# Polyethylene-based Anion Exchange Membrane for Alkaline Fuel Cell and Electrolyser Application: Synthesis, Characterisation and Degradation Studies

A thesis submitted for the degree of

Doctor of Philosophy

By

**RICHARD DE VILLA ESPIRITU**

School of Chemical Engineering and Advanced Materials

Newcastle University

Newcastle upon Tyne, United Kingdom

April 2017

# ABSTRACT

Alkaline anion exchange membranes (AAEM) have been fabricated using polyethylene as the base polymer offering a low cost AAEM for electrolyser and fuel cell applications. This study focused on the synthesis and characterisation of AAEM with controlled degree of grafting (DOG) and ion-exchange capacity (IEC) with the following parameters investigated: low density polyethylene (LDPE) film thickness 30-130 µm, gamma radiation dose and monomer concentration. The corresponding IEC, water uptake (WU) and degree of swelling (DS) are reported. The performance of 74.6% DOG membrane in a hydrogen fuel cell showed a high open circuit voltage of 1.06 V, with a peak power density of 608 mW cm$^{-2}$ at 50 °C under oxygen. The use of a membrane with a high DOG does not impact fuel cross-over significantly and provides improved fuel cell performance due to its high conductivity, water transport and resilience to dehydration.

The AAEMs showed long term stability, at 80 °C, exhibiting a conductivity of ca. 0.11 S cm$^{-1}$ over a period of 3300 h under nitrogen. The membrane showed a degradation rate of 5.7 and 24.3 mS kh$^{-1}$ under nitrogen and oxygen, respectively. With the membrane lifetime defined as the duration of fuel cell operation until the conductivity of the membrane has reduced to a cut-off value of 0.02 S cm$^{-1}$, the estimated lifetime of the membrane is 2 years under nitrogen and 5 months under oxygen operating at 80 °C.

The fabricated anion exchange membranes were subjected to degradation tests in deionised water for electrolyser/fuel cell operation. After the degradation test, the decrease in ion exchange capacity (IEC) of the AEM, hence decrease in ionic conductivity, was influenced by the applied gamma radiation dose rate. The use of a high radiation dose rate produced membranes with improved stability in terms of % IEC loss due to shorter, more uniformly distributed vinylbenzyl chloride (VBC) grafts. For LDPE-based AEMs, increasing the applied radiation dose rate during grafting from 30 to 2000 Gy h$^{-1}$ significantly reduced AEM % IEC loss from 38 to 11%, respectively. Analyses of both the aged functionalised membranes and their resulting degradation products confirmed the loss of not only the functional group, but also the VBC group, which has not been reported previously in the literature. Investigation of other amine functional groups revealed similar degradation via the removal of both VBC and head group. Oxidation reactions

taking place at pH close to neutral are the main contributor to the IEC loss, in contrast to the widely reported E2 or $S_N2$ attack on the head group in high alkalinity solutions. A parallel degradation mechanism is proposed to explain head group loss of AEMs, that involves peroxide radicals which are more dominant in low alkalinity solutions.

The investigation of the degradation of a commercially available AEM (A201, Tokuyama Corp.) was performed and compared with the fabricated LDPE AEMs. Using similar membrane thickness, results revealed that the fabricated AEM exhibited superior stability to the commercial A201 membrane in terms of % IEC loss and ionic conductivity, both in fuel cell and electrolyser modes. It is believed that the faster degradation rate of the A201 membrane could possibly be due to the attack of $OH^-$ ions on both the head group and on the polymer backbone, the latter of which was not observed on the fabricated AEMs.

# ACKNOWLEDGMENT

# TABLE OF CONTENTS

**Part II. Stability and Degradation Studies of Anion Exchange Membrane**

# LIST OF FIGURES

**Part II. Stability and Degradation Studies of Anion Exchange Membrane**

# LIST OF SCHEMES

**Part II. Stability and Degradation Studies of Anion Exchange Membrane**

# LIST OF TABLES

**Part I. Synthesis and Characterisation of Anion Exchange Membrane**

**Part II. Stability and Degradation Studies of Anion Exchange Membrane**

**Appendices**

# ABBREVIATIONS AND GLOSSARY OF TERMS

AEM
anion exchange membrane

a semi-permeable membrane generally made from ionomers and designed to conduct anions while being impermeable to gases such as oxygen and hydrogen

ABCO
1-azabicyclo[2.2.2]octane

also known as quinuclidine is a bridged bicyclic tertiary amine containing 1 nitrogen with empirical formula $C_7H_{13}N$

AFC
alkaline fuel cell

a type of fuel cell that utilises alkaline electrolyte to produce electric current

ATR
attenuated total reflectance

a sampling technique used in conjunction with infrared spectroscopy where infrared light is introduced into a prism at an angle exceeding the critical angle for internal reflection

AWE
alkaline water electrolyser

a type of electrolyser that utilises alkaline electrolyte to split water into hydrogen and oxygen

CP-MAS
cross polarisation magic angle spinning

a technique combined with magic angle spinning which is used in order to enhance the signal of the weakly coupled nuclei (i.e. $^{13}C$ nuclei) in solid state nuclear magnetic resonance spectroscopy

DABCO
1,4-diazabicyclo[2.2.2]octane

also known as triethylenediamine is a bridged bicyclic tertiary amine containing 2 nitrogens with empirical formula $N_2(C_2H_4)_3$

DE-MAS
Direct excitation magic angle spinning

a technique combined with magic angle spinning which involves direct application of energy to produce net transverse magnetisation in solid state nuclear magnetic resonance spectroscopy

DOG
degree of grafting

a measure of the extent of polymerisation which is expressed in terms of percentage mass of the grafted component within the copolymer matrix

| | |
|---|---|
| DS<br>degree of swelling | a measure of water absorbance in terms of difference in dimensions (length, width and thickness) of the hydrated and dry membrane |
| EIS<br>electrochemical impedance spectroscopy | a technique of determining the impedance by applying AC potential to an electrochemical cell and then measuring the current |
| electrolyser | an electrochemical device that converts electrical and thermal energy into chemical energy stored in a fuel (i.e. hydrogen) |
| ETFE<br>ethylene tetrafluoroethylene | a type of plastic containing partially fluorinated copolymer of ethylene and tetrafluoroethylene |
| FRA<br>frequency response analyser | a technique that involves applying a low-voltage signal to an electrochemical system wherein the output spectrum is plotted in terms of gain and phase-shift |
| FTIR<br>Fourier transform infrared spectroscopy | a technique which is used to obtain an infrared spectrum of a sample that is used to identify the molecular components and structures |
| fuel cell | an electrochemical device capable of converting chemical energy from the reaction of fuel and oxidant directly into electrical energy |
| HDPE<br>high density polyethylene | a thermoplastic polyolefin which exhibits higher mechanical properties than low density polyethylene due to lower degree of branching |
| hydration number | expressed as the number of water molecules per unit of functional group |
| IEC<br>ion exchange capacity | measure of the ability of the anion exchange membrane to allow preferential displacement of the initially attached OH ion on the tethered head group by another OH ion, which is a function of the number of exchange sites within a given quantity of the membrane |

| | |
|---|---|
| IEC$_{theo}$<br>theoretical ion exchange capacity | ion exchange capacity of the membrane assuming complete amination, ion exchange and complete removal of water upon drying |
| KOH<br>potassium hydroxide | a strong base commonly called as caustic potash with a molecular weight of 56.11 g/mol |
| LDPE<br>low density polyethylene | a type of thermoplastic polyolefin exhibiting high degree of short and long chain branching with low crystallinity and melting point |
| LLDPE<br>linear low density polyethylene | a type of thermoplastic polyolefin with high number of short chain branches and higher crystallinity than low density polyethylene |
| MAS<br>magic angle spinning | a technique commonly employed in solid-state nuclear magnetic resonance spectroscopy wherein the sample is spinning at an angle of 54.74º with respect to the direction of the magnetic field |
| membrane lifetime | duration of fuel cell operation until the conductivity of the membrane has reduced to a cut-off value of 0.02 S cm$^{-1}$ |
| MCFC<br>molten carbonate fuel cell | a type of fuel cell that operates above 600 °C and utilises molten carbonate mixture material as electrolyte to produce current |
| NMP<br>*N*-methylpiperidine | a type of cycloaliphatic amine with empirical formula $C_6H_{13}N$ |
| NMR<br>nuclear magnetic resonance spectroscopy | a technique in which a sample when subjected to a known magnetic field strength absorbs and emits electromagnetic radiation producing a resonance frequency that provides information about the structure and chemical environment of the sample |
| PAFC<br>Phosphoric acid fuel cell | a type of fuel cell that utilises liquid phosphoric acid as electrolyte to produce electric current |
| PEMFC<br>polymer electrolyte membrane fuel cell | a type of fuel cell that uses solid acid membrane as electrolyte operating at low temperatures to produce current |

| | |
|---|---|
| PEMWE<br>polymer electrolyte membrane water electrolyser | a type of electrolyser that uses solid acid membrane as electrolyte operating at low temperatures to split water into hydrogen and oxygen |
| RH<br>relative humidity | the ratio of the partial pressure of water vapour in air to the saturation vapour pressure of water at the same temperature, expressed in percentage |
| SEM<br>scanning electron microscopy | a type of electron microscope that produces image using a focused beam of electrons to scan the surface of the sample |
| SOFC<br>solid oxide fuel cell | a type of high temperature fuel cell that uses solid oxide (e.g. yttria stabilised zirconia) as electrolyte to produce electric current |
| SOWE<br>solid oxide water electrolyser | a type of high temperature electrolyser that uses solid oxide (e.g. yttria stabilised zirconia) as electrolyte to split water into hydrogen and oxygen |
| TMA<br>trimethyl amine | a clear and colourless tertiary amine with chemical formula $N(CH_3)_3$ |
| UHMWPE<br>ultra high molecular weight polyethylene | a type of thermoplastic polyethylene containing extremely long chains with a molecular mass of 3 to 7 million atomic mass units |
| UTS<br>Ultimate tensile strength | maximum stress that a material can withstand prior to fracture upon elongation |
| UV<br>ultraviolet | an electromagnetic radiation shorter than visible light with a wavelength between 10 nm to 400 nm |
| VBC<br>vinylbenzyl chloride | also known as chloromethyl styrene, is a type of monomer containing polymerisable double bonds and benzylic chloride group |
| WU<br>water uptake | measure of the amount of water a membrane can absorb expressed in terms of weights of the hydrated and dried polymer membrane |

## OVERVIEW AND OUTLINE OF THE THESIS

This research has investigated a wealth of different parameters in terms of base polymer types, initial film thickness, monomer concentration, radiation source and grafting conditions in fabricating anion-exchange membranes (AEM) as shown in Table A. The produced AEMs were evaluated in terms of their physico-chemical, morphological, mechanical and electrical properties in order to obtain an AEM with the desired properties (Table B).

Table A. Different grafting parameters investigated in this study.

| Base film and base film thickness | Monomer concentration | Radiation source | Grafting condition |
|---|---|---|---|
| LDPE (20, 30, 50, 75 and 130 µm) | Vinylbenzyl chloride 10% and 31% | UV | Two 400 W lamp UV source |
| | | Gamma radiation | Total dose: 10 and 20 kGy |
| | | | Dose rate: 2 kGy h$^{-1}$ |
| LLDPE (cast) HDPE (40 µm) UHMWPE (40 µm) | | Gamma radiation | Total dose: 10 and 20 kGy |
| | | | Dose rate: 2 kGy h$^{-1}$ |
| ETFE (50 µm) | | Electron beam | 4.5 MeV electron beam source |
| | | | Total dose: 70 kGy |

It was originally envisaged that polyethylene base film precursors will be prepared and cast in the laboratory so that the properties of the initial films can be controlled. This is because polyethylene films procured from commercial sources have varying quality and properties (i.e. molecular weight, degree of polymerisation, melting and glass transition temperature, presence and amount of additives, etc.) which play significant role in the resulting copolymer characteristics and will greatly affect the consistency of the measured properties of the fabricated polyethylene-based AEM. However, after numerous attempts, polyethylene pellets were found

difficult to melt with a suitable solvent and cast into films. The study therefore proceeds with the use of polyethylene films from commercial suppliers.

Table B. Important AEM properties that are evaluated.

| | |
|---|---|
| Physico-chemical | Degree of grafting |
| | Ion exchange capacity |
| | Water uptake |
| | Hydration number |
| | Degree of swelling |
| Morphological | Grafting distribution (surface and cross-section) |
| Mechanical | Ultimate tensile strength |
| Electrical | Ionic conductivity |
| | Fuel cell performance |

An initial approach to fabricate the AEMs is with the use of ultraviolet (UV) radiation source and using low density polyethylene (LDPE) as the base polymer and vinylbenzyl chloride (VBC) as the grafting monomer. However, due to the low energy emitted by UV, hence low depth of penetration through the LDPE film to enact grafting, the synthesis of AEM shifted to the use of gamma radiation source. In order to investigate the effect of the applied radiation dose, two total exposure doses are used, namely, 10 kGy and a higher dose of 20 kGy, with a fixed radiation dose rate of 2 kGy h$^{-1}$. These choices of exposure parameters were based on equipment's settings and limitations as the mutual radiation grafting was performed by Synergy Health plc (Wiltshire, UK).

Aside from LDPE, the first batch of samples sent for gamma radiation grafting include other polyethylene-type of base polymers such as linear low density (LLDPE), high density (HDPE) and porous ultra-high molecular weight polyethylene (UHMWPE). The next batch of samples sent for gamma radiation grafting focused chiefly on LDPE from a single commercial source, however, with different initial film thicknesses, namely, 20, 30, 50, 75 and 130 µm. On the other hand, employing ethylene-tetrafluoroethylene (ETFE) as base polymer requires high radiation energy

source and total dose exposure hence, electron beam source with 70 kGy total dose was used to prepare the membrane.

The fabricated AEMs, after assessment in terms of fuel cell performance, are subsequently subjected to degradation test in order to evaluate its suitability for fuel cell and water electrolyser application. The degradation test is done by immersing the $OH^-$ exchanged AEM in deionised water placed in water bath for different time and temperatures. This approach of performing degradation test (i.e. in deionised water and prolonged period of up to 1440 h) is novel, and contrary to those reported in literature where AEM degradation tests were performed using solutions of high alkalinity and immersion for only several days (< 200 h), which is not sufficient to confirm with certainty any observable degradation on the membrane and is very far from the real operating conditions of alkaline fuel cells and electrolysers. Furthermore, typically reported AEM degradation studies in literature were performed under inert atmosphere and use simple benzyl trimethylammonium compound instead of the actual polymer membrane.

The study of AEM degradation is expanded to include other functional groups aside from trimethyl amine (TMA) in order to compare and identify the most stable cation group for the AEM. The other functional groups include N-methylpiperidine (NMP), 1,4-diazabicyclo[2.2.2]octane (DABCO) and 1-azabicyclo[2.2.2]octane (ABCO). The original and aged membranes together with the solid and degradation solutions are subjected to Fourier transform infrared (FTIR) spectroscopy and to solid state- and solution-NMR spectroscopy. The summary of degradation test conditions performed on the fabricated AEMs is shown in Table C. The degradation tests were performed at temperatures of up to 60 $^{\circ}$C, which is normally the highest operating condition for low-temperature alkaline fuel cells and electrolysers. The use of deuterium oxide ($D_2O$) for some samples offers the advantage of having the dissolved degradation products in deuterated water to be directly analysed and identified by solution-NMR spectroscopy.

Due to the vast number of parameters to be investigated and with the limited amount of fabricated radiation-grafted membranes and considering further the long duration of each degradation test (up to 1440 h in deionised water and 5000 h in nitrogen-saturated atmosphere) for each type of functionalised membrane and under different test conditions, performing several trials for each degradation test were deemed tedious and impracticable.

Table C. Summary of degradation test conditions of the different fabricated AEMs.

| Base polymer | Functional group* | Degradation test condition** | |
| --- | --- | --- | --- |
| | | Temperature (ºC) | Time (h) |
| - | TMA | 60 | 2160 |
| LDPE | TMA (unexchanged) | 60 | 2160 |
| LDPE | DABCO (unexchanged) | 60 | 2160 |
| LDPE | TMA | 20, 40, 60<br><br>60 | 720<br><br>1440 |
| HDPE | | | |
| ETFE | | | |
| LDPE | TMA<br><br>DABCO<br><br>ABCO<br><br>NMP | 60<br>(in D$_2$O) | 720<br><br>1440<br><br>(in D$_2$O) |
| LDPE | TMA | 60<br>(in D$_2$O)<br>under Nitrogen<br>under Oxygen | 1080<br>(in D$_2$O)<br>under Nitrogen<br>under Oxygen |

*OH$^-$ exchanged, unless otherwise specified.

**Immersed in deionised water, unless otherwise specified.

In order to have a systematic and easy-to-follow flow of discussions, this doctoral thesis is hereby presented in two major parts. Part I includes the synthesis and characterisation of the anion-exchange membrane prepared by radiation grafting employing different base polymer films and vinylbenzyl chloride as the grafting monomer. The produced copolymers were subsequently functionalised with TMA. The functionalised membrane was chemically analysed by FTIR spectroscopy and was characterised in terms of different AEM properties enumerated in Table B.

Part II focuses on the stability and degradation studies of the fabricated membranes functionalised with different head groups. This involves stability assessment of the membranes in both vapour phase (fuel cell) and in liquid phase (deionised water) conditions. The initial and aged membranes functionalised with different head groups were characterised in terms of ion exchange capacity and ionic conductivity measurement while scanning electron microscopy was utilised to investigate the morphology and structure of the membrane. The aged membranes were subjected to $^{13}$C, $^{15}$N, $^{17}$O solid state magic angle spinning NMR analysis while the degradation solutions were analysed using $^{1}$H and $^{13}$C solution-NMR spectroscopy. The solid degradation by-products were chemically analysed by FTIR spectroscopy.

Furthermore, this thesis is partially based on the following publications of the author:

**R. Espiritu**, B. Golding, K. Scott and M. Mamlouk. Degradation of radiation grafted hydroxide anion exchange membrane immersed in neutral pH: removal of vinylbenzyl trimethylammonium hydroxide due to oxidation. *Journal of Materials Chemistry A*. **2017**, 5(3), 1248-1267. DOI: 10.1039/c6ta08232g

**R. Espiritu**, M. Mamlouk, and K. Scott. Study on the effect of the degree of grafting on the performance of polyethylene-based anion exchange membrane for fuel cell application. *International Journal of Hydrogen Energy*. **2016**, 41(2), 1120-1133. DOI: 10.1016/j.ijhydene.2015.10.108

K. Scott, M. Mamlouk, **R. Espiritu** and X. Wu. Progress in alkaline membrane fuel cells and regenerative fuel cells. *ECS Transactions*. **2013**, 58(1), 1903-1906. DOI: 10.1149/05801.1903ecst

# INTRODUCTION

Over the recent decades, there has been aggressive research on the development of alternative renewable energy technologies. Such undertaking was driven by the increasing consumer demand for energy, unabated cost of power production and the rising public awareness for environmental protection. Though there are several established renewable energy resources (e.g. wind, geothermal and sunlight), fuel cell technology has been recognised as a promising clean power source for future energy systems [1, 2].

The fuel cell is an electrochemical device capable of converting chemical energy from the reaction between the fuel and the oxidant directly into electrical energy. It consists mainly of three important components, namely, the anode where the fuel is externally supplied, the cathode where the oxidant is fed and the electrolyte which effectively separates the two electrodes but allows the flow of ions through it. The chemical energy conversion of hydrogen (fuel) and oxygen (oxidant) into electric energy and heat takes place by electrochemical redox reactions at the anode and the cathode, respectively.

The fuel cell offers the advantage of providing higher energy conversion efficiency compared with an internal combustion engine. Furthermore, it basically has no moving parts thus produces less noise and so is more reliable. Therefore it is expected to have lower maintenance cost and longer service life [3]. Fuel cells are mainly classified according to the type of electrolyte they employ. Currently, there are five major types of fuel cells, namely, alkaline fuel cells (AFCs), proton-exchange membrane fuel cells (PEMFCs), solid oxide fuel cells (SOFCs), phosphoric acid fuel cells (PAFCs) and molten carbonate fuel cells (MCFCs). Comparison between different types of fuel cells is shown in Table D. The choice of suitable fuel cell type depends on the particular desired application, the kind of catalyst used, the temperature range in which the fuel cell operates and required fuel input.

Among all of these types of fuel cells, PEMFCs and AFCs are the most studied for practical service applications, particularly in low temperature regime of operating conditions. Though AFCs are considered to be the most matured fuel cell technology [4], having been extensively studied as early as the 1960s, PEMFCs

Table D. Comparison of different types of fuel cells [2, 3, 5, 6].

| | PEMFC | PAFC | AFC | MCFC | SOFC |
|---|---|---|---|---|---|
| **Electrolyte** | Polymer membrane | Liquid $H_3PO_4$ (immobilised) | Liquid KOH (immobilised) | Molten carbonate | Ceramic |
| **Charge carrier** | $H^+$ | $H^+$ | $OH^-$ | $CO_3^{2-}$ | $O^{2-}$ |
| **Operating Temperature** | 60 – 100 ºC | 175 – 220 ºC | 60 – 220 ºC | 600 – 650 ºC | 800 – 1000 ºC |
| **Catalyst** | Platinum | Platinum | Platinum, nickel | Nickel | Perovskite (cathode) Nickel (anode) |
| **Fuel Compatibility Efficiency (%)** | $H_2$, methanol 40 – 50 | $H_2$ 40 – 45 | $H_2$ 50 – 70 | $H_2$, $CH_4$ 50 – 60 | $H_2$, $CH_4$, CO 50 – 60 |
| **Power density (kW/m³)** | 3.8 – 6.5 | 0.8 – 1.9 | ~ 1.0 | 1.5 – 2.6 | 0.1 – 1.5 |
| **Capacity** | 30W, 7kW, 250kW | 100kW – 1.3 MW | 10 – 100 kW | 155kW – 2MW | 1kW – 1.7MW |
| **Advantages** | High power density, quick start-up | Tolerant to impure $H_2$ | High efficiency, fast cathode reaction, quick start-up | High efficiency | High efficiency, generate high grade waste heat |
| **Disadvantages** | Expensive platinum catalyst, Intolerant to CO in impure $H_2$ | Corrosive electrolyte, Low power density, sulfur poisoning | Expensive platinum catalyst, Intolerant to $CO_2$ in impure $H_2$ and air | High cost, corrosive electrolyte, slow start-up, sulfur poisoning | High temperature, high cost, thermal stress failure |
| **Application** | portable power, distributed generation, transportation | Distributed generation, transportation | Transportation, military, space and portable power | Electric utility, distributed generation | Auxiliary power, electric utility and distribution generation |

have emerged as the preferred technology and have effectively displaced AFCs for low temperature and moderate power applications [7]. This is due to the flexibility of PEMFCs for using solid electrolyte and its capability of preventing electrolyte leakage [4].

Many types of fuel cell require hydrogen as fuel. Although hydrogen is ubiquitous in nature, it rarely exists in its pure form. Commercial large scale production of hydrogen is performed by reforming of natural gas, gasification of coal and petroleum coke, and reforming of fossil fuels [8]. The process of producing hydrogen through water electrolysis has been known for around 200 years and offers the advantage of producing extremely high purity of hydrogen, however, it is confined to small scale setup with limited application to large scale pure hydrogen production. Thus water electrolysis accounts only for 4% of world total hydrogen production [9].

Table E. Different types of water electrolyser technologies [10, 11].

|  | AWE | PEMWE | HT-SOWE |
| --- | --- | --- | --- |
| **Electrolyte** | Liquid KOH | Polymer membrane | Ceramic |
| **Charge Carrier** | $OH^-$ | $H^+$ | $O^{2-}$ |
| **Electrode** | Ni | Pt/C | Ni, ceramics |
| **Operating Temperature** | 60 – 90 °C | 20 – 100 °C | 700 – 1000 °C |
| **Advantages** | well-established, non-noble catalyst, relative low cost | high current densities, high gas purity, rapid system response | 100% efficiency High-pressure operation, non-noble catalyst |
| **Disadvantages** | low current densities, gas crossover, corrosive electrolyte | high component costs, corrosive environment | laboratory stage, brittle electrolyte |

Water electrolysis is an electrochemical process which utilises supplied electricity to split water in to separate components, namely, hydrogen and oxygen. In this process, water is fed to an electrochemical cell (electrolyser) in which the hydrogen evolves at the cathode while the oxygen evolves at the anode. It is

basically a reverse process of a fuel cell. There are currently three types of water electrolysers available, namely, alkaline water electrolyser (AWE), polymer electrolyte membrane water electrolyser (PEMWE) and high-temperature solid oxide water electrolyser (HT-SOWE) as shown in Table E.

Similar with fuel cell, AWE and PEMWE are employed for low-temperature applications, however AWE provides higher efficiency in comparison with PEMWE. Furthermore, PEMWE requires ultrapure water feed while AWE is tolerable to caustic electrolytes [12].

**Motivation for the Study**

Renewed interest to the research and development of AFCs and AWEs has grown rapidly with the advent of solid anion-exchange membrane (AEM) instead of liquid KOH as the electrolyte. The alkaline anion-exchange membrane fuel cell (AEMFC) and water electrolyser (AEMWE) have been developed to address the challenges and limitations of the conventional AFCs and AWEs. Alkaline-type fuel cell and electrolyser regain fame against their PEM-type counterparts as they offer the following advantages, namely, (a) faster oxygen reduction reaction (ORR) under alkaline fuel cell conditions, thus providing lower activation losses [4, 13, 14], (b) possibility of using non-noble metal catalysts [15-17], (c) osmotic drag associated with ion transport opposes the cross-over of liquid methanol fuels [18, 19] and (d) lower membrane cost and cheaper cell components due to less corrosive environments [13, 15, 19]. Figure A shows the comparison of mechanism between PEM and AAEM containing fuel cells.

Owing to these advantages, this particular study focuses on the synthesis and characterisation of AEMs for alkaline fuel cells and electrolysers using low density polyethylene as the base polymer thus offering an essentially cheaper alternative than commercially available AEM. Vinylbenzyl chloride is used as the monomer to produce the graft co-polymer which exhibits high ion conductivity coupled with good mechanical, chemical and thermal stability. This research further investigates the use of different grafting techniques and employing several amine functionalities in fabricating the most suitable AEM for fuel cell and electrolyser applications.
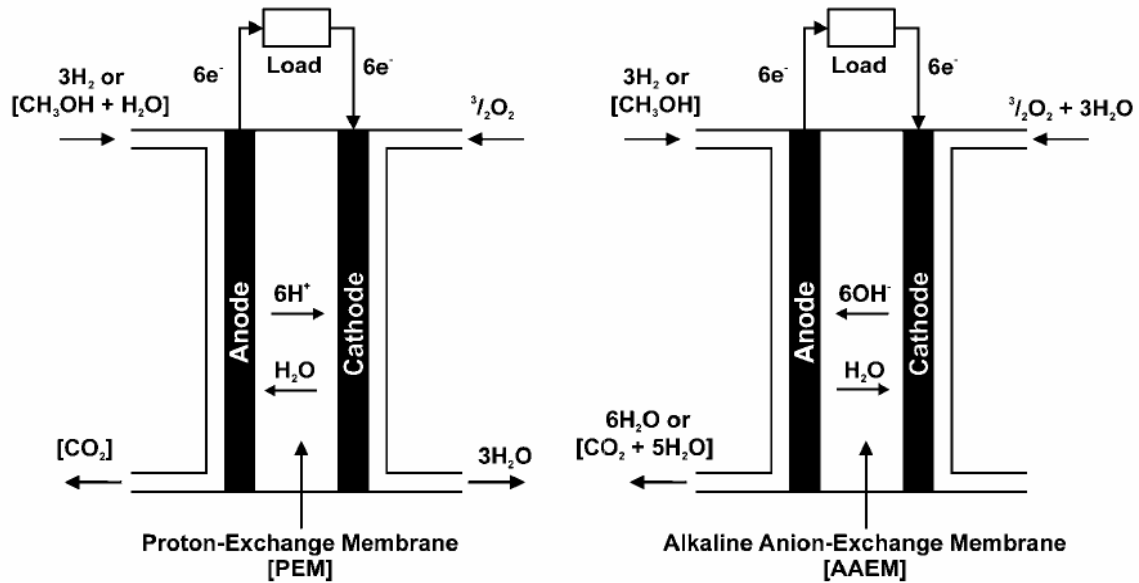
Figure A. Schematic of proton exchange membrane and alkaline anion exchange membrane both fuelled with pure hydrogen or methanol [20, 21].

**Research Aim and Objectives**

The aim of this research is to synthesise an alkaline AEM using low density polyethylene (LDPE) as base polymer and poly(vinylbenzyl chloride) as the grafting monomer. Such AEM is envisioned to have excellent properties that can be seamlessly applied for fuel cell and electrolyser operation. Particularly, this study intends to:

1. Establish a procedure of synthesising an alkaline polymer anion-exchange membrane via radiation grafting techniques.

2. Evaluate the different parameters such as the type of radiation source (e.g. gamma and UV), radiation dose, exposure time, monomer concentration and functionalisation/amination (head group) type to the properties of the resulting graft co-polymer.

3. Characterise the AEM in terms of its hydrophysical, morphological, chemical, mechanical and electrical properties and relate them to their respective stability characteristics.

4. Perform fuel cell performance testing; and

5. Assess the stability of the AEM by performing degradation tests.

**PART I. SYNTHESIS AND CHARACTERISATION OF ANION EXCHANGE MEMBRANE**

# CHAPTER 1

# REVIEW OF RELATED LITERATURE

The basic principle of the fuel cell was discovered by the Swiss scientist Christian Friedrich Schonbein in 1838 and the following year, the first fuel cell was developed when Sir William Grove in his experiment accidentally reversed the electrolysis of water [5]. The alkaline fuel cell is considered to be the first type of fuel cell to be developed where Francis T. Bacon later gained prominence. Bacon commenced his research in 1932 and successfully constructed a 5-kW hydrogen-oxygen fuel cell in 1952 [22]. In the 1960s, AFC was the first fuel cell type to be used for space application and were installed in NASA's Apollo spacecraft [23].

## 1.1 Alkaline fuel cell

The alkaline fuel cell (AFC) is an electrochemical device that converts the chemical energy of hydrogen (as fuel) directly into electric current. AFC uses a liquid electrolyte solution of potassium hydroxide (KOH) because it is the most conducting of all alkaline hydroxides [22, 24]. Of all the types of fuel cells available, AFC offers the highest electrical efficiency when using very pure gas fuels [25]. The schematic diagram and overall chemical reactions are shown in Figure 1.1.



Anode: $2H_2 + 4OH^- \longrightarrow 4H_2O + 4e^-$    $E_a^0 = -0.83V$

Cathode: $O_2 + 2H_2O + 4e^- \longrightarrow 4OH^-$    $E_c^0 = 0.40V$

Overall: $2H_2 + O_2 \longrightarrow 2H_2O$    $E_{cell} = 1.23V$
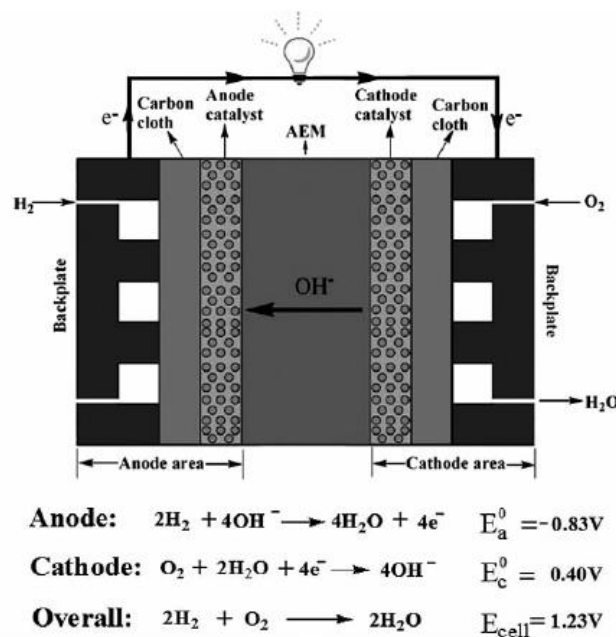
Figure 1.1. Fundamentals of an alkaline fuel cell [26].

Unlike in PEMFC where $H^+$ is transmitted from the anode to the cathode, in an AFC, $OH^-$ is conducted from the cathode to the anode. In the anode, hydrogen reacts with the hydroxyl ions producing water and electrons. The generated electrons are then transported to the cathode thru an external circuit which then react with water and oxygen to produce hydroxyl ions. It is also evident from the overall chemical reaction that the anode produces twice as much water as the anode can consume, thus water recirculation is an integral component of a fuel cell. This can be done by recirculating the electrolyte and using the excess water as the coolant liquid, thereby allowing removal of water by evaporation.

As mentioned earlier, one of the important advantages of AFC is that the activation overvoltage at the cathode is generally less than that with an acid electrolyte. This is because the reduction of oxygen to a hydroxide ion is much faster in AFC than in the acidic counterpart of oxygen to water [25]. Such improved kinetics allow AFCs to have operating voltages considerably higher than their PEMFC counterparts [23]. This high electrical efficiency also allows the use of alternative noble metal catalyst instead of platinum which is very expensive. Furthermore, AFCs are relatively easy to handle as the operating temperature is relatively low.

Albeit the numerous advantages of the use of AFCs, no fuel cell system is perfect. One of the main problem of AFCs is that the liquid KOH electrolyte reacts with $CO_2$ forming carbonates and/or bicarbonate ($CO_3^{2-}$/$HCO_3^-$) which cause the degradation of the electrodes and the electrolyte solution [21, 24]. Consequently, it has been a major constraint to keep the $CO_2$ concentration to the minimum. In order to address this concern, the search for an alternative electrolyte has been the focus of intensive research, which resulted in the development of anion-exchange membranes for alkaline fuel cell applications.

## 1.2 Alkaline water electrolyser

Electrolysis is a well-established method of generating hydrogen and oxygen by applying electric current to water. The very high purity of hydrogen that can be obtained from this process significantly attracts attention of its viability as hydrogen fuel source for low-temperature fuel cell applications. In water electrolysis, electric current flows between two electrodes immersed in an electrolyte and are separated

by a membrane with high ionic conductivity to avoid the recombination of the generated hydrogen (cathode) and oxygen (anode) [9].



| | | | |
|---|---|---|---|
| Anode: | $4OH^- \rightarrow O_2 + 2H_2O + 2e^-$ | $E_o = 0.4$ V | (1) |
| Cathode: | $2H_2O + 2e^- \rightarrow 2H_2 + 4OH^-$ | $E_o = -0.83$ V | (2) |
| Overall: | $2H_2O \rightarrow 2H_2 + O_2$ | $E_o = 1.23$ V | (3) |
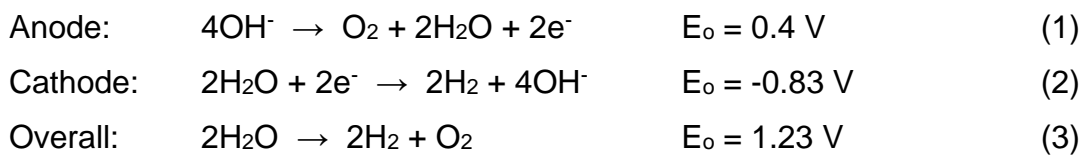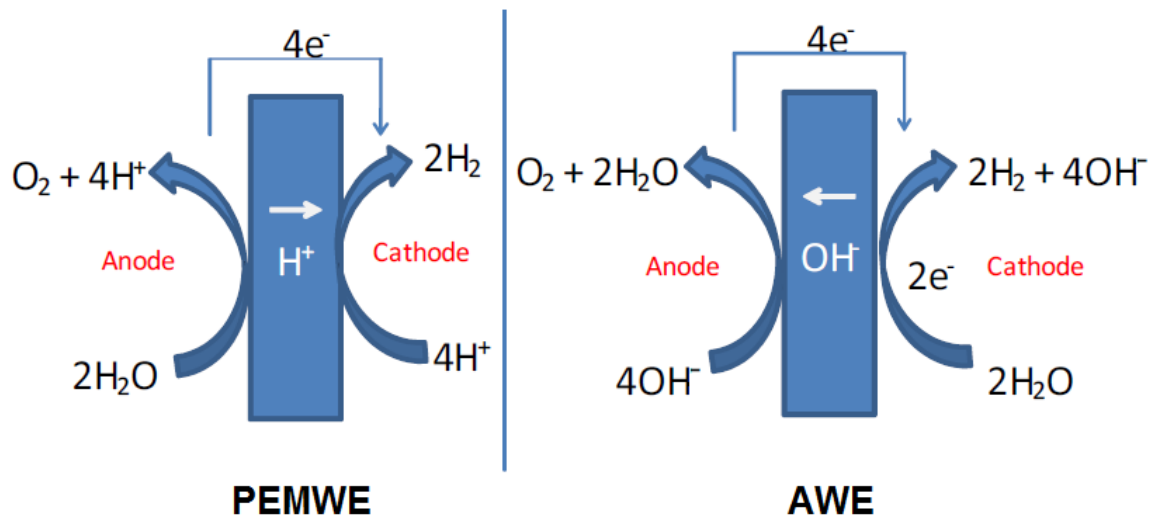
Figure 1.2. Comparison of electrode reactions for AWE and PEMWE [27].

A water electrolyser is an electrochemical device that converts electrical and thermal energy into chemical energy stored in a fuel (hydrogen). There are two main types of low-temperature water electrolysers namely, alkaline water electrolyser (AWE) which uses $OH^-$ ions as charge carrier and polymer electrolyte membrane water electrolyser (PEMWE) that uses protons instead, comparison of which is shown previously in Table E. Figure 1.2 further shows the comparison between AWE and PEMWE in terms of half-cell reactions wherein the major difference between the two, aside from the type of charge carrier involved, is that water reacts at the opposite sides of the cell. Such difference great influences the appropriate system configuration and the choice of electrolyser type for a particular application. The low operating potential at the anode side (0.4 V) enables the use of non-platinum based catalysts for AWE systems thereby offering a lower operating cost.

Similar to fuel cell systems, the membrane that separated the two electrodes plays a very important role in attaining the highest electrolyser operation efficiency possible. It is therefore incumbent for the anion-exchange membrane for AWE application to have superb ionic conductivity, high chemical and thermal stability and enhanced mechanical strength while reducing gas cross-diffusion [28].

## 1.3 Alkaline anion-exchange membrane

Anion-exchange membranes (AEMs) are solid polymer electrolyte membranes that contain positive ionic groups, typically containing quaternary ammonium groups: $-N^+(CH_3)_3$, and mobile negatively charged anions, usually $OH^-$ [20, 29]. With the use of AEMs as electrolyte for AFCs, the oxygen reduction reaction is improved [1] and electrolyte leaking and carbonate precipitation are prevented [4] due to the effective separation of the fuel and oxidant.

There have been several classes of alkaline anion-exchange membranes fabricated for fuel cell and electrolyser operations reported in literature. As previously mentioned, the most common class of AEMs are those based on quaternary ammonium groups due to their appreciable stability under alkaline environment [30]. Examples of anion exchange membranes for fuel cells and electrolysers reported in literature are quaternised poly(ether sulfone) [31], quaternised poly(phenylene) [32], aminated poly(oxy ethylene) [13], methacrylates [33] and poly(epichlorhydrin [34]. Polybenzimidazole-doped AEMs were also investigated for their feasibility for fuel cell [21, 35] and electrolyser [36, 37] applications were found to possess excellent endurance both in alkali medium [38] and at elevated temperature [39].

The materials and methods needed to synthesise the AEM are influenced by the desired properties of the resulting membrane wherein it should meet stringent performance, durability, stability, and low cost. The chemical and thermal stability are greatly dependent on the nature of the polymer backbone and on the type of functional groups that enables the transfer of hydroxyl ions [40]. With these in mind, the major challenge is to synthesise AEM with a high $OH^-$ ion conductivity which can be done by using a polymer backbone with high ion exchange capacity. This challenge has been adequately solved by employing polymer modification via a grafting technique.

## 1.4 Polyethylene-based anion exchange membranes

Polyethylene is a thermoplastic olefin composed of long chains of ethylene monomer. It is used extensively in various industrial applications and has gained significant attention in fuel cell technology particularly as an attractive base polymer for anion exchange membranes. Polyethylene has been found to be a lucrative polymer backbone for AEMs due to its low cost, superior chemical stability, high crystallinity and hydrophobicity, good mechanical properties [41, 42] and versatility to radiation grafting both for electrolyser and fuel cell applications [43-45]. Masson et al. [46] utilised a gamma radiation source to graft low density polyethylene (LDPE) with acrylic acid followed by sulfonation while Faraj et al. [47] utilised a UV-radiation source to graft LDPE with vinylbenzyl chloride (VBC) with subsequent amination to fabricate AEMs for water electrolysis. In terms of fuel cell application, Mamlouk et al. [48, 49] successfully fabricated AEMs for alkaline fuel cells using LDPE and high density polyethylene (HDPE) as base polymer and employing VBC as the graft monomer. Aside from LDPE and HDPE based membranes for alkaline fuel cells, ultrahigh molecular weight polyethylene (UHMWPE) has also been used for radiation grafting but requires a melt pressing method to produce the membrane [50]. Shen et al. [51] on the other hand, performed methanol permeation studies on LDPE-based AEM for direct methanol fuel cells while Cheng et al. [52] evaluated the performance of LDPE-based AEM for direct borohydride fuel cell application.

There were reports in literature that used LDPE as base polymer for AEM however used a chemical synthesis route rather than the radiation-induced grafting method. Kostalik et al. [53] have functionalised crosslinked-polyethylene with a tetraalkyl ammonium group through ring-opening metathesis polymerisation and successfully produced AEM with good ionic conductivity and improved mechanical strength. Another study [41] synthesised AEM by employing metallocene-mediated copolymerisation in order to introduce flexible pendant ammonium groups to the crosslinked and uncrosslinked polyethylene matrix.

Evolving research trends on polyethylene-based membranes involve grafting of polyethylene with another polymer in order to obtain the desired chemical and mechanical properties of the resulting copolymer backbone prior to functionalisation. Kim et al. [42] exploited the innate hydrophobicity of polyethylene and chemically grafted it with sulfonated poly(arylene ether sulfone) to produce membranes with high ion exchange capacity but with controlled swelling and water

uptake. The grafting of 4-vinylpiridine on polyethylene was also reported to increase the ion-exchange properties of the resulting polymer product [54]. The work of Noonan et al. [55] showed the preparation of membranes with superb alkaline stability by chemically attaching phosphonium-based functional groups to polyethylene. The crosslinking of tetrafluoroethylene with polyethylene was reported to enhances the tensile strength of the resulting membrane [56]. Moreover, pore-filled composite membranes based on porous polyethylene exhibited high durability [57] and enhanced mechanical stability for high temperature fuel cell operation [58].

## 1.5 Monomers for AEM fabrication by radiation-induced grafting

As the base polymer film provides the backbone structure of the membrane, the grafting monomer acts as the bridge between the polymer backbone and the attached ion exchange site functionality. Expectedly, the choice of grafting monomer is a major consideration that affect the uniformity and yield of grafting. Based on the reactivity and sensitivity of the monomer to radiation, grafting monomers can be classified either reactive or non-reactive. Reactive or radiation-sensitive monomers are those that exhibit high susceptibility to homopolymerisation due to formation of free radicals, which is in contrast compared with the non-reactive grafting monomers. Furthermore, the monomer of choice should have low viscosity to enhance monomer diffusion through the base polymer and should have low dipole strength to reduce the tendency of the monomer to form free radicals [45].

Vinyl monomers have been the most commonly employed for radiation grafting reactions wherein styrene has been the most extensively used monomer for anion-exchange membrane fabrication due to the following advantages, namely, availability due to low cost, established reaction kinetics, and the presence of a benzene ring making it highly amenable to host a variety of functionalities [59]. However the lack of stability of the styrene-functionalised membranes resulted in exploring styrene-based substitutes (Figure 1.3) that can enhance the stability of the resulting membrane [43]. Among the styrene-based monomers available, VBC has been widely used due to its versatility as a single monomer or as a starting monomer (i.e. cross-linker) for radiation-induced grafting copolymerisation.

Monomer concentration is the major governing parameter that significantly influences the outcome of the grafting process. The concentration of the monomer

in the bulk solution dictates the diffusion rate to the base polymer, hence the extent of grafting degree [45]. The unimpeded access of the monomer to the active sites ensures effective and uniform grafting, thus increasing the amount of monomer available for grafting leads to a higher degree of grafting of the resulting polymer membrane. This is observed with either simultaneous or pre-irradiation grafting schemes [44].
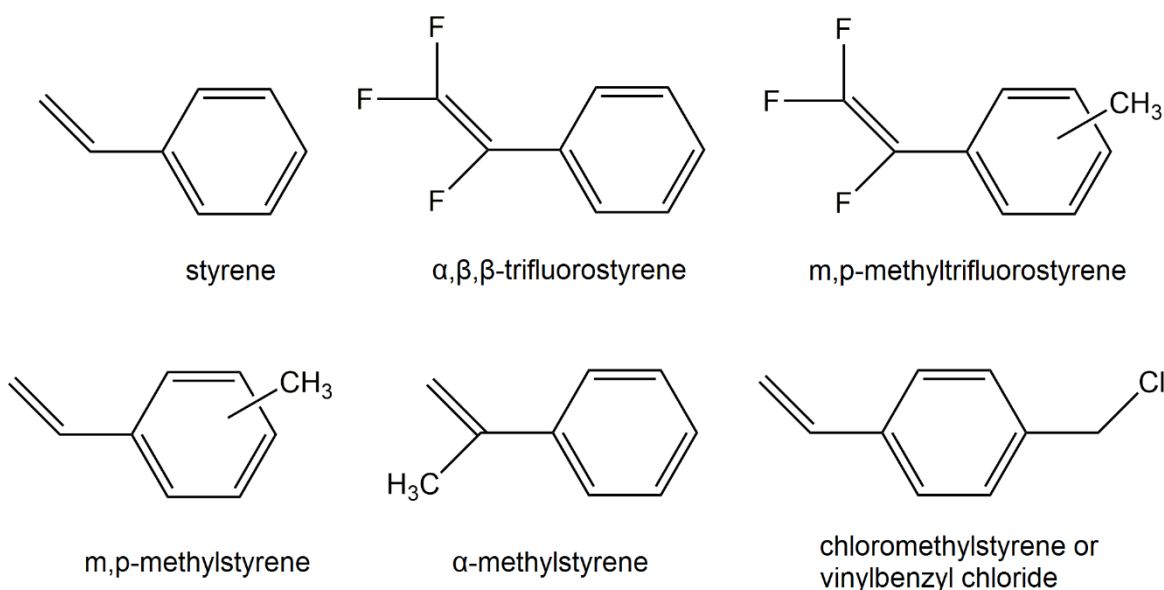


Figure 1.3. Chemical structures of some styrene and styrene-based monomers used for AEM fabrication through radiation-induced grafting [43].

## 1.6 AEM preparation by the radiation-induced grafting method

Radiation grafting is a widely used technique in industrial applications in order to improve the properties of the resulting polymer product [60] without altering their individual inherent properties [61]. In this method, active sites are formed on the polymer backbone using high energy radiation (gamma radiation, ultraviolet or electrons) and the irradiated base polymer is allowed to react with the monomer units which then propagate to form side chain grafts [62]. Radiation grafting can be performed through three different ways [40, 44]: (1) simultaneous irradiation of the polymer in the presence of the monomer, (2) irradiation of the polymer under air or oxygen atmosphere resulting in the creation of radicals along the polymer backbone which initiates polymerisation, and (3) irradiation of the polymer in an inert

atmosphere or vacuum condition wherein the monomer is subsequently added to commence polymerisation.

In fuel cell and electrolyser applications, in particular, radiation grafting is a cheaper way of producing ionomer membranes and offers a wealth of adjustable experimental parameters (e.g. radiation source, radiation dose, temperature, film thickness) thus providing a large degree of tailorability. Furthermore, the radiation grafting method offers the following advantages, namely, uniformly distributed reaction sites within the bulk of the polymer due to effective penetration of the high energy radiation, facile membrane synthesis that can be performed at room temperature and with the absence of catalysts, and the radiation grafting can be performed on polymer substrates regardless of the form and shape [63].

## 1.6.1 Ultraviolet-induced radiation grafting method

Ultraviolet (UV) radiation has been used as radiation source for anion exchange membrane, however was not popular because the UV range of radiation is not efficient in breaking sigma bonds to form radicals [64]. UV-radiation however, is less invasive compared with other radiation sources thus only penetrates a few millimetres of depth of the polymer. As expected, cross-linking by UV radiation is a slow process, and photo-initiators are usually required to induce grafting (Figure 1.4). Ketones such as benzophenone and benzyl dimethyl ketal are suitable photo-initiators for crosslinking of polyethylene [65, 66]. The process involves abstraction of the hydrogen on the polymer surface by the benzophenone photo-initiator resulting in the formation of radicals and in the presence of the monomer initiates graft polymerisation under UV radiation [67].
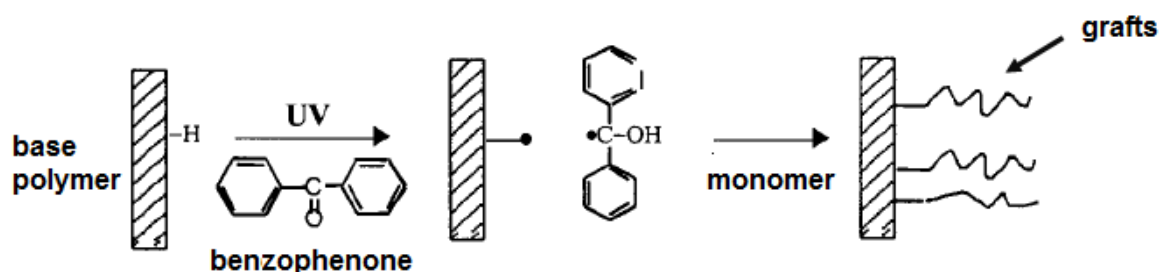


Figure 1.4 Schematic of AEM preparation by UV-radiation grafting [67].

Faraj et al. [47] successfully grafted VBC with LDPE using UV-radiation and subsequently functionalised it with 1,4-diazabicyclo[2.2.2]octane to be used as AEM for water electrolysis. The fabricated AEM exhibited an ion exchange capacity of 1.5 meq $g^{-1}$ and through-plane ionic conductivity of 10 mS $cm^{-1}$ (30°C). Choi et al. [68] reported fabrication of AEM using LDPE as base polymer and grafted with divinylbenzene (DVB) crosslinked with VBC prior to functionalisation with TMA. Another experiment of the same authors [69] again utilised a single-beam UV-radiation source setup to crosslink divinylbenzene (DVB) with polystyrene and LDPE base polymer prior to functionalisation and obtained a modest ion-exchange capacity of 1.8 meq $g^{-1}$. In order to obtain an improved AEM, this research designed an AEM fabrication setup utilising a double-beam UV-radiation source (one on each side of the polymer substrate) to produce membranes with a more uniform grafting on both side of the LDPE film due to improved penetration of UV radiation.

## 1.6.2 Gamma radiation-induced grafting method

Unlike a UV source, gamma radiation can provide stronger energy radiation and improved penetration depth to cause production of radicals in the inner part of the polymer structure without the need for initiators [70]. The reaction is completed in a fraction of a second, thus high product yields can be obtained [65]. Expectedly, preparing AEM with a high degree of grafting can be easily achieved via the gamma radiation grafting method. Among the different sources of gamma radiation available today, the most versatile is $^{60}$Co which has a long half-life of 5.3 years and is capable of emitting gamma radiation between 1.17 to 1.33 MeV [44]. The amount of exposure to gamma radiation of a given material is expressed in terms of the absorbed dose. The most widely used unit of absorbed radiation dose is Gray (Gy) which corresponds to 1 x $10^4$ erg $g^{-1}$. Similarly, the radiation dose rate is defined as the absorbed gamma radiation per unit time (Gy $min^{-1}$).

Mamlouk et al. [48, 49] and Scott et al. [71] successfully fabricated AEM by using low density (LDPE) and high density polyethylene (HDPE) as base polymer immersed in vinylbenzyl chloride (VBC) monomer solution and via simultaneous gamma radiation grafting (Figure 1.5). Kolhe and Kumar [72] also successfully grafted VBC with LDPE in the presence of 2-hydroxyethyl methacrylate (HEMA) via simultaneous irradiation using $^{60}$Co as the gamma radiation source, however key properties such as ion exchange capacity and water uptake are reportedly low.

Figure 1.5. Reaction mechanism of gamma radiation grafting of polyethylene with VBC monomer [50].

Horsfall and Lovell [73], Fang et al. [74], Herman et al. [75] and Sundell et al. [76] have utilised gamma radiation to pre-irradiate the base polymer film (i.e. LDPE, ETFE and PVDF) which was later immersed in a VBC monomer to produce graft copolymer prior to functionalisation.  Pre-irradiation method however, requires higher irradiation dose to produce a sufficient number of active sites needed for subsequent contact with the monomer to effect grafting.  As the electron beam radiation can supply a higher dose rate than $^{60}$Co source, it is widely regarded as the most effective high energy radiation source if the pre-irradiation route is desired [45].  However, this may adversely lead to degradation of the base polymer during fuel cell and water electrolyser operation [63].

## 1.7 Functionalisation of PE-g-VBC

After chloromethylation of polyethylene by grafting with vinylbenzyl chloride, the copolymer will be converted to an anion exchange membrane via amination reaction.  This is commonly done by reacting the grafted copolymer with compounds containing tertiary amine groups, the reaction of which is shown in Figure 1.6.  The compositional ratio of the ortho and the para isomers in the VBC dictates the extent of the amination reaction.  Trimethylamine reacts more readily with the para isomer compared with that of the ortho derivative which gives a sluggish reaction [77].  After

16

amination, the cationic end group is then reacted with KOH solution to produce hydroxide ion-conducting AEM.
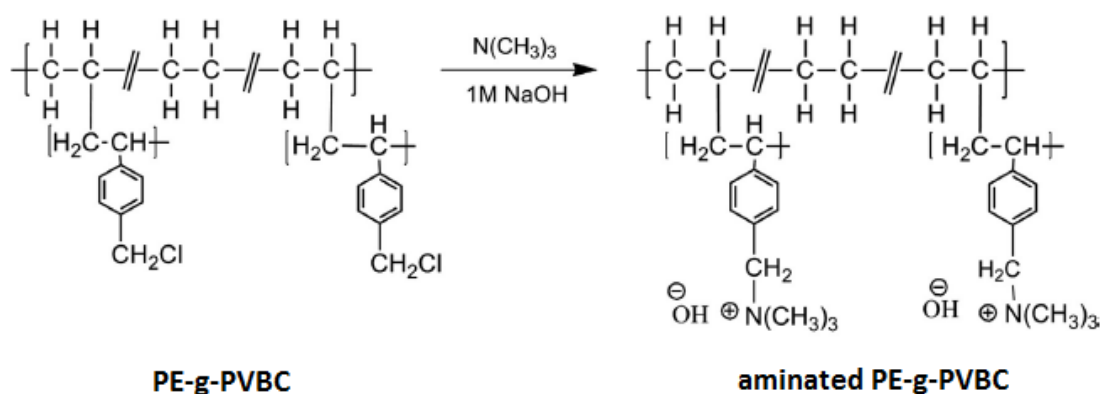


Figure 1.6.  Amination and alkalisation reactions of the VBC grafted PE [50].

## 1.8 Characterisation of alkaline anion exchange membrane

As mentioned earlier, the AEM is the heart of the fuel cell, thus its properties (i.e. physical, thermal, mechanical and structural) are of paramount importance in determining the suitability and performance of the fabricated membrane.  These properties are dependent on several factors like the nature and type of base polymer used, the type of co-polymer(s) used if any, the extent of polymerisation or grafting and the choice of grafting route.

Essentially, characterisation of AEM greatly depends on the polymer matrix properties and the nature and concentration of the cation group.  Properties of the polymer matrix dictate the mechanical, structural and thermal stability while the parameters related to the cation functional group determines the ion-exchange capacity, transport number and ionic conductivity [24].  The chemical stability of the AEM however, is influenced by the synergistic effect of both polymer matrix and the tethered functional group [24, 78].  Table 1.1 summarises the important properties that are determined for each anion exchange membrane and the corresponding technique used to measure them.

Table 1.1.  Important AEM properties and the techniques to measure them [79].

| Properties | | Technique/Equipment |
|---|---|---|
| Physico-chemical Properties | Ion-exchange capacity | Back Titration |
| | Water uptake | Gravimetry |
| | Ionic conductivity | Impedance spectroscopy |
| Thermal Properties | Melting temperature | Differential scanning calorimetry (DSC) |
| | Thermal stability | Thermal gravimetric analysis |
| Structural and Morphological Properties | Grafting distribution | X-ray microprobe analysis or EDX |
| | Degree of crystallinity | X-ray diffractometer (XRD) or DSC |
| Mechanical Properties | Tensile strength | Universal testing machine |
| | Elongation (%) | |

## 1.8.1 Degree of grafting

The measure of the extent of polymerisation is often expressed in terms of the degree of grafting (DOG).  It is defined as the percentage mass of the grafted component within the copolymer matrix [44].  It is a very important property of the anion exchange membrane since it influences the resulting properties of most of the characterisation studies performed, i.e. ion exchange capacity, swelling and water uptake, ionic conductivity and thermal stability. Needless to say, obtaining the optimum DOG will lead to the desired membrane characteristics.  Table 1.2 lists the factors that should be taken into consideration in the proper manipulation of the DOG when using the radiation-grafting route.

Table 1.2. Parameters affecting the degree of grafting of the membrane using radiation-grafting method [43, 45].

| Parameters related to the radiation source | Parameters related to the grafting mixture |
|---|---|
| <ul><li>Nature of radiation</li><li>Dose rate</li><li>Dose</li></ul> | <ul><li>Nature of monomer</li><li>Nature of base film</li><li>Monomer concentration</li><li>Addition of diluent</li><li>Addition of crosslinking agent</li><li>Reaction temperature</li><li>Addition of inhibitor</li><li>Film thickness</li></ul> |

### 1.8.2 Ion-exchange capacity

The ion-exchange capacity (IEC) is the measure of the ability of the ion-exchange membrane to allow preferential displacement of the initially attached ion on the tethered functional group by another ion present in the solution [80], hence it is a function of the number of exchange sites within a given quantity of membrane [81]. It is often expressed in millimoles of the ion-exchange groups present in a gram of the dry membrane (mmol $g^{-1}$). The IEC is determined by titration (Table 1.1) and increases as a function of the DOG [44]. The IEC however, only dictates the overall capability of the AEM to exchange anions and does not give information about the distribution profile of the ion exchange sites throughout the membrane structure [82]. This could indicate that membranes with high IEC do not necessarily translate to high ionic conductivity [63, 78]. Therefore, the uniformity of grafting across the membrane is a major consideration during membrane preparation to assure effective hydroxide ion transport from the cathode to the anode during fuel cell operation.

### 1.8.3 Water uptake and hydration number

As the functional group attached to the polymer backbone dissociates for the charged ion ($H^+$ or $OH^-$) to become mobile, the amount of water present in the membrane greatly influences the conductivity of the charged ions. Transport of mobile ions occurs via hopping from one water molecule to another (Grotthus

mechanism, Figure 1.7) thus higher membrane water content results in improved ionic conductivity. Expectedly, as the DOG is increased resulting in higher concentration of ion exchange sites, hence higher IEC, the hydrophilicity of the membrane also increases evidenced by increased water uptake [44]. The water uptake (WU) is determined by gravimetry (Table 1.1) where the mass of the wet and dry membrane are taken into account. The WU is commonly expressed in terms of hydration number ($\lambda$), which is the number of water molecules per unit of functional group [83].

### 1.8.4 Degree of swelling

Similar to the WU is the degree of swelling (DS) of the membrane which is also dependent on the water content of the membrane. The DS corresponds to the change in dimensions (expansion) of the membrane in terms of length, width and thickness as a function of water content. Though increased amount of water in the membrane increases IEC, hence increase in ionic conductivity, excessive WU leads to weaker mechanical properties and decreased structural stability of the membrane [84]. A calibrated balance between WU and ionic conductivity is therefore desired.

### 1.8.5 Mechanical testing

In both AFC and AWE, the membrane is expected to exhibit mechanical stability during operation. Tensile strength, elongation and creep are important mechanical properties that have to be taken into consideration in order to ensure long term service conditions. The polymer backbone of the AEM has the primary role of providing mechanical strength and stability which is essentially achieved by chain entanglements during radiation grafting. It is therefore of paramount importance to choose a polymer backbone composed of rigid repeating units and with relatively high molecular weight capable of chain entanglement formation during grafting [85]. Although increased WU is desired to obtain high OH$^-$ ion conductivity through the membrane, it also causes increased DS that imperils dimensional stability leading to structural defects (i.e. pinholes and crack propagation) on the membrane. The increased swelling of the membrane can also cause delamination in the catalyst layer [86]. Furthermore, membrane creep is likely to occur due to the continuous compaction experienced by the hydrated membrane under elevated working temperature and prolonged service operation [44].

Therefore a balance between the optimum WU uptake and the required mechanical properties is desired.

The tensile strength and elongation are commonly measured using a universal testing machine (UTM).  The membrane sample, both hydrated and unhydrated, are placed in between the grips and pulled apart (tensile stress) under a predetermined load.  Upon application of constant cross-head speed during the mechanical test, the stress-strain plot can be obtained.

### 1.8.6 Conductivity measurement

Ionic conductivity is a key performance property of the anion exchange membrane wherein a higher ionic conductivity will translate to better fuel cell and water electrolyser performance.  It has been an ardent challenge for AFC and AWE to deliver high ionic conductivity since $OH^-$ ions transport is inherently about 2 times slower compared with its acidic ($H_3O^+$) counterpart [63, 78].  This can be generally offset by fabricating membranes with sufficiently high IEC which is possible through the radiation grafting route.  In the molecular level, the $OH^-$ ion transport through the hydrated or humidified membrane can be explained by three transport mechanisms namely, the Grotthuss transport mechanism, diffusion or vehicular mechanism and convection mechanism [87] (Figure 1.7).  The Grotthuss mechanism or commonly called "ion hopping" mechanism is wherein, as the name implies, the $OH^-$ ions hop from one hydrolysed exchange site to another across the membrane, similar to what is observed with protons ($H_3O^+$) [88].  On the other hand, the diffusion or vehicular mechanism involves water as the vehicle of $OH^-$ ion transport driven by an electrochemical potential gradient while the convection mechanism is attributed to the electro-osmotic drag as $OH^-$ ions carried by water move through the membrane generating convective flow of water molecules [24].  Expectedly, the level of hydration, i.e. water uptake, of the membrane has a significant influence to its ionic conductivity wherein $OH^-$ ion transport happens simultaneously through these three mechanisms.  However, among the three $OH^-$ ion transport mechanisms, the Grotthuss transport route is considered to be the most dominant [89].
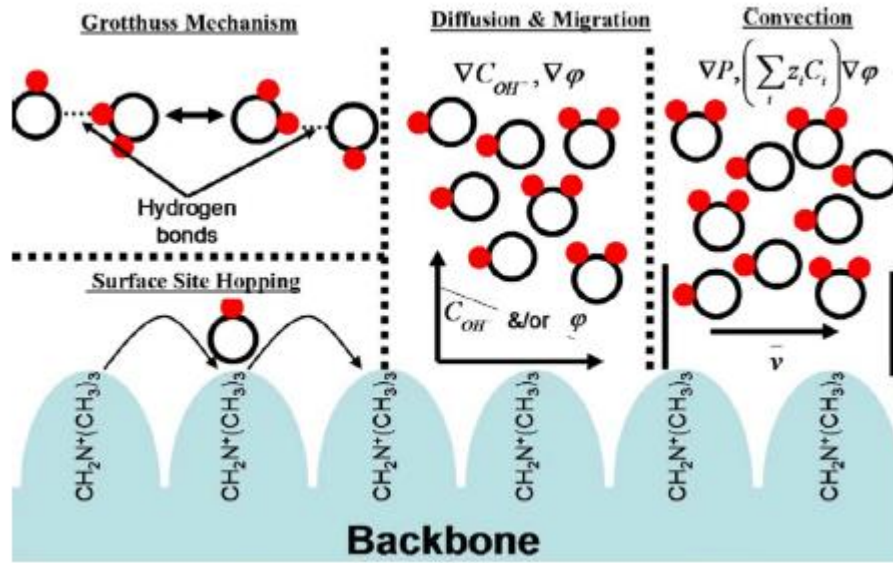
Figure 1.7. Transport mechanism for OH⁻ ions in AAEM [87].

Though the membrane ionic conductivity cannot be directly measured, it is the resistance or impedance that is experimentally determined wherein the conductivity is conversely derived. Conductivity is therefore defined as the ease with which hydroxyl ions can pass through or within the membrane and can be computed by the following formula:

$$\sigma = \frac{L}{RA} \tag{4}$$

where $\sigma$ is the conductivity, L is the membrane thickness, A is the electrode area and R is the measured resistance. Conductivity measurement can be performed in two ways, one is done within the plane of the membrane (in-plane direction) and the other is through the thickness of the membrane (through-plane direction). Although through-plane conductivity is more important for fuel cell design considerations, in-plane conductivity measurement is more easily implemented.

There are several factors that could affect the measured conductivity most influential of which is the distribution of the graft component across the membrane. Studies have also shown that in some cases, a thicker starting polymer film will yield higher conductivity after grafting and functionalisation [44]. The operating

temperature also plays a key role in determining the membrane conductivity. As the temperature is increased, the conductivity increases exponentially following an Arrhenius behaviour, thus

$$\sigma(T) = \sigma_0 \exp\left(\frac{-E_a}{kT}\right) \tag{5}$$

where $\sigma$, $\sigma_0$ and $k$ are the ionic conductivity, the pre-exponential factor and the Boltzmann constant, respectively. With respect to the effect of relative humidity (RH) to the conductivity of the membrane, higher RH gives higher conductivity. It is because at a particular temperature, the increase in RH gives higher moisture or water content that presumably lowers the viscosity within the membrane. Such decrease in viscosity with the membrane translates to higher ion mobility and conductivity [90].

### 1.8.6.1 Electrochemical impedance spectroscopy

Although resistance can be simply measured using the DC method, other phenomena like polarisation, the distribution of chemical potential and changes in the electrode reaction would greatly affect the measured resistance of the fuel cell system thus requiring a more accurate measuring equipment. Electrochemical impedance spectroscopy (EIS) is a method wherein an electrochemical system is excited by a perturbation voltage of which the effect on the frequency response of the system is analysed. Such frequency response to the applied potential is related to the electrochemical impedance of the fuel cell system. With the use of the impedance data, EIS can be routinely used as a technique of measuring conductivity and performance of fuel cell operations. The impedance (Z) is defined as the ratio of the sinusoidal voltage to the current at a particular frequency and is represented mathematically as a complex system that consists of the real (Z') and imaginary part (Z''), wherein $\theta$ is the phase angle.

$$Z' = |Z|\cos\theta \tag{6}$$

$$Z'' = |Z|\sin\theta \tag{7}$$

$$\theta = \tan^{-1}\left(\frac{Z'}{Z''}\right) \tag{8}$$

The impedance can be graphically represented in two ways, one using a rectangular coordinate form of Z' + jZ'', also known as the Nyquist plot or using the logarithm of the absolute magnitude of the total impedance |Z| versus the logarithm of the angular frequency (log ω), also known as the Bode plot [91].

### 1.8.7 Fuel cell performance

The polarisation curve is the most common method of representing the electrochemical efficiency of a fuel cell at any operating current. It is a plot which describes the magnitude of potential drop with increasing current draw brought about by the resistance to the passage of current. An excellent fuel cell has a polarisation curve which exhibits high current density and cell voltage, thus indicating high power output [92]. Figure 1.8 shows the typical polarisation curve of the fuel cell describing the prominent slopes in the plot.
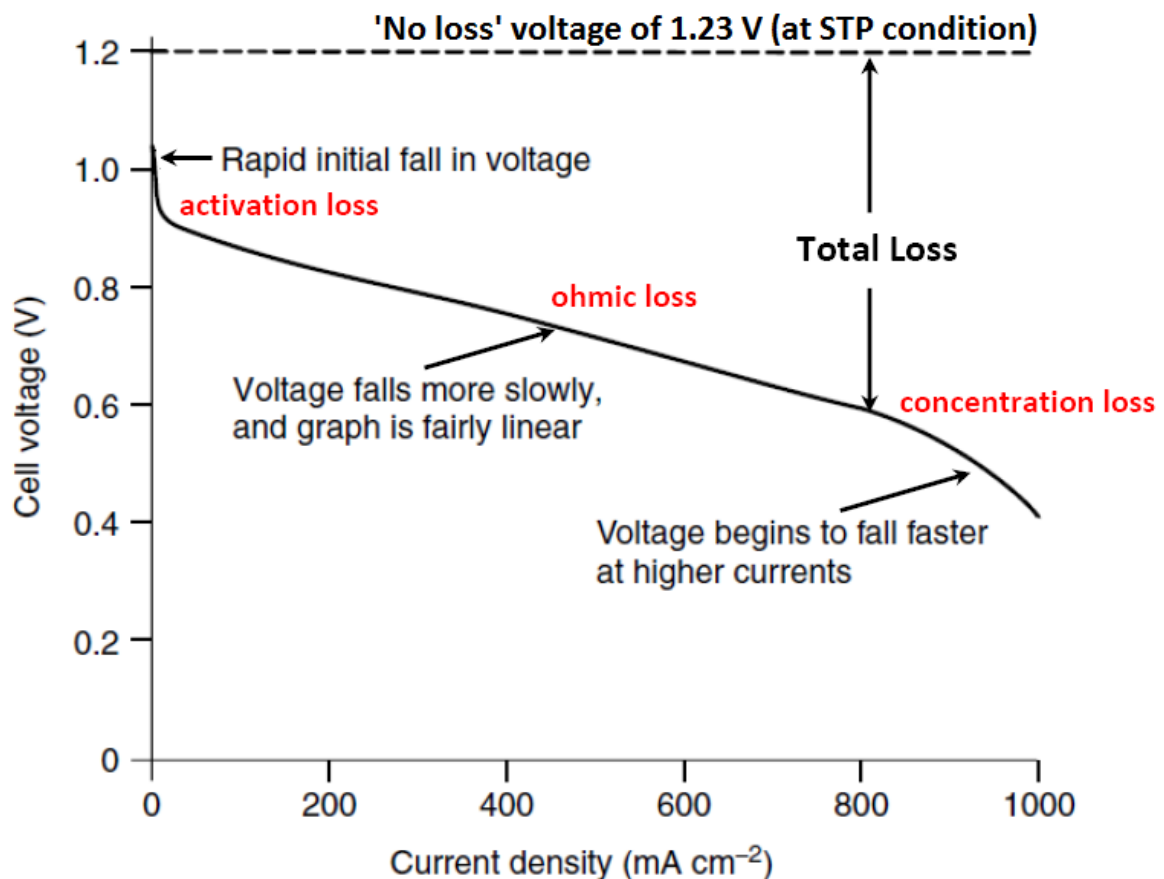


Figure 1.8. A typical polarisation curve in a fuel cell [23, 92].

From the graph, the 1.23 volts indicate the highest theoretical voltage that a fuel cell can operate.  But in reality, due to the losses within the fuel cell, this is never achieved wherein the potential is slightly lower than the theoretical voltage even with no external current generation.  Such potential corresponds to the open circuit voltage (OCV).  Once the circuit is closed or a load is applied, current starts to be produced which further contribute to the decrease in cell voltage.  Further increase in current drawn will lead to a decreasing linear slope due to resistance to the flow of electrons.  Consequently, as more current is drawn, fuel transport poses a limitation to sustain the current requirement whereupon the cell voltage quickly drops.  These phenomena are the three voltage drop regimes shown on Figure 1.8, namely, the activation loss, ohmic loss and the concentration loss.

### 1.8.7.1 Activation loss

Activation losses are primarily due to the sluggish reaction kinetics on the surface of the electrodes [93].  The initial drop in cell voltage is attributed to the loss of potential needed to drive the chemical reaction that will transfer the electrons to and from the electrode [23].  This drop is indicated as the steep slope in the initial portion of curve in Figure 1.8.  The relationship between the activation voltage and the current density is conveniently expressed in terms of the following equation [94]:

$$V_{act} = A \ln\left(\frac{i}{i_o}\right) \tag{9}$$

This equation above is also called the Tafel equation where A is the Tafel slope which is usually high if the electrochemical reaction is slow, i is the current density and $i_o$ is the exchange current density.  This equation only holds true if the current density is greater than the exchange current density.

### 1.8.7.2 Ohmic loss

As the current is increased, the steepness of the slope of the I-V curve becomes less which indicates that activation polarisation is no longer the significant factor that contributes to the potential drop.  At this point another phenomenon causes the polarisation which is the ohmic loss.  It is the polarisation due to the resistance to the flow of hydroxyl ions through the membrane in addition to

electronic resistance of bipolar plates and various fuel cell interconnections. The ohmic loss ($\eta_{ohmic}$) therefore has two contributing factors, namely, the electronic resistance ($R_{electronic}$) and the ionic resistance ($R_{ionic}$) [95]:

$$\eta_{ohmic} = \left(R_{electronic} + R_{ionic}\right) \times I \tag{10}$$

Furthermore, the ohmic resistance is strongly dependent on both the operating temperature and membrane humidity [94, 96].

### 1.8.7.3 Concentration loss

Lastly, as a larger current is drawn, more fuel needs to be delivered to the electrodes to drive electrochemical reactions resulting for a concentration gradient to occur. Consequently, a drastic potential drop is observed due to the failure to transport sufficient reactant to the electrode surface. The voltage loss due to concentration polarisation ($V_{conc}$) is computed using the formula [93]:

$$V_{conc} = \frac{RT}{nF} \ln\left(\frac{i_L}{i_L - i}\right) \tag{11}$$

where R is the gas constant, T is the operating temperature, n is the number of electrons per molecule of hydrogen, F is the Faradays constant (96,485 C mol$^{-1}$), i is the current density and $i_L$ is the limiting current density.

Alternatively, Kim et al. [97] proposed a more convenient empirical approximation of the concentration loss using the following equation:

$$V_{conc} = c \times \exp\left(\frac{i}{d}\right) \tag{12}$$

where c and d are empirical coefficients having values of 3 x 10$^{-5}$ V and 0.125 A/cm$^2$, respectively. Furthermore, the empirical coefficients are dependent on the conditions inside the fuel cell and should be determined experimentally as each fuel system is unique.

# CHAPTER 2
# METHODOLOGY

## 2.1 Materials

Low-density polyethylene (melt index of 25 g / 10 min) and linear low-density polyethylene (melt index of 1 g / 10 min) pellets were procured from Sigma-Aldrich. Commercial polyethylene films were sourced from different suppliers, namely, British Polythene Industries plc (BPI) and VWR International (VWR). Microporous ultra-high molecular weight polyethylene (UHMWPE) films, with 40% porosity, were purchased from Entek Membrane LLC (ENTEK, USA). Vinylbenzyl chloride (mixture of 3– and 4–isomers, 97%) and trimethyl amine (in 45% solution in $H_2O$) were also procured from Sigma-Aldrich. Benzophenone initiator, toluene solvent, potassium hydroxide pellets, acetone, methanol, sulphuric acid and sodium chloride were all analytical reagent grade and were used as received.

## 2.2 Anion exchange membrane preparation

### 2.2.1 Polyethylene casting

Pre-calculated amounts of low-density polyethylene (LDPE) and linear low-density polyethylene (LLDPE) were dissolved in 30 mL toluene solvent to obtain solutions of 5% by weight and 2% by weight of LDPE and LLDPE, respectively. Dissolution of polyethylene was performed by heating with agitation. After complete dissolution of polymer in hot toluene, appropriate amounts of 5% LDPE and 2% LLDPE were extracted using a syringe and were transferred to a pre-heated Petri dish placed inside a metal chamber submerged in a Grant GD120 hot water bath set to 90 °C. Toluene solvent was allowed to completely evaporate to produce the membrane films.

### 2.2.2 Heat treatment of cast polyethylene films

In order to obtain strong polyethylene films and to completely remove trapped solvent, cast membranes were subjected to heat treatment. LDPE-cast membranes were placed inside the Lenton ECF 12/30 furnace at 130 °C while the temperature setting for LLDPE-cast membranes was 150 °C. Polyethylene samples were heat-

treated for 30 min and were allowed to cool to room temperature inside the furnace. After which, polyethylene films were then peeled from the Petri dish.

## 2.2.3 Preparation of PE-g-VBC copolymer

### 2.2.3.1 UV radiation grafting route

LDPE film was cut into 12 cm x 17 cm dimension and was soaked in acetone for 5 minutes to remove surface impurities.  The polymer film was subsequently dried and the initial weight measured.  An appropriate amount of benzophenone (BP) initiator was dissolved in a small amount of THF.  The BP photoinitiator was added to the VBC monomer, pre-washed with 0.5% KOH solution to extract the inhibitor.  The LDPE film was then soaked in the VBC monomer and was left overnight under the dark cupboard.
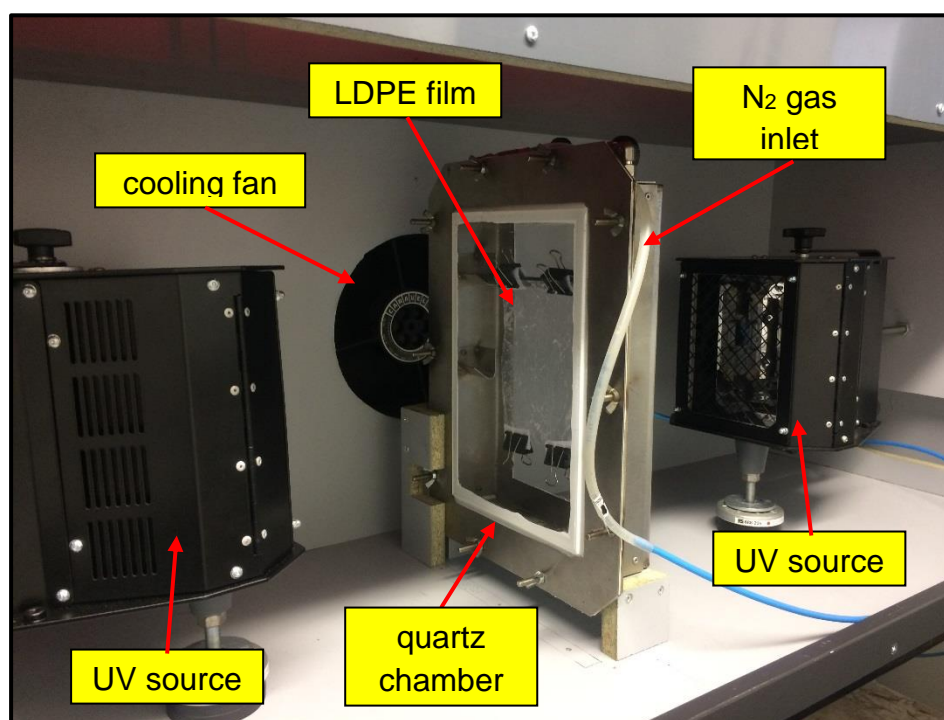


Figure 2.1.  AEM synthesis using double-beam UV radiation source.

The wet LDPE was then placed inside the sealed quartz chamber (Figure 2.1) with continuous flow of nitrogen gas.  The polymer film was subjected to UV radiation using two 400 W UV beam sources spaced 25 cm apart on both sides at varying exposure time (Figure 2.2).  After which, the grafted film was washed with

acetone to remove surface VBC homopolymers and subsequently allowed to dry. The weight of the grafted membrane was determined and the DOG was computed.

Another set of LDPE films were prepared and subjected to stepwise-radiation exposure.  After the initial exposure of the LDPE film to UV radiation, the irradiated film was immersed back in the VBC solution and was allowed to stay overnight.  The initially grafted polymer film was subjected again to UV radiation under the same exposure time.  The resulting DOG was subsequently computed.
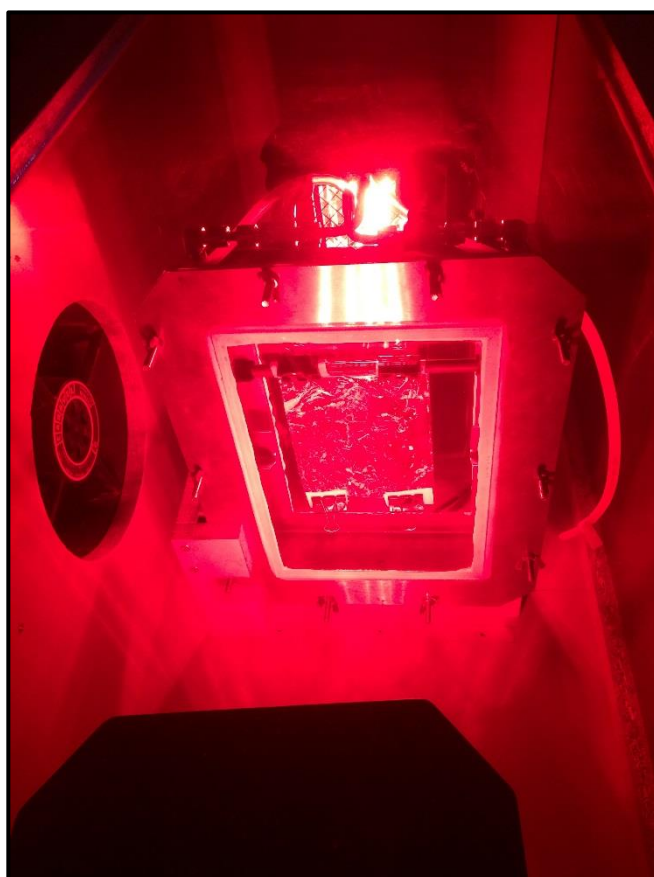


Figure 2.2 UV irradiation of LDPE film.

## 2.2.3.2 Gamma radiation grafting route

Figure 2.3 shows the schematic of the preparation of LDPE-based AAEM. Both commercially procured and as-cast polyethylene films of a constant thickness of 50 μm, were cut into 4 cm x 8 cm dimension.  The films were washed with acetone and allowed to dry.  Two samples of each polyethylene film were prepared and their initial weights were recorded.  They were then subsequently placed inside a screw-cap vial.  VBC monomer was added to each vial in the following concentration ratios: 10:36:54 and 31:26:45 by volume VBC/toluene/methanol, respectively.   Samples

were then sent to Synergy Health plc (Wiltshire, UK) for gamma radiation treatment. The samples were subjected to gamma radiation with total dose of 10 kGy and 20 kGy at dose rate of 2.0 kGy h$^{-1}$. Radiation grafted membranes were then washed with toluene, then with acetone and were subsequently ultrasonicated for 5 min. The membranes were allowed to dry and the final weights were recorded. To investigate the effect of varying the initial polyethylene thickness, another set of polyethylene films with thicknesses of 30, 50, 75 and 130 μm were prepared and were subjected to the same radiation grafting.
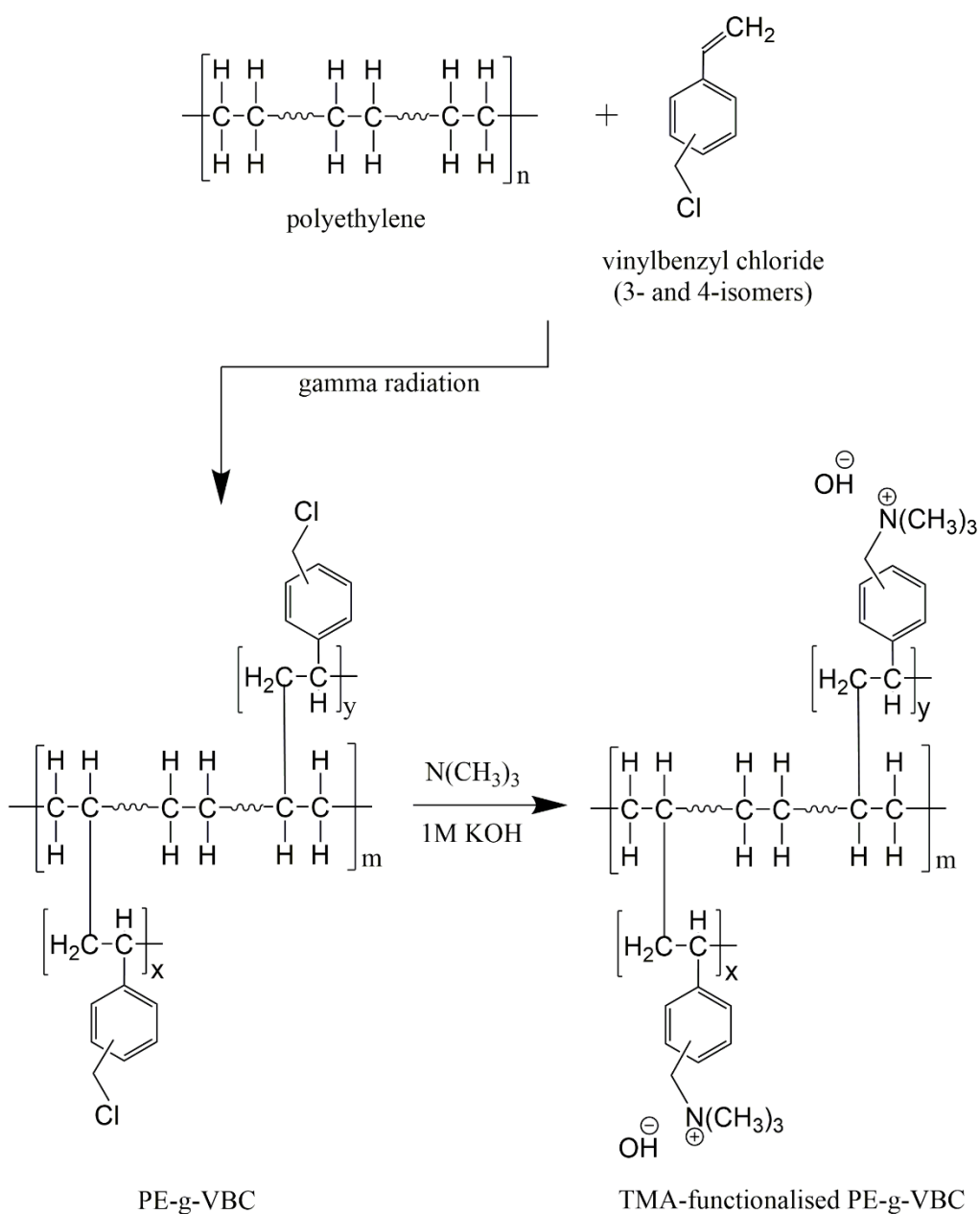


Figure 2.3. Schematic of synthesis of polyethylene based AAEM.

## 2.3 Functionalisation of the membranes

A previous study [71] revealed that, from a selection of various amines and sulfide functional groups investigated, TMA functionalised membranes offered the highest conductivity and superior fuel cell performance in comparison with other functional groups.   Therefore, TMA was used to functionalise each PE-g-VBC membrane sample (Figure 2.3) and allowed to soak for sufficient amount of time. The membranes were then washed repeatedly with deionised water.

## 2.4 Characterisation of anion exchange membranes

### 2.4.1 Degree of grafting

The degree of grafting (DOG) of the membrane was measured from the weights of the membrane before and after gamma irradiation using the following formula:

$$\text{Degree of Grafting (\%)} \ = \ \frac{W_a - W_o}{W_a} \times 100 \tag{10}$$

where $W_o$ and $W_a$ are the weights of polymer before and after irradiation, respectively.

### 2.4.2 Scanning electron microscopy (SEM)

SEM analysis of the UV-grafted membranes was performed using a JEOL JSM-5300LV machine.   The cross-section micrographs were obtained by first dipping the polymer membranes in liquid nitrogen prior to cutting in order to reveal a crisp edge side.

### 2.4.3 Fourier-transform infrared (FTIR) spectroscopy

Verification of chemical structure and presence of functional groups were performed using Varian 800 FTIR Spectrometer at scan range of 3800 to 600 cm$^{-1}$ equipped with Pike Technologies diamond crystal plate Attenuated Total Reflectance (ATR) unit.   Samples of original polyethylene, VBC-grafted polyethylene and TMA-functionalised PE-g-VBC were subjected to analysis.

### 2.4.4 Measurement of ion exchange capacity

The ion exchange capacity (IEC) of each membrane was measured using acid-base titration. Membranes were treated with fresh 1.0 M KOH solution every 20 min for three times (total OH⁻ exchange time of 1 h) to completely exchange the chloride ions with hydroxide ions. The membrane was then washed with copious amount of deionised water to remove residual hydroxide ions. Removal of excess OH⁻ ions was confirmed by using pH paper. The membrane was subsequently immersed in a known volume of 1.0 M NaCl solution and was let to stand overnight. The liberated hydroxide ions were then titrated with 0.05 M $H_2SO_4$ solution using Brand GMBH Titrette bottle-top burette and the endpoint was determined visually using methyl red indicator. The membrane was thoroughly washed with deionised water to remove excess salt and was allowed to dry. The IEC was computed using the amount of OH⁻ ions neutralised, expressed in mmol divided by the dry weight of the membrane, in grams. The measured IEC was then compared with the theoretical IEC, computed as shown in equation below which assumes complete amination, ion-exchange and full removal of water upon drying.

$$\text{IEC}_{theo} \text{ (mmol g}^{-1}) = \frac{1000 \times \frac{\left(W_{LDPE-g-VBC} - W_{LDPE}\right)}{MW_{VBC}}}{W_{LDPE-g-VBC} + \left[\frac{\left(W_{LDPE-g-VBC} - W_{LDPE}\right)}{MW_{VBC}} \times MW_{TMA}\right]} \tag{11}$$

where $W_{LDPE-g-VBC}$ and $W_{LDPE}$ are the weights of the grafted membrane and initial LDPE respectively; and $MW_{VBC}$ and $MW_{TMA}$ are molecular weights of VBC and TMA, respectively.

### 2.4.5 Water uptake, hydration number and swelling measurement

Water uptake (WU) was determined from the difference in weights between the hydrated and the dried polymer membrane. OH⁻ exchanged membranes were immersed in deionised water at room temperature. After 48 h, wet membranes were collected and pat dried with tissue paper to remove surface water. The thickness, dimensions and weight of the hydrated membrane were subsequently measured. To obtain the weight of the dry membrane, the hydrated membranes were oven-

dried at 60 °C and weighed repeatedly until constant weight and dimensions were obtained. The WU, in terms of wt%, was computed as follows:

$$WU \ (wt \ \%) \ = \ \frac{W_{wet} - W_{dry}}{W_{dry}} \times 100 \tag{12}$$

where $W_{wet}$ and $W_{dry}$ were the wet and dry weights of the membrane, respectively. Consequently, the volumetric WU was determined taking into consideration the density of the polymer and with the assumption that the total volume is simply the sum of volume of the water phase and the polymer phase of the swollen membrane (Equation 13) [98]

$$WU \ (vol \ \%) \ = \ \frac{\dfrac{(W_{wet} - W_{dry})}{\rho_{water}}}{\dfrac{(W_{wet} - W_{dry})}{\rho_{water}} + \dfrac{W_{dry}}{\rho_{polymer}}} \times 100 \tag{13}$$

where $\rho_{water}$ and $\rho_{polymer}$ are the densities of water (1 g cm$^{-3}$) and the grafted and functionalised polymer (0.95 g cm$^{-3}$), respectively.

The hydration number ($\lambda$), which is the number of water molecules per trimethyl amine group, was calculated using the IEC and the gravimetric WU data as shown below:

$$\lambda \ = \ \frac{WU \ (wt\%) \times 10}{MW_{water} \times IEC} \tag{14}$$

where $MW_{water}$ is the molecular weight of water, 18.01 g mol$^{-1}$.

The degree of swelling (DS) was measured as the average of swelling in width, in length and in thickness, of the membrane before and after drying, as shown below:

$$DS \ (\%) \ = \ \frac{D_{wet} - D_{dry}}{D_{dry}} \times 100 \tag{15}$$

where $D_{wet}$, is the dimension, of the wet membrane in a given direction (width (x-axis), length (y-axis) or thickness (z-axis)) and $D_{dry}$, is the corresponding dimension of the dry membrane in a given direction.

### 2.4.6 Mechanical testing

Tensile testing of the LDPE base film, dry AEM and fully hydrated AEM of different DOG was performed. A fully hydrated Nafion 212 film was also tested for comparison. To prepare fully hydrated AEMs, membranes were soaked in deionised water for at least 48 hours prior to tensile testing. A Shimadzu Autograph AGS-X Universal Testing Machine was employed to obtain the stress-strain plot applying a constant crosshead speed of 2 mm min$^{-1}$ for all the test specimens.

### 2.4.7 Conductivity measurement

Grafted membranes were OH$^-$ exchanged using 1.0 M KOH solution for initial 20 min. The solution was then replaced with fresh 1.0 M KOH solution and was allowed to exchange for another 20 min. The process was repeated until a total OH$^-$ exchange time of 1 h was achieved. After which, the membranes were thoroughly washed with deionised water. Removal of excess OH$^-$ ions was confirmed by using pH paper. Initial thickness of the membrane was measured using a Mitutuyo No. 293-240 micrometre calliper. Each membrane was then sandwiched in between two Freudenberg FCCT H2315-C2 gas diffusion layer carbon electrodes and was placed in a gold-plated titanium test cell. The environment inside the test cell was maintained at atmospheric pressure and the humidifier temperature was set to ensure 100% relative humidity inside the cell. The relative humidity inside the fuel cell was verified using a Vaisala HUMICAP humidity sensor. The through-plane conductivity was measured using a four-point technique with one probe placed on either side of the membrane. The impedance was measured using an N4L NumetriQ PSM 1735 Frequency Response Analyser within the frequency range of 200 kHz to 20 kHz with a perturbation voltage amplitude of 15 mV (Figure 2.4). Three readings of the impedance in 5 min intervals were made and the average was reported. Consequently, the conductivity of the membrane was computed based on the following formula [14]:

$$\sigma = \frac{4L}{R(\pi d^2)} \tag{16}$$

where σ is the hydroxyl ion conductivity, L is the membrane thickness, R is the resistance derived from the impedance value at zero-phase angle and d is the diameter of the membrane test area.
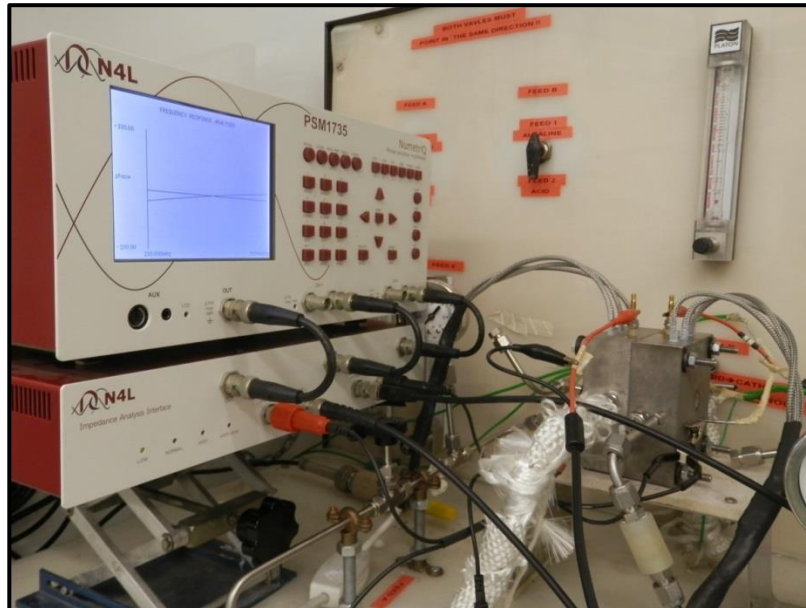


Figure 2.4.  AEM conductivity measurement setup.

### 2.4.8 Fuel cell performance test

Fuel cell electrodes made from catalyst inks were used for testing as previously prepared [13, 48].  A titanium-made hydrogen fuel cell, with a 1 cm$^2$ gold-coated serpentine flow field was used. Each membrane was OH$^-$ exchanged using the same alkaline treatment.   The polarisation curve of each anion exchange membrane was obtained using an Autolab PGSTAT302 Potentiostat with a scan rate of 2 mV s$^{-1}$.  The test cell was subjected to several cycle runs until stable performance was obtained at hydrogen and oxygen stoichiometry of 1.2 and air of 2.2.

# CHAPTER 3
# RESULTS AND DISCUSSION

## 3.1 Polyethylene film casting

One of the parameters investigated in this research is to study the influence of the variability in polyethylene films supply source onto the fabricated polyethylene-based AAEM. This is because batches of commercial polyethylene films could differ in properties like molecular weight, melting and glass transition temperature, melt index and the type and content of additives. Several trials have been performed to obtain a working procedure of casting polyethylene films into desired concentration, thickness and consistency. Different types of polyethylene were subjected to trials, namely, low density polyethylene (LDPE), linear low density polyethylene (LLDPE), medium density polyethylene (MDPE) and ultrahigh molecular weight polyethylene (UHMWPE). Toluene was used as the non-polar solvent suitable for polyethylene. Unfortunately, polyethylene is not soluble in toluene at room temperature, thus requires heating by a heat gun.

Of the different types of polyethylene used, only LDPE and LLDPE were successfully cast. Due to limited solubility of polyethylene in hot toluene, the highest concentrations that can be produced are 5% and 2% by weight for LDPE and LLDPE, respectively. On the other hand, MDPE was brittle and shrank upon heat treatment while UHMWPE was found to be quite difficult to be dissolved in hot toluene solvent in a manageable concentration.

Finding the suitable casting technique was also found to be difficult. It was found out that LDPE transforms from its liquid phase to its solid, swollen state at around 60ºC. The rate of solvent evaporation below this temperature will be high, therefore producing a cracked LDPE cast. The optimum casting temperature should be higher than 60ºC to produce a smooth and consistent LDPE film. Unlike that of LDPE, the phase transformation temperature for LLDPE was higher at 91ºC.

The influence of pressure on the production of the polyethylene films was also investigated. Initial casting runs were made inside a metal chamber pressurised at about 2 bars. The pressurised metal chamber was subjected both to room temperature and elevated temperature. Placing the polyethylene solution under pressure drastically decreased the evaporation rate of the solvent thus required venting from time to time. No polyethylene film was successfully cast under

pressurised environment.  Table A.1 (Appendix A) shows the different sample runs performed with varying parameter conditions.  Table 3.1 on the other hand, summarises the best procedure of polyethylene casting so far been developed.

Table 3.1. Summary of optimum polyethylene casting procedure.

| Polymer | Concentration | Casting Procedure |
|---|---|---|
| Low density polyethylene (LDPE) | 5% by weight | 1. Place 1.3737g LDPE in 30 ml toluene then dissolve with heating.<br>2. Syringe 6 mL of 5% LDPE on Petri dish<br>3. Cast in a metal chamber submerged in 91ºC hot water bath for 25 min.<br>4. Heat treatment at 125ºC for 30 minutes then allow to cool to room temperature inside the furnace. |
| Linear low density polyethylene (LLDPE) | 2% by weight | 1. Place 0.5326g LLDPE in 30 ml toluene then dissolve with heating.<br>2. Syringe 12 mL of 2% LLDPE on Petri dish<br>3. Cast in a metal chamber submerged in 91ºC hot water bath for 120 minutes.<br>4. Heat treatment at 150ºC for 30 minutes then allow to cool to room temperature inside the furnace. |

## 3.2 UV radiation grafting of polyethylene films

An attempt to fabricate AEM utilising UV radiation is hereby reported.  The polymer film initially soaked in VBC monomer with BP photoinitiator was placed in between two UV radiation lamps to effect grafting.  This is envisioned to provide more uniform grafting through the polymer structure due to improved radiation penetration on both sides of the base polymer film compared with using only one radiation source.

The initial attempt was 30 min irradiation time where the grafting of LDPE with VBC was low with only 6.29% DOG.  The low DOG can be attributed to the VBC monomer not sticking on the LDPE surface even with overnight immersion and probably due to the vertical position of the LDPE film during UV irradiation rather

than lying flat.  The surface grafting appeared to be rough (Figure 3.1a), and the SEM image of the cross-section revealed very thin grafting as the bulk of the LDPE film remains unreacted (Figure 3.1b).  When the grafted polymer was removed from the quartz chamber, the polymer turn yellowish indicating oxidation of VBC on the surface of LDPE.  This suggests VBC monomer on the surface remains unreacted, hence another preparation trial was made with prolonged UV exposure time.
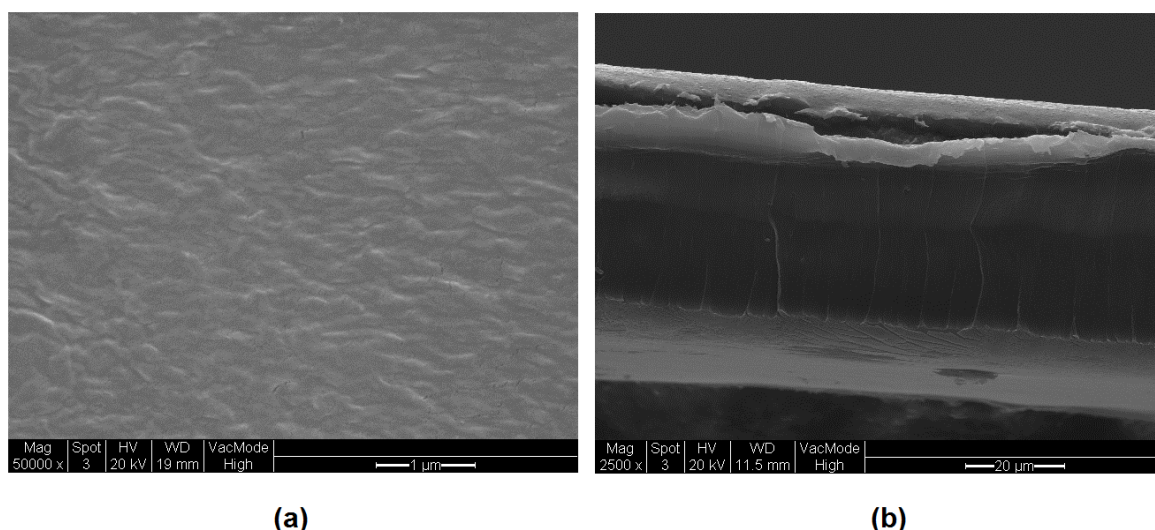


Figure 3.1 SEM micrograph of the (a) surface at 50000x and (b) cross-section at 2500x of UV-grafted LDPE-g-VBC.

A subsequent test was performed with increased irradiation time to 45 min. Though the DOG slightly improved from 6.29% to 11.27% from 30 to 45 min irradiation time, the grafting was still not uniform and also patchy due to dripping of the VBC monomer during irradiation.  Measurement of the through plane ionic conductivity revealed very low conductivity not useful for fuel cell application.

To address the issue of dripping VBC monomer from the polymer surface, the monomer-wet LDPE base film was sandwiched between two quartz glass plates and sealed with cellotape before placing it inside the quartz chamber.  Placing the polymer film in between two quartz glass plates provides some advantage namely, the grafting was smooth and homogenous, and the base film had complete contact with the VBC since the evaporation of the monomer was impeded (Figure 3.2). However, placing the LDPE film between two quartz glass plates limits the amount

of VBC monomer that can be spread onto the surface of the polymer and also limits the movement (i.e. expansion) of the copolymer during UV grafting.



(a)    (b)
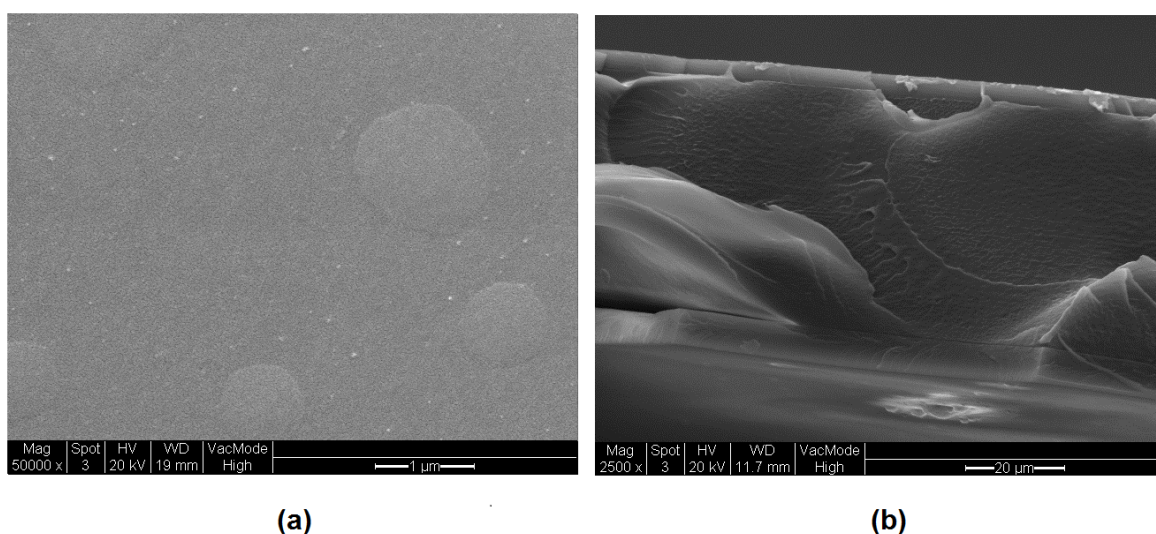
Figure 3.2 SEM micrograph of the (a) surface at 50000x and (b) cross-section at 2500x of UV-grafted LDPE-g-VBC sandwiched between quartz glass plates.

The DOG significantly improved to 30.11% at 45 min irradiation time evinced by the thicker LDPE–VBC grafts on both sides of the LDPE film (Figure 3.2b). Though 30.11% is a modest DOG value, through-plane ionic conductivity of the membrane remained very poor as the bulk of the LDPE film in the middle remains unreacted. Even with prolonged exposure to UV, the grafted LDPE film still turned yellowish after removal from the chamber suggesting the presence of unreacted VBC-radicals on the surface that consequently reacted with the surrounding air. This could indicate limited penetration of UV radiation even with prolonged exposure to radiation and cannot be solely attributed to excess VBC monomer on the LDPE surface.

In order to obtain AEM with higher DOG, step-wise UV irradiation was realised. In this way, initially UV-irradiated films were re-immersed into the VBC-BP solution overnight and subjected again to UV radiation. Figure 3.3 shows the surface and cross-section of LDPE-g-VBC subjected to 2 UV radiation treatments. The bulk of the surface appears to be saturated with the VBC monomer and was not uniformly distributed (Figure 3.3a) while the cross-section shows an inner layer of LDPE-g-VBC but the subsequent exposure to UV radiation only produced VBC

homopolymers on both the outermost layer of the copolymer (Figure 3.3b). The added layers are probably responsible to the significant increase of the resulting DOG to 45.40%. However, high DOG does not necessarily reflect to increased ionic conductivity. There is still a significant layer of LDPE film in the middle which remained unreacted, expectedly resulting in a very low through plane ionic conductivity.



(a)                                                          (b)
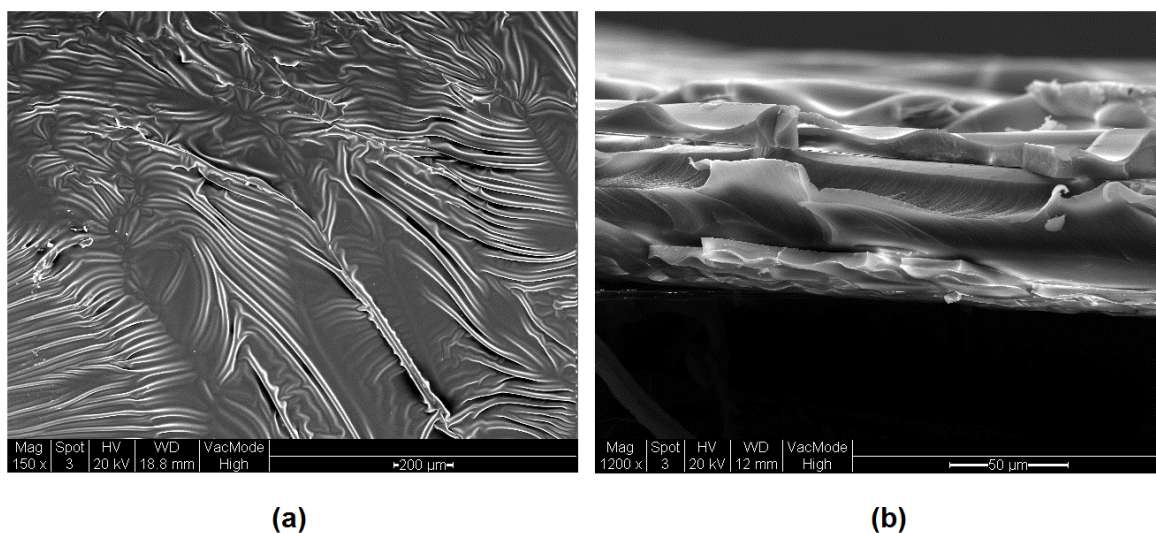
Figure 3.3 SEM micrograph of the (a) surface at 150x and (b) cross-section at 1200x of LDPE-g-VBC subjected to consecutive UV radiation treatments.

Lastly, in order to obtain a copolymer with uniform surface grafting, the wet LDPE film was sandwiched between two quartz glass plates before placing inside the quartz chamber prior to 2 UV radiation treatments. The resulting graft copolymer showed a smooth and uniform surface (Figure 3.4a), however, was still unsuccessful in obtaining a completely grafted copolymer throughout the base film structure. While the initial exposure to UV radiation resulted in formation of LDPE-g-VBC (inner layer), the subsequent UV exposure only resulted in the formation of VBC homopolymers on the surface of the initial LDPE-g-VBC (Figure 3.4b). There was still a thick LDPE film that remained in the middle. The several preparation trials under UV radiation confirmed its limited penetration capability (i.e. UV radiation source should be higher than 400 W power output). Therefore, the use of a higher radiation source was necessary to produce membranes with improved grafting uniformity.

<div align="center">(a)          (b)</div>
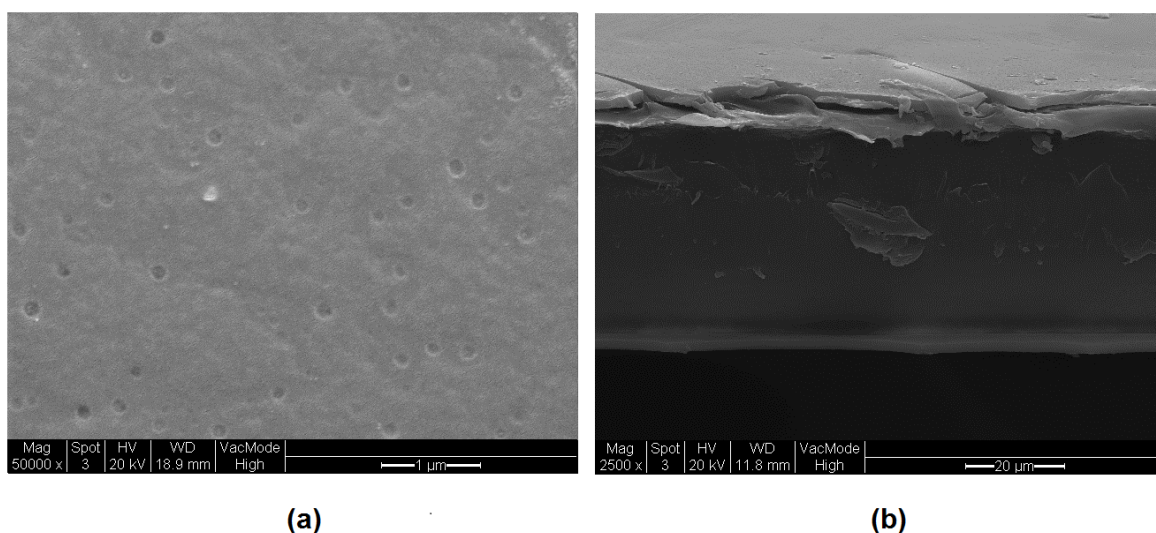
Figure 3.4 SEM micrograph of the (a) surface at 50000x and (b) cross-section at 2500x of UV-grafted LDPE-g-VBC sandwiched between quartz glass plates and subjected to consecutive UV radiation treatments.

## 3.3 Gamma radiation grafting of polyethylene films

The polyethylene films were placed in a vial and added with 10:36:54 and 31:26:43 by volume VBC/toluene/methanol solution adapting the procedure of Horsfall and Lovell [99] and Cheng et al. [52], with modifications. The toluene served as the solvent for the VBC while methanol was used to swell the LDPE film so that that VBC monomer can more effectively penetrate the LDPE structure. They were then subjected to gamma radiation of 10 kGy and 20 kGy total dose. The results are shown in Table 3.2. Both the as-cast and commercial LDPE-based membranes grafted poorly at low VBC concentration and low gamma radiation dose (Appendix B). Increasing the concentration of the VBC monomer produced a marked increase in the degree of grafting (DOG). The BPI-polyethylene based membrane, in particular, showed the highest percentage increase in DOG from 16.3% to 74.6% both subjected to 20 kGy radiation dose. This is due to the presence of more monomer available (higher concentration) for grafting to the polymer backbone. It can be also observed that an increase in the total gamma radiation dose results in an increase in the DOG of the membranes. This is due to the fact that more high energy radiation is supplied to cause the formation of active sites for the VBC monomer to tether to the polyethylene backbone.

Table 3.2. Degree of grafting for polyethylene membranes subjected to different VBC monomer concentration and gamma radiation dose.

| Polyethylene | | Approximate Degree of Grafting (DOG) based on single measurement, % | | | |
| | | 10:36:54 by volume VBC/toluene/methanol | | 31:26:43 by volume VBC/toluene/methanol | |
| Type | Source | 10 kGy | 20 kGy | 10 kGy | 20 kGy |
| --- | --- | --- | --- | --- | --- |
| LDPE | BPI | 4 | 16 | 50 | 75 |
| LDPE | VWR | 6 | 13 | 48 | 71 |
| Cast-LDPE | Sigma-Aldrich | 7 | 22 | 53 | 70 |
| Cast-LLDPE | Sigma-Aldrich | 1 | 13 | 49 | 71 |
| UHMWPE | ENTEK | 21 | 46 | 57 | 84 |

The ENTEK UHMWPE porous membrane showed the highest DOG for all VBC concentrations and gamma radiation doses as compared with all of the other studied non-porous PE membranes. The ENTEK UHMWPE exhibited a four-fold increase in DOG from 21.0% at low VBC concentration and low gamma radiation dose to 83.9% DOG at both high VBC concentration and gamma radiation dose. At low VBC concentration and low radiation dose, the ENTEK-based membrane showed three-fold higher DOG in comparison with any of the other studied membranes. This is because even at low VBC concentration, the monomer can still easily penetrate within the porous structure of the ENTEK base polymer with high mass transport rate in comparison with the non-porous films. Unfortunately, while the grafting resulted in a decrease in the porosity from the original 40%, the ENTEK-based membrane remained porous (>5%) after grafting with very high rate of hydrogen cross-over rendering it not suitable for fuel cell applications. When the concentration of the monomer was increased, the mass transport of the VBC monomer through the LDPE film became no longer a limiting factor and the observed DOG became similar to the other non-porous LDPE-based membranes.

In the case of cast-PE membranes, both the cast-LDPE and cast-LLDPE showed almost the same high value of DOG at both high VBC concentration and gamma radiation dose. At low VBC concentration however, cast-LDPE showed

higher DOG than cast-LLDPE.  This is attributed to the difference in the polymer architecture between LDPE and LLDPE.  Due to the absence of long chain branching in LLDPE, fewer sites are available for monomer attachment, requiring higher energies and resulting in a lower DOG. Radiation grafting favours a more branched structure wherein more sites for grafting are present compared with just a fixed long chain.  However, with the increase in VBC concentration and radiation dose, the difference in DOG became negligible between the two structures.

The use of low-density polyethylene films from different sources showed no effect on the observed DOG at both high VBC concentration and gamma radiation dose.  Even at low monomer concentrations, similar structure LDPE-based membranes showed very minimal variation in the observed DOG.  This indicates that varying the PE supplier source has minimal effect on the PE grafting.

## 3.4 Characterisation of the membranes by FTIR Analysis

The chemical structures of polyethylene, PE-g-VBC and functionalised PE-g-VBC were analysed by FTIR analysis, as shown in Figure 3.5.  The polyethylene spectra (i), being predominantly composed of methylene groups, is characterised by the presence of methylene stretches and bends.  The spectra revealed four sharp peaks, namely the $-CH_2$ asymmetric stretching at 2916 $cm^{-1}$ (■) and symmetry stretching at 2849 $cm^{-1}$ (*) and $-CH_2$ deformation (stretching and bending) at 1463 $cm^{-1}$ (●) and 719 $cm^{-1}$ (□)  [100].  Comparison between the non-irradiated and the irradiated polyethylene film as shown in (ii) revealed presence of only the same dominant bands indicating that no structural damage to the polymer backbone was observed after gamma irradiation [101].  This is because the radiation dose of 20 kGy was not high enough to cause significant damage to the polyethylene structure [102, 103].
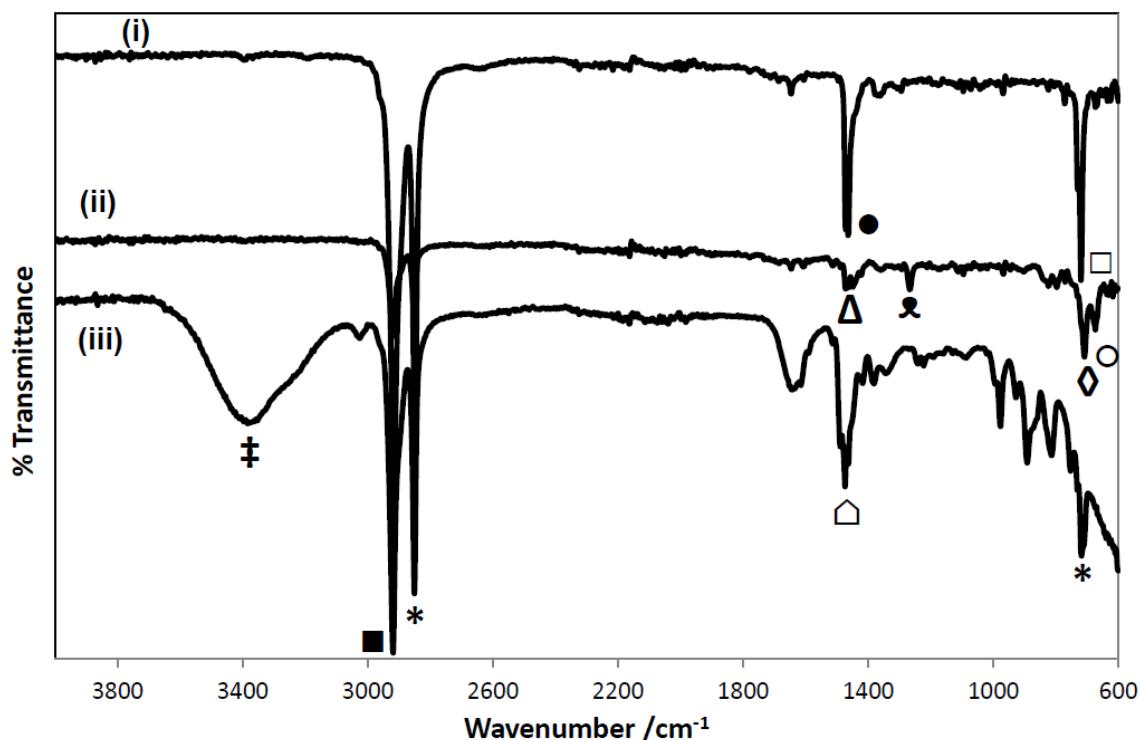
Figure 3.5. FTIR spectra of (i) original polyethylene, (ii) VWR-based PE-g-VBC and (iii) functionalised PE-g-VBC.

The VBC-grafted polyethylene (ii) showed additional peaks attributed to the presence of chlorobenzyl functional groups. The stretching of C=C aromatic double bonds was observed at peaks between 1400 cm$^{-1}$ to 1600 cm$^{-1}$ ($\triangle$). Bands observed at 823, 796 and 708 cm$^{-1}$ ($\lozenge$) were consistent with the meta and/or para benzene ring substitution of the VBC. Furthermore, the C–Cl stretching was observed at 673 cm$^{-1}$ ($\circ$) and CH$_2$–Cl wagging band at 1266 cm$^{-1}$ ($\mathbf{\star}$) [104].

The spectra of TMA-functionalised PE-g-VBC (iii) exhibited additional peaks, particularly at 3377 cm$^{-1}$ ($\ddagger$) which can be attributed to –OH stretching from the residual water present in the membrane. The band at 1474 cm$^{-1}$ ($\triangle$) can be attributed to symmetric N–CH$_3$ deformation. Also, it can be observed that the CH$_2$–Cl wagging band and the C–Cl stretching peak both observed in (ii) were no longer present, confirming the release of Cl$^-$ and bonding with N$^+$ upon successful quaternisation [47].

### 3.5 IEC, membrane swelling and WU

Representative samples of grafted membranes were subjected to IEC measurement, by measuring the amount of $OH^-$ ions released by exchanging it with $Cl^-$ ions employing acid-base titration. IEC is the measure of the number of functional groups available for $OH^-$ ion exchange per weight of dry membrane.

Table 3.3 shows the computed IEC in relation to the corresponding DOG for the prepared membrane from different polymer sources. The IEC increased with increasing DOG, as more functional groups were attached to the polymer backbone and more sites available for $OH^-$ ion exchange.

Table 3.3. IEC of membranes with different polyethylene sources with the same initial thickness of 50 μm.

| Polyethylene | | DOG (%) | IEC (mmol g$^{-1}$) |
|---|---|---|---|
| Type | Source | | |
| UHMWPE | ENTEK | 46 | 2.0 |
| | | 57 | 2.5 |
| LDPE | VWR | 52 | 2.3 |
| | | 71 | 3.0 |
| Cast-LLDPE | Sigma-Aldrich | 71 | 2.9 |
| LDPE | BPI | 50 | 2.4 |
| | | 75 | 3.2 |

Table 3.4 shows the effect of increasing the initial polyethylene thickness on the IEC and DOG of the produced membrane. The use of varying initial thickness of polyethylene film showed no effect on the resulting IEC of 2.7 mmol g$^{-1}$ for a given value of DOG. This is because as shown in the previous section, the use of high VBC concentration enhanced monomer mass transport through LDPE film even at high dose rate of 20 kGy thereby the influence of varying the thickness was not observed. Furthermore, based on the results, the thinnest membrane will be the most desirable due to better water transport and lower resistance. However, this

will come at the cost of increase in the gas cross-over ($H_2$).

The measured IEC (Table 3.4) is lower than the estimated theoretical value from the DOG values due to the following reasons: incomplete amination of the LDPE-g-VBC copolymer, limitation of accessing all the functional sites and incomplete ion exchange between $OH^-$ and $Cl^-$. The calculated value of hydration number ($\lambda$) is also high of 52 (IEC 2.7 mmol $g^{-1}$). This is around double that of fully hydrated Nafion and mainly caused by the high IEC. The IEC of most of the prepared membranes in Table 3.4 are ca. 3 times higher than that of Nafion 117 (0.91 mmol $g^{-1}$). This high IEC and consequently high $\lambda$ is required to achieve high $OH^-$ ionic conductivities in the order of 0.1 S $cm^{-1}$. Conductivity of ions is a function of both the ion mobility and the concentration of charge carriers. The ratio of the ion mobility in dilute solution of that of $H^+$ to $OH^-$ is around 1.77 [29]. Which means that to achieve similar $H^+$ ionic conductivity in Nafion, AEM should have IEC ca. double that of Nafion to balance the slow diffusion of hydrated $OH^-$ in comparison with that of the hydrated $H^+$. Moreover, Nafion binds water more strongly than the relatively weak base in AEM, the absorbed water is less bound within the AEM polymer structure because there are not as many ion pairs dissociated [105] and higher IEC is required to stop AEM from dehydration at temperatures above 60°C. An IEC over 2 mmol $g^{-1}$ is required for AEM to achieve similar effective water self-diffusion coefficients in Nafion of $10^{-9}$ $m^2$ $s^{-1}$ at 25 °C [105]. However excessive water uptake will lead to excessive swelling leading to dimensional deformation and structural instability of the membrane. Therefore, a good balance between IEC and WU is desired.

Similar with $\lambda$, the water uptake, WU, is also a measure of the amount of water in the membrane in terms of wt% or vol% which results in membrane swelling DS%. Consequently, high DOG, hence high IEC, will lead to high WU and high DS. Since all membranes regardless of initial polyethylene thickness showed essentially constant IEC and DOG at the same grafting conditions (Table 3.4), expectedly the membranes exhibited the same high value of WU around 255 wt% (IEC 2.7 mmol $g^{-1}$). While an initial look at this value suggests significantly higher number than Nafion WU ca. 30 wt% (Table 3.5), WU based on wt% has its limitations due to its failure to consider the density of the polymer (Nafion of ca. 2 g $cm^{-3}$ [106] in comparison with LDPE-VBC-TMA of ca. 0.95 g $cm^{-3}$). A more relevant comparison

Table 3.4. DOG, IEC, WU, λ, and swelling of membranes with increasing initial LDPE thickness measured at room temperature.

| Initial polyethylene film thickness (μm) | Membrane thickness after grafting (μm) | DOG (%) | $IEC_{theo}$ (mmol g$^{-1}$) | Measured IEC (mmol g$^{-1}$) | WU (wt %) | WU (vol %) | λ | Membrane Swelling | | | |
|---|---|---|---|---|---|---|---|---|---|---|---|
| | | | | | | | | $DS_z$ (%) | $DS_x$ (%) | $DS_y$ (%) | Average (%) |
| 30 | 49 | 67.5 | 3.5 | 2.7 | 255 | 70.8 | 52.4 | 57.9 | 41.5 | 60.3 | 53.2 |
| 50 | 63 | 32.0 | 1.9 | 1.4 | 130 | 54.8 | 53.5 | 30.2 | 20.8 | 17.9 | 23.0 |
| 50 | 75 | 65.4 | 3.4 | 2.7 | 253 | 70.6 | 52.0 | 53.9 | 52.5 | 36.9 | 47.8 |
| 50 | 95 | 74.6 | 3.8 | 3.2 | 285 | 73.1 | 49.5 | 58.9 | 57.1 | 50.7 | 55.6 |
| 75 | 96 | 65.6 | 3.4 | 2.7 | 254 | 70.7 | 52.2 | 49.6 | 34.6 | 32.3 | 38.8 |
| 130 | 169 | 59.9 | 3.2 | 2.7 | 259 | 71.0 | 53.3 | 51.1 | 43.1 | 38.9 | 44.4 |

is to look at the WU in vol% [107].  The WU vol% for AEM with IEC of 2.7 mmol g$^{-1}$ was ca. 71% (Table 3.4) around 2.5 times that of Nafion (Table 3.5) which is in agreement with the ratio of IEC and λ.

The WU is also related to the swelling, which can be measured by the increase of membrane thickness or by dimensional expansion due to the water content at room temperature.  Higher WU causes higher swelling of the membrane. The membrane exhibited isotropic swelling wherein dimensional change was similar both along the in-plane (width and length) direction and the through-plane (thickness) direction.  As expected, average swelling was essentially constant at given IEC and WU of ca. 50% for IEC of 2.7 mmol g$^{-1}$.  As expected, the observed swelling is found to be higher to that exhibited by Nafion membranes as shown in Table 3.5.  The swelling varied with IEC when the measured IEC for LDPE membrane with initial thickness of 50 μm increased from 1.4 to 2.7 to 3.2 mmol g$^{-1}$, the DS increased from 23.0 to 47.8 to 55.6%.

Table 3.5. WU, λ and swelling of Nafion membranes having IEC of 0.91 mmol g$^{-1}$.

| Membrane Code | Nominal thickness (μm) | WU (wt %) | WU[a] (vol %) | λ[a] | DS (%) | Reference |
|---|---|---|---|---|---|---|
| 212 | 51 | 30.3[c,1] | 37.7 | 18.5 | 39.6[b,2] | [1]Takamuku [108] [2]Sherazi et al. [109] |
| 117 | 183 | 19.22[d] | 27.8 | 11.7 | 37.4[d] | Xu et al. [110] |

[a] calculated based on reported WU (wt %) and using Nafion density of 2 g cm$^{-3}$ [106].
[b] measured at 20 °C
[c] measured at room temperature
[d] measured at 30 °C

## 3.6 Tensile test

Mechanical testing was performed to determine the effect of swelling and WU on the resulting tensile strength of the hydrated membranes of different DOG. A sample of the initial LDPE film and fully hydrated commercial Nafion 212 film were also tested for comparison wherein the stress-strain curves of all the samples are shown in Figure 3.6.  As summarised in Table 3.6, both dry AEMs, 32% and 65%

DOG, showed comparable ultimate tensile strength (UTS) of 9.5 and 11.2 MPa, respectively. This indicates that the amount of VBC monomer did not significantly affect the tensile strength of the dry membranes. These values are also slightly lower than that of pristine LDPE film of 15.5 MPa.

Table 3.6. Ultimate tensile strength of single test specimens.

| | Test Specimen | Ultimate Tensile Strength (MPa) |
|---|---|---|
| LDPE base film | | 15.5 |
| Fully hydrated Nafion 212 film | | 9.0 |
| 65% DOG | Dry LDPE-AEM | 11.2 |
| | Fully hydrated LDPE-AEM | 2.4 |
| 32% DOG | Dry LDPE-AEM | 9.5 |
| | Fully hydrated LDPE-AEM | 6.6 |
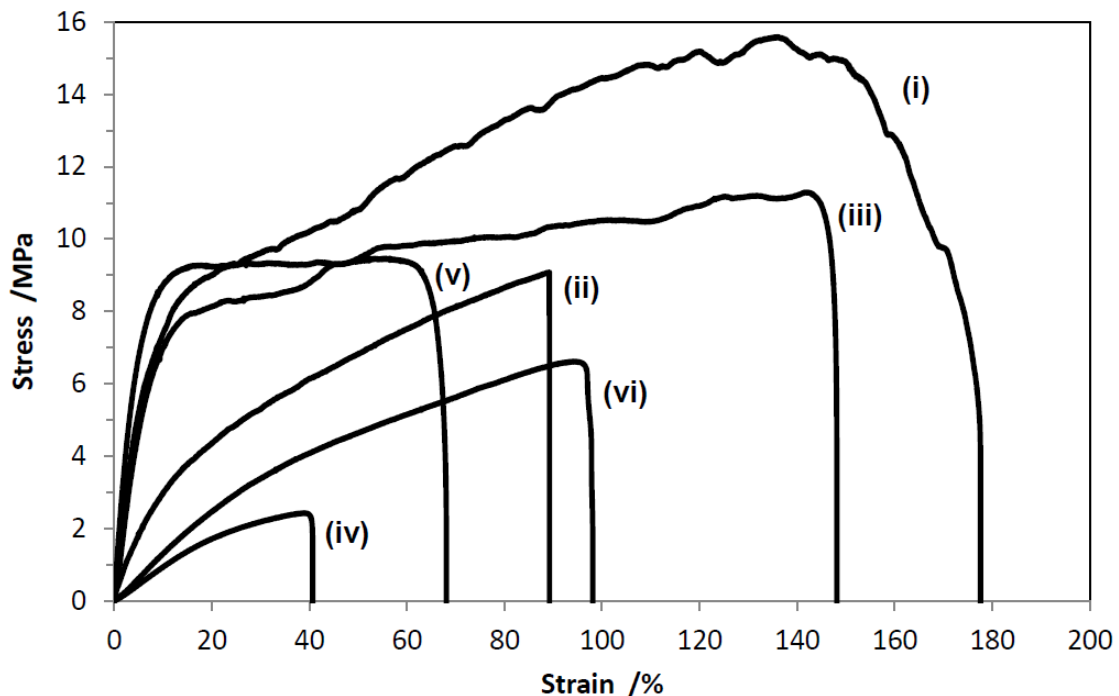


Figure 3.6. Stress–strain curves of the (i) LDPE film, (ii) fully hydrated Nafion 212 film, (iii) dry LDPE-AEM (65% DOG), (iv) fully hydrated LDPE-AEM (65% DOG), (v) dry LDPE-AEM (32% DOG), and (vi) fully hydrated LDPE-AEM (32% DOG).

Fully hydrated membranes, on the other hand, have as expected significantly lower UTS of 6.6 and 2.4 MPa for AEMs with DOG of 32% and 65%, respectively. The higher the grafting degree (65% – Table 3.4) the higher the membrane degree of swelling (DS of 48%) and the poorer the mechanical properties, i.e. decrease by 79% of UTS (from 11.2 to 2.4 MPa) compared with AEM with lower DOG (32%) and consequently lower DS (23%) and lower loss of UTS of 30% (from 9.5 to 6.6 MPa).

The commercial Nafion film exhibited a UTS of 9.0 MPa (Table 3.6) which is in agreement with values reported in literature [56]. While the AEM with low DOG of 32% has an IEC 1.5 that of Nafion (and lower ionic conductivity), the UTS of the hydrated AEM is lower than that of Nafion by only 26%. Furthermore, when compared with other polymers, the tensile strength of the AEM with the use of LDPE as the base polymer is still inferior compared with that of polytetrafluoroethylene (PTFE) [111] and ethylene tetrafluoroethylene (ETFE) [56] as the base polymers. HDPE and UHMWPE can be used in the future instead of LDPE to improve the mechanical strength of the initial base polymer and consequently the final produced AEM. As mentioned earlier, since the OH$^-$ diffusion is ca. 2 times slower than H$^+$ in dilute solutions, the optimum balance between IEC and mechanical properties shifts towards higher IEC values, in comparison with PEM, at the cost of mechanical properties.

## 3.7 Ionic conductivity

The IEC and DOG data from Table 3.3 are important membrane parameters that can be directly correlated with the measured ionic conductivity. Figure 3.7 shows the variation in conductivity of the radiation grafted membranes with temperature as a function of increasing DOG. It can be observed that as the DOG increased, the ionic conductivity also increased. As shown for ENTEK-based porous membrane, an increase from 46.0% to 57.4% DOG exhibited an increase in ionic conductivity at 70 °C from 0.05 to 0.08 S cm$^{-1}$, respectively. Similarly, BPI-based non-porous membrane showed an increase in ionic conductivity from 0.09 to 0.11 S cm$^{-1}$ at 60 °C when the DOG was increased from 50.4% to 74.6%, respectively.
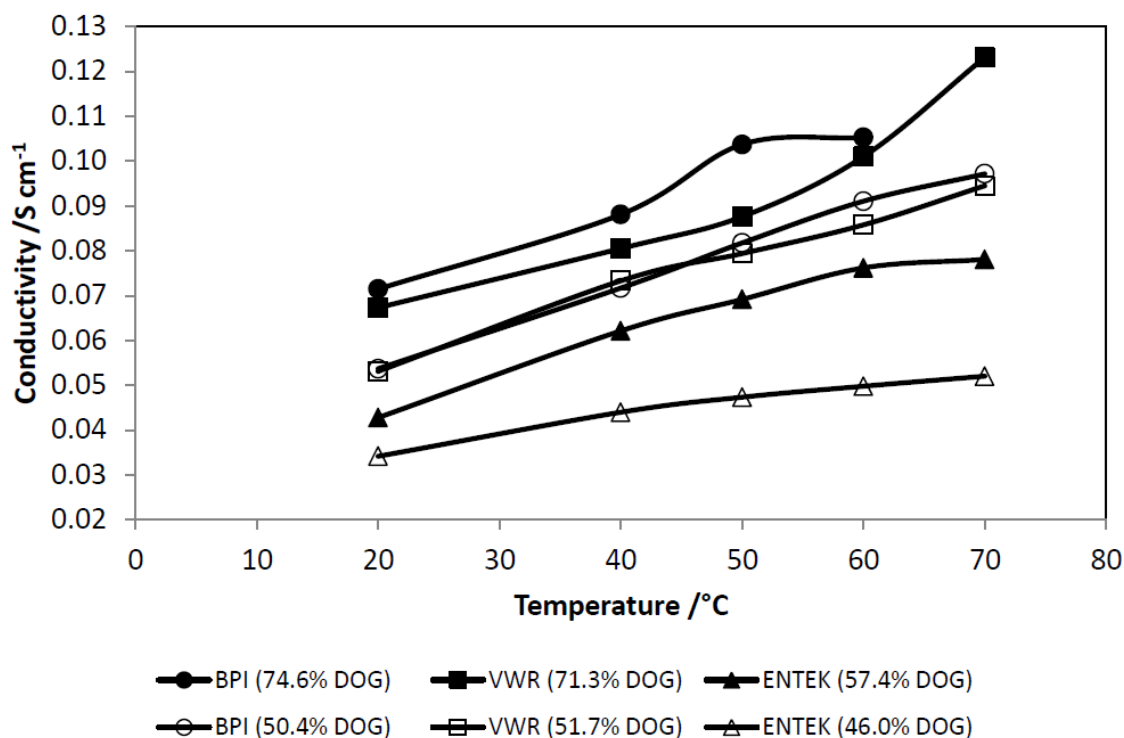
Figure 3.7. Through-plane conductivity of membranes at different temperatures.

By comparing relatively similar DOG of membranes from different polyethylene sources, namely VWR-based AEM (51.7% DOG) and BPI-based AEM (50.4% DOG), we can establish that varying the commercial polyethylene supply source has minimal effect on the ionic conductivity of the fabricated AEM. It can be observed that both membranes exhibited essentially the same ionic conductivity at all temperatures tested ruling out the effect of variation in supplier on the properties of the resulting AEM, particularly in terms of ionic conductivity.

The ENTEK-based porous membranes were compared with non-porous VWR-based membranes, at similar DOG. The non-porous VWR-based membrane showed superior conductivity compared with the porous ENTEK-based membrane. At 70 °C, the non-porous VWR-based membrane with 51.7% DOG showed higher conductivity of 0.097 S cm$^{-1}$ compared with 0.078 S cm$^{-1}$ exhibited by the porous ENTEK-based membrane with 57.4% DOG. The observed difference in conductivity by ca. 20% is believed to be caused by the remaining porosity in ENTEK membranes after grafting. This porosity led to a very high hydrogen fuel cross-over through the membrane and the recorded OCV was lower than 0.4 V, thus the fuel cell performance data was no longer collected.

Among the different AEMs tested, the VWR-polyethylene based membrane with DOG of 71.3% (IEC 3.0 mmol g$^{-1}$) showed the highest conductivity of 0.12 S cm$^{-1}$ at 70 °C. This value is much higher compared with similar studies of polyethylene-based AEMs at the same temperature [50]. This makes the fabricated membrane a good candidate for alkaline fuel cell systems being capable of supporting large currents with minimal resistances loss.

Figure 3.8 shows the effect of varying the thickness of polyethylene on the ionic conductivity of the produced membrane. As the initial thickness of the polyethylene increased, the ionic conductivity of the resulting membrane also increased. However from Table 3.4, the IEC remained essentially constant regardless of the initial thickness of polyethylene used, thereby inferring that the expected ionic conductivity should be also constant. A parallel study by Ko et al. [112] which investigated the effect of fluoropolymer film thickness in the preparation of fuel cell membranes, also showed a similar trend wherein the conductivity of the membrane increased as the fluoropolymer film thickness increased even with essentially the same membrane IEC.
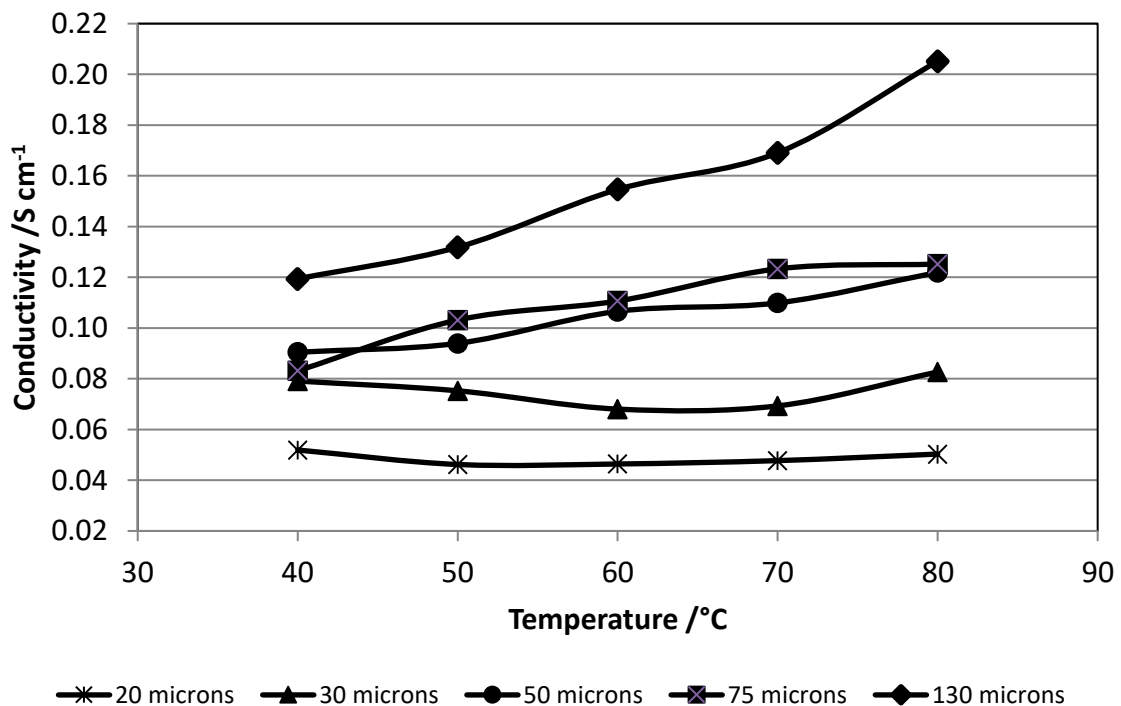


Figure 3.8. Effect of varying initial polyethylene thickness to the average through-plane ionic conductivity.

The observed increase in ionic conductivity could not be due to the variation in water uptake or swelling since data from Table 3 showed similar WU and swelling regardless of the initial polyethylene thickness. The membranes exhibited superb performance in terms of ionic conductivity in the range of 0.08 to 0.12 S cm$^{-1}$ under fully humidified environment at 80 °C. The observed high conductivity of the thickest membrane can be attributed to the variation in degree of anisotropy among the membranes. The degree of anisotropy is the ratio of the in-plane conductivity to that of the through-plane conductivity. Thus, the anisotropy is largely influenced by the variation in the uniformity of VBC grafting on the polymer backbone whereby larger amount of VBC grafted onto the polymer surface than within the polymer will result in higher in-plane over through-plane conductivity (anisotropy).

A low degree of anisotropy is desired which indicates successful penetration of monomer through the polyethylene film resulting in improved grafting. Thicker polyethylene film were reported to graft more uniformly than thinner films [48] wherein the grafting is chiefly controlled by the concentration of the radicals rather than by the monomer transport [113]. The thickest membrane showed the highest through-plane conductivity of 0.21 S cm$^{-1}$ at 80 °C.

## 3.8 Fuel cell performance

Figures 3.9 shows the fuel cell polarisation curve for anion-exchange membranes with 74.6% and 32.0% DOG at 40 °C, using air and oxygen feed under atmospheric pressure. Under oxygen feed, the measured OCV were 1.06 and 1.08 V for 74.6% and 32.0% DOG, respectively. The high recorded OCVs indicate that the studied DOG range and the resulting membrane swelling degrees are suitable for fuel cells application with low fuel cross-over across the cell. The DS of AAEM with DOG of 74.6% was ca. 55.6% and the DS of AEM with DOG of 32.0% was 23.0% (Table 3.4) in comparison with that of Nafion 212 of 40% and Nafion 117 of 37% as shown in Table 3.5.
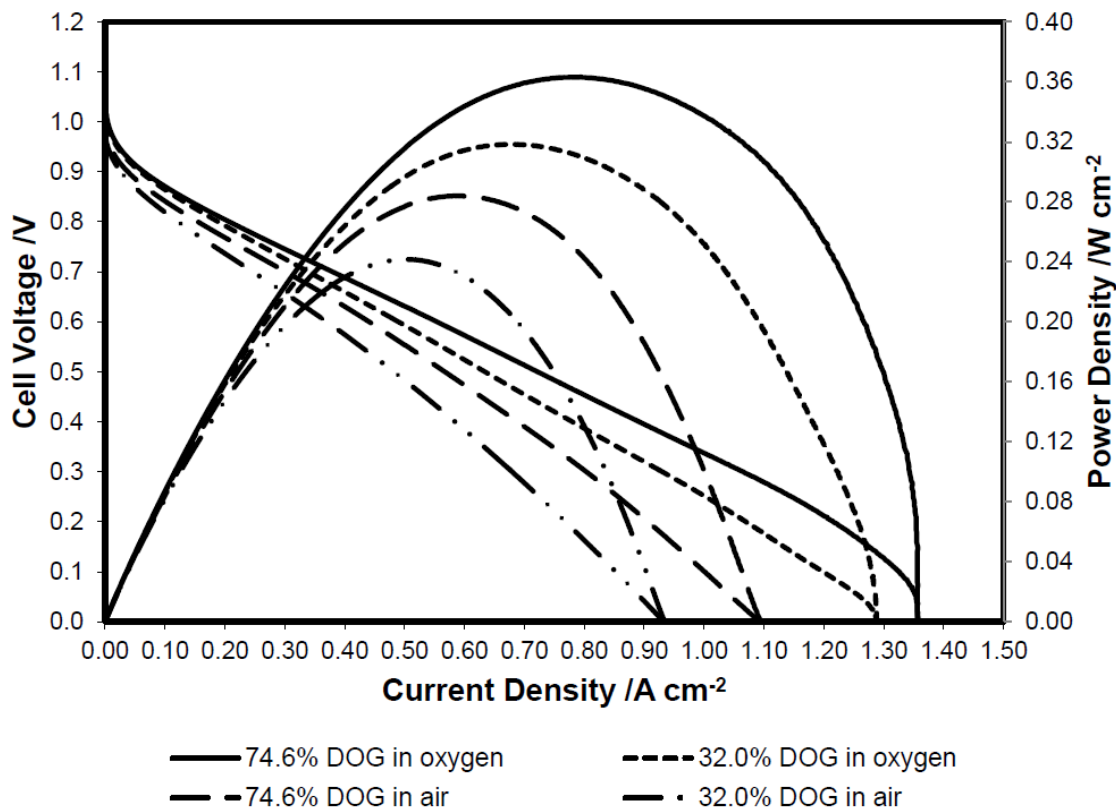
Figure 3.9. Polarisation and power density curves of LDPE-based anion exchange membranes at 40 °C both at oxygen and air atmosphere.

The use of AEM with increased DOG is beneficial in attaining higher performance of the fuel cell due to better conductivity, resilience to dehydration and water transport from anode to cathode. As can be seen in Figure 3.9, the slope of the I-V curve improved upon using AAEM with higher DOG due to lower membrane resistivity from 158 m$\Omega$ cm$^2$ for 32.0% DOG to 143 m$\Omega$ cm$^2$ for 74.6% DOG (measured using FRA) resulting in an increase in current density from 502 to 544 mA cm$^{-2}$ at 0.6 V, respectively. The resistivity decrease translates to ionic conductivity increase by a factor of 2 considering the difference in thickness between the two membranes (Table 3.7). While both polymer films had the same initial thickness of 50 µm, the thickness of the dry film with higher DOG of 74.6% was 1.5 that of the lower DOG of 32.0% after grafting (Table 3.4). The consequent difference in IEC and WU when hydrated resulted in even larger difference in the final hydrated films thickness by a factor of 1.84 (Table 3.7).

Table 3.7. MEAs through plane resistivity at 40 °C under oxygen with different DOG and corresponding membrane thickness.

| Membrane DOG (%) | Initial PE thickness (μm) | Hydrated thickness (μm) | FRA through-plane resistance (mΩ cm$^2$) |
|---|---|---|---|
| 32.0 | 50 | 82 | 158 |
| 74.6 | 50 | 151 | 143 |

Data further shows that the difference between oxygen and air performance at 40 °C is rather small indicating good electrode architecture and good hydration level with minimal transfer losses at the cathode.  For the membrane having 74.6% DOG, the current density at 0.6 V was 544 mA cm$^{-2}$ under oxygen and 415 mA cm$^{-2}$ under air.  The plot shows approximately linear behaviour at medium current densities. While normally this region is referred to as the ohmic region, contribution from mass transport effects are also present [29, 49]. This can be seen from the difference in the polarisation slopes between air and oxygen operation.

Figures 3.10 shows the fuel cell polarisation curve for anion-exchange membranes with 74.6% and 32.0% DOG at 50 °C, both using air and oxygen feed under atmospheric pressure.  It can be seen that for the membrane electrode assembly (MEA) utilising a 74.6% DOG membrane under oxygen feed, the obtained current density at 0.6 V was 643 mA cm$^{-2}$, higher compared with that at 40 °C of 544 mA cm$^{-2}$.  Similarly, for the MEA with 32.0% DOG membrane, the current density at 0.6 V under oxygen increased from 502 to 546 mA cm$^{-2}$ when the working temperature was increased from 40 to 50 °C, respectively.  Despite the observed increase in current density under oxygen with temperature, the dehydration of MEA with 32.0% DOG membrane became evident at a closer look. A clear mass transport limitation represented by a limiting current even under oxygen operation at ca. 1.2 A cm$^{-2}$ was observed (32.0% DOG, Figure 3.10). This is an indication of membrane/ionomer dehydration and consequently decrease in oxygen permeability (through ionomer) and water permeability (through ionomer and membrane) both of which are reactants at the cathode. This is also supported by the resistivity

measurements where the through plane resistivity of MEA utilising the membrane with 32.0% DOG increased from 158 to 199 ohm cm$^2$ (Table 3.8). The dehydration effect became more apparent under air operation where higher flow rates were used at the cathode. The current density under air at 0.6 V decreased (32.0% DOG) from 372 to 342 mA cm$^{-2}$ with temperature increase from 40 to 50 °C, respectively.
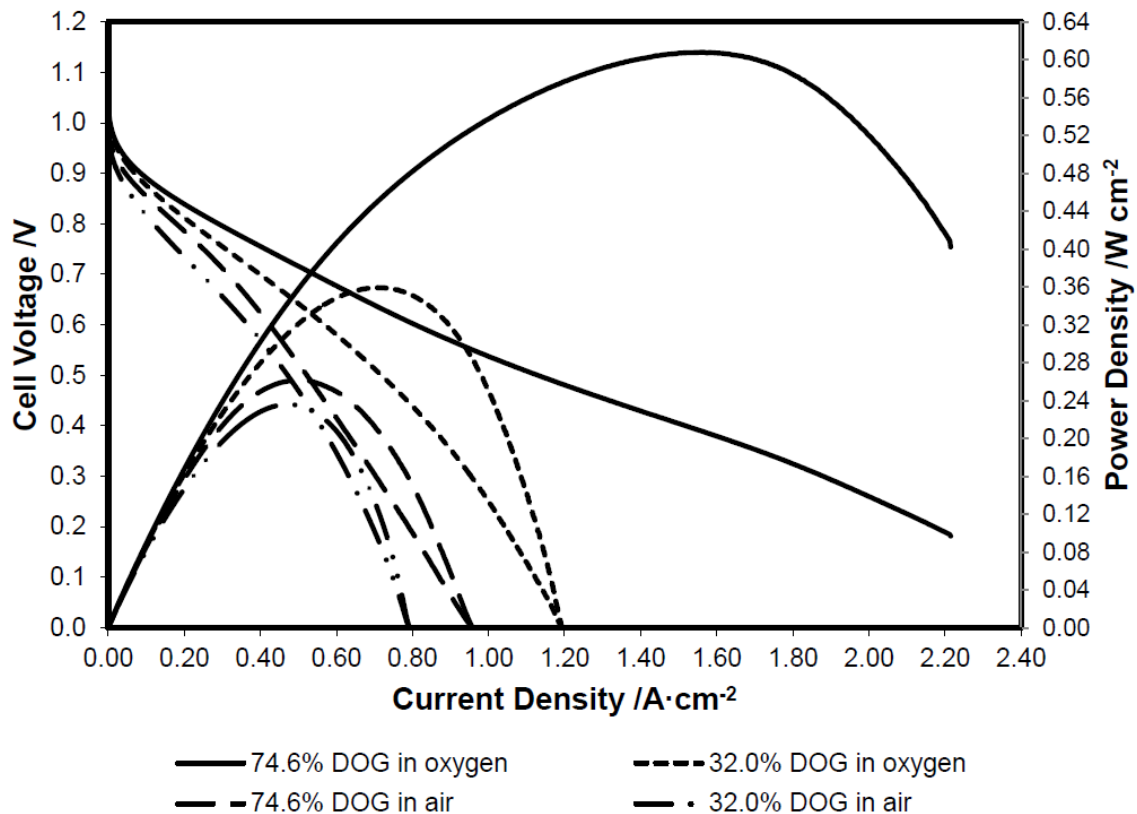


Figure 3.10. Polarisation and power density curves of LDPE-based anion exchange membranes at 50 °C both at oxygen and air atmosphere.

On the other hand, the MEA utilising the membrane with 74.6% DOG did not suffer dehydration at 50 °C under oxygen. This can be seen by no clear limiting current even at a current density of 2.2 A cm$^{-2}$ under oxygen. This was additionally confirmed by a decrease in the measured resistivity from 143 to 122 mΩ cm$^2$ with a temperature increase from 40 to 50 °C, respectively.

Table 3.8. MEAs through plane resistivity at 50 °C under oxygen with different DOG.

| Membrane DOG (%) | FRA through-plane resistance ($m\Omega$ cm$^2$) |
|---|---|
| 32.0 | 199 |
| 74.6 | 122 |

The measured WU of the 32.0% DOG membrane was 130 wt%, considerably lower compared with 285 wt% for the 74.6% DOG membrane (at room temperature) explaining the observed dehydration limitation in the case of the 32.0% DOG membrane. It can be therefore reiterated that in order to operate AEM for prolonged periods at temperatures of 50 °C and above, the use of membranes with high DOG is required.

Table 3.9. Summary of peak power density and current density at 0.6 V of the fabricated membranes.

| DOG (%) | Temperature (°C) | Gas Feed | Peak Power Density (mW cm$^{-2}$) | Current Density at 0.6 V (mA cm$^{-2}$) |
|---|---|---|---|---|
| 74.6 | 40 | Oxygen | 363.3 | 543.5 |
| | | Air | 284.0 | 414.6 |
| | 50 | Oxygen | 607.8 | 643.0 |
| | | Air | 261.6 | 460.6 |
| 32.0 | 40 | Oxygen | 318.5 | 502.3 |
| | | Air | 241.7 | 372.2 |
| | 50 | Oxygen | 359.3 | 546.0 |
| | | Air | 235.9 | 342.4 |

Peak power density and current density values at 0.6 V are summarised in Table 3.9.   Under oxygen gas feed at 50 °C, the membrane with 74.6% DOG exhibited peak power density and current density at 0.6 V of 608 mW cm$^{-2}$ and 643 mA cm$^{-2}$, respectively.   On the other hand, using air as the feed showed peak power density and current density at 0.6 V of 262 mW cm$^{-2}$ and 461 mA cm$^{-2}$, respectively. Similarly for the 32.0% DOG membrane, the peak power density and current density at 0.6 V at 50 °C under oxygen were 359 mW cm$^{-2}$ and 546 mA cm$^{-2}$, respectively, while under air were 236 mW cm$^{-2}$ and 342 mA cm$^{-2}$, respectively.

# CHAPTER 4
# CONCLUSION

The fabrication of polyethylene-based alkaline anion-exchange membranes (AAEM) was attempted employing a double-beam UV radiation source, to supply a high radiation dose rate and potentially ensure uniform grafting on both sides of the base polymer film. However, after several trials and varying synthesis parameters (i.e. irradiation time, placing the base film between quartz glass plates, step-wise and simultaneous grafting) the grafting was patchy and not uniform. Even with prolonged exposure to UV, the grafted LDPE film turned yellowish suggesting presence of unreacted VBC radicals on the surface.

The successful fabrication of a polyethylene-based AAEM was performed by mutual radiation graft polymerisation using both laboratory-cast and commercially procured polyethylene films. AEM conductivity increased with VBC concentration and gamma radiation dose. Cast-LDPE membrane showed higher DOG than cast-LLDPE membrane at low VBC concentration due to the absence of chain branching in LLDPE. The variation in commercial polyethylene films had an insignificant effect on the ionic conductivity of the fabricated AEMs. The use of porous ENTEK polyethylene as base polymer film resulted in higher DOG compared with non-porous LDPE at the same grafting conditions due to the ease with which the VBC monomer can penetrate the porous structure of the base polymer. However, the AEM remained porous (over 5%) after radiation grafting rendering it not useful for fuel cell applications. Mechanical testing revealed that when fully hydrated, the AEM ultimate tensile strength (UTS) was significantly reduced with an increase in DOG and consequent increase in swelling. At 32% DOG, the value was 26% lower than Nafion UTS. However, due to slower $OH^-$ diffusion (ca. 2 times) in comparison with $H^+$, the optimum balance between conductivity and mechanical strength shifts towards higher IEC values, in comparison with PEM, at the cost of mechanical properties.

The observed ionic conductivity and the IEC increased with increase in DOG, wherein VWR-based AEM with 71.3% DOG exhibited the highest conductivity of 0.12 S cm$^{-1}$ at temperature of 70 °C, amongst the membranes prepared with 50 μm initial LDPE thickness. The initial thickness of the polyethylene film was found to have no influence on the resulting IEC and DOG of the produced membrane.

59

Similarly, the WU and swelling were essentially constant at fixed DOG, regardless of the initial polyethylene thickness. To achieve similar $H^+$ ionic conductivity as Nafion (0.1 S cm$^{-1}$ at 80°C, 100%RH), the AEM should have IEC > 2.0 mmol g$^{-1}$ double that of Nafion to balance the slow diffusion of hydrated $OH^-$ in comparison with that of the hydrated $H^+$. Moreover, Nafion binds water more strongly than the relatively weak base in AEM, and higher IEC is required to stop AEM dehydration at temperatures above 60°C.

Membrane electrode assemblies based on fabricated AEM showed high OCVs of 1.06 and 1.08 V for 32.0% and 74.6% DOG membranes, respectively. This shows that membranes with DOG <75% are suitable for fuel cell application with low fuel cross-over. Furthermore, the use of membranes with high DOG provided improved fuel cell performance due to better ionic conductivity and water transport from anode to cathode. The fuel cell performance can be improved by increasing the operating temperature from 40 to 50 °C. The best performing AEM with a hydrated thickness of 151 μm (74.6% DOG) achieved a peak power density of 608 mW cm$^{-2}$ and a maximum current density at 0.6 V of 643 mA cm$^{-2}$ under oxygen at 50 °C. In order to operate AEM for prolonged periods at temperatures of 50°C and above, the use of membranes with high DOG >32% is required.

**PART II.    STABILITY AND DEGRADATION STUDIES OF ANION EXCHANGE MEMBRANE**

# CHAPTER 1
# REVIEW OF RELATED LITERATURE

Alkaline anion exchange membranes (AEMs) are solid polymer electrolytes that contain positive ionic groups, typically containing quaternary ammonium groups: $-N^+(CH_3)_3$, and mobile negatively charged anions, usually $OH^-$ [20, 29]. There have been several classes of AEMs fabricated for alkaline fuel cell (AFC) and water electrolyser (AWE) operations reported in literature. As the ionic conductivity and fuel cell / electrolyser performance are important properties of AEM, its chemical and thermal stability for long term service life is equally paramount. The chemical and thermal stability of AEMs greatly depend on the nature of the polymer backbone and on the type of functional group that enables the transfer of hydroxide ions [40].

## 1.1 Stability and degradation of polymer backbone

A variety of base polymers for AEM synthesis have been extensively investigated in literature from vinyl polymers to aromatics such as LDPE [47, 114], HDPE [48, 50], poly(2,6-dimethyl-1,4-phenylene oxide) (PPO) [115, 116], poly(ether ether ketone) (PEEK) [70, 117], poly(arylene ether sulfone) (PES) [42, 110, 118], and poly(methyl methacrylate) (PMMA) [119, 120], to  fluorinated or partially fluorinated polymers such as poly(tetrafluoroethene-co-hexafluoropropylene) (FEP) [121, 122], poly(vinilydine fluoride) (PVDF) [123], poly(ethylene tetrafluoroethylene) (ETFE) [56, 74, 124], and poly(tetrafluoroethylene) (PTFE) [125, 126]. As mentioned in the previous section, the polymer backbone provides the mechanical strength and stability of the AEM and perceived degradation of the polymer backbone will eventually lead to the failure of the AEM to deliver the desired performance.  The fluorinated base polymers have emerged to be the preferred polymer backbone for AEM preparation owing to their inherently inert properties and electrochemical and thermal stability due to the presence of the strong electron-withdrawing fluorine atom (C–F) [127].  However, it has been reported that partially fluorinated polymers like PVDF-based AEMs are known to degrade in alkaline media via dehydrofluorination [121, 128].

Since fluorinated-type of AEM still undergo degradation under an alkaline environment, it paved the way to revisit the use of hydrocarbon-based backbones

for AEM preparation due to some definite advantages, namely, low cost, commercial availability and structures that are amenable for tethering pendant groups [88]. The study of Nunez et al. [129] however, has reported that grafting of cationic functional groups to an innately stable and chemically inert polymer backbones, i.e. PES and PPO, negatively affects the nature of the polymer backbone. It has been reported that even though polysulfone polymer is tolerant to a highly basic environment, the polymer backbone gradually degrades in alkaline medium when quaternised with ammonium functional groups [129, 130]. The PPO-based AEM, on the other hand, undergoes backbone degradation by chain scission via hydrolysis of the ether bonds [131, 132]. In order to address this concern, Pan et al. [133] suggested that the DOG to be in minimum while tethering the grafted membrane with functional groups containing multiple cations. In this way, the polymer backbone is minimally altered while delivering the same IEC, hence same ionic conductivity, brought by the increased number of cation sites.
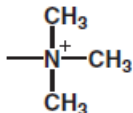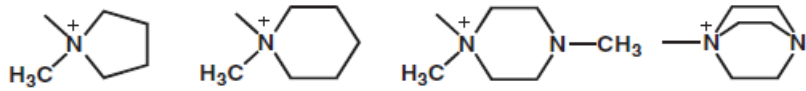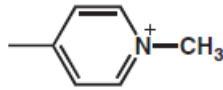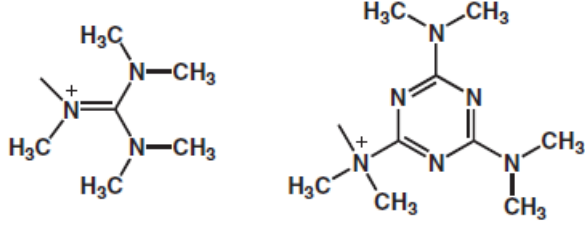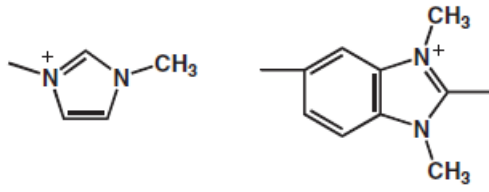
Since the degradation of the polymer backbone is triggered by the proximity of the attached functional group, another approach to improve the stability of the backbone is to move the tethered functionality farther by using pendant spacers. The long spacer chain was predicted to increase the barrier for Hofmann elimination thus further preventing cation degradation [134]. However, it was reported that a spacer length of more than 4 units provided little improvement in terms of alkaline stability of the resulting AEM [135] and will only increase the hydrophobicity of the AEM [136], hence decreasing ionic conductivity. Parrondo et al. [137] even reported that the use of hexyl spacers for PPO-based AEMs offered insignificant alkaline stability which suggests that the envisioned advantage of using spacers does not apply to all types of polymer backbones and preparation conditions.

## 1.2 Stability and degradation of tethered functional group

The fact that novel fluorocarbon-type AEMs are still unstable under strong basic conditions [21, 138] suggests that the functional ion-exchange groups rather than the cross-linked polymer network undergoes degradation. Therefore, it can be assumed that the alkaline stability of an AEM is given by the stability of the weakest link, which is generally considered to be the head group. The most common class of AEMs are those based on quaternary ammonium groups (Table 1.1) [63, 139] due to their appreciable stability in an alkaline environment [140, 141] compared

with phosphonium or sulfonium groups [24]. However, it was reported that phosphonium groups have demonstrated their potential and seem to be more stable towards attack by the hydroxide ion than the more conventional quaternary ammonium [142].

Table 1.1. Chemical structures of representative ammonium-based functional groups [139].

| Example | Chemical structure |
| --- | --- |
| Tetraalkyl ammonium |  |
| Cycloalkyl ammonium |  |
| Pyridinium |  |
| Guanidinium |  |
| Imidazolium |  |

Alkaline stability and degradation of AEMs are mainly assessed in the purview of cation stability. Literature has abundantly discussed mechanisms of the degradation of AEMs, namely, Hofmann elimination, nucleophilic substitution and formation of ylide derivatives [24, 78, 130, 134, 143-148]. Hofmann elimination is when OH$^-$ ions attack a β-hydrogen atom (with respect to N) of the cation which leads to the elimination of the tertiary amine from the neighbouring carbon [24, 134, 144] as shown in Scheme 1.1.
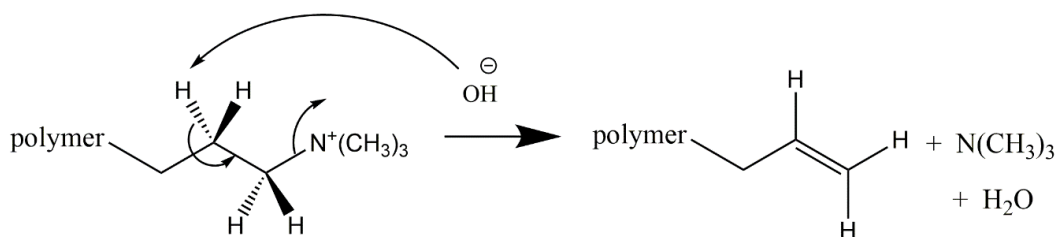
Scheme 1.1. Degradation mechanism of OH⁻ ion attack on the TMA cation group via Hofmann elimination [24].

Nucleophilic substitution involves OH⁻ ions acting as a strong nucleophile which can either (1) attack the α-carbon atom of the cation converting the quaternary ammonium group to tertiary amine and releasing an alcohol or (2) attack the benzylic carbon atom causing the detachment of the tertiary amine [78, 130, 146]. Lastly, the ylide formation route is through OH⁻ ions abstracting the proton (α-hydrogen) of the methyl group producing nitrogen ylide intermediates which transform to tertiary amine and water [145, 147, 148]. These ylide intermediates can further undergo degradation through Stevens rearrangement or the Sommelet-Hauser mechanism [143, 149-151], the selectivity of which is dependent on the electronic properties of the substituents attached to the aromatic ring, the steric effect and the type of solvent used [151]. These three degradation mechanisms can occur simultaneously which can lead to a combination of degradation products. It is thus important to synthesise membranes with chemical structures capable of circumventing these degradation mechanisms to ensure long term stability of AEMs.

Table 1.2 shows the relative basicity and half-life of the head-groups investigated in this study. ABCO shows the highest pKa (10.76) making it the strongest base among the head-groups investigated and TMA is found to be the weakest base in terms of pKa (9.76). NMP-functionalised membranes exhibited the longest half-life (in 6 M NaOH solution at 160 °C) suggesting that it is the most stable among the investigated membranes in medium with high alkaline concentration. The same study also revealed that DABCO-based membranes will be the least stable compared with TMA, NMP and ABCO having the least half-life of 1.4 h measured at 160 °C in 6 M NaOH solution.

Table 1.2. Basicity and half-life of amine functionalities of AEMs investigated.

| Name | Functional Group | pKa (at 25 °C) | Half-life[a] (h) |
|---|---|---|---|
| TMA | Trimethyl amine | 9.81[b] | 4.2 |
| DABCO | 1,4-diazabicyclo[2.2.2]octane | 8.72[c] | 1.4 |
| NMP | N-methylpiperidine | 10.13[c] | 7.3 |
| ABCO | 1-azabicyclo[2.2.2]octane | 10.76[d] | - |

[a]in 6 M NaOH and 160 °C [135]
[b]Hall and Bates [152]
[c]Frenna et al. [153]
[d]Beltrame et al. [154]

## 1.2.1 Trimethyl amine-based AEM

The use of trimethyl amine (TMA) to impart functionality to AEMs provides tetraalkyl ammonium cations considered to be the most chemically stable [155]. This is due to the absence of longer subgroups (e.g, ethyl or propyl) that could introduce β-hydrogens making it susceptible to degradation via the Hofmann elimination mechanism.

The ionic conductivity and fuel cell performance of several benzyl ammonium and sulfonium head groups for AEMs has been reported and it has been found that trimethylamine (TMA)–functionalised ionomers show superior ORR performance and higher ionic conductivities in comparison with other studied head groups including 1,4-diazabicyclo[2.2.2]octane [29, 71]. Another report [49] showed an increase of around 60% of the power density at 0.4 V when TMA was used instead of N,N,N',N'-tetramethyl-1,6-hexanediamine (TMHDA) at 60 °C. Our TMA-functionalised vinylbenzyl chloride (radiation) grafted on low-density polyethylene backbone (LDPE-$g$-VBC-TMA) showed low activation energy of 12 kJ mol$^{-1}$ for OH$^-$ ionic conductivity close to the reported value for H$^+$ conductivity in Nafion [156] with OH$^-$ through plane conductivity of 0.11 S cm$^{-1}$ at 80 ºC and 100% RH [49]. These (LDPE-$g$-VBC-TMA) AEMs have superior fuel cell peak power densities, at a high potential of 500 mV, one of the highest reported in the literature for AAEMFCs of

823 mW cm$^{-2}$ under oxygen (atm) and 506 mW cm$^{-2}$ under air (1 bar gauge) at 60 $^{\circ}$C [48].

Benzyl-trimethylammonium (benzyl-TMA) is far more stable than its phenyl equivalent [141]. 90% of benzyl-TMA was found to be stable after 29 days alkaline treatment compared with only 30% in the case of phenyl-TMA [147]. Among the several studied quaternary ammonium head groups, benzyl-TMA and benzyl-DABCO showed the highest stability in 2 M KOH at 160 $^{\circ}$C (under N$_2$) with half-time disintegration of 29 and 42 min, respectively [155].

For the TMA-functionalised membranes, the attachment of TMA to VBC during functionalisation did not produce β-hydrogens, thus the Hofmann elimination route can be conveniently disregarded [50, 157, 158]. When the Hofmann elimination is impossible, nucleophilic substitution proceeds preferably towards the release of TMA rather than producing benzyl-dimethylamine [145, 155, 159] as shown in Scheme 1.2. This is because TMA is an excellent leaving group in the nucleophilic substitution reaction [155, 160]. The reaction consequently leaves behind a benzylic alcohol [159] that readily transforms to dibenzylic ether, and together with TMA, are the major decomposition products [161].
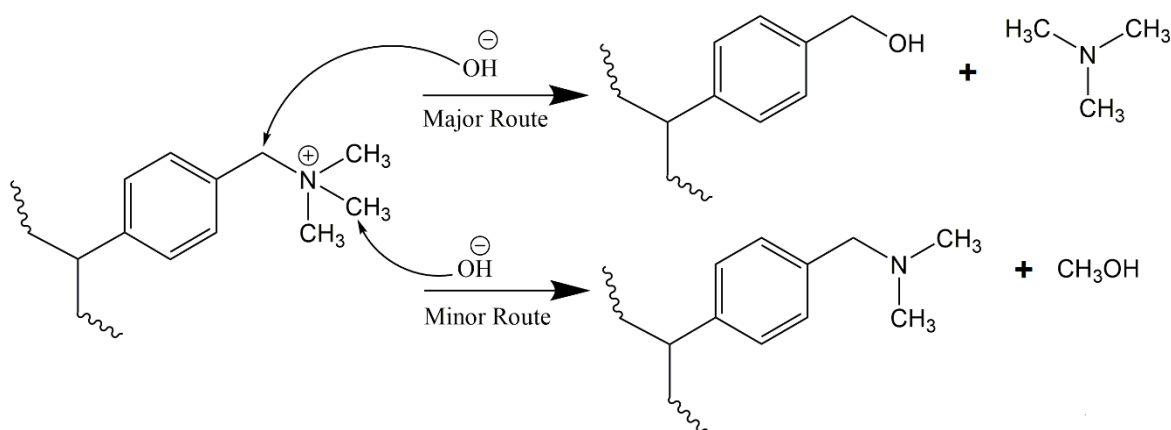
Scheme 1.2. Degradation mechanism of OH$^-$ ion attack on TMA cation group via nucleophilic substitution [159].

Stevens rearrangement for the benzyl-TMA group in basic media involves abstraction of the acidic proton of the α-carbon connecting the aromatic group and the TMA to form ylide. This ylide intermediate undergoes rearrangement to produce

a tertiary amine and water as final products (Scheme 1.3) [150]. Similar to the Stevens rearrangement, the Sommelet-Hauser mechanism also involves abstraction by $OH^-$ ions, however the attack is on the acidic proton of the α-carbon of the methyl group attached to the quaternary nitrogen atom and the resulting carbanion attacks the ortho-position of the aromatic ring (Scheme 1.3) [151].

For benzyl-TMA cation, Stevens rearrangement is the only ylide reaction observed as the $OH^-$ ion prefers the acidic proton attached to the α-carbon connecting the aromatic ring and the TMA, rather than the methyl attached to the quaternary nitrogen atom [149, 150]. However, recent studies have suggested that this ylide reaction pathway is reversible and does not lead to cation degradation [55, 140, 148, 162].
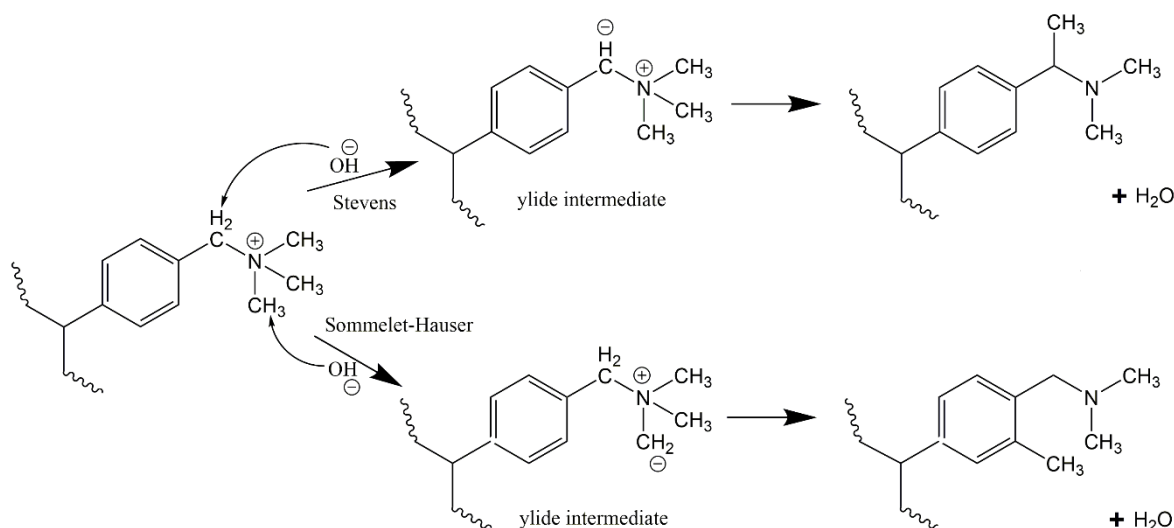


Scheme 1.3. Stevens rearrangement [163] and Sommelet-Hauser mechanism [164] for benzyl-TMA cation group.

## 1.2.2 ABCO- and DABCO-based AEM

The use of functionalities, namely, 1-azabicyclo[2.2.2]octane (ABCO) and 1,4-diazabicyclo[2.2.2]octane (DABCO), for AEM was realised owing to its cyclic bulky structure that can provide the needed chemical and thermal stability. This is because the rigid structures of ABCO and DABCO make them not amenable to the Hofmann elimination mechanism [134, 165]. Unlike the TMA-functionalised membranes, the linkage between ABCO or DABCO with VBC results in the presence of β-carbons, however, their structures do not allow the stereoelectronics

necessary for a Hofmann elimination mechanism. In order for the Hofmann elimination to proceed, the β-hydrogen and the quaternised nitrogen should be in trans-position to each other with a dihedral angle of 180 °C (anti-periplanar) [78, 146] (Scheme 1.4a). For the caged structure of ABCO and DABCO in the fixed boat conformation, the carbon atoms are in eclipsed conformation (Scheme 1.4b) therefore, an anti-periplanar conformation is not possible [155].



(a)                                      (b)
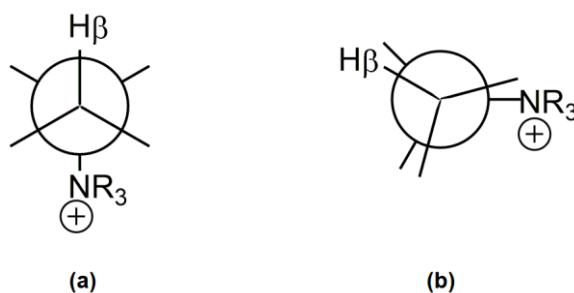
Scheme 1.4. The (a) anti-periplanar conformation required for Hofmann elimination and the (b) eclipsed conformation [78].

Using polysulfone as base polymer, Di Vona et al. [166] reported that the ionic conductivity and water uptake of the DABCO-functionalised membrane doubled compared with TMA-functionalised membrane at the same degree of chloromethylation of 76%. Thermogravimetric analysis also reported [167] that the DABCO-functionalised membrane exhibits better thermal stability than its TMA-based AEM counterpart. However, in terms of AFC performance, Maurya et al. [157] reported 81 mW cm$^{-2}$ maximum power density of a DABCO-functionalised membrane using porous polyethylene base film which is inferior to our TMA-based AEM having a non-porous LDPE base polymer and the same thickness of 50 μm.

Parrondo et al. [137] compared the stability of TMA and ABCO functionalities tethered to PPO base film via hexyl spacers and both were found to undergo degradation in 1 M KOH solution at 60 °C. DABCO unlike ABCO, has two nitrogens which provides better stabilising effect wherein the positive charge can balance the over-all charge therefore, mono-substituted DABCO-membrane is preferred [166]. Expectedly, a mono-quaternised DABCO-based membrane will exhibit better chemical stability than ABCO-functionalised AEMs. However, the mono-quaternised ABCO/DABCO undergoes a nucleophilic displacement reaction

causing the release of ABCO or DABCO to the solution as shown in Scheme 1.5 [145, 155].



R = CH (ABCO) or N (DABCO)
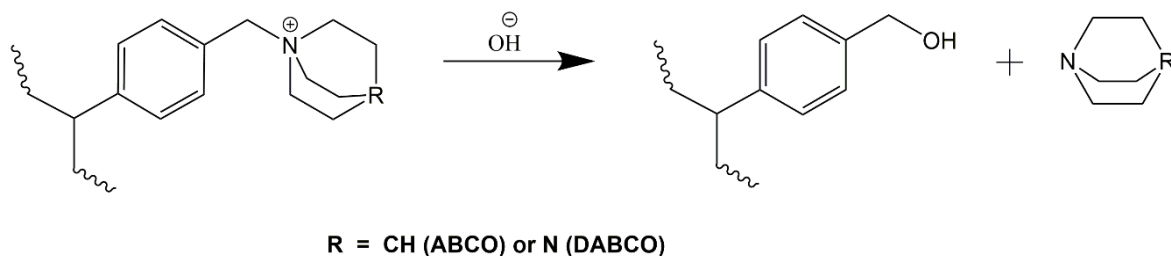
Scheme 1.5.  Degradation mechanism of OH⁻ ion attack on ABCO/DABCO cation group via nucleophilic substitution [155].

If both the DABCO nitrogens are quaternised, the IEC tends to decrease due to increased mass of the repeating unit.  Furthermore, the bis-quaternised DABCO converts into a piperazine structure which is less stable due to rapid elimination via the mononuclear E1 (two-step) mechanism (Scheme 1.6).  At 160 °C in 2 M KOH solution under nitrogen atmosphere, the half-life ($t_{1/2}$) of bis-quaternised DABCO drops to 2.3 min compared with 42 min for the mono-quaternised DABCO [155]. Therefore, the combined faster degradation and decrease in IEC rendered it inferior to mono-substituted DABCO and unsuitable for fuel cell and electrolyser application.
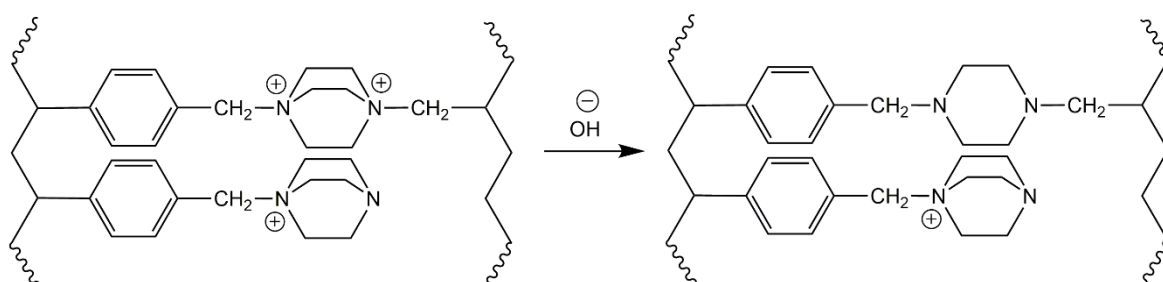


Scheme 1.6. Degradation of bis-quaternised DABCO compared with mono-quaternised DABCO [155].

### 1.2.3 NMP-based AEM

N-methylpiperidine (NMP) is another cycloaliphatic quaternary ammonium group used to functionalise AEMs. Dang and Jannasch [168] investigated the use of quaternary piperidinium groups for AEMs using PPO base polymer film placing heptyl spacers in between. Thermogravimetric data indicates that NMP-based AEMs offer slightly better thermal stability than TMA-functionalised AEMs at the same IEC with the use of PPO base polymer film and heptyl spacers. The same study also indicated insignificant degradation in terms of IEC loss under alkaline stability test using 1 M NaOH solution at 90 °C for 8 days.

Degradation of NMP-functionalised AEM is due to OH⁻ ion attack through nucleophilic substitution (Scheme 1.7a). NMP-based AEMs also degrades by ring-opening elimination (Scheme 1.7b) and ring-opening substitution (Scheme 1.7c). Among the three possible pathways, nucleophilic substitution is considered to be dominant [135].
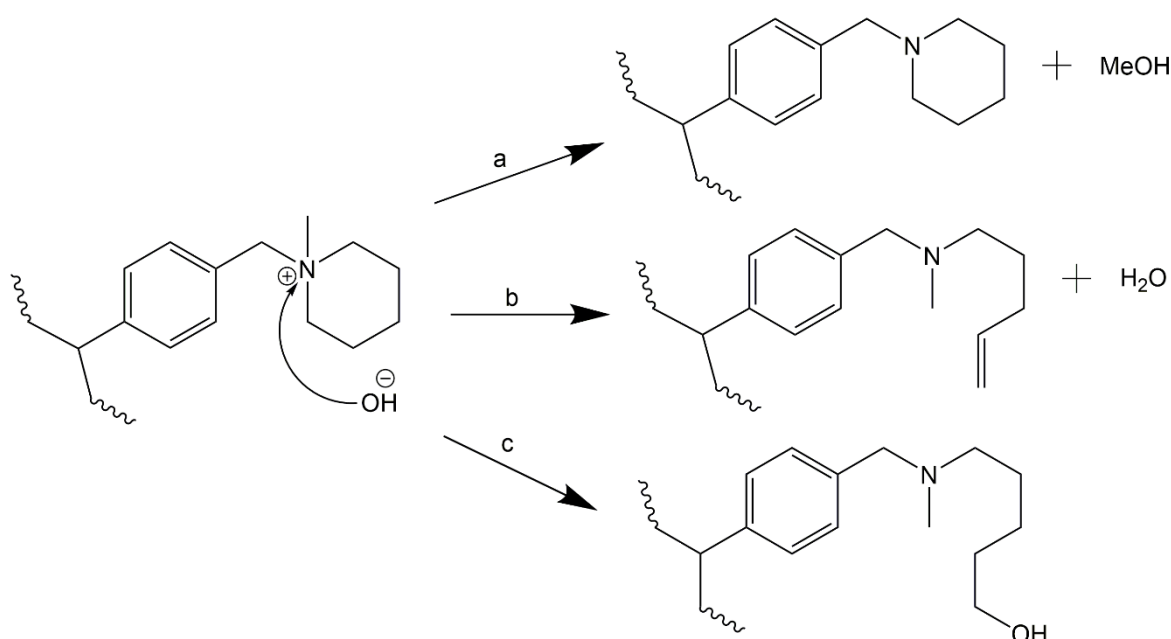


Scheme 1.7. Three possible degradation mechanisms of OH⁻ ion attack on NMP cation group: (a) nucleophilic substitution, (b) ring-opening elimination and (c) ring-opening substitution [135].

## 1.3 Motivation and Research Objectives

The chemical stability of AEMs in the OH$^-$ form, particularly at high temperatures, poses a critical challenge that limits the wide scale use of AEMFCs. In some of our published results [114], we have successfully demonstrated the long term stability of the fabricated polyethylene-based AEMs for AFC operating at temperatures of up to 80 °C. We have shown that the degradation rate is strongly dependent on the oxidant concentration, where the degradation rate under oxygen (atm) was 4 times faster than that under nitrogen. However, limited chemical analysis has been conducted regarding the chemical stability of AEMs, wherein a more fundamental understanding of the chemical stability of AEMs is required to adequately design robust solid-state AFCs and electrolysers [145]. Degradation tests of membranes having quaternary ammonium groups reported in literature were all performed in high alkaline concentrations [50, 169] and elevated temperature [141, 145, 170]. This study is the first attempt to illustrate the observed degradation of the OH$^-$ exchanged AEM stored in deionised water, which is the usual medium for electrolyser operations. Furthermore, the majority of the published work assessed membrane stability by measuring the decrease in its weight, ion exchange capacity and ionic conductivity with time [50, 55, 119, 145, 157, 169, 171, 172]. However, very limited research has been done to analyse the decomposing products. This is partially due to the insoluble nature of some of these products [173], limiting the technique available for chemical analysis needed to identify their structure. Due to such difficulty, we have gathered results from several chemical analyses to elucidate the structure and identity of the degradation products. Most importantly, all of the available literature has so far reported that the degradation of AEMs is due to the removal of the ion-carrying functional groups and not the graft monomer [21, 24, 26, 63, 78, 140, 155, 174]. This research is the first to report that the degradation of the AEMs is not only due to the removal of the functional group, but also attributed to the loss of the benzene ring, namely vinylbenzyl chloride, in the AEMs we have synthesised and investigated. Such findings will have a significant implication on the way we design and fabricate AEMs in order to obtain excellent thermal and chemical stability properties.

# CHAPTER 2
# METHODOLOGY

## 2.1 Materials

Low-density polyethylene films were sourced from two suppliers, namely, British Polythene Industries plc and VWR International. The ETFE film was procured from Nowoflon Kunststoffprodukte GmbH while the high-density polyethylene film was obtained from Metal Box Co. All commercial polymer films were used as received. Poly(vinylbenzyl chloride) (60/40 mixture of 3- and 4-isomers, $M_n$ = 55000, $M_w$ = 100000), vinylbenzyl chloride (mixture of 3- and 4-isomers, 97%), 1,4-diazabicyclo[2.2.2]octane, trimethylamine (45% in water) and N-methylpiperidine were acquired from Sigma-Aldrich while 1-azabicyclo[2.2.2]octane was purchased from Alfa Aeser. Deuterium oxide (99.8 atom % D) was purchased from Acros Organics. Toluene solvent, potassium hydroxide pellets, acetone, sulfuric acid, methanol and sodium chloride were all analytical reagent grade and were used as received.

## 2.2 Anion exchange membrane preparation

The AEMs were synthesised as previously discussed in Part I using low-density polyethylene (LDPE), high-density polyethylene (HDPE) and ethylene-tetrafluoroethylene (ETFE) as base polymers immersed in a vinylbenzyl chloride (VBC) monomer. PE-g-VBC copolymer was prepared with LDPE film (20 to 130 µm thickness) immersed in 31:26:43 ratios by volume VBC/toluene/methanol via mutual gamma radiation grafting while ETFE-g-VBC was produced utilising electron beam as radiation source. The samples were sent to Synergy Health plc (Wiltshire, UK) and irradiation was carried out for a predetermined time and known dose rate. The obtained grafted copolymers were then washed thoroughly with acetone to completely remove VBC homopolymers. To produce the AEM, a selection of several amines were utilised to impart functionality to the PE-g-VBC copolymer (Table 2.1). Scheme 2.1 shows an idealised schematic of the preparation of polyethylene-based AEM functionalised with TMA.
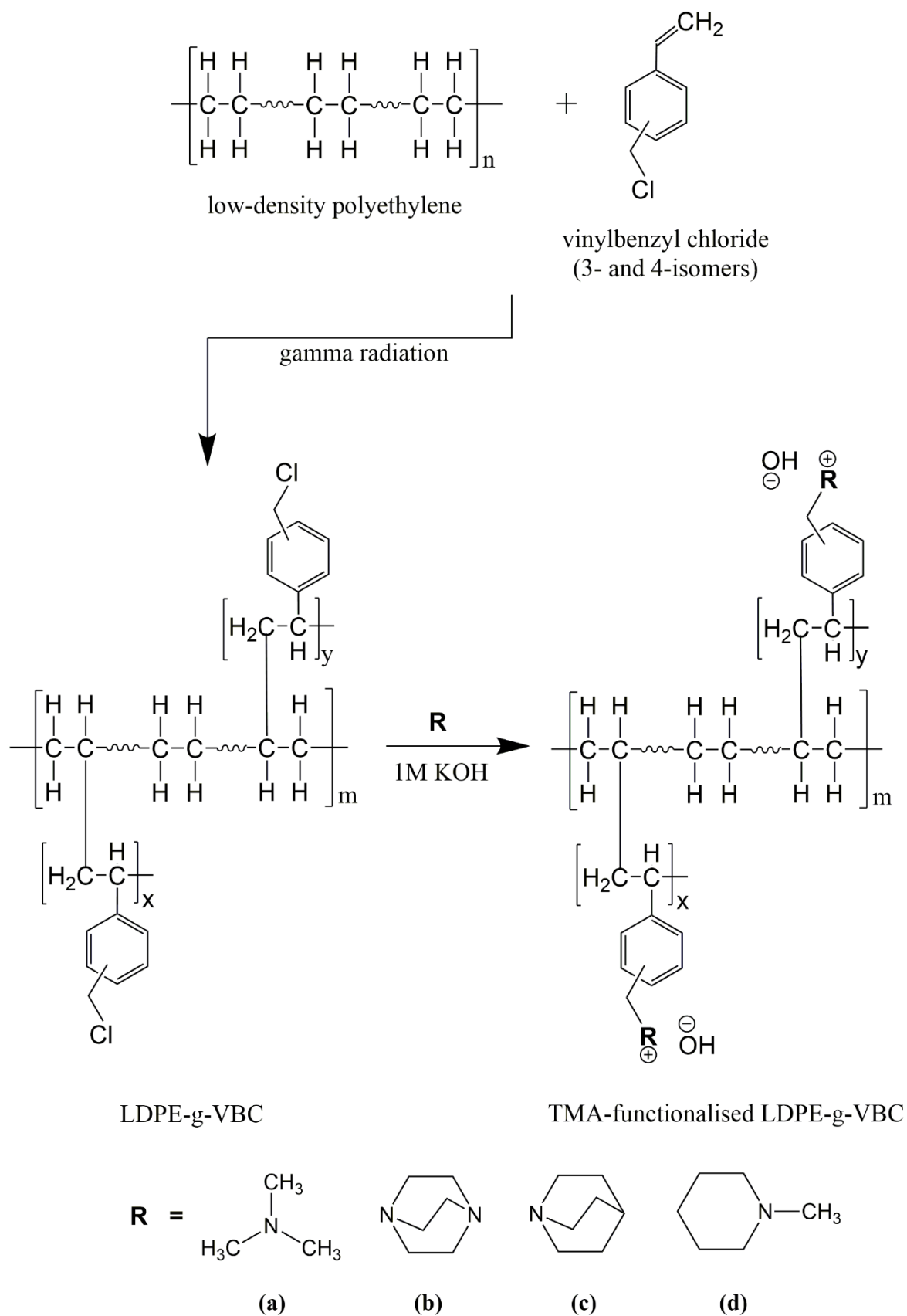
Scheme 2.1. Synthesis of LDPE-based AEM functionalised with different amine head groups.

Table 2.1. Functionalisation of LDPE-g-VBC with different amines.

| Name | Functional Group | Condition* |
|---|---|---|
| (a) TMA | Trimethyl amine | 7.6 M solution at room temperature |
| (b) DABCO | 1,4-diazabicyclo[2.2.2]octane | 1 M solution at 60 °C |
| (c) ABCO | 1-azabicyclo[2.2.2]octane | 1 M solution at 60 °C |
| (d) NMP | N-methylpiperidine | 8.2 M solution at 60 °C |

*All copolymers were functionalised for 72 h.


## 2.3 Membrane stability tests

### 2.3.1 Membrane stability test under vapour phase condition

The LDPE-g-VBC functionalised with TMA was converted to OH⁻ form in sealed bottles at room temperature. The membrane was washed several times with deionised water prior to conductivity measurement following the procedure stated earlier. Conductivity measurements were made at 40, 50, 60, 70 and 80 °C taking note to obtain a stable conductivity reading at each temperature regime before shifting to a higher temperature.

### 2.3.2 Membrane stability test under liquid phase (deionised water) condition

#### 2.3.2.1 Stability test of PVBC–TMA copolymer

The stability of the poly(VBC)–TMA copolymer was initially assessed. A precalculated amount of PVBC was dissolved in a Petri dish with a small amount of tetrahydrofuran (THF) and mixed thoroughly until homogenous. The PVBC was allowed to dry at room temperature to remove the THF solvent, after which, it was immersed in TMA for 72 h. The PVBC-TMA copolymer was then allowed to dry and was subsequently placed in a vacuum oven to completely remove excess TMA. The solid PVBC-TMA copolymer was dissolved in deuterium oxide ($D_2O$) and a measured amount of KOH pellets were added to obtain a 0.4 M alkaline solution. The PVBC–TMA solutions were then placed inside a water bath at 60 °C for 1440

h.  The PVBC–TMA solutions for every 720 h interval were then submitted for analysis. An initial solid PVBC-TMA copolymer was set aside for comparison.

### 2.3.2.2 Stability test of PE–g–VBC copolymer and the un-exchanged functionalised membrane

The PE–g–VBC copolymer and the functionalised membrane ($Cl^-$ form) were immersed in deionised water in sealed bottles and were placed inside a water bath at 60 °C for three months (2160 h).  The ion-exchange capacity (IEC) of the TMA- and DABCO-functionalised membranes before and after the stability test were measured and compared.

### 2.3.2.3 Stability test of $OH^-$ exchanged membranes with different head groups

Functionalised AEMs were treated with 1.0 M KOH solution for 20 min.  The solution was then replaced with fresh 1.0 M KOH solution and the process was repeated until a total $OH^-$ exchange time of 1 h was achieved to ensure complete exchange of chloride ions to hydroxide ions. The membrane was then washed with copious amount of deionised water to remove residual hydroxide ions. Removal of excess $OH^-$ ions was confirmed by using pH paper.  $OH^-$ exchanged membranes were then placed in sealed bottles immersed in deionised water and were placed inside the water bath.  Stability tests were performed with varying temperature and degradation time.

### 2.3.2.4 Stability of $OH^-$ exchanged membranes under oxygen and nitrogen gas feed

The $OH^-$ exchanged TMA-functionalised membrane was immersed in $D_2O$ inside a sealed polypropylene bottle placed in water bath at 60 °C.  A continuous feed of oxygen gas was supplied.  A similar setup was prepared but with nitrogen gas feed instead.  After the stability test for 1440 h, both the membrane and the $D_2O$ solution were sent for analysis.

## 2.4 Characterisation of the membrane and the degradation products

### 2.4.1 Measurement of the ion-exchange capacity

The ion-exchange capacity (IEC) of each membrane was measured using acid-base titration. Membranes were treated with fresh 1.0 M KOH solution every 20 min for three times (total OH$^-$ exchange time of 1 h) to completely exchange the chloride ions with hydroxide ions. The membrane was then washed with a copious amount of deionised water to remove residual hydroxide ions. Removal of excess OH$^-$ ions was confirmed by using pH paper. The membrane was subsequently immersed in a known volume of 1.0 M NaCl solution and was left to stand overnight. The liberated hydroxide ions were then titrated with 0.10 M H$_2$SO$_4$ solution using Titrette GMBH bottle-top digital burette and the endpoint was determined visually using methyl red indicator. After titration, the membranes were washed with deionised water to completely remove the salt and dried using an MTI Model DZF-6020-FP vacuum oven. Measurements of the weight were performed until no change in the dry weight remained. The IECs were computed using the amount of OH$^-$ ions neutralised, expressed in mmol, divided by the dry weight of the membranes, in grams.

### 2.4.2 Measurement of the ionic conductivity

The membranes were OH$^-$ exchanged using 1.0 M KOH solution for initial 20 min. The solution was then replaced with fresh 1.0 M KOH solution and was allowed to exchange for another 20 min. The process was repeated until a total OH$^-$ exchange time of 1 h was achieved. The membranes were thoroughly washed with deionised water. Removal of excess OH$^-$ ions was confirmed by using pH paper. Each membrane was then sandwiched between two Freudenberg FCCT H2315-C2 gas diffusion layer carbon electrodes and was placed in a gold-plated titanium test cell. The environment inside the test cell was maintained at atmospheric pressure and the humidifier temperature was set to ensure 100% relative humidity inside the cell. The relative humidity inside the fuel cell was verified using a Vaisala HUMICAP humidity sensor. The through-plane conductivity was measured using a four-point technique with each probe placed on either side of the membrane. The impedance was measured using an N4L NumetriQ PSM 1735 Frequency Response Analyser within the frequency range of 200 to 20 kHz with a perturbation voltage amplitude

of 15 mV. Three readings of the impedance in 5 min intervals were made and the average was reported. Consequently, the conductivity of the membrane was computed based on the following formula:

$$\sigma = \frac{4L}{R(\pi d^2)} \qquad (16)$$

where σ is the hydroxide ion conductivity, L is the membrane thickness, R is the resistance derived from the impedance value at zero-phase angle and d is the diameter of the membrane test area.

### 2.4.3 Chemical analysis

The following were the equipment utilised to characterise the membrane before and after the stability test and the resulting degradation products.

### 2.4.3.1 Scanning electron microscopy (SEM) analysis

SEM analysis was performed using JEOL JSM-5300LV equipment.

### 2.4.3.2 Nuclear Magnetic Resonance (NMR) spectroscopy

Solid-state ($^{13}$C and $^{15}$N) NMR analysis employing magic-angle spinning with cross-polarisation (CP-MAS) of the AEMs before and after degradation and the resulting degradation products were performed using tetramethylsilane (TMS) and nitromethane as chemical shift references, respectively. For the solid-state $^{17}$O NMR analysis of the membrane, direct-excitation (DE-MAS) was employed with water as the chemical shift reference. All solid-state ($^{13}$C, $^{15}$N and $^{17}$O) NMR spectra obtained with two-pulse phase-modulated (TPPM) decoupling were acquired using a Varian VNMRS spectrometer of the EPSRC National Solid-State NMR Service in Durham University, UK. The enriched water-$^{17}$O (70 - 75.9 atom % $^{17}$O, Aldrich) was used to prepare 0.1 M NaOH solution in a glove box by adding the appropriate amount of Na and then the membrane was immersed in the solution for 1440 h at 60 °C. The membrane was then rinsed with deionised water and dried under vacuum at 50 °C. Similarly, the isotope-labelled degradation solution was subjected to solution NMR analysis using a Bruker 500 Avance III HD spectrometer to obtain the $^{17}$O NMR spectra.

The $^1$H and $^{13}$C NMR spectra of the other degradation solutions were obtained using the same Bruker 500 Avance III HD NMR spectrometer operating at 500.15 MHz with TMS as the chemical shift reference.  All solution and solid-state NMR spectra were processed using MestReNova 11.0 (Mestrelab Research S.L.) software.

### 2.4.3.3 Fourier-transform Infrared (FTIR) spectroscopy

Determination of chemical structure and presence of functional groups were performed using a Varian 800 FTIR Spectrometer at scan range of 4000 to 500 cm$^-$$^1$ equipped with Pike Technologies diamond crystal plate Attenuated Total Reflectance (ATR) unit.

### 2.5 Membrane stability of commercial membrane

A commercially procured AEM (A201, Tokuyama Corp.) was subjected to similar stability test for 720 and 1440 h degradation period.  The aged membrane was characterised in terms of IEC and ionic conductivity.  The ionic conductivity of the A201 membrane was measured (a) using a four-point probe technique in a fuel cell under fully humidified gas stream and (b) using an electrolyser cell for 5 days with circulating alkaline electrolyte (0.5 M NaOH) operating at atmospheric pressure.

# CHAPTER 3
# RESULTS AND DISCUSSION

## 3.1 Membrane stability under vapour phase condition

The stability of the LDPE-g-VBC membrane (71.3% DOG) was investigated in terms of ionic conductivity in vapour phase condition for a total of 4800 h. The test was performed with a stepwise increase in temperature from 40 to 80 °C wherein a stable conductivity reading was obtained before shifting to the higher temperature. The plot of membrane conductivity for different temperature regime is shown in Figure 3.1. The observed fluctuations in the conductivity data at 80 °C were due to regular replenishment of deionised water into the humidifier.
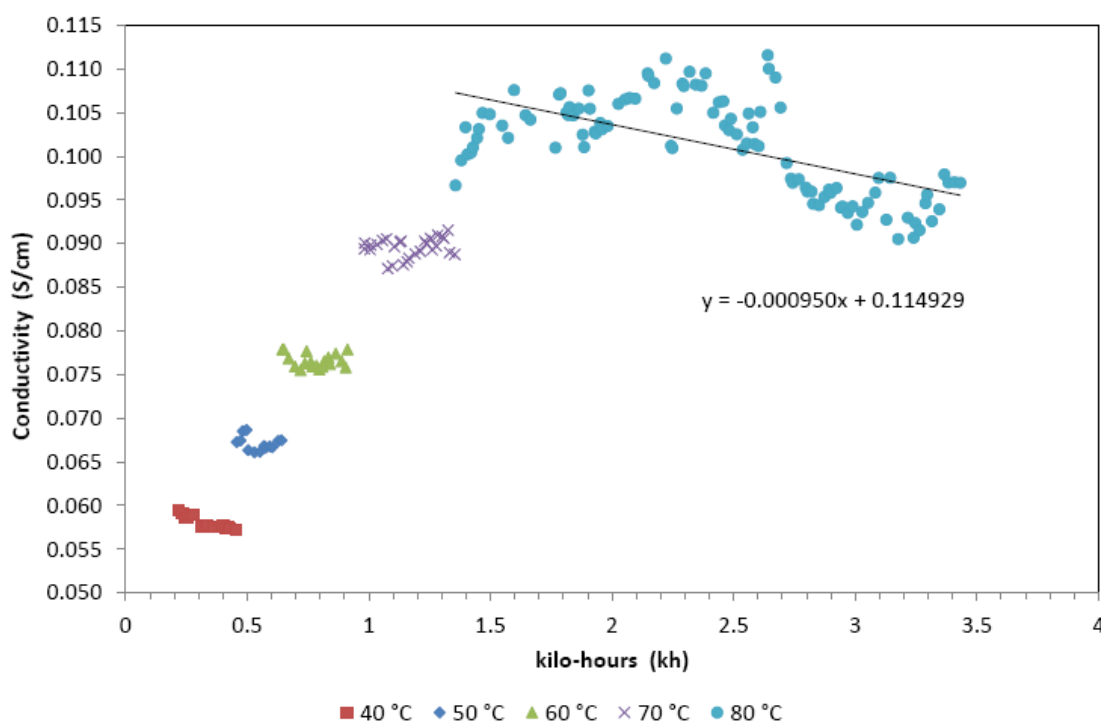


Figure 3.1. Through-plane conductivity of LDPE-g-VBC membrane (71.3% DOG) with increasing temperature under nitrogen.

As expected, the conductivity of the membrane increased with increasing cell temperature from 0.06 to 0.11 S cm$^{-1}$ peak conductivity. At the highest temperature of 80 °C, the conductivity was extremely stable at an average ca. 0.11 S cm$^{-1}$ for a 2000 h continuous run under nitrogen with a degradation rate of 5.7 mS kh$^{-1}$. At a

conductivity cut-off point of 0.02 S cm$^{-1}$ for the membrane, the estimated life time under nitrogen would be 2 years. This demonstrated that the produced membrane exhibited superb stability considering the fact that the membrane was subjected to a harsh test temperature of 80 °C.  Typical alkaline fuel cells usually do not operate above 50 °C because of dehydration which results in faster degradation [175].  Thus it is expected that the calculated life time of the produced membrane will be significantly longer at 50 °C.

After obtaining a stable conductivity of the membrane for 3300 h under nitrogen, the gas feed was changed to oxygen at the same temperature of 80 °C to determine its effect on membrane stability.  On a closer look at the data shown in Figure 3.2, it can be seen that the conductivity gradually and continuously decreased from around 0.10 to 0.07 S cm$^{-1}$ in 1000 h resulting in an average degradation rate of 24.3 mS kh$^{-1}$.  At a conductivity cut-off point of 0.02 S cm$^{-1}$ for the membrane, the estimated life time under oxygen would be 5 months operating under 80 °C.
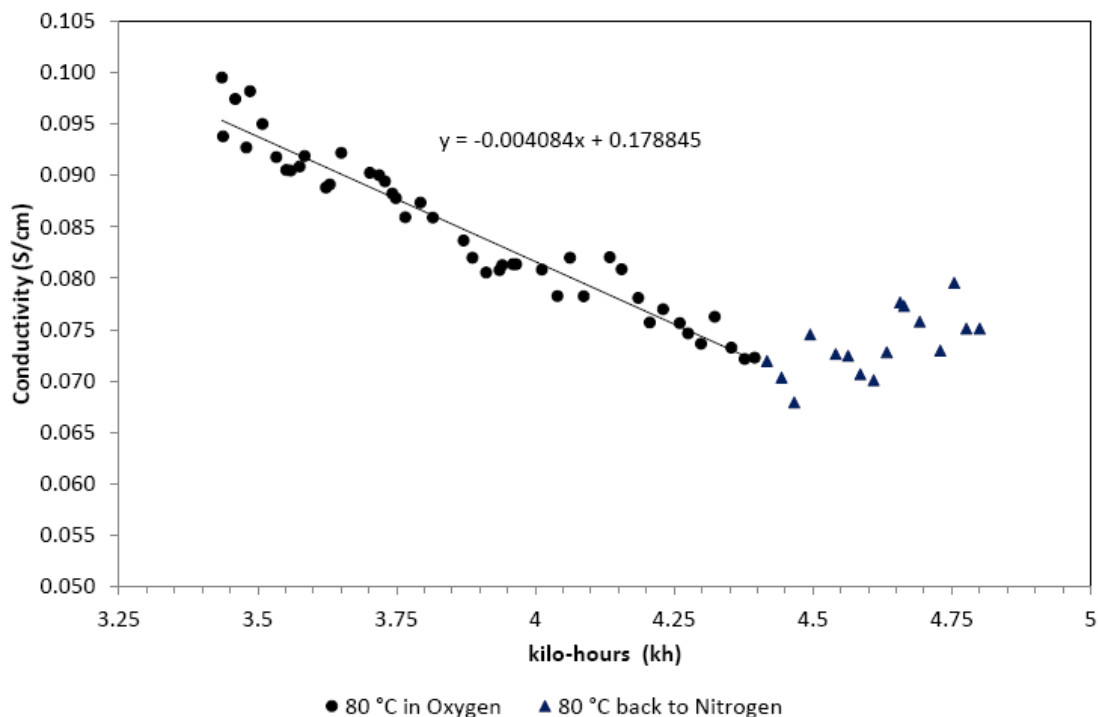


Figure 3.2. Degradation of LDPE-g-VBC membrane (71.3% DOG) under oxygen gas feed at 80 °C.

The results indicate that the degradation rate in terms of ionic conductivity is around 4 times faster in oxygen than in nitrogen gas stream. After the 1000 h period, the gas feed was reverted to nitrogen to check whether the conductivity decline of the membrane will stop. It can be observed from Figure 3.2 that the decrease in conductivity was abated but the membrane did not recover its original high conductivity. It can be concluded that membrane degradation caused by oxidation was permanent.

## 3.2 Stability of PVBC–TMA polymer

The stability test of the PVBC–TMA polymer was performed to assess the stability of the membrane components prior to AEM fabrication. In this way, the effect of the base polymer on the degradation can be isolated from the PVBC-TMA. $OH^-$ exchanged PVBC–TMA in excess alkaline solution were subjected to degradation test for every month (720 h) interval. Figure 3.3 shows the $^{13}C$ solution-NMR spectra of the PVBC–TMA polymer after 1440 h degradation test.
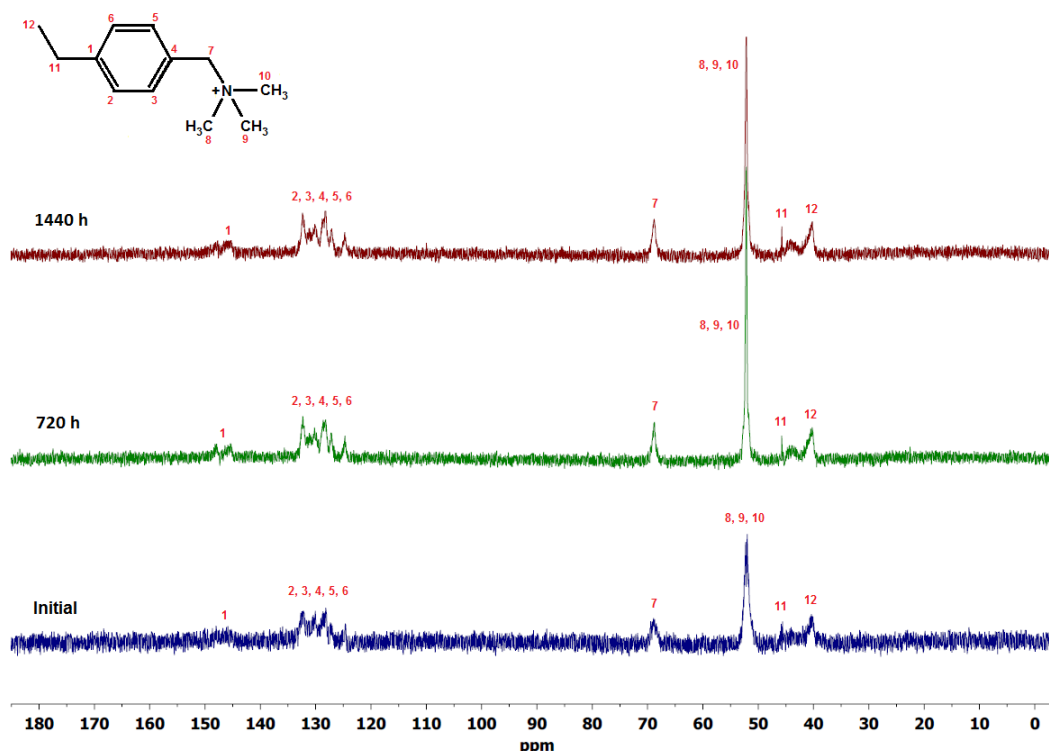


Figure 3.3. The $^{13}C$ solution-NMR of PVBC–TMA polymer after 720 and 1440 h degradation test at 60 °C.

The $^{13}C$ solution-NMR of PVBC–TMA polymer (Figure 3.3) shows the same resonance peaks after every 720 h degradation period when compared with the initial polymer. There were no new peaks detected indicating no by-products formed and confirmed the stability of PVBC–TMA after 1440 h degradation test.
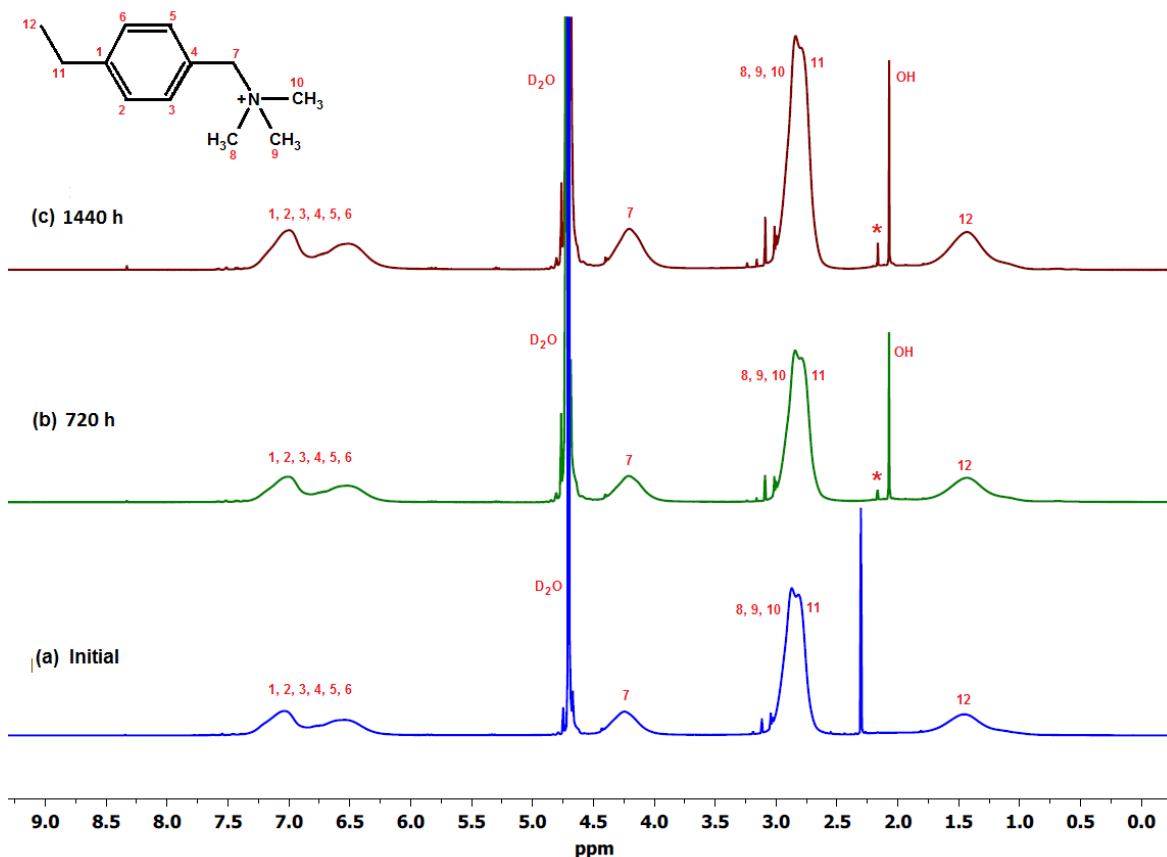


Figure 3.4. The $^1H$ solution-NMR of PVBC–TMA polymer after 720 and 1440 h degradation test at 60 °C.

Similarly, the same PVBC–TMA polymer was subjected to $^1H$ solution-NMR as shown in Figure 3.4. The $^1H$ solution-NMR spectra shows a similar set of resonance before and after degradation test confirming the stability of the polymer. The observed upfield shift of peak from 2.30 ppm of the initial to 2.08 ppm of that after 720 and 1440 h degradation test could be due to the unexchanged (Cl⁻ form) and exchanged (OH⁻ form) of the un-attached TMA in the solution, respectively.

### 3.3 Stability of LDPE–g–VBC copolymer and the fabricated membrane

The stability of the fabricated membranes was assessed by measuring the IEC of the unexchanged (Cl⁻ form) membranes before and after immersing the membranes in deionised water at 60 °C for 3 months (2160 h).  Table 3.1 indicates the stability of the synthesised membranes having the same degree of grafting (DOG) wherein IEC did not change after the stability test.  Both the DABCO- and TMA-functionalised membranes in their unexchanged (Cl⁻) forms were found to be stable at 60 °C for 2160 h.  The solutions wherein the membranes were immersed were also oven dried and no solid precipitates were recovered indicating that there was no degradation of the membrane.

Table 3.1.  The IEC of membranes (Cl form) immersed in deionised water at 60°C.

| DOG (%) | Functionality | IEC (mmol g$^{-1}$) | |
| --- | --- | --- | --- |
| | | Initial | After 2160 h |
| 65.5 | DABCO-functionalised | 2.2 | 2.2 |
| | TMA-functionalised | 2.8 | 2.8 |

### 3.4 Effect of initial base polymer (LDPE) thickness

Varying thicknesses (20 to 130 μm) of the LDPE base polymer films were subjected to a 2000 Gy hr$^{-1}$ gamma radiation dose rate (total dose of 2 kGy) which resulted in a ca. 65.5% degree of grafting (DOG) for all LDPE-g-VBC copolymer produced.  The AEMs were subsequently prepared by functionalising the copolymer with TMA and DABCO.  The TMA- and DABCO-functionalised AEMs prepared from different initial LDPE base polymer thickness were then subjected to stability test and the initial IECs of the membranes and the IECs after 1440 h in deionised water at 60 °C are shown in Tables 3.2 and 3.3, respectively.  It is observed that using varying thickness of LDPE base polymer showed insignificant effect on the measured IEC of the resulting membrane at essentially constant DOG of 65.5%. This is due to the use of high VBC concentration during radiation grafting which enhances monomer mass transport through the LDPE base film coupled with a high dose rate of 2000 Gy hr$^{-1}$ [114].  However, the measured initial membrane IECs of

ca. 2.7 and ca. 2.3 mmol g$^{-1}$ for TMA- and DABCO-functionalised membranes, respectively, indicates influence of the nature of the tethered functionality to the IEC. DABCO cannot effectively penetrate the structure of the LDPE-g-VBC copolymer due to its bulkier structure compared with TMA [157], thus DABCO shows lower initial IEC.

Table 3.2. IEC profile of TMA-functionalised AEM with varying initial LDPE thickness.

| Initial LDPE thickness (µm) | IEC (mmol g$^{-1}$) | | | % IEC loss |
|---|---|---|---|---|
| | Initial | After 720 h | After 1440 h | |
| 20 | 2.7 | 2.5 | 2.2 | 18.3 |
| 30 | 2.8 | 2.7 | 2.4 | 14.2 |
| 50 | 2.8 | 2.6 | 2.5 | 9.1 |
| 75 | 2.7 | 2.6 | 2.5 | 5.5 |
| 130 | 2.9 | 2.8 | 2.5 | 11.1 |

The TMA-functionalised membranes showed a decrease of IEC after 720 h degradation test and further decreased after 1440 h, for all membranes regardless of the initial LDPE base film thickness. This could indicate either deactivation of the tethered functional group (i.e. exchange with carbonates and/or other competing ions with OH$^-$) or detachment of the functional group responsible for the transfer of charge from the AEM backbone. A linear relationship of the decrease in IEC from the initial, to 720 h and then further to 1440 h is observed for all TMA-based AEMs investigated. However, from the initial IEC of ca. 2.7 mmol g$^{-1}$, membranes with thicker initial LDPE base film (50 to 130 µm) ended up with similar IEC of 2.5 mmol g$^{-1}$ after 1440 h degradation test, slightly higher than those of thinner initial LDPE films, 20 and 30 µm, of 2.2 and 2.4 mmol g$^{-1}$, respectively. This suggests that even though membranes have the same initial DOG and IEC, thinner membranes degrade faster than thicker ones. This is due to ease with which the membrane structure can be attacked because of its thinner cross-section.

Table 3.3. IEC profile of DABCO-functionalised AEM with varying initial LDPE thickness.

| Initial LDPE thickness (μm) | IEC (mmol g$^{-1}$) | | | % IEC loss |
|---|---|---|---|---|
| | Initial | After 720 h | After 1440 h | |
| 20 | | 2.1 | 1.9 | 18.2 |
| 30 | | 2.2 | 2.0 | 13.2 |
| 50 | 2.3 | 2.1 | 2.0 | 15.6 |
| 75 | | 2.1 | 2.0 | 12.7 |
| 130 | | 2.2 | 2.0 | 11.5 |

Similar with the TMA-based AEMs, the DABCO-functionalised membranes showed a decrease of IEC after 720 and 1440 h for all the membranes with varying initial LDPE film thickness as shown in Table 3.3. The same linear relationship of the decrease in IEC was observed, from the initial to 1440 h, though starting with a lower initial IEC of ca 2.3 mmol g$^{-1}$. After 1440 h degradation test, all the DABCO-functionalised membranes regardless of the initial LDPE base film thickness showed IEC of 2.0 mmol g$^{-1}$. Expectedly, the % IEC loss is essentially constant at average of 14%.

## 3.5 Effect of radiation dose rate

The IEC of the OH$^-$ exchanged aged TMA-functionalised membranes were measured after 1440 h and compared with their initial IECs as shown in Table 3.4. The initial IECs of the membranes varied as expected based on their DOG for each type of base polymer. The resulting DOG upon grafting is influenced by the applied dose rate and total radiation dose. With all of the other parameters remaining constant (i.e. VBC monomer concentration, amination time, and total radiation dose), a higher dose rate results in a higher DOG as more high energy radiation is supplied to grafting [114], which is observed in LDPE and HDPE (Table 3.4). The IEC of the membrane decreased after 1440 h of soaking in deionised water at 60 °C for all types of OH$^-$ exchanged AEM investigated. Such a decrease in IEC is an

indication of the loss of the functional groups that enable the transfer of charge.  The data further demonstrates that AEM with higher DOG exhibits slower degradation in terms of % IEC loss compared with that of AEM with lower DOG having the same type of base polymer.  This suggests that the degradation rate is limited by factors other than the functional group concentration (IEC).  This further suggests that there is a stability benefit as well as conductivity benefit from the use of membranes with high DOG for electrolyser/fuel cell application that is operating at a very low alkaline concentration.

The differences obtained in membrane DOGs are the direct result of the influence of the applied radiation dose rate (at the same total dose) during mutual radiation grafting.  It can be observed that the variation in % IEC loss is directly related to the dose rate used.  For example, LDPE-based AEM with a dose rate of 30, 35 and 67 Gy h$^{-1}$, exhibited % IEC loss after 1440 h of 37, 33 and 21%, respectively.  Similarly with the HDPE-based AEM, at dose rate of 30, 35 and 67 Gy h$^{-1}$, the % IEC loss observed after 1440 h was 50, 46 and 28%, respectively.  This leads to the conclusion that subjecting the base polymer to a higher dose rate will lead to a slower rate of degradation and hence to a more stable membrane.  Lower dose rates can cause oxidative degradation to the base polymer, which decreases the extent of crosslinking compared with subjecting the base polymer to high dose rates which is normally favourable [176, 177].  High dose rate treatment increases the degree of crosslinking of the base polymer, which provides structural strength and stability to the AEM [178, 179].  When polymers are exposed to ionising radiation, even at low doses, they often undergo structural changes accompanied by molecular cross-linking, grafting and chain-scission reaction.  It should however be mentioned that the highest total radiation dose (70 kGy for ETFE and 20 kGy for LDPE) used to fabricate the AEMs is still relatively low to cause substantial damage to the base polymer structure [102, 103, 180] and was confirmed  previously by FTIR (Figure 3.5, Part I) [114].  Furthermore, subjecting the polymer to a high dose rate quickly consumes available oxygen and thus effectively prevents any dissolved oxygen from penetrating into the polymer and causing undesirable side reactions as the time of high energy application is so short [176, 181].  Expectedly, when radiation grafting was performed with a very high dose rate of 2000 Gy h$^{-1}$, the AEM stability further improved with only 11% IEC loss over a 1440 h test.

Table 3.4.  The effect of mutual radiation grafting conditions on the IEC of TMA-functionalised membranes.

| Radiation source | Base polymer | Total dose (kGy) | Dose rate (Gy h$^{-1}$) | DOG (%) | IEC (mmol g$^{-1}$) | | IEC loss (%) |
|---|---|---|---|---|---|---|---|
| | | | | | Initial | After 1440 h | |
| Gamma radiation | LDPE | 10 | 30 | 32 | 1.6 | 1.0 | 37.5 |
| | | 10 | 35 | 58 | 2.4 | 1.6 | 33.3 |
| | | 10 | 67 | 68 | 2.8 | 2.2 | 21.4 |
| | | 20 | 2000 | 65 | 2.7 | 2.4 | 11.1 |
| | HDPE | 10 | 30 | 27 | 1.4 | 0.7 | 50.0 |
| | | | 35 | 58 | 2.6 | 1.4 | 46.2 |
| | | | 67 | 66 | 2.9 | 2.1 | 27.6 |
| Electron beam | ETFE | 70 | 400 | 29 | 1.3 | 1.1 | 15.4 |
| | | | | 37 | 1.5 | 1.3 | 13.3 |

Another important factor that should be considered is the effect of dose rate on the distribution and the length of VBC chains in the grafted polymer.  Ideally during simultaneous radiation grafting, each VBC unit should be attached to each of the polyethylene chain upon creation of a free radical (Scheme 3.1a) leading to very short length graft.  However, there is a competition between the grafting process and the VBC polymerisation.  After the initial VBC unit attached itself to the polyethylene backbone, subsequent VBC units attach to the VBC unit (VBC polymerisation) instead of the polyethylene chain (Scheme 3.1b) resulting in longer grafts.   Using higher dose rates will result in faster decay of radicals by recombination and consequently faster termination of the growing VBC chains. This results in a shorter VBC grafted chains due to a decrease in styrene concentration in the internal grafting layers [182, 183].    While at slow dose rates, VBC diffusion through the base polymer is sufficiently fast and the lifetime of the radicals formed is long enough to result in longer and fewer VBC chain grafts [184] i.e. faster dose

rates will result in better distributed VBC throughout the grafted polymer and more LDPE–VBC links and shorter VBC–VBC links for a given DOG (Scheme 3.1a).

There seems to be also an effect of the base polymer on the stability of the grafted AEM. While this effect is minimal compared with the dose rate effect, it is still significant. At similar grafting conditions (dose rate, DOG, etc.), the LDPE-based AEM showed a 25% slower degradation rate compared with that of HDPE across the studied dose rates. This might arise from the differences in the structural change, e.g. cross-linking, that the base polymer is undergoing under radiation. Since crosslinking takes place between carbon atoms in neighbouring chains or chain branches joining together with other branches of the chain, a highly branched polymer like LDPE is more amenable to crosslinking compared with a linear polymer like HDPE [65]. It has been shown that under our radiation dose (maximum of 20 kGy for LDPE/HDPE) i.e. below total dose of 100 kGy, LDPE polymer experiences significantly higher cross-linking under radiation than HDPE, with both approaching similar cross-linking values at 250 kGy [185]. Additionally, the highly branched LDPE provides more accessible grafting sites in comparison with HDPE (seen by higher DOG for the same grafting conditions) which could translate to better grafting distribution and consequently shorter grafts.

The large variation in grafting requirements of LDPE/HDPE (10 to 20 kGy) and that of ETFE (70 kGy) makes direct comparison of the degradation rate difficult. In the case of ETFE, membrane fabrication using gamma radiation as source did not produce high enough graft of VBC monomer [48]. ETFE-based membranes were then synthesised via electron beam radiation grafting since a high energy electron beam is capable of providing a higher dose rate [186]. At a dose rate of 400 Gy h$^{-1}$, ETFE-based AEM showed an IEC loss of 13–15% somewhere in the middle range of IEC loss of LDPE of 21% for 67 Gy h$^{-1}$ and 11% for 2000 Gy h$^{-1}$.
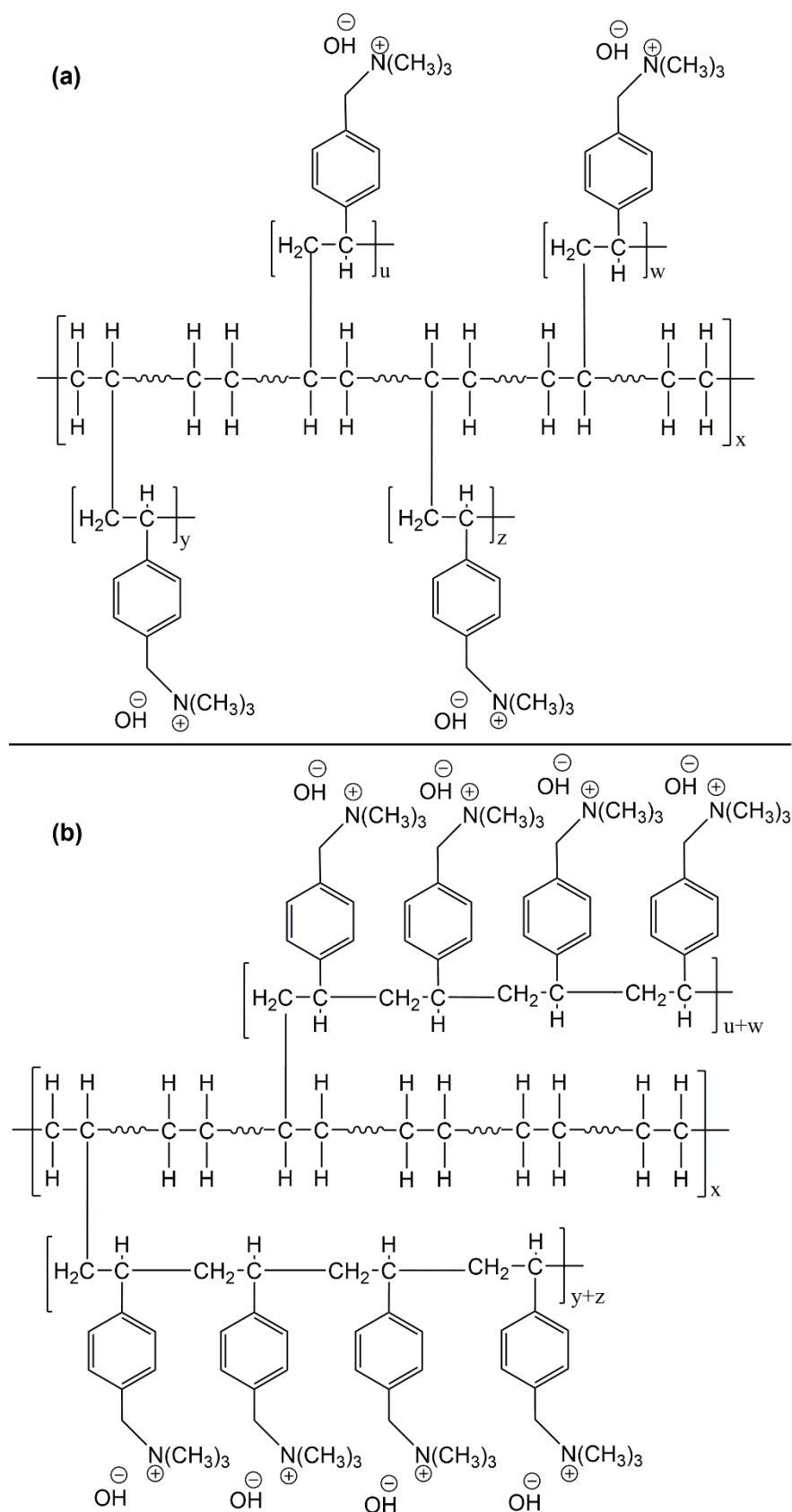
Scheme 3.1. Possible structures of functionalised AEM after radiation grafting.

## 3.6 Effect of functional head-group

Figure 3.5 shows the comparison in IEC drop of the membranes tethered with different amine functionalities having the same DOG of 65% (2000 Gy hr$^{-1}$). The TMA-functionalised membrane exhibited the highest initial IEC than other amine groups since TMA can more effectively penetrate the LDPE−g−VBC copolymer compared with other amine functional groups due to their bulkier structure. The lower IEC with the use of other amine functionalities is still acceptable, provided that the resulting membrane is more chemically and thermally stable [187].
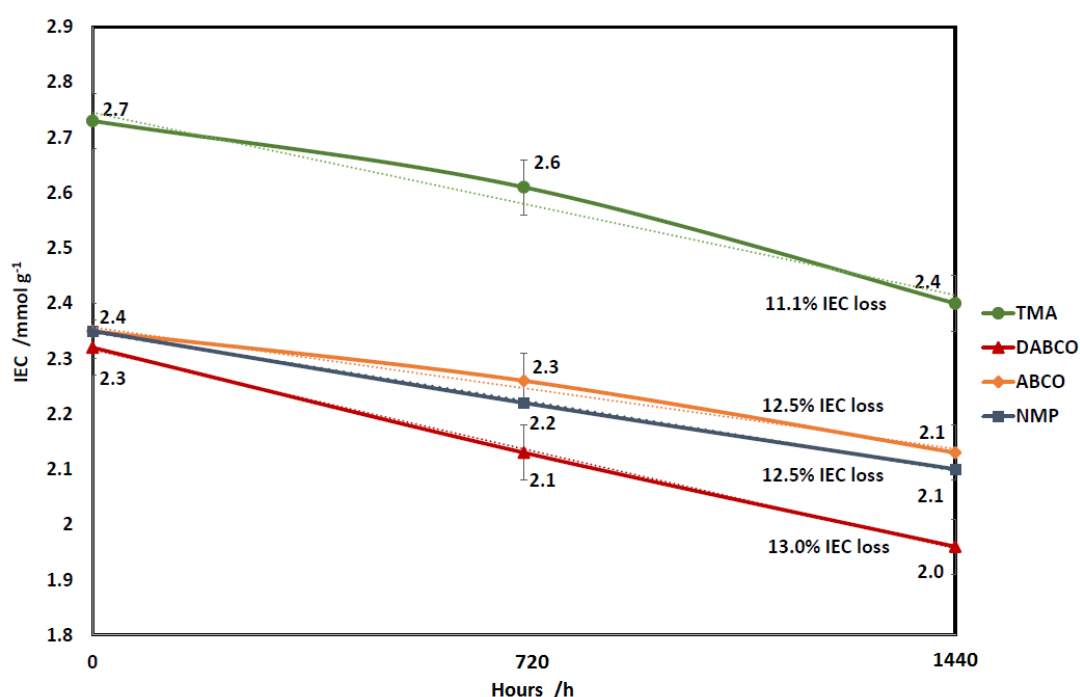


Figure 3.5. The IECs of membranes functionalised with different amines (2000 Gy h$^{-1}$, 65% DOG) after soaking in deionised water at 60°C.

The degradation rate for the membranes investigated were very similar, with IEC loss in the range of 11 to 13%. These results were obtained under neutral pH (deionised water) and not in highly alkaline media, where the hydroxide counter ions associated with the head group might not be able to start the nucleophilic attack leading to head group loss under Scheme 1.2 but rather could undergo reversible ylide reaction (Scheme 1.3). It can be seen that the degradation rate in our tests was less dependent on the head group in comparison with the accelerated tests on the head groups alone in high temperature and alkaline concentration (2M KOH at

160 °C) which showed much better stability of DABCO than TMA with half-time disintegration of 42 and 29 min, respectively [155]. It also suggests that the degradation mechanism under low alkaline concentration and relatively low temperature of 60 °C might be different to the mechanisms reported under accelerated testing using high alkaline concentrations and temperature using single monomer unit.

## 3.7 Effect of temperature and degradation time on the membrane stability

The effect of temperature on the degradation rate was studied where representative samples of AEM with varying base polymers (LDPE and HDPE, 35 Gy hr$^{-1}$ and ETFE, 400 Gy hr$^{-1}$; Table 3.4) were subjected to the stability test employing the same procedure but with increasing temperature and time (Table 3.5). There was negligible decrease in IEC at low temperature of 20 and 40 °C after 720 h period indicating that the AEMs are stable at temperatures up to 40°C. At 60 °C, a measurable decrease of IEC was recorded after 720 h period as discussed earlier.

Table 3.5. The IECs of membranes in deionised water soaked for different time intervals and temperatures.

| Base polymer | DOG (%) | Initial IEC (mmol g$^{-1}$) | IEC after 720 h (mmol g$^{-1}$) | | | IEC after 1440 h (mmol g$^{-1}$) |
|---|---|---|---|---|---|---|
| | | | 20 °C | 40 °C | 60 °C | 60 °C |
| LDPE | 58 | 2.4 | 2.3 | 2.2 | 2.0 | 1.6 |
| HDPE | 58 | 2.6 | 2.5 | 2.5 | 2.4 | 1.4 |
| ETFE | 37 | 1.5 | 1.5 | 1.5 | 1.4 | 1.3 |

## 3.8 Ionic conductivity of the initial and aged membranes

IEC is a measure of the concentration of the functional groups present to transfer the hydroxide ions and a higher IEC consequently results in a higher ionic conductivity. Loss of functional groups due to membrane degradation results in lowering its IEC and decreases its measured ionic conductivity.

Table 3.6 shows the through-plane ionic conductivity at 60 °C of HDPE-based membranes prepared under a radiation dose rate of 35 and 67 Gy h$^{-1}$, respectively. Degradation tests on the membranes after 1440 h revealed a decrease in ionic conductivity of the membrane (at 60 °C) by 37.0% (84 to 53 mS cm$^{-1}$) and 24.7% (101 to 76 mS cm$^{-1}$). Similarly, LDPE-based membranes showed a decrease in ionic conductivity (at 60 °C) of 19.0% (84 to 68 mS cm$^{-1}$) and 14.1% (99 to 85 mS cm$^{-1}$) for AEM with dose rate of 67 and 2000 Gy h$^{-1}$, respectively. The decrease in ionic conductivity agrees well with the observed decrease in IEC reported in Table 3.4 and confirms the earlier conclusion that membranes prepared under high radiation dose rate demonstrate slower degradation compared with using low dose rate. Furthermore, it also confirms that the degradation rate using LDPE-based AEM is lower compared with that of HDPE-based AEM using the same grafting conditions.

Table 3.6. Through-plane ionic conductivity at 60 °C of AEMs before and after 1440 h degradation test.

| Base polymer | Radiation Dose Rate (Gy h$^{-1}$) | Functionality | Average Ionic Conductivity (mS cm$^{-1}$) | |
| --- | --- | --- | --- | --- |
| | | | Initial | After 1440 h |
| HDPE | 35 | TMA | 84 | 53 |
| | 67 | | 101 | 76 |
| LDPE | 67 | TMA | 84 | 68 |
| | 2000 | | 99 | 85 |
| | 2000 | DABCO | 69 | 52 |

The TMA-functionalised membrane showed lower decrease in conductivity at 60 °C after 1440 h of 14.1% compared with the DABCO-functionalised membrane, which showed a decrease of 24.6% (using the same radiation dose rate of 2000 Gy h$^{-1}$). While both AEMs using TMA and DABCO showed the same % IEC loss after 1440 h, the bulkier structure of DABCO and its lower basicity (p$K_a$ = 8.72) compared with TMA (p$K_a$ = 9.81) (Table 1.2) results in lower conductivity at

similar DOG and IEC. This translates to a larger activation energy of DABCO-based AEM (Ea = 14 kJ mol$^{-1}$) for OH$^-$ ion conductivity and consequently larger effect of IEC decrease on ionic conductivity in comparison with TMA-based AEM (Ea = 12 kJ mol$^{-1}$) [29].

## 3.9 Scanning electron microscopy analysis

Figures 3.6a and 3.6b show the scanning electron microscopy (SEM) images of the surface and cross-section of the aged LDPE-based membrane prepared under 35 Gy h$^{-1}$ dose rate, respectively. The observed voids (bubbles) suggest that part of the polymer was lost and dissolved in the surrounding water during the degradation process leaving the void behind. This is most likely to be the grafted vinylbenzyl groups and not simply the functional head group alone.
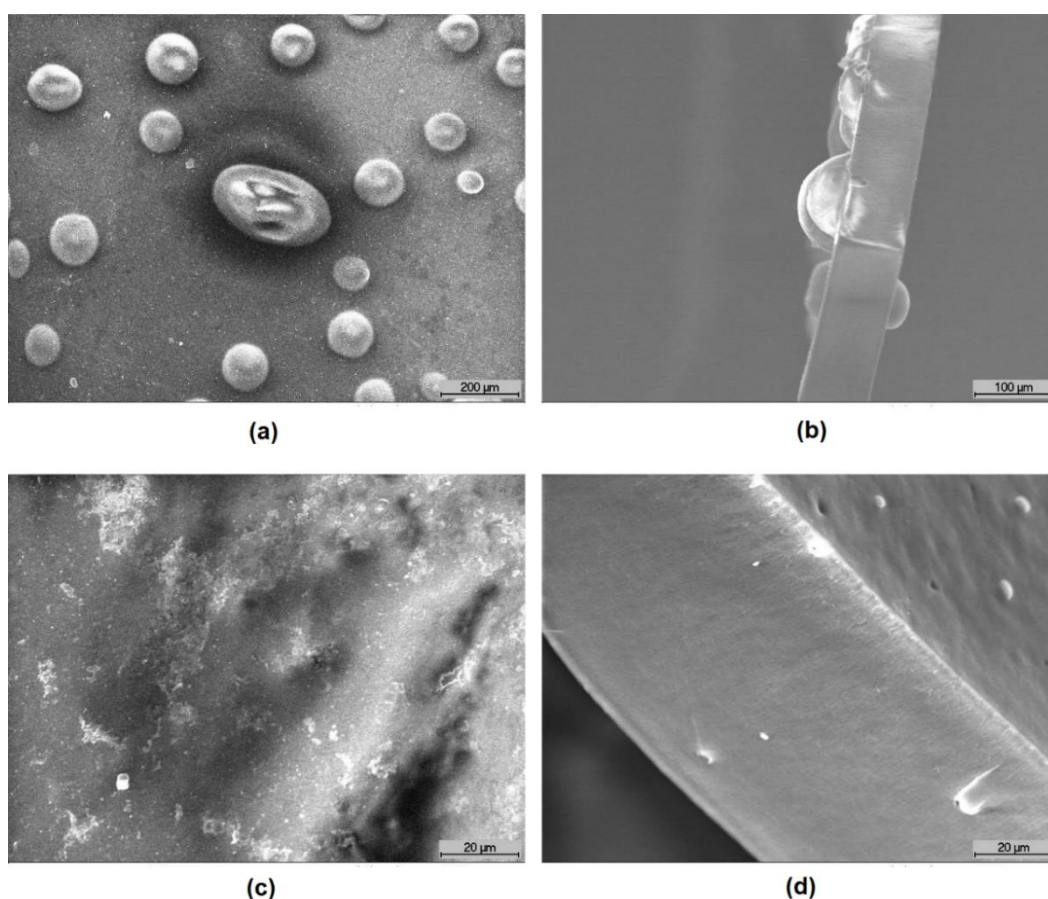


Figure 3.6. SEM micrographs of (a) surface at 100x and (b) cross-section at 200x magnification of the aged membrane prepared under 35 Gy h$^{-1}$ dose rate, and (c) surface and (d) cross-section at 1000x magnification of the aged membrane prepared under 2000 Gy h$^{-1}$ dose rate.

While polyvinylbenzyl trimethylammonium chloride or hydroxide is water soluble, the grafted LDPE–g–VBC–TMA–OH is not and the potential loss of polymer seen by the SEM must be caused by the degradation mechanism using OH$^-$ ion attack as such degradation/loss was not observed with LDPE–g–VBC–TMA–Cl (Table 3.1). It also suggests that at such dose rate, the VBC has relatively longer chains and is less distributed throughout the grafted polymer (for a given DOG). Hence, upon scission of the VBC–VBC link, long chains of water soluble vinylbenzyl trimethylammonium hydroxide are lost leaving the large void space observed behind. The image of the cross-section of the aged membrane seems to suggest that the degradation starts on the surface then progresses through the membrane.

Figures 3.6c and 3.6d show the surface and cross-sectional structure of an aged LDPE-based AEM prepared under higher radiation dose rate of 2000 Gy h$^{-1}$, respectively. SEM micrographs were taken at higher magnification (1000x) and the membranes were still visibly smooth and lacked any bubbles. This supports the earlier results concluding that mutual radiation grafting performed under high dose rate produces more stable AEMs compared with applying low radiation dose rate and suggests that the loss of VBC is more uniform in the structure. This can be explained by better distribution of VBC in the grafted polymer with shorter grafted chains and higher cross-linking resulting in less water soluble by-products. This will be discussed further below using various chemical analysis techniques.

## 3.10 NMR analysis of the aged membranes and the degradation products

Solid-state NMR spectroscopy was employed on both the original and the aged TMA- and DABCO-functionalised membranes (in OH$^-$ form stored in deionised water at 60°C for 1440 h) to determine the decrease of various chemical groups present as an initial attempt to identify the decomposition products (Figures 3.7 and 3.8). The $^{13}$C CP-MAS NMR peaks were observed to be broad, which is usually expected for polymers, while the intensities of the signals are not normally proportional to the number of equivalent $^{13}$C atoms (unlike $^1$H NMR) and are instead strongly dependent on the number of surrounding spins (typically $^1$H). This means for example, that the ratio of aromatic ring $^{13}$C peaks to that of LDPE $^{13}$C is lower than the estimated molar ratio value from the DOG. However, a decrease in that ratio under the same NMR test conditions (relaxation time, etc.) suggests a

decrease in the aromatic group content. The $^{13}$C CP-MAS NMR spectra obtained were normalised against LDPE peaks since the base polymer was not detected in the degradation products.

Comparison of the spectra of the initial and aged membranes revealed a decrease in the intensity ratio of the benzyl group to that of LDPE, which indicates a decrease in the amount of the particular group in the membrane structure [188]. Furthermore, no new signals were detected in both $^{13}$C and $^{15}$N CP-MAS NMR spectra suggesting no degradation by-products on the membrane surface had formed. This suggests that the degradation products are water soluble and can be identified in the solution.

Figure 3.7a shows the $^{13}$C CP-MAS NMR spectra of the initial and aged TMA-functionalised membrane (67 Gy h$^{-1}$, 68% DOG). The aromatic ring carbons (benzyl groups) give the resonance between 125 and 150 ppm. The signals between 190 and 220 ppm and the smaller broad signal between 55 and 85 ppm are spinning sidebands associated to the aromatic carbons. The CH–CH$_2$ groups resonate at 40-50 ppm, N(CH$_3$)$_3$ at 53 ppm and LDPE aliphatic carbons around 20 to 35 ppm. The 69 ppm resonance is assigned to the –CH$_2$N [47, 189, 190].

It is clear from the spectra that there are losses in the VBC and ammonium (TMA) group peak size. The results show 1:1 ratio of VBC to TMA loss wherein the percentage of the loss to their initial values after 1440 h degradation was ca. 30%. This agrees well with the observed loss of IEC of ca. 22% and indicates that the majority of the degradation is caused by the loss of the whole vinylbenzyl trimethylammonium hydroxide and not simply just the TMA head group. This is significant since all the proposed mechanisms in the literature involve loss of only the head group (TMA) and not the VBC groups. It was further observed that the ratio of VBC to TMA loss remained close to 1 using high radiation dose rate (2000 Gy h$^{-1}$, 66% DOG).

Figure 3.7b on the other hand, shows the $^{15}$N CP-MAS NMR spectra of the same LDPE-based AEM. The same quaternised nitrogen peak of TMA at -330 ppm [191] can be seen and no other resonance peaks were observed after degradation suggesting that no other nitrogen-containing by-products have formed on the membrane.
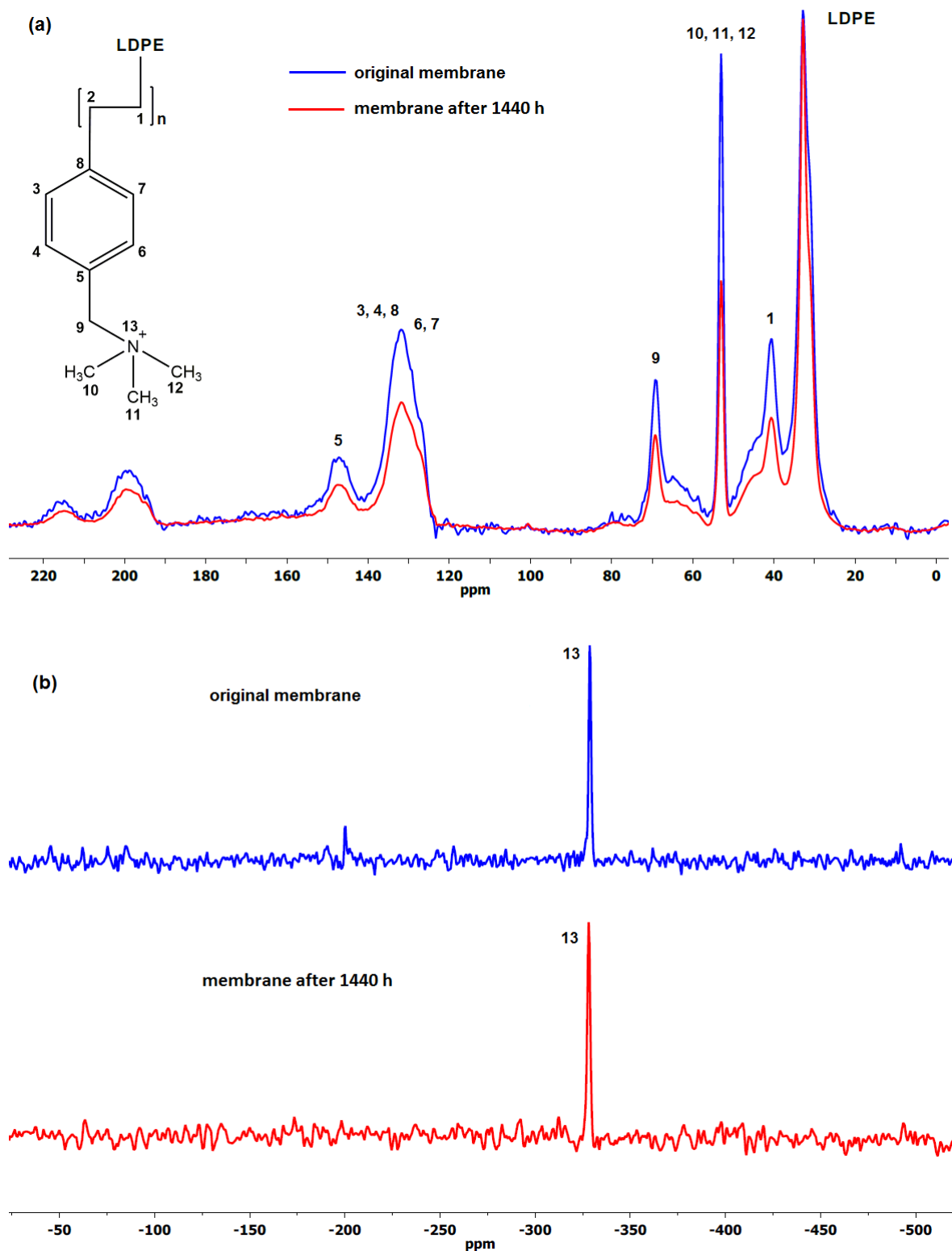
Figure 3.7. The (a) $^{13}$C and (b) $^{15}$N CP-MAS NMR spectra of the original and aged TMA-functionalised membrane (67 Gy h$^{-1}$, 68% DOG).

Similarly for the DABCO-functionalised membrane (2000 Gy h$^{-1}$, 65% DOG), the $^{13}$C CP-MAS NMR spectra shown in Figure 3.8a share common peaks with that of TMA-based AEM namely, the aliphatic carbon peaks of LDPE at 20 to 35 ppm and the aromatic carbons between 120 to 150 ppm. Total Suppression of Spinning Sidebands (TOSS) was employed during analysis in order to minimise the impact of the spinning sidebands. There are two strong peaks at 46 and 53 ppm representing the carbons attached to the unquaternised and quaternised nitrogen, respectively [192]. It can be seen that the sizes of both of those peaks are very similar suggesting equal amounts of unquaternised and quaternised nitrogen, i.e. mono-substituted DABCO which is supposed to offer better stability over double substitution [155]. After 1440 h degradation period, there is a marked decrease in the peak intensity at 40 ppm indicating loss of VBC, similar to what was observed with the TMA-functionalised membrane (Figure 3.7a). However, unlike the aged TMA-functionalised membrane, the results indicate VBC to DABCO loss of 1:2 ratio with loss to its initial values of ca. 15% which is in agreement with the observed IEC loss of 13% (Figure 3.5).

The resonance peak at -330 ppm in the $^{15}$N CP-MAS NMR spectra shown in Figure 3.8b is consistent with the quaternised nitrogen in the DABCO structure and the peak at -368 ppm can be associated with the unquaternised nitrogen, both present in the original and degraded membrane [193]. Furthermore, no other additional resonance peaks were observed. Unfortunately, the peaks in $^{15}$N CP-MAS NMR spectra cannot be integrated to quantify the relative loss of DABCO-nitrogen in both original and degraded membranes.
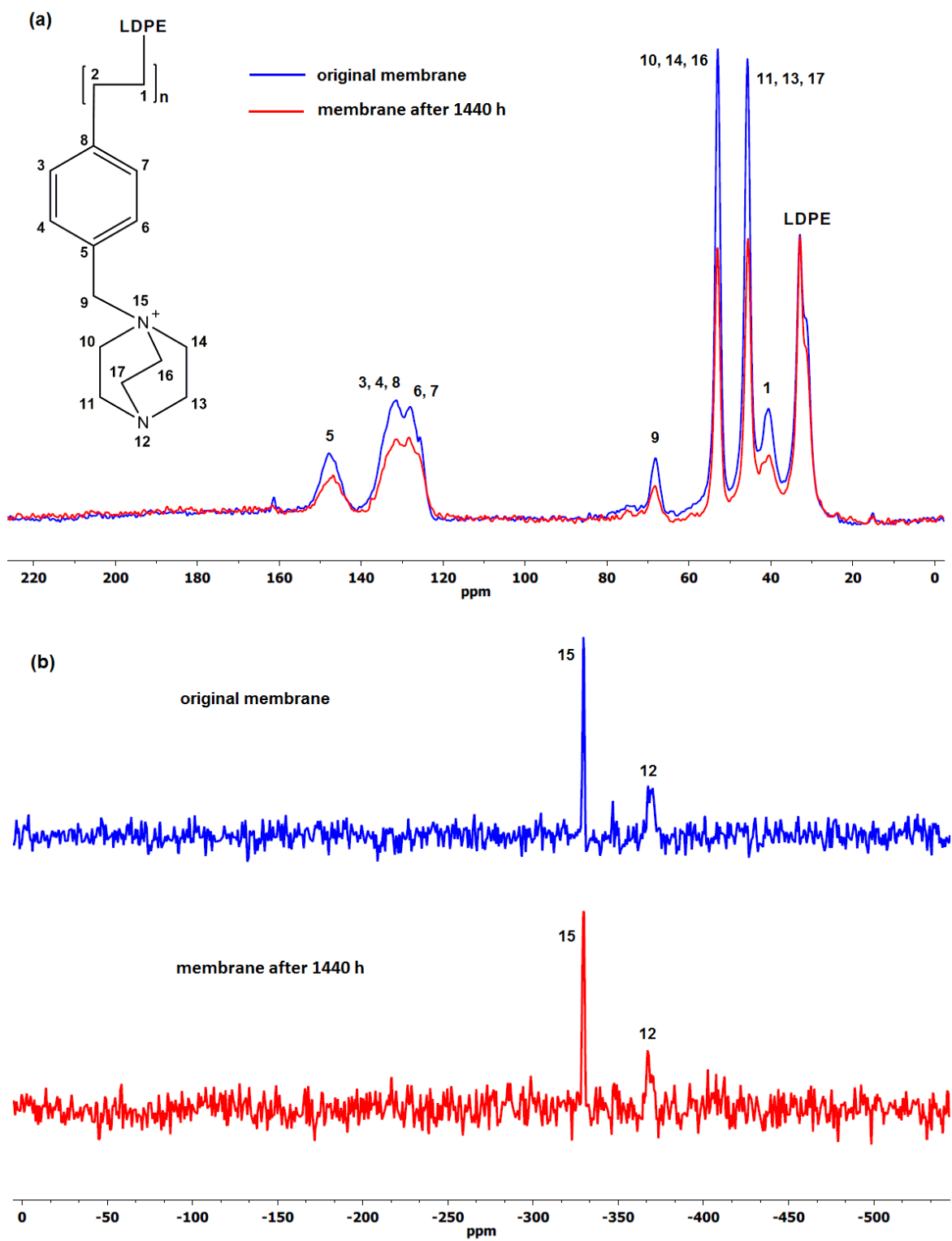
Figure 3.8. The (a) $^{13}C$ and (b) $^{15}N$ CP-MAS NMR spectra of the original and aged DABCO-functionalised membrane (2000 Gy h$^{-1}$, 65% DOG).

Nuclear magnetic resonance (NMR) has been the most commonly established method of analysing and monitoring degradation of ionomer membranes [159, 194, 195]. In order to shed more light on the role of OH⁻ ion on the degradation process, both solid-state and solution $^{17}O$ NMR spectroscopy were utilised in order to determine the presence of possible oxygen-containing compounds which could help elucidate the AEM degradation reactions [196]. The $^{17}O$ DE-MAS NMR spectra of the aged TMA-functionalised membrane revealed clear identifiable peaks even with a moderate signal-to-noise ratio that suggests oxidation of the aged membrane as shown in Figure 3.9a. Similarly, the water-$^{17}O$ solution wherein the isotope-labelled TMA-functionalised membrane had undergone degradation, was subjected to $^{17}O$ solution-NMR (Figure 3.9b). As expected, the spectra of the solution appear to show predominantly oxygen from $H_2^{17}O$ solvent and alkaline $^{17}OH^-$ ion [197], but also show other peaks indicating the presence of degradation products.

Experimental data obtained at 120 °C employing $Ag_2O$-mediated ion exchange reaction have verified mechanism (Scheme 1.2) indicating formation of a benzylic alcohol and release of TMA as predominant degradation products [173]. However, the presence of a benzylic alcohol cannot be ascertained from the $^{17}O$ NMR spectra (Figure 3.9) since its expected chemical shift (0.7 ppm) [198] is masked by the predominant oxygen resonance of $H_2^{17}O$ and $^{17}OH$. This can also be due to the conversion of benzylic alcohol to dibenzylic ether [161], whose possible presence can be attributed to the 127 ppm (C–O) and 48 ppm (–O–) resonances [199] (Figure 3.9a). Furthermore, the presence of carbonyl-containing (C=O) compounds [200] suggests that the benzylic alcohol, if present, is not the final form of the degradation product, but rather could have undergone subsequent oxidation reactions. Considering that the membrane was subjected to a degradation period of 1440 h at 60 °C, the benzylic alcohol by-product may have undergone auto-oxidation to produce aromatic aldehydes and/or other carbonyl compounds [201]. Aromatic aldehydes can readily transform to the corresponding carboxylic acid and/or benzylic peroxide radicals [202]. This benzylic peroxide radical could lead to a variety of side reactions, which may cause release of benzyl-TMA group from the membrane. The benzylic peroxide radical could have also been responsible for the oxidation of TMA indicated by the presence of N-oxide (N–O) groups (resonances at 409 and 500 ppm) [199] detected on the aged membrane

(Figure 3.9). The peak at 379 ppm (C=O) coupled with the single-bond O resonance at 127 ppm indicates the possible presence of an ester (–O–C=O) functionality [199], while the 242 ppm signal may arise from an anhydride [200]. In addition, the broad resonance at 170 ppm in the $^{13}$C CP-MAS spectra (Figure 3.10) and the FTIR signals at 1057 (□) and 1730 (▲) cm$^{-1}$ of the degradation products (Figure 3.12) provide further evidence of the presence of carbonyl-containing compounds indicating that either both the benzylic alcohol and TMA group might underwent subsequent oxidation and such auto-oxidation reactions could have caused the decrease in IEC of the membrane, or other peroxide radicals could have attacked the VBC-TMA group resulting in the observed carbonyl and N-oxide groups.
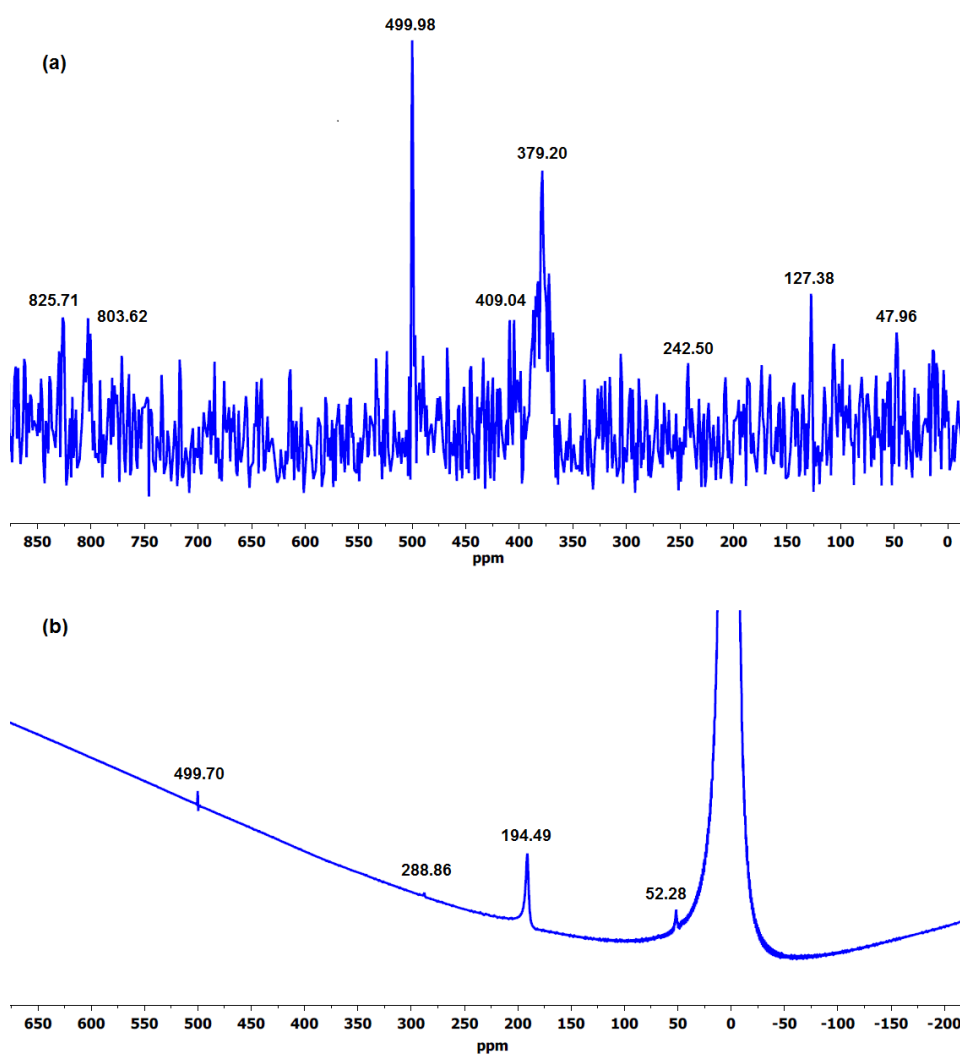


Figure 3.9. The (a) $^{17}$O DE-MAS NMR spectra of aged TMA-functionalised AEM and (b) $^{17}$O solution-NMR spectra of the degradation solution after stability test.

The presence of degradation products in the solution was confirmed by the detected resonance peaks as shown in Figure 3.9b. The peak at 194 ppm is attributed to peroxides (O–O) and/or soluble carbonate ($CO_3^{2-}$) compounds [203] present in the solution. There are also common peaks observed in both the solution and solid-state $^{17}O$ NMR spectra, such as the peak at 500 ppm indicative of oxidised TMA group (N–oxides) and the resonance at 52 ppm (–OH and –O– group) [204] suggesting the presence of similar functional groups in both the degradation solution and the aged membrane. However, further studies are required to identify all of the oxygen-containing products observed.

Figures 3.10 and 3.11a show the $^{13}C$ CP-MAS NMR spectra of the degradation products for both TMA- and DABCO-functionalised membranes after the stability test, respectively. The characteristic resonance of the aliphatic carbons of the base polymer between the 20 to 35 ppm range for the degradation products for both TMA- and DABCO-functionalised membranes is clearly absent, proving that the LDPE is not part of the degradation products. The strong peak at 53 ppm corresponding to the methyl groups in TMA and the resonance peaks within the 130 to 160 ppm region attributed to aromatic ring carbons are both present in the degradation product of the TMA-functionalised membrane (Figure 3.10). Furthermore, the peak at 69 ppm ($CH_2$–N) indicates that the benzyl–TMA groups were detached as a whole from the polymer backbone which is consistent with the observed 1:1 ratio of VBC to TMA loss between the original and aged membrane (Figure 3.7). Such loss of benzyl-TMA groups can explain the observed decrease in IEC and the large voids seen in SEM (Figure 3.6). This is in contrast with typically suggested elimination degradation mechanism which produces only TMA and/or methanol as proposed by-products [78, 147]. It should be stressed that the later mechanisms are typically suggested in high alkaline media. The broad resonance in the 170 ppm region indicates the presence of carbonyl groups (C=O) suggesting formation of oxidative degradation products discussed earlier. Unfortunately, an attempt to obtain a $^{15}N$ CP-MAS NMR spectra for the degradation product of the TMA-functionalised membrane was unsuccessful due to low absolute intensity of the carbon spectrum.
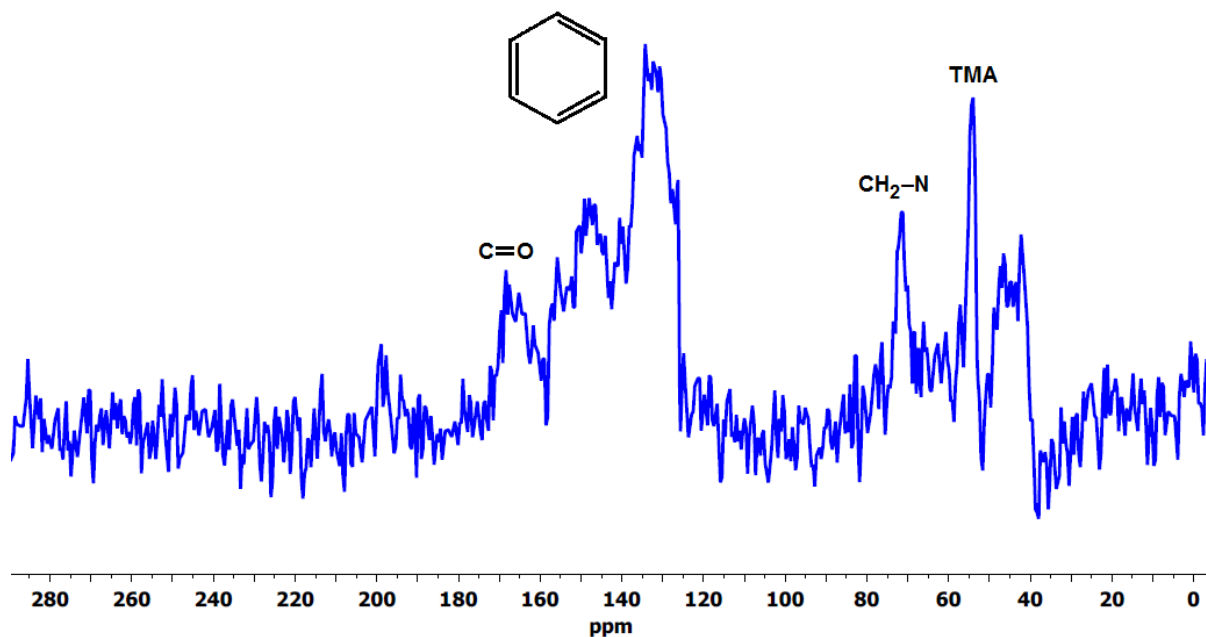
Figure 3.10. The $^{13}$C CP-MAS NMR spectra of the degradation products of TMA-functionalised membranes after stability test.

Unlike TMA, some of the DABCO upon detachment from the membrane were observed to recrystallise from the solution upon cooling to room temperature. DABCO was subsequently separated by centrifuge and was present predominantly in mono-quaternised form as indicated by the two strong carbon peaks at 45 and 53 ppm as shown in Figure 3.11a. Furthermore, the resonance at -330 ppm attributed to quaternised nitrogen in the $^{15}$N CP-MAS NMR spectra (Figure 3.11b) suggest the loss of benzyl trimethylammonium groups from the polymer backbone. The intense resonance of DABCO compared with weak VBC peaks indicates presence of DABCO in excess than VBC in the degradation product which is in agreement with the 1:2 ratio of VBC to DABCO loss as observed in Figure 3.8a. Since the prepared DABCO-functionalised AEM is largely mono-quaternised (weak -368 ppm resonance, Figure 3.8b), the unquaternised nitrogen is expectedly too weak to be detected in the degradation products. (Figure 3.11b).
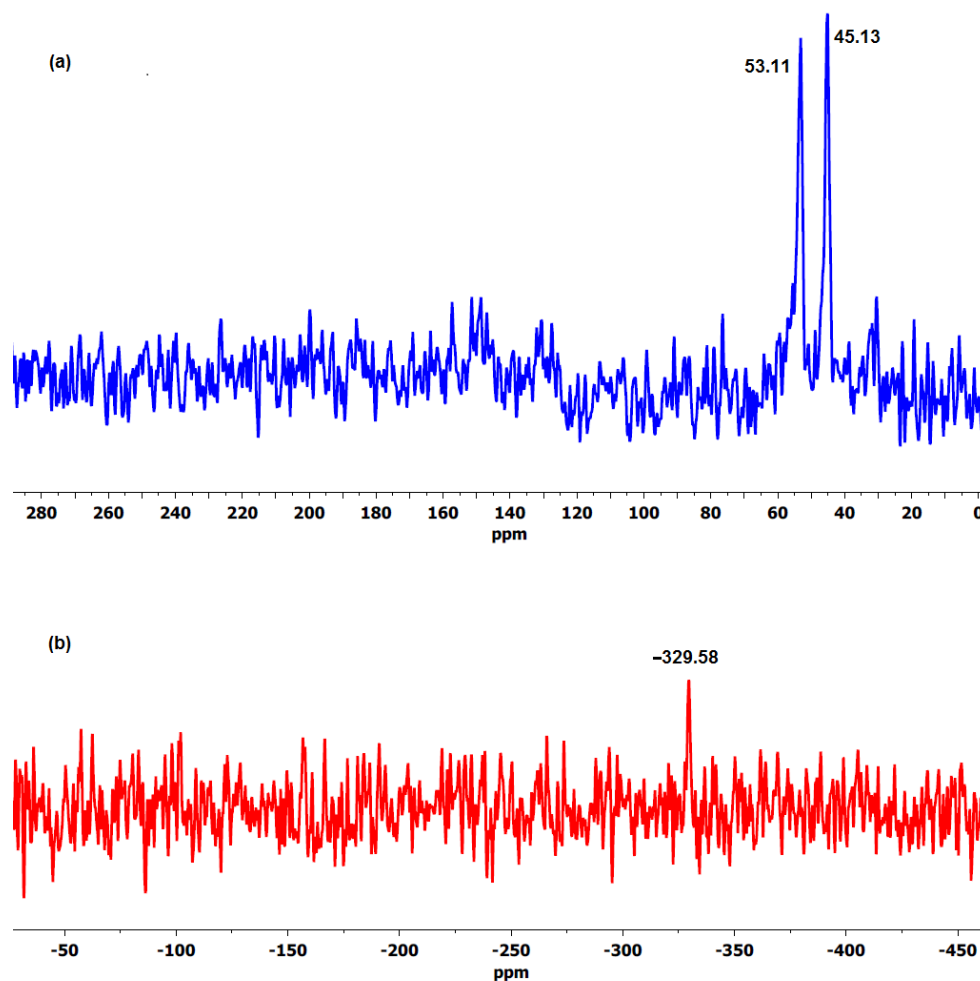
Figure 3.11. The (a) $^{13}$C and (b) $^{15}$N CP-MAS NMR spectra of the degradation products of DABCO-functionalised membrane after stability test.

## 3.11 FTIR analysis of the degradation products

Figure 3.12 shows the FTIR spectra of the degradation products (residue isolated from the solution) of TMA-functionalised membrane having different base polymers. It was very evident in all spectra of the degradation products (deg prdt) that there were no detectable strong peaks between the 2800 and 3000 cm$^{-1}$ region. The 2850 (‡) and 2920 (†) cm$^{-1}$ peaks are attributed to the –CH$_2$ symmetric and asymmetric stretching, respectively, both of which are characteristic peaks of the ETFE, LDPE and HDPE [100, 205, 206]. Additionally for ETFE deg prdt, there is a clear absence of intense peaks in the 1100 to 1300 cm$^{-1}$ region than can be associated with C–F stretching vibrations [74, 126]. This agrees with the NMR analysis (Figure 3.10) wherein the absence of these characteristic peaks indicates

that the base polymers were thermally stable and did not degrade as they were not detected in the degradation products.

Figure 3.12 clearly shows that the spectra of the degradation products for all the different base polymers are identical. This indicates that same degradation products were recovered after the stability test regardless of the type of polymer backbone used. The precipitate contains VBC groups evinced by bands observed at 840 ($\bullet$) and 700 ($\blacklozenge$) cm$^{-1}$ which are consistent with the meta and/or para benzene ring substitution [104]. The presence of TMA is attributed to the C–N stretch at 880 cm$^{-1}$ ($\maltese$) and the N–CH$_3$ symmetric bending deformation at 1393 cm$^{-1}$ ($\triangle$) [207] while the band at 1440 cm$^{-1}$ ($\blacksquare$) refers to the –CH$_2$ scissoring vibrations [208]. The peak at 1660 cm$^{-1}$ ($\circ$) is due to the O–H bending of hydrogen bonded water associated with tetramethylammonium hydroxide (TMAH) hydrate [209]. This is different with the weak signal observed between 3300 and 3400 cm$^{-1}$ region ($\lozenge$) that is associated with the O–H stretching due to possible presence of residual water and/or OH in the degradation product.
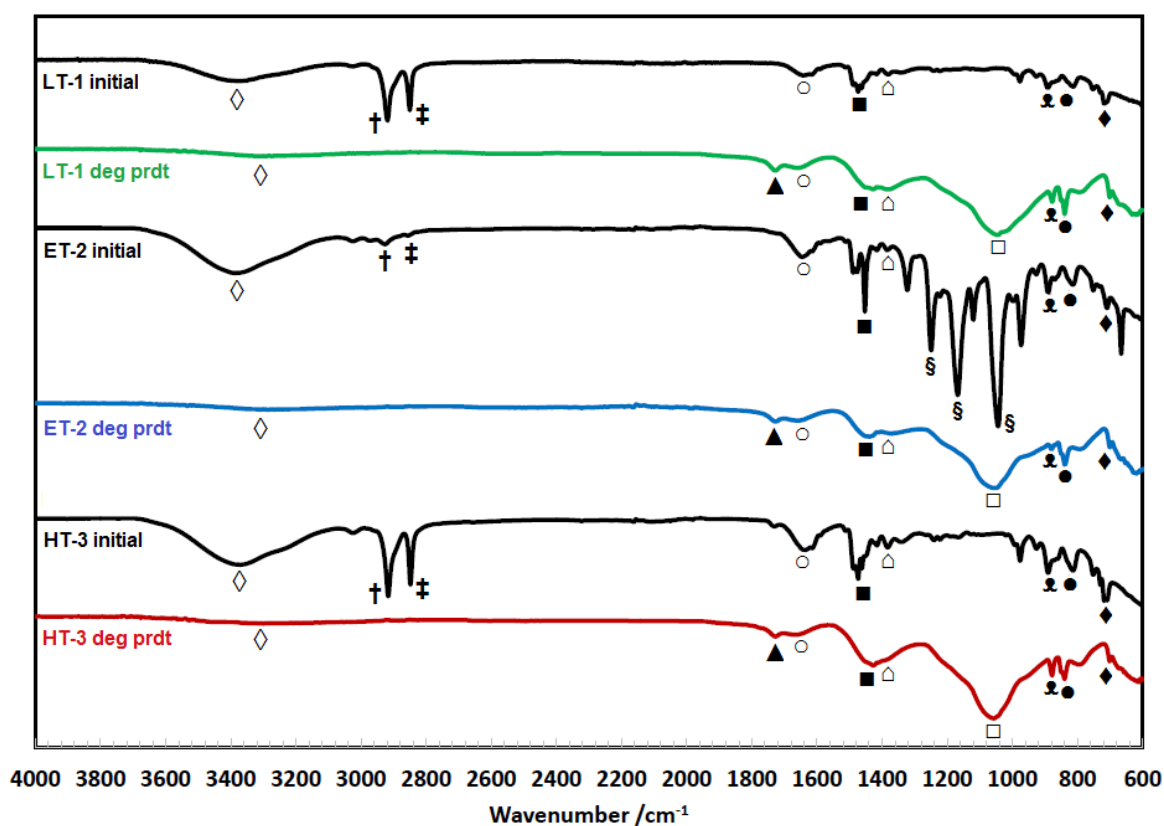


Figure 3.12. FTIR spectra of the degradation products of TMA-functionalised membranes with different polymer backbones.

The possible presence of carbonyl-containing compounds in the degradation products is shown by the strong C–O and C=O stretching vibrations at 1057 (□) and 1730 (▲) cm$^{-1}$, respectively [210].

The FTIR spectra of the degradation product from the LDPE-based membrane functionalised with DABCO is shown in Figure 3.13. Similar to the TMA-functionalised membrane (Figure 3.12), there is no detected presence of LDPE base polymer in the degradation products as there were no strong peaks observed between the 2800 and 3000 cm$^{-1}$ region, which also confirms with the NMR analysis (Figure 3.11). The peaks observed at 1700 (▲), 1057 (□) and 583 cm$^{-1}$ (ℸ) suggest existence of carbonyl-containing (aldehyde and/or ketone) by-products, while the bands at 848 (●) and 796 cm$^{-1}$ (Δ) are attributed to the meta and/or para substitutions of the VBC [104] indicating presence of aromatic compounds in the degradation product.
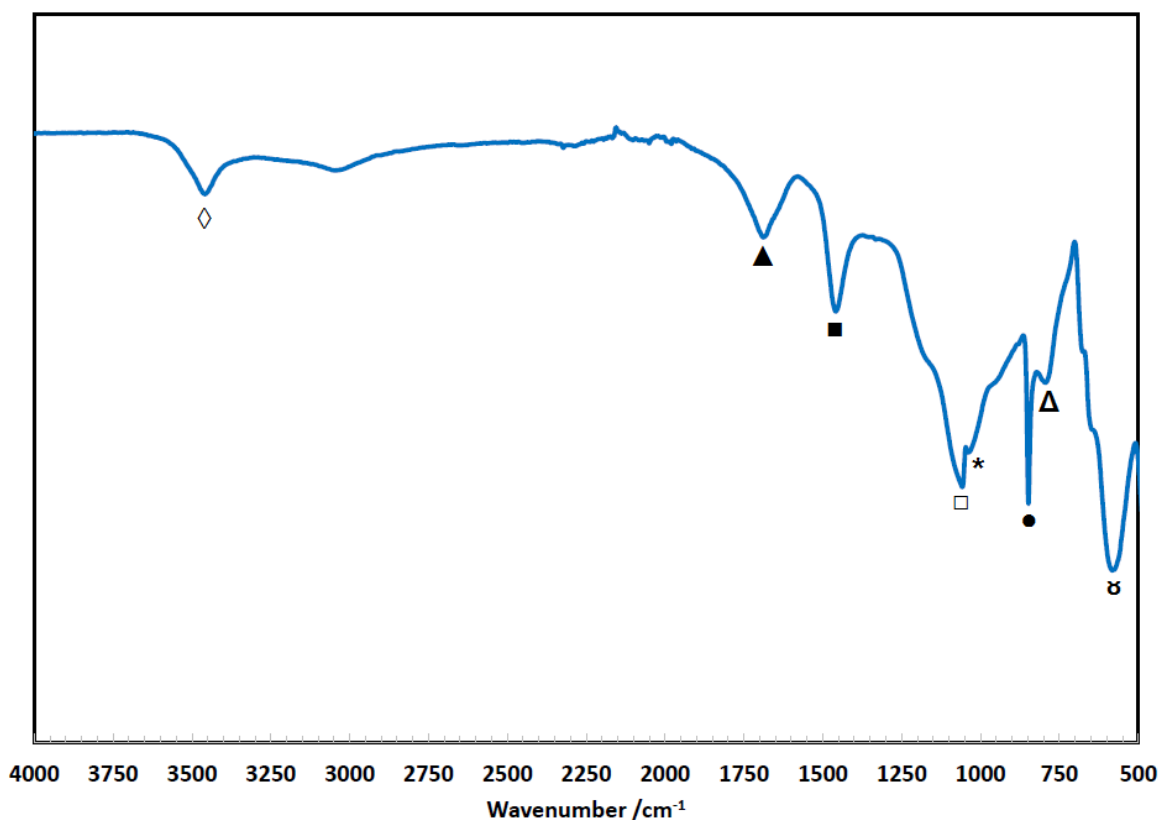


Figure 3.13. FTIR spectra of the degradation products of LDPE-based membrane functionalised with DABCO.

The presence of DABCO in the degradation product was confirmed by the bending deformation at 1460 cm$^{-1}$ (■) of the $CH_2$ groups [211] while the strong signal at 1030 cm$^{-1}$ (*) is due to C–N stretching vibrations in the DABCO structure [212, 213]. Lastly, the band observed at 3460 cm$^{-1}$ (◊) is associated to stretching vibration of N–H bond and/or O–H stretching due to possible presence of residual water and OH in the degradation product.

## 3.12 Mechanism of AEM degradation

Studies on the mechanisms of degradation and measurements of the degradation rates of fabricated membranes reported in the literature were all performed in media with high alkaline concentration and temperature. The degradation rates reported therein are driven predominantly by the loss of head group due to very high alkaline concentration (OH$^-$ ion attack) at elevated temperature. However, such test conditions are actually very far from the real operating environments of low-temperature fuel cells and electrolysers (i.e. close to neutral medium). As previously discussed, AEM degradation due to IEC loss was observed even at very low alkaline concentration (deionised water) at temperature of 60 °C. Results suggest that not only the loss of TMA head group and VBC monomer were responsible for the loss of IEC but also parallel oxidation processes are taking place that provide other routes to degradation. Therefore, in actual fuel cell and electrolyser systems that use media with very low alkalinity and constantly exposed to oxygen gas, the investigation of membrane degradation should shift to the effect of varying the oxygen concentration rather than simply the OH$^-$ ion concentration on stability. Consequently, this suggests that the rate of membrane degradation due to auto-oxidation can have a significant impact aside from the established degradation mechanisms due to loss of head group.

The decrease in ionic conductivity brought about by the decrease in IEC due to the degradation of the fabricated membrane via auto-oxidation of the functional group (TMA), is more pronounced under 100% humidified stream of oxygen than nitrogen at 80 °C (Figure 3.2). The degradation rate in terms of ionic conductivity is 4 times faster in oxygen than in nitrogen which suggests that at very low alkaline concentration, such four-fold increase in degradation rate indicates another degradation mechanism taking place alongside (i.e. oxidation) or at very low

alkaline concentration with negligible head group loss (Scheme 1), one mechanism is accelerated by oxygen concentration.

The result was compared with our ex-situ degradation test of membranes immersed in deuterium oxide ($D_2O$) at 60 °C, one fed with continuous flow of oxygen, another with nitrogen gas feed, and both under reflux (later shown in Section 3.14). NMR spectra only revealed decrease in resonance intensities for both membranes before and after the degradation test and $^1$H-NMR confirmed the same soluble degradation by-products under nitrogen and oxygen atmospheres. Furthermore, the membrane fed with oxygen gas exhibited higher % IEC loss than the membrane with nitrogen gas feed, which indicates that the membrane degradation is faster with oxygen gas feed compared with nitrogen similar to the results observed with the fuel cell degradation test.

The ca. 5.5 % loss after 1 month (720 h) in deionised water at 60 °C (Figure 3.5) was compared with reported degradation rates in literature. Einsla et al. [160] observed a 10% loss of benzyltrimethylammonium (BTMA) cation (compound) at 80 °C after 1 month under 1 M alkaline and there was no change in degradation rate in the studied alkaline concentration range between 1–5 M. Using the reported activation energy (15.8 kcal mol$^{-1}$), the degradation rate at 60 °C of the same BTMA cation was estimated to be 2.6% after 1 month in 1 M KOH. This is less than half of the % loss after 1 month (720 h) in air saturated deionised water we obtained of 5.5% with the highest radiation dose and an order of magnitude lower than the lowest dose rate (25%) indicating that the degradation of the fabricated membranes investigated is not only due to the removal of the head group but could also due to other mechanisms involving oxygen.

We therefore suggest an alternative AEM degradation mechanism at very low alkaline concentration that involves auto-oxidation of the initial degradation products and the ylide intermediate (Scheme 3.2) which can explain the above observations. A parallel observation that suggests peroxide radicals could be generated from ylide (Scheme 1.3) was recently reported [131] employing $^{31}$P NMR spectroscopy and using polyphenylene oxide (PPO) as base polymer for the TMA-based AEM. It was reported that auto-oxidation is favoured under alkaline conditions and the degradation of AEM was due to hydroxyl and superoxide anion radicals formation which were found to be responsible for the PPO backbone chain scission.
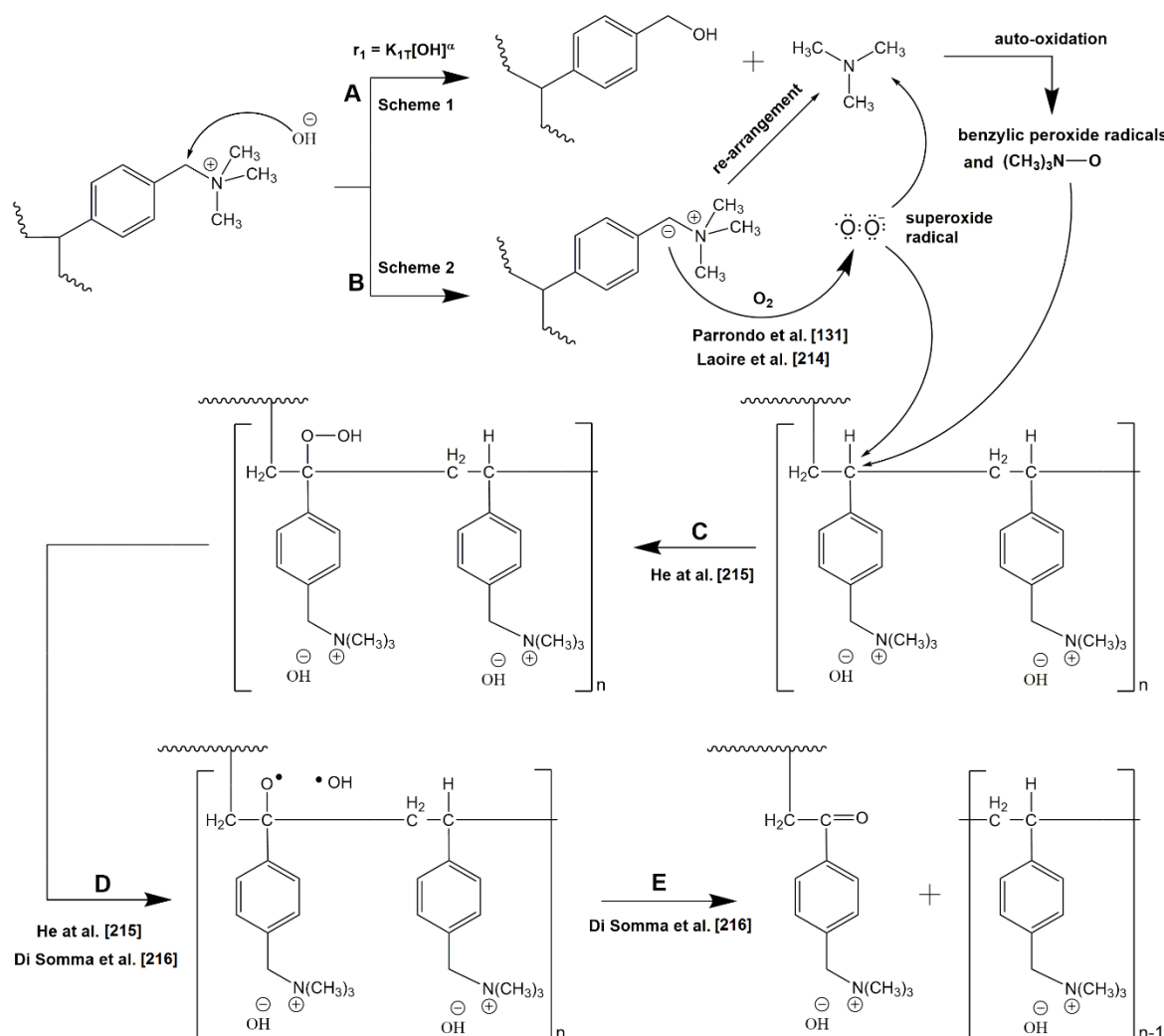
Scheme 3.2. Proposed degradation pathways for TMA-functionalised AEM in media with very low alkaline concentration.

In the proposed mechanism (Scheme 3.2), the degradation of the membrane is governed by 2 reaction routes (A and B) which can proceed simultaneously. Initially, in alkaline environment, AEM degradation proceeds with the loss of the head group (Scheme 1.2) as widely reported, hereby indicated as Reaction A. The reaction rate ($r_1$) in terms of loss of head group is a function of the OH$^-$ ion concentration and operating temperature, wherein subjecting the membrane to highly alkaline media and temperature expect a high degradation rate via head group loss. The initial degradation products of Reaction A could subsequently undergo oxidation/auto-oxidation to form benzylic peroxide radicals and TMA–oxide radicals. The reaction rate in terms of auto-oxidation reaction is dependent on

temperature and on degradation products and oxygen concentrations, wherein as more oxygen is fed to the system at constant alkaline concentration and temperature, more N-oxide and peroxide radicals will be created.  These benzylic peroxide radicals and TMA–oxide radicals could possibly attack the benzylic carbon liberating VBC–TMA groups-grafts causing further decrease in IEC of the AEM depending on the length of the VBC grafts, n.  However, we observed 1:1 ratio of VBC to TMA loss of prepared AEM (67 Gy h$^{-1}$, Figure 3.7), suggesting that at very low alkaline concentration, the loss of head group due to OH$^-$ ion attack (Reaction A) has minor contribution to membrane degradation and is rather mainly attributed to the loss of VBC–TMA group as a whole (Reaction B).

The degradation route via Reaction A can be applicable to DABCO-based AEM (2000 Gy h$^{-1}$) where a 1:2 ratio of VBC to DABCO loss was observed (Figure 3.8) indicating better stability of TMA than DABCO even at same radiation dose rate due to more loss of DABCO head group than VBC.  This suggests that the degradation of DABCO-functionalised membrane is not solely due to removal of the whole VBC–DABCO group but could also involve the auto-oxidation of the initial degradation products of the nucleophilic substitution reaction (i.e. membrane degradation proceeds through both Reaction A and B).  Therefore, this indicates that at very low alkaline concentration, the ratio of VBC to head group loss dictates the relative yields of degradation routes and that different head group types could follow one or more degradation pathways depending on the applied radiation dose rate.

Reaction B proceeds as proposed by Parrondo et al. [131] wherein the carbanion reduces the dissolved oxygen present in the solution to produce superoxide radicals.  Such process involves one-electron reduction of the dissolved oxygen leading to the formation of $O_2/O_2^-$ (superoxide) redox couple [214].  The ylide formation and consequently the superoxide explain why degradation in terms of IEC loss is not due to direct oxygen reaction with VBC–TMA as IEC loss was only observed when the membranes were in the OH$^-$ form and was not observed in Cl$^-$ form (Table 3.1).  The presence of carbonyl-containing compounds and N-oxide groups (Figure 3.9) provides evidence of formation of these superoxides. Consequently, in the absence of high OH$^-$ ion concentration in the surrounding media, these superoxide radicals can attack the vulnerable benzylic carbon of the LDPE–VBC chain resulting in the release of VBC–TMA groups.

The attack of free radicals (benzylic peroxide, TMA-oxide, or superoxide radicals) on the vulnerable carbon (carbon in para position with respect to the trimethyl ammonium hydroxide group) gives rise to the formation of a hydroperoxide moiety (Reaction C) reported for cumene [215]. The hydroperoxide group is expectedly unstable and is easily fragmented to hydroxyl and oxide radicals upon thermal decomposition (Reaction D) [215, 216], which subsequently rearranges to form ketone (C=O) by-product and cause the detachment of VBC–TMA chains [216].

The reaction rate in terms of free radical attack is influenced by the applied radiation dose rate. Therefore, at a fixed operating temperature with constant OH⁻ ion and oxygen concentration, the degradation rate is solely dependent on the applied radiation dose rate during AEM synthesis. Membranes prepared under low radiation dose rate produce longer VBC–VBC chains (high value of n) resulting in higher IEC loss upon chain scission of the long VBC grafts. As observed in the SEM image (Figure 3.6), the even distribution of bubbles (voids) suggests long VBC–VBC grafts as few active sites for LDPE–VBC were created due to low applied radiation dose rate. On the other hand, membranes prepared under high radiation dose rate will have more uniform VBC monomer distribution producing more LDPE–VBC grafts and shorter VBC–VBC links (low value of n), hence slower degradation due to lower IEC loss per attack.

## 3.13 Investigation on other amine-functionalised membranes

### 3.13.1 Measurement of ionic conductivity

LDPE-based membranes (65% DOG) were prepared with high radiation dose rate (2000 Gy h⁻¹) and functionalised with different amine groups, namely, TMA, DABCO, ABCO and NMP. Table 3.7 shows the through-plane ionic conductivity of the membranes tethered with different amine functionalities at 60 °C. Degradation resulted in a decrease in the through-plane ionic conductivity for each 720 h interval for all AEMs investigated. Expectedly from the IEC measurement (Figure 3.5), TMA exhibited the highest ionic conductivity due to its high initial IEC attributed to its effective penetration of the LDPE-g-VBC copolymer compared with the bulkier cyclic structure of the other amine functional groups, namely, ABCO,

NMP and DABCO. The observed decrease in ionic-conductivity is in agreement with the observed decrease in IEC (Figure 3.5) for each 720 h degradation test.

Table 3.7. Through-plane ionic conductivity at 60 °C of LDPE-based AEMs functionalised with different amine groups before and after degradation test.

| Functional Group | Average Ionic Conductivity (mS cm$^{-1}$) | | |
|---|---|---|---|
| | Initial | After 720 h | After 1440 h |
| TMA | 101 | 87 | 85 |
| ABCO | 87 | 81 | 71 |
| NMP | 75 | 71 | 65 |
| DABCO | 70 | 57 | 47 |

The TMA-functionalised membrane showed lower decrease in ionic conductivity at 60 °C after 1440 h of 15.8% compared with DABCO-functionalised membrane of 32.8% (using the same high radiation dose rate of 2000 Gy h$^{-1}$) similar with that observed in Table 3.6. The decrease in ionic conductivity at 60 °C after 720 h of the TMA-functionalised membrane of 13.8% was found to be similar to that after 1440 h (15.8%). However, the measured decrease in ionic conductivity at 60 °C after 720 h of the DABCO-functionalised membrane of 18.6% was about half of that after 1440 h of 32.8%.

The ABCO- and NMP-functionalised membranes also showed evidence of degradation in terms of ionic conductivity loss due to the observed decrease in their respective IECs after every 720 h of degradation test. While the three cyclic-structured head groups showed similar % IEC loss after 1440 h degradation period (Figure 3.5), the measured ionic conductivity of ABCO- (71 mS cm$^{-1}$) and NMP-functionalised AEM (65 mS cm$^{-1}$) were found superior to the 47 mS cm$^{-1}$ ionic conductivity of DABCO-functionalised AEM, which is primarily due to the lower basicity of DABCO (p$K_a$ = 8.72) compared with NMP (p$K_a$ = 10.13) and ABCO (p$K_a$ = 10.76) (Table 1.2).

### 3.13.2 CP-MAS NMR analysis

The original and aged membranes (after 720 and 1440 h degradation period) with different amine functionalities were subjected to the same solid state NMR analysis to measure the decrease of the chemical groups present at every 720 h. Figures 3.14 to 3.17 show the $^{13}$C and $^{15}$N CP-MAS NMR spectra of the original and aged membranes functionalised with TMA, DABCO, ABCO, and NMP, respectively. The obtained $^{13}$C CP-MAS NMR spectra were normalised against LDPE peak since the base polymer was found to be stable and did not participate in the degradation reactions.

Figure 3.14a shows the $^{13}$C CP-MAS NMR spectra of the original and aged TMA-functionalised membrane (2000 Gy h$^{-1}$, 65% DOG). The resonance assignments are similar with that of Figure 3.7a, hence will no longer be discussed. Figure 3.14a however, shows the spectra of the aged and original TMA-functionalised membrane prepared with higher radiation dose rate (2000 Gy h$^{-1}$) compared with Figure 3.7a (67 Gy h$^{-1}$). It was also observed that the ratio of VBC to TMA loss remained close to 1 using high radiation dose rate of 2000 Gy h$^{-1}$ (Table 3.8). Furthermore, even with the same VBC to TMA ratio of 1 for both 67 and 2000 Gy h$^{-1}$, the decrease in intensity of each particular group for the aged membrane prepared with higher radiation dose rate (Figure 3.14a) is less at each 720 h interval compared with that prepared with lower radiation dose rate (Figure 3.7a). This indicates improved stability of membranes when prepared with high radiation dose rate that provides structural strength to the AEM brought about by the increase in the degree of crosslinking. Furthermore, the application of high radiation dose rate also produces shorter chain grafts which results in a lower % IEC loss.

Figure 3.14b shows the $^{15}$N CP-MAS NMR spectra of the same TMA-functionalised membrane (2000 Gy h$^{-1}$, 65% DOG). Similar with that of Figure 3.7b, the same quaternised nitrogen peak of TMA at -330 ppm [191] was observed and no other resonance peaks were detected after degradation suggesting that no other nitrogen-containing by-products have formed on the membrane.
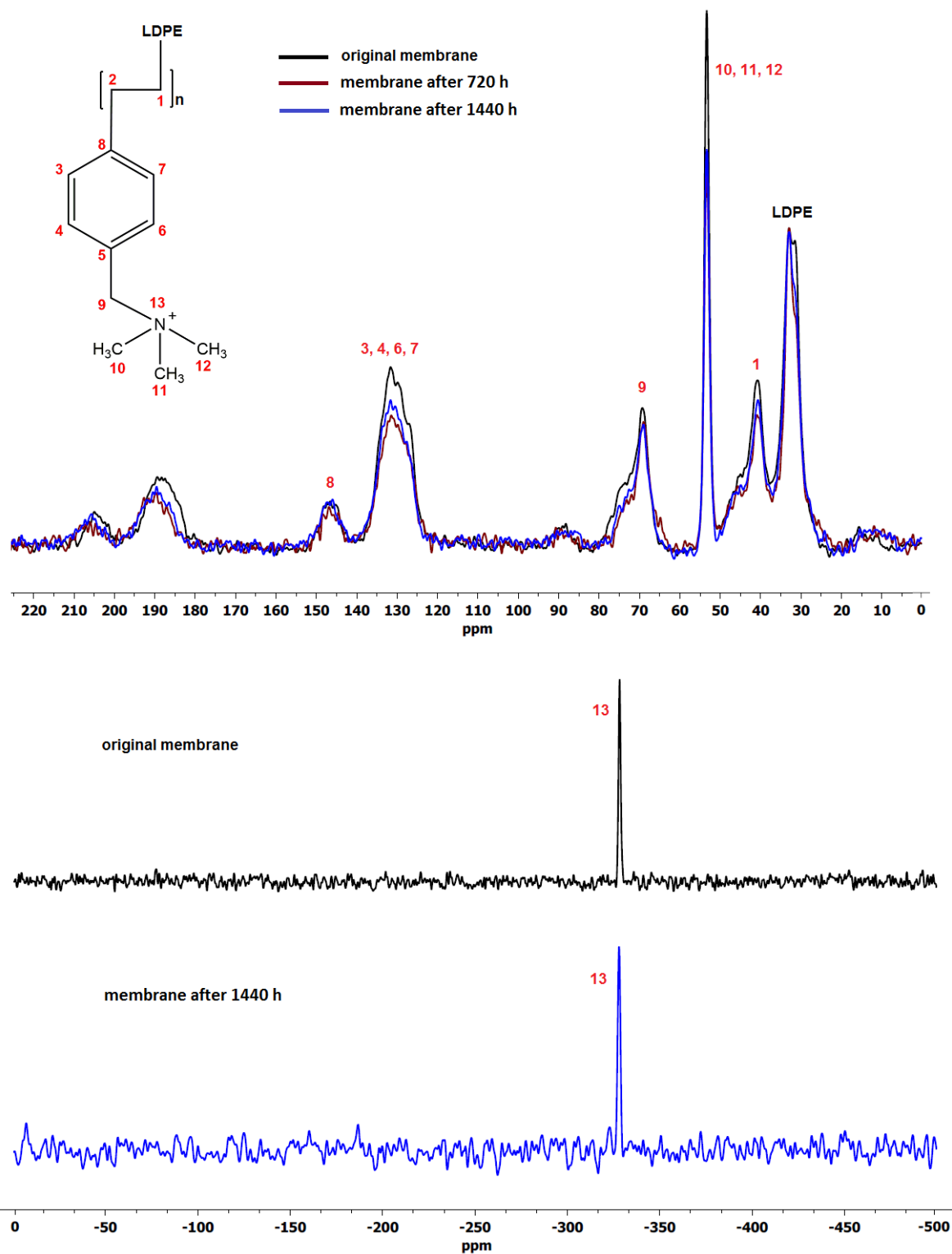
Figure 3.14. The (a) $^{13}$C and (b) $^{15}$N CP-MAS NMR spectra of the original and aged TMA-functionalised membrane (2000 Gy h$^{-1}$, 65% DOG).

Figure 3.15 shows the $^{13}$C CP-MAS NMR spectra of the initial and aged DABCO-functionalised membrane prepared under high radiation dose rate of 2000 Gy h$^{-1}$ similar to that of Figure 3.8a. However, Figure 3.15a further shows the progression of the decrease from the initial, after 720 h and after 1440 h degradation tests. The marked decrease in the intensity of DABCO from initial, after 720 h and finally to 1440 h degradation period compared with that of VBC verified the observed ratio of VBC to DABCO loss of 1:2.

The resonance assignments of the initial and aged DABCO-functionalised membranes have been amply discussed in Figure 3.8a which is just similar to Figure 3.15a. The resonance peak at -330 ppm in the $^{15}$N CP-MAS NMR spectra as shown in Figure 3.15b is consistent with the quaternised nitrogen in the DABCO structure and the peak at -368 ppm can be associated with the unquaternised nitrogen, both present in the original and degraded membrane [193]. Furthermore, no other additional resonance peaks were observed suggesting that no other nitrogen-containing by-products have formed on the membrane.

Figure 3.16 shows the $^{13}$C and $^{15}$N CP-MAS NMR spectra of the original and aged ABCO-functionalised membrane (2000 Gy hr$^{-1}$, 65% DOG). ABCO has similar structure with that of DABCO but with only one nitrogen present, thus the only difference in the $^{13}$C CP-MAS NMR spectra is the additional intense CH$_2$–CH$_2$ peaks at 25 ppm. There is a noticeable rapid decrease in intensity of ABCO functional group after 720 h and further after 1440 h of degradation run compared with that of DABCO (Figure 3.15) which indicates better stability of mono-quaternised DABCO than ABCO as proposed in the literature.

Having a single quaternised nitrogen similar with TMA, the $^{15}$N CP-MAS NMR spectra of the original and aged ABCO-functionalised membrane (Figure 3.16b) both show single resonance at -330 ppm. No other additional resonance peaks were detected.
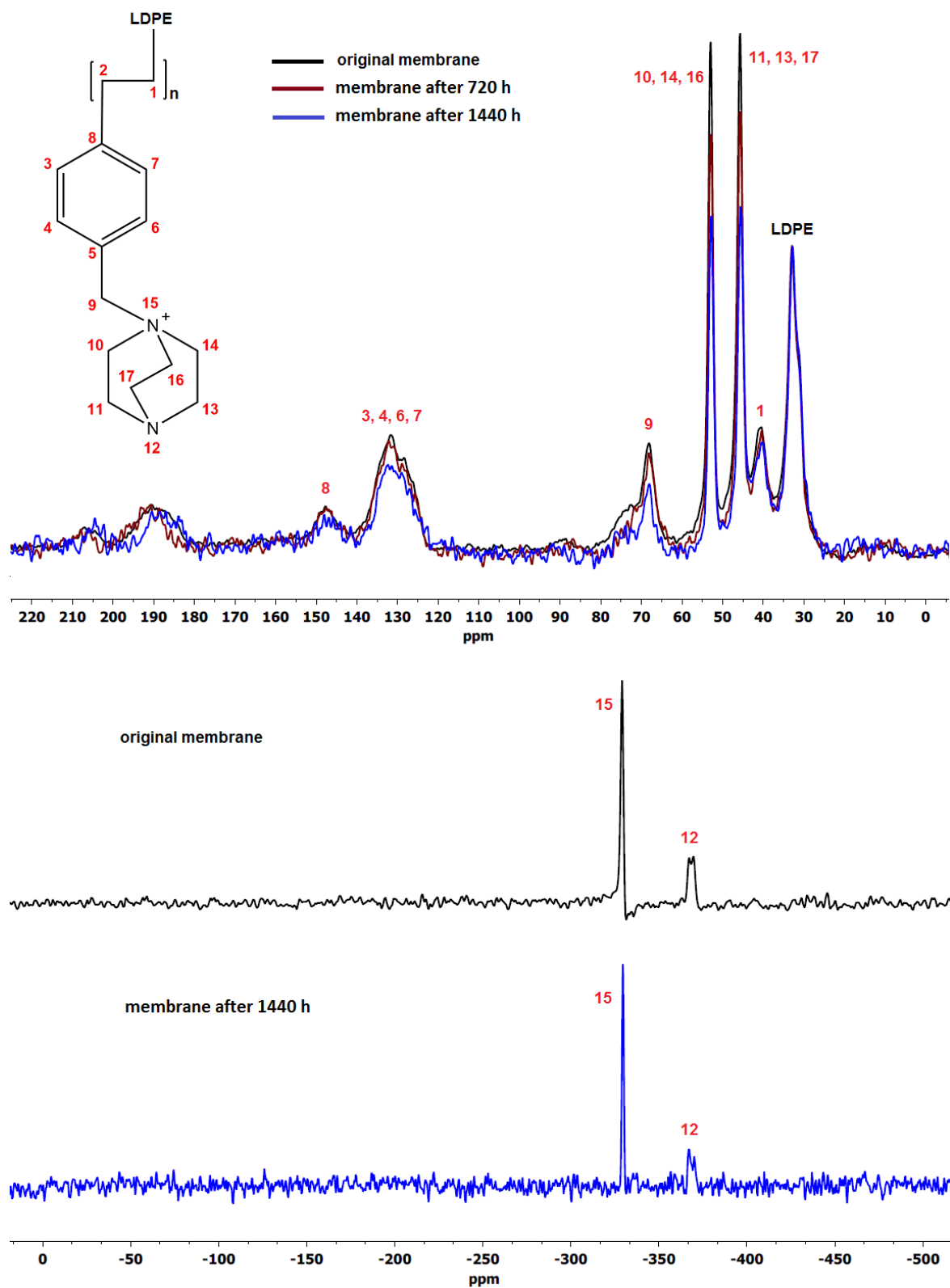
Figure 3.15. The (a) $^{13}$C and (b) $^{15}$N CP-MAS NMR spectra of the original and aged DABCO-functionalised membrane (2000 Gy h$^{-1}$, 65% DOG).
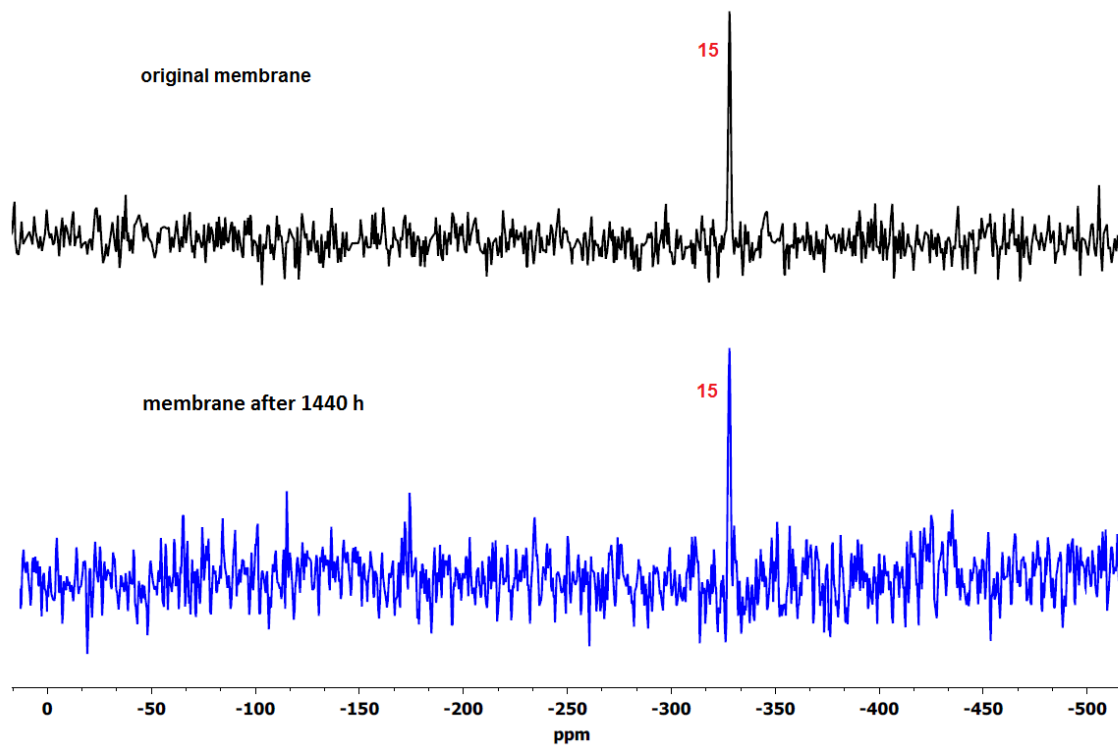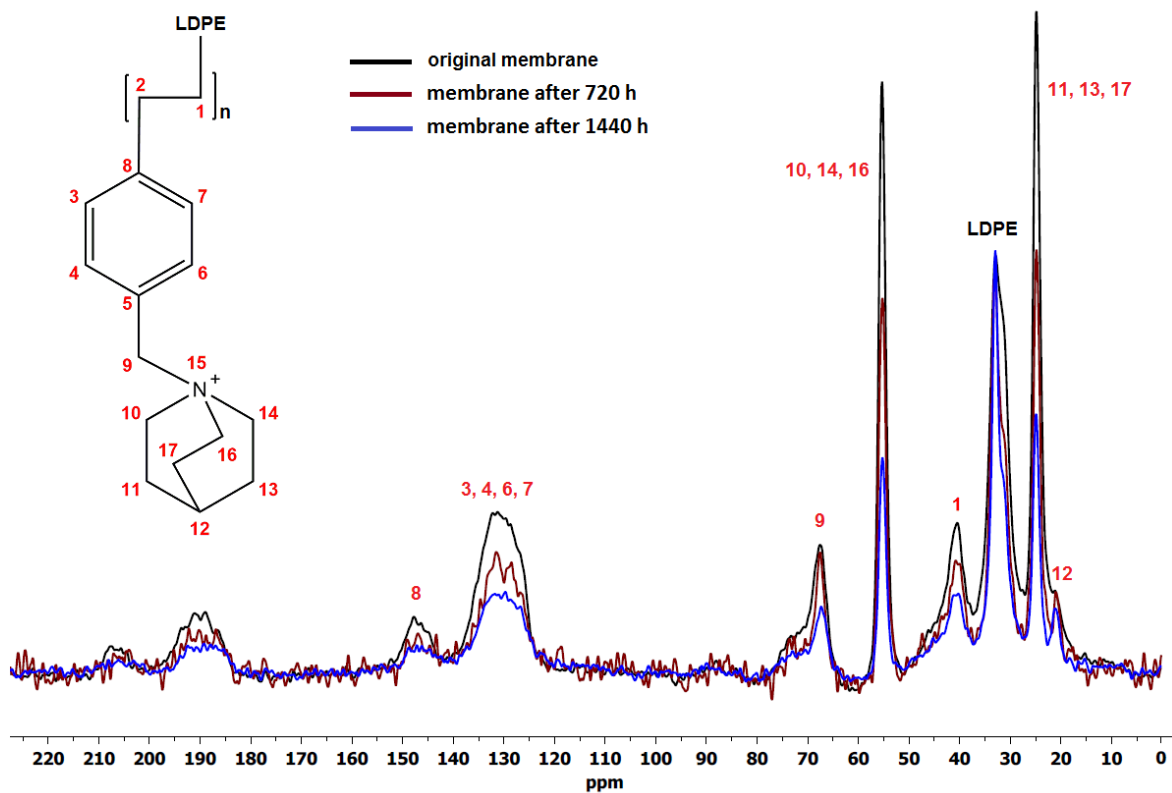
Figure 3.16. The (a) $^{13}C$ and (b) $^{15}N$ CP-MAS NMR spectra of the original and aged ABCO-functionalised membrane (2000 Gy h$^{-1}$, 65% DOG).

Lastly is the NMP-functionalised membrane (2000 Gy hr^{-1}, 65% DOG) wherein the ^{13}C and ^{15}N CP-MAS NMR spectra of the original and aged membranes are shown in Figure 3.17. Similar with previous spectra, the aromatic VBC resonance is observed at 125 to 150 ppm and exhibited a decrease in intensity with every 720 h degradation period suggesting loss of VBC from the polymer backbone. The cyclic alkyl structure of NMP made it difficult to distinguish from LDPE as the alkyl $CH_2$–$CH_2$ resonance overlaps that of the intense LDPE peaks, which consequently complicates the estimation of the VBC and NMP (head group) loss (Table 3.8).

Similar with previous spectra of mono-quaternised nitrogen, the ^{15}N CP-MAS NMR spectra of the original and aged NMP-functionalised membrane (Figure 3.17b) both show single resonance at -330 ppm. No other additional resonance peaks were detected.

The superimposition of the ^{13}C CP-MAS NMR spectra of the original and aged membranes showed the decrease of the chemical components of the AEM at each period of degradation test. As all measurements were performed under similar CP-MAS NMR test conditions, the loss of each component (i.e. VBC and head group) and their ratios at every period of degradation can be estimated. Table 3.8 shows the estimated VBC to head group loss for each membrane investigated at every 720 h degradation period.

Table 3.8 VBC and head group loss of AEMs (2000 Gy h[-1], 65% DOG) for each period of degradation test estimated from the ^{13}C CP-MAS NMR spectra.

| Degradation test | | Head group | | | |
|---|---|---|---|---|---|
| | | TMA | DABCO | ABCO | NMP |
| After 720 h | VBC loss (%) | 2.0 | 8.5 | 28.2 | 37.6 |
| | Head group loss (%) | 1.9 | 18.6 | 25.9 | 20.8 |
| | VBC:Head group | 1:1 | 1:2 | 1:1 | 1:2 |
| After 1440 h | VBC loss (%) | 12.1 | 15.1 | 47.2 | 61.7 |
| | Head group loss (%) | 9.0 | 26.9 | 49.3 | 38.9 |
| | VBC:Head group | 1:1 | 1:2 | 1:1 | 1.5:1 |
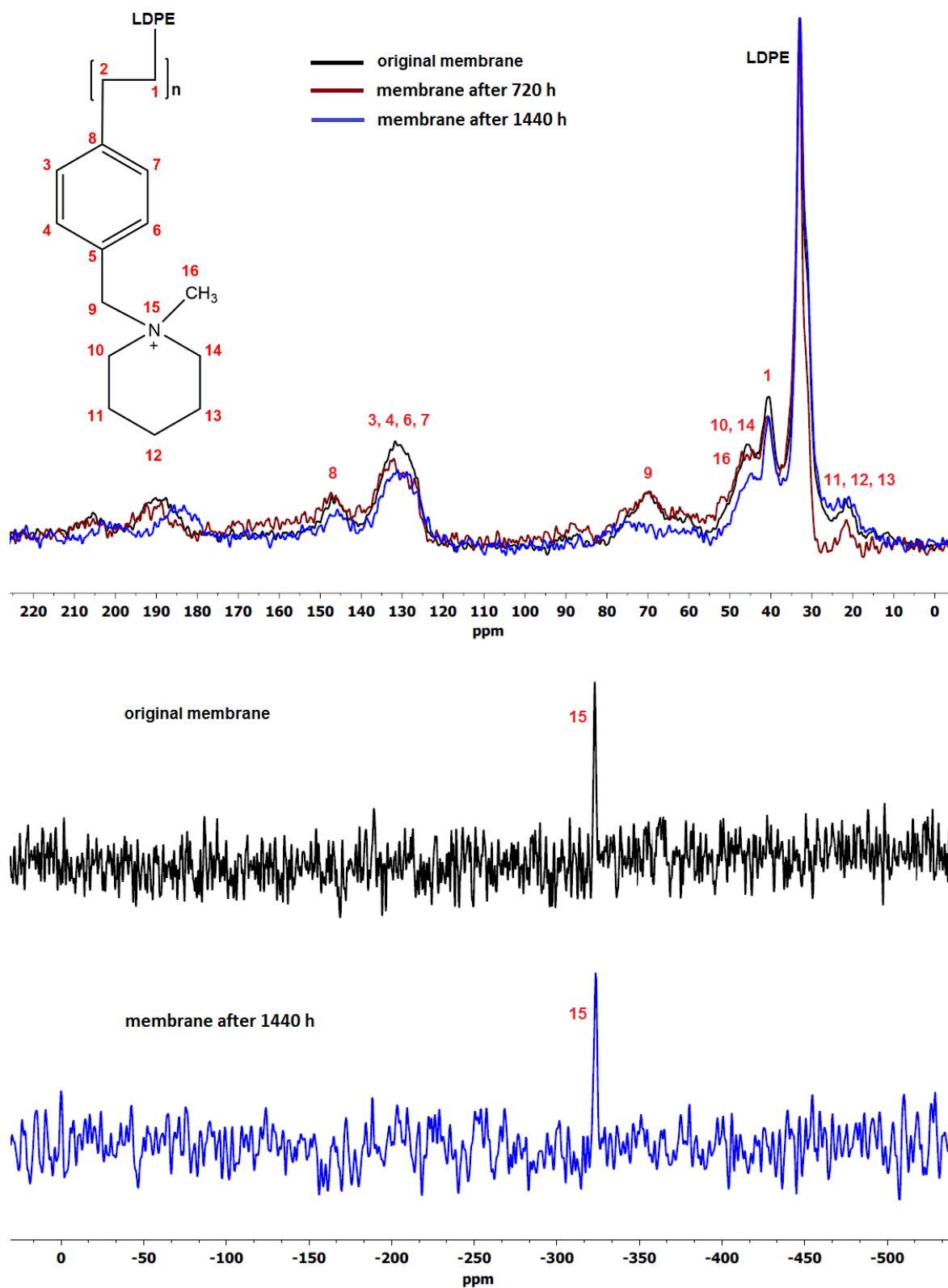
Figure 3.17. The (a) $^{13}$C and (b) $^{15}$N CP-MAS NMR spectra of the original and aged NMP-functionalised membrane (2000 Gy h$^{-1}$, 65% DOG).

The TMA-functionalised membrane emerged as the most stable among the AEMs investigated having minimal VBC loss of 2 and 12% for after 720 and 1440 h degradation test, respectively, and head group (TMA) loss of 2 and 9% for after 720 h and 1440 h degradation test, respectively. The ratio of VBC to TMA loss remained close to 1 for both after 720 and 1440 h degradation. The observed stability of TMA compared with the other cyclic-structured head groups is consistent with the IEC data (Figure 3.5) that shows TMA having the slowest degradation rate.

Table 3.8 also shows that the cyclic-structured head groups, namely, NMP and DABCO, exhibited ratios of VBC to head group loss greater than 1 after 720 h degradation, which indicates more head group units were detached for every unit of VBC present in the membrane. This can be due to the bulkier structures of these head groups in comparison with the facile structure of TMA. In the case of DABCO-functionalised AEM, the ratio of VBC to DABCO loss is 1:2 for both materials after 720 and 1440 h degradation test. The greater loss of DABCO head group compared with VBC suggests more than one degradation mechanism could be taking place simultaneously, as previously proposed. These are (1) nucleophilic substitution reaction caused by the attack of $OH^-$ ions resulting in the release of DABCO, and (2) superoxide and/or benzylic peroxide radical attack on the vulnerable benzylic carbon of the LDPE-VBC, leading to the removal of the VBC-DABCO groups [217].

Comparison of the aged DABCO- with ABCO-functionalised AEMs revealed that, in terms of % VBC loss and % head group loss, ABCO-functionalised AEM appears to lose more VBC and ABCO (Figure 3.16) than the DABCO-functionalised AEM with 28% loss of VBC, which is three times higher than that of DABCO-functionalised membrane of only 8.5% VBC loss after 720 h. While after 1440 h degradation run, the % loss of VBC of ABCO-functionalised AEM is also three times higher at 47% than 15% VBC loss of DABCO-functionalised AEM and the % loss of head group of ABCO-functionalised AEM is almost double that of DABCO-functionalised membrane at 49% and 27%, respectively. Thus, the much greater loss of both VBC and ABCO indicates that the ABCO-functionalised AEM is inferior to the DABCO-functionalised AEM in terms of cation stability. This is consistent with that propounded in literature that a mono-quaternised DABCO (Figure 3.15b) offers improved stability as the unquaternised nitrogen balances the positive charge of the other nitrogen [166], effectively reducing the acidity of the molecule thereby making it less susceptible to nucleophilic substitution through $OH^-$ ion attack [218].

The observed order of cation stability in terms of % VBC loss of the cyclic-structured head groups, DABCO>ABCO>NMP, is possibly due to the more rigid or caged structure of DABCO and ABCO compared with NMP, however such conclusion cannot be correlated with the IEC data (Figure 3.5) as the difference in % IEC loss between AEMs is minimal.  Furthermore, some measurements showed higher % VBC loss than the head group (i.e. ABCO after 720 h and NMP after 1440 h) that results in inconsistencies with the calculated estimates and can be attributed to personal bias in identifying the peak areas in the NMR spectra, particularly to that of NMP (and to some extent on ABCO) where the resonance of the alkyl $CH_2$–$CH_2$ in the head group structure overlaps that of the peaks of the base polymer (LDPE) making their stability assessment in terms of VBC and head group loss ratios inconclusive.

### 3.13.3 $^1$H solution-NMR analysis

The degradation solutions ($D_2O$ solution where the AEM was immersed during degradation test) of AEMs functionalised with different head groups were analysed using NMR.  With the use of $D_2O$ as the solvent, the obtained degradation solutions can be directly subjected to $^1$H solution-NMR spectroscopy. Figures 3.18 to 3.21 show the $^1$H NMR spectra of the degradation solutions of TMA-, DABCO-, ABCO- and NMP-functionalised AEMs, respectively.

The $^1$H NMR spectra of the degradation solution of TMA-functionalised AEM (Figure 3.18) confirms the removal of VBC (6.25 to 7.25 ppm region) [219] and TMA (2.89 ppm) [133] from the base polymer chain.  The ratio of VBC to TMA loss is 1 for both after 720 and 1440 h degradation tests (Table 3.9), which is consistent with the ratios of VBC to TMA loss estimated from the $^{13}$C CP-MAS NMR spectra (Table 3.8).  Furthermore, the presence of 4.25 ppm peak (9) [220] suggests that VBC–TMA detaches from the polymer backbone as a whole.
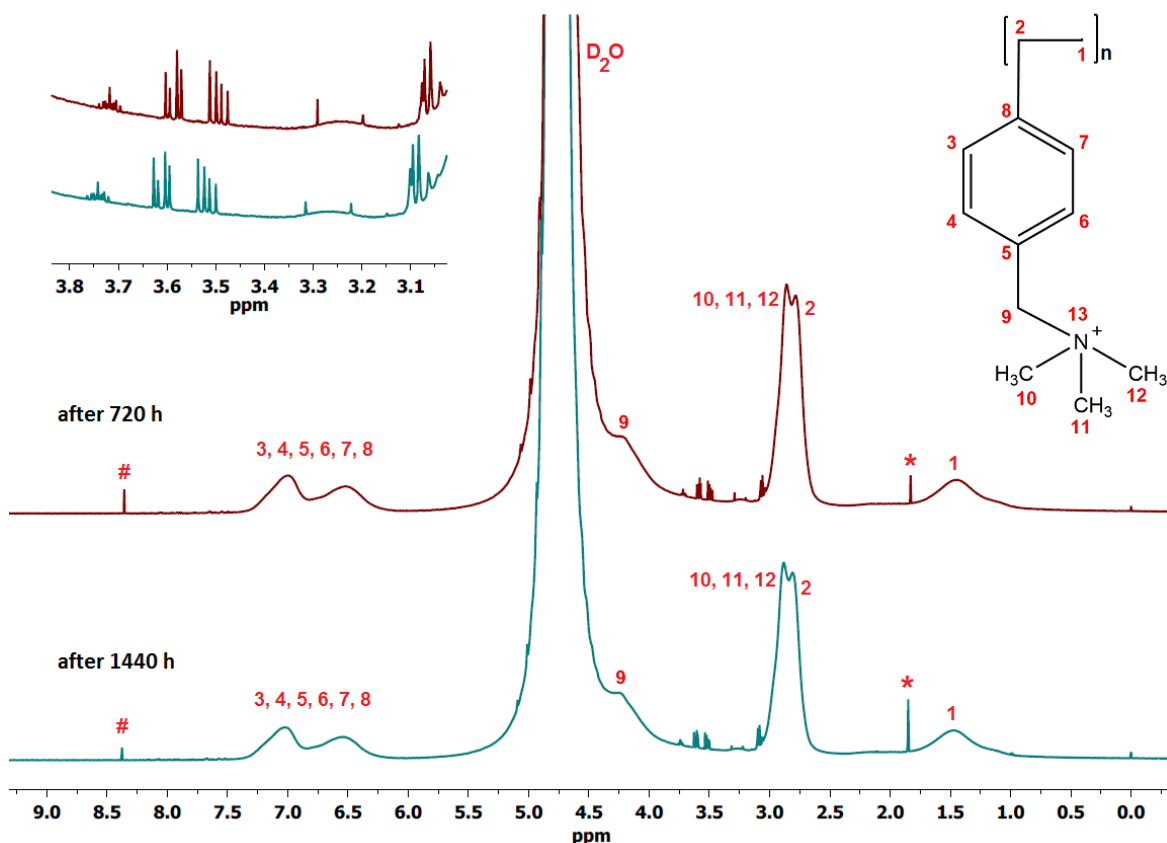
Figure 3.18. $^1$H NMR spectra of the degradation solution of TMA-functionalised AEM.

Table 3.9. The ratios of VBC to head group loss of AEMs (2000 Gy hr$^{-1}$, 65% DOG) for each period of degradation test from the $^1$H solution-NMR spectra.

| Degradation test | | Head group | | | |
|---|---|---|---|---|---|
| | | TMA | DABCO | ABCO | NMP |
| Ratio of VBC to head group loss | After 720 h | 1:1 | 1:2 | 1:2 | - |
| | After 1440 h | 1:1 | 1:2 | 1:2 | - |

Aside from the expected functional groups and chemical components (i.e. VBC and TMA), the $^1$H NMR spectra of the degradation solution of TMA-functionalised AEM (Figure 3.18) revealed formation of new peaks at 1.85 ppm (singlet), 8.36 ppm (singlet) and clusters of peaks between the 3.0 to 3.8 ppm

region.  The observed new peaks were detected after 720 and 1440 h degradation indicating the presence of identical degradation products.  The degradation products proposed in literature as shown in Schemes 1.2 and 1.3 were compared with the obtained NMR spectra.  There is a possible presence of dibenzylic ether as a proposed degradation product by Musker [161] due to the presence of aromatic group (around 7.0 ppm region) and the ether (–O–) group detected in the $^{17}O$ solution-NMR (Figure 3.9b) of the degradation solution.  The proposed presence of benzylic dimethylamine as a minor product of degradation (Schemes 1.2 and 1.3) is untenable due to the clear absence of resonance within the 2.15 to 2.25 ppm region characteristic to the dimethyl groups attached to the nitrogen atom [221].  The downfield resonance at 8.36 ppm (#) can be attributed to the benzylic hydroperoxy proton (O–O–H) with the corresponding alcohol (O–H) signal at 1.85 ppm (*) [222], which conforms with the 194 ppm peroxide peak in the $^{17}O$ solution-NMR (Figure 3.9b).  Furthermore, the cluster of unsymmetrical splitting resonance within the 3.0 to 3.8 ppm region (inset, Figure 3.18) can be considered as noise in the signal or from impurities due to their very weak intensities (in comparison with other degradation products) and they are similarly observed in other spectra of degradation products of different head groups investigated as shown later.  Moreover, the resonance at around 3.1 ppm were confirmed to be impurities innate to the membrane as it was originally present in the $^1H$ solution-NMR spectra of the PVBC-TMA polymer (without the LDPE base polymer) as shown in Figure 3.4.

The $^1H$ NMR spectra of the degradation solution of DABCO-functionalised AEM (Figure 3.19) revealed removal of both the VBC (6.25 to 7.25 ppm region) and DABCO head group (at 2.7 ppm (11, 13, 17) for protons neighbouring the unquaternised nitrogen; and at 3.1 ppm (10, 14, 16) for protons neighbouring the quaternised nitrogen) [223].  Both spectra of degradation solutions showed the same set of resonance, indicating similar degradation products were produced and increased in concentration after the longer degradation test as evidenced by the increased intensity of resonance from 720 to 1440 h period.
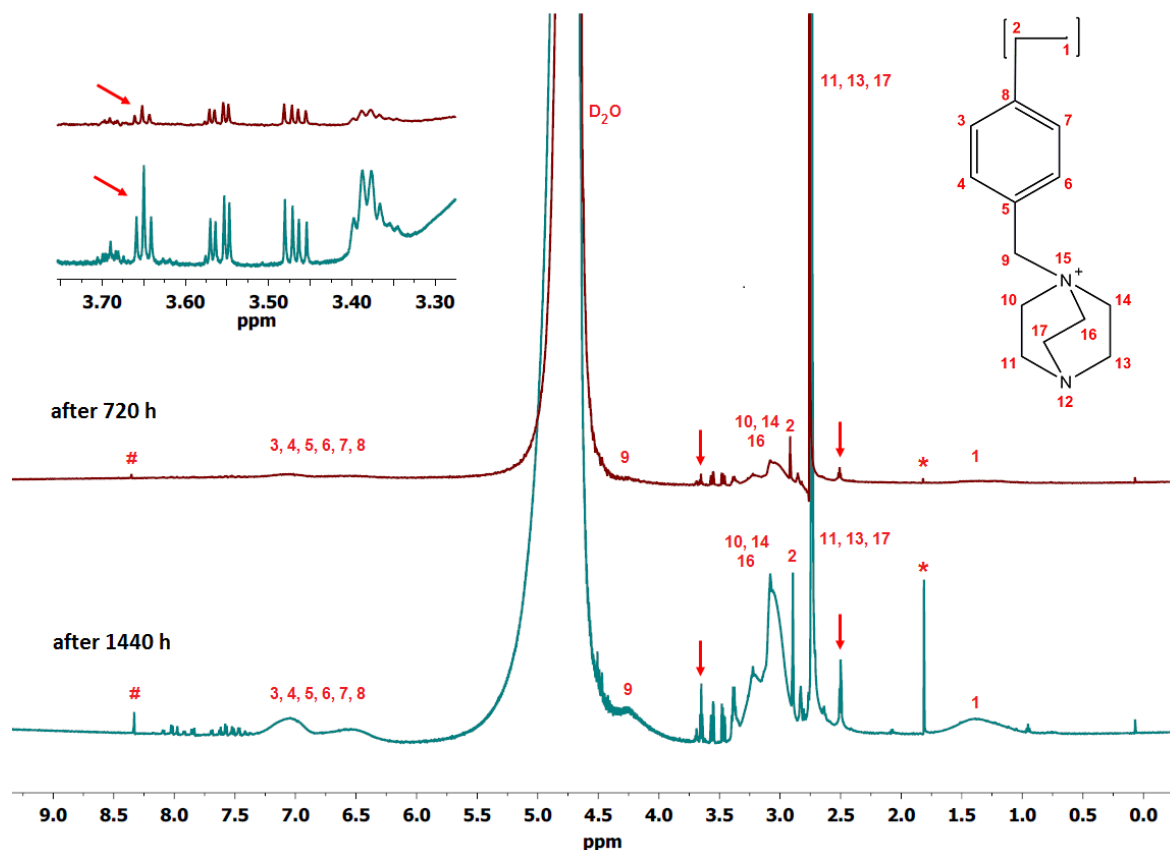
Figure 3.19. $^1$H NMR spectra of the degradation solution of DABCO-functionalised AEM.

The ratio of VBC to DABCO loss is 1:2 after both 720 and 1440 h degradation (Table 3.9), which is consistent with the ratios of VBC to DABCO loss estimated from the $^{13}$C CP-MAS NMR spectra (Table 3.8). This suggests that DABCO was detached from the membrane in addition to removal of the VBC–DABCO group as evidenced by the presence of 4.25 ppm peak (9, Figure 3.19). Similar with the spectra of the degradation products of TMA-functionalised AEM, there is a peak at 1.81 ppm and at the downfield 8.34 ppm suggesting the presence of benzylic peroxide in the degradation solution of DABCO-functionalised AEM. Furthermore, there are new peaks detected in both spectra aside from the expected VBC and DABCO resonances, namely, 2.50, 3.38 and 3.65 ppm indicating the presence of other degradation products.
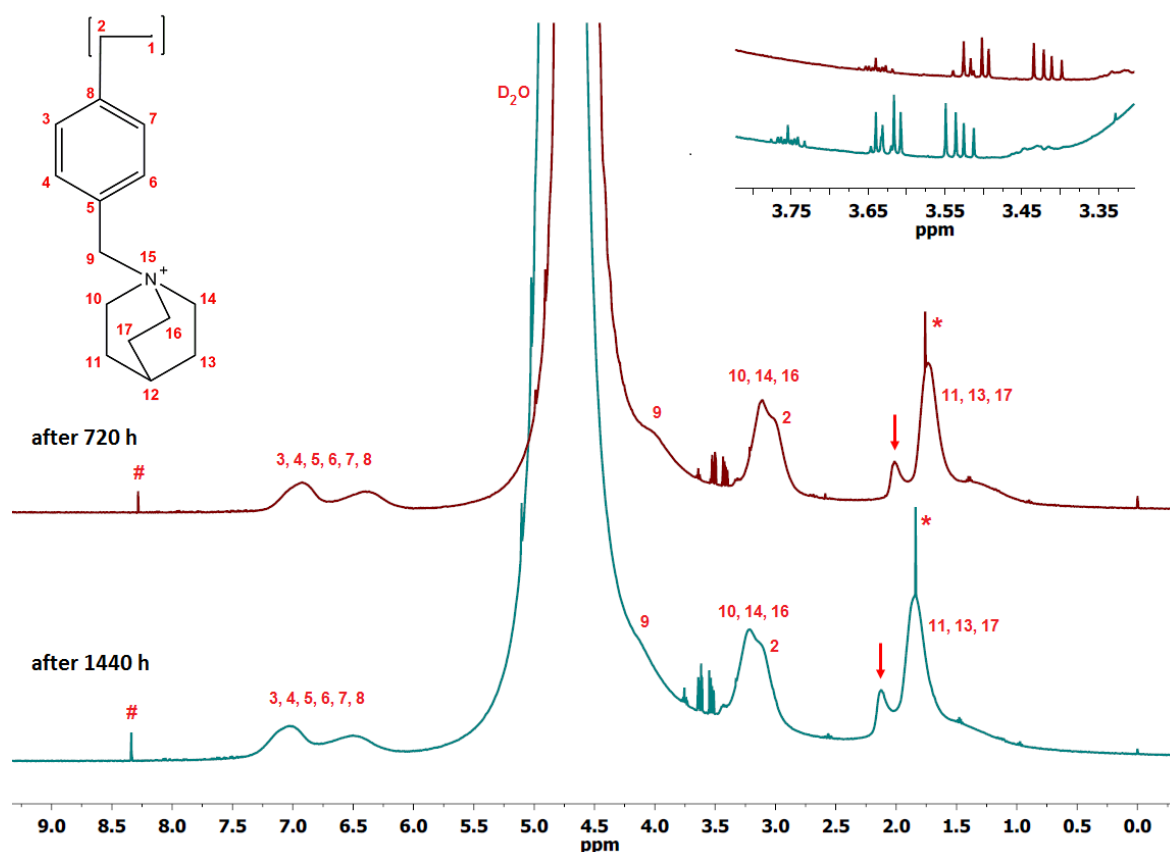
Figure 3.20. $^1$H NMR spectra of the degradation solution of ABCO-functionalised AEM.

Figure 3.20 shows the $^1$H NMR spectra of the degradation solution of ABCO-functionalised membrane. Similar with the $^1$H NMR spectra of the degradation solution of TMA- and DABCO-functionalised membranes, there's an observed loss of both the VBC and the ABCO head group from the membrane in both 720 and 1440 h degradation. The two spectra are identical, indicating similar species are present after 720 and 1440 h degradation, although with a slight shifting of the resonances. The spectra after 1440 h degradation showed increased intensity of peaks, indicating more loss of both VBC and ABCO with the same ratio. Upon integration of the spectra, the ratio of VBC to ABCO loss is 1:2 for both 720 and 1440 h degradation test (Table 3.9). The similar ratio of VBC to ABCO loss is due to their removal as a whole evidenced by the 4.0 ppm peak shown in the spectra (9, Figure 3.20). Furthermore, aside from the expected spectra of VBC and ABCO, there are new peaks observed in the spectra which suggests the presence of other degradation products. The unsymmetrical splitting spectra between 3.4 to 3.8 ppm

region is considered to be either noise in the signals or from impurities as they were detected in the same region regardless of the head-group investigated as detected in previous spectra (Figures 3.18 and 3.19).

The $^1$H NMR spectra of the degradation solution of the NMP-functionalised AEM is shown in Figure 3.21. Similar to those observed in previous spectra, the resonance after 720 and 1440 h degradation are identical suggesting the presence of similar degradation products and there is an observed increase in peak intensity as the degradation test is prolonged to 1440 h.
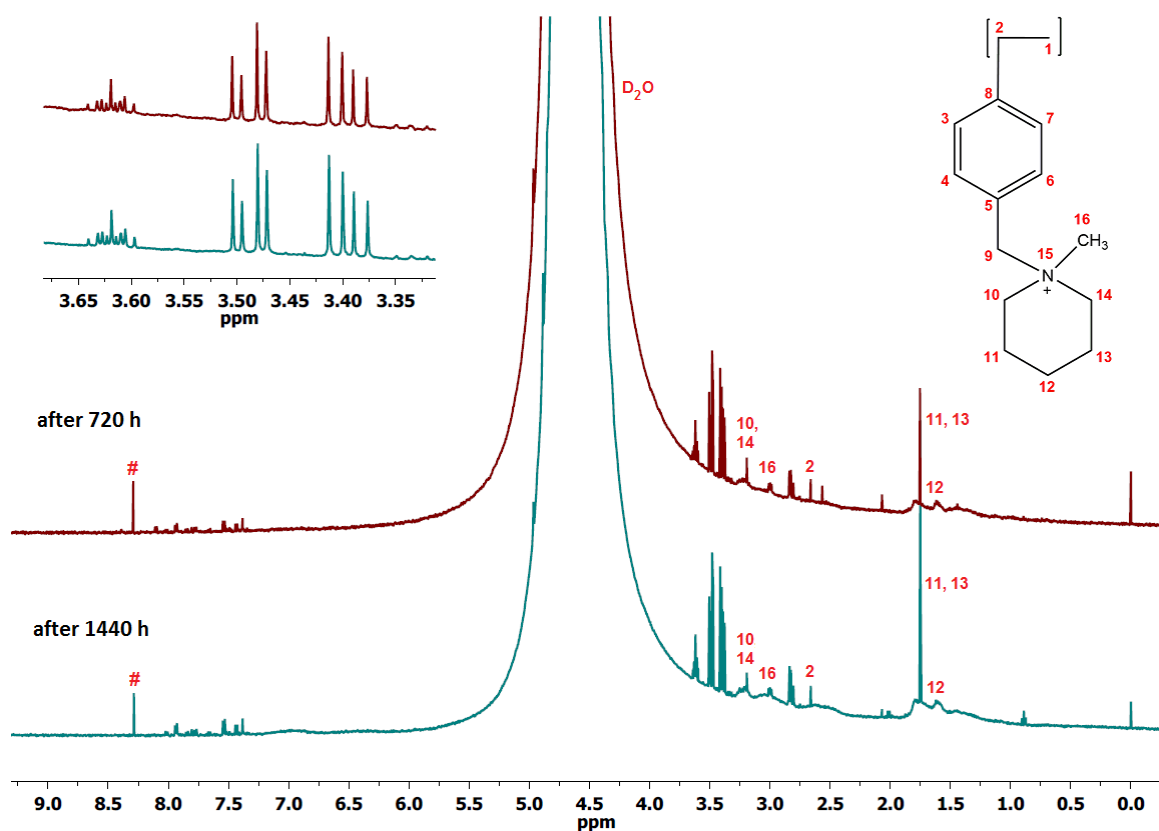


Figure 3.21. $^1$H NMR spectra of the degradation solution of NMP-functionalised AEM.

There is no or very little loss of VBC observed from both spectra hence ratio of VBC to NMP loss was not computed (Table 3.9). It is more likely that the estimation of % VBC loss using the $^{13}$C NMR spectra is inaccurate due to the reasons mentioned earlier (i.e. personal bias in measurement) and considering the fact that solution-NMR is more sensitive and accurate than solid-state NMR.

However, there is identified presence of NMP in the degradation solution confirming loss of the head group. Furthermore, the asymmetric signals between the 3.35 to 3.65 ppm region were considered to be from noise or impurities. There are also new peaks detected but these are considered as impurities due to their very weak absolute intensities.

## 3.14 Degradation test under nitrogen and oxygen atmospheres

In order to investigate the effect of oxygen gas feed (oxidation) to the degradation of membrane, $OH^-$ exchanged TMA-functionalised AEM (2000 Gy $h^{-1}$, 65% DOG) was subjected to 1440 h degradation test with continuous oxygen gas feed under reflux. A similar membrane was subjected to the same degradation test but with nitrogen gas feed for comparison. Table 3.10 shows the IEC of the membranes after the degradation test.

Immediately after the degradation test, both membranes were immersed in 1.0 M NaCl solution (without prior $OH^-$ ion exchange) for IEC measurement. Table 3.10 shows decrease in IEC of the membranes after the degradation test wherein from the initial 2.7 mmol $g^{-1}$, the IEC dropped to 1.9 and 2.4 mmol $g^{-1}$ with oxygen and nitrogen gas feed, respectively. However, when the IEC of the membranes were measured again by re-exchanging with 1.0 M NaOH solution prior to titration, the membrane that undergone degradation test under nitrogen gas feed recovered its initial IEC. The result indicates that the membrane remains stable under nitrogen gas feed which agrees well with earlier observation.

Table 3.10. The IEC of TMA-functionalised membranes immersed in $D_2O$ supplied with different gas feeds at 60 °C.

| Gas Feed | IEC (mmol $g^{-1}$) | |
|---|---|---|
| | Initial | After 1440 h |
| Oxygen | | 1.9 |
| Nitrogen | 2.7 | 2.4 |

The observed loss of IEC immediately after the degradation test suggests the presence of other anions (aside from OH⁻) attached to the AEM active sites, which consequently reduce the OH⁻ ions present that could react with the titrant during acid-base titration. The decrease in IEC can be due to the possible presence of carbonates and/or bicarbonates ($CO_3^-/HCO_3^-$) that were exchanged with the OH⁻ ions in the active site but not necessarily detaching the functional head group from the membrane, especially in the case of aged TMA-functionalised AEM under nitrogen gas feed. This might also indicate that some of the OH⁻ ions initially present in the membrane could have been neutralised or have been transformed or reacted to form other compounds.

However, in the case of the aged TMA-functionalised AEM under oxygen gas feed, the loss of IEC after 1440 h is not entirely due to the possible presence of other anions (i.e. $CO_3^-$ and/or $HCO_3^-$) but also due to the removal of both the VBC and TMA head group as shown in Figure 3.22. The ratio of VBC to head group loss is very close to 1, which is consistent with TMA-functionalised AEM as previously discussed and that the accelerated AEM degradation is caused by exposure to increased concentration of oxygen gas feed.
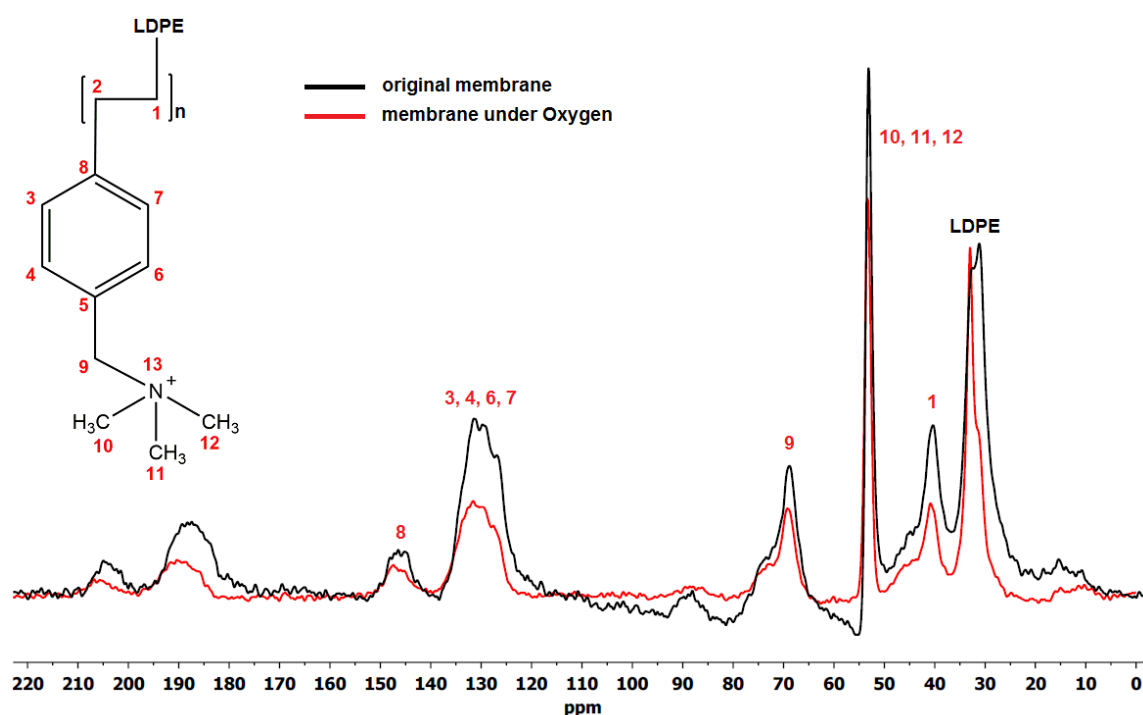


Figure 3.22. The ¹³CP-MAS NMR spectra of the original and aged TMA-functionalised membrane under oxygen gas feed after 1440 h.

The $^1$H NMR spectra of the degradation products of TMA functionalised membranes under oxygen and nitrogen atmospheres after stability tests are shown in Figure 3.23. The $^1$H NMR spectra revealed similar resonances both under oxygen and nitrogen gas feeds indicating presence of the same soluble degradation products. The peak at 3.3 ppm is associated to TMA while the resonances between the 7.5 to 8.0 ppm region represent the aromatic benzyl group. Similar with that previously mentioned, the additional peaks can be associated with other degradation products or possibly just impurities due to their very weak absolute intensities.
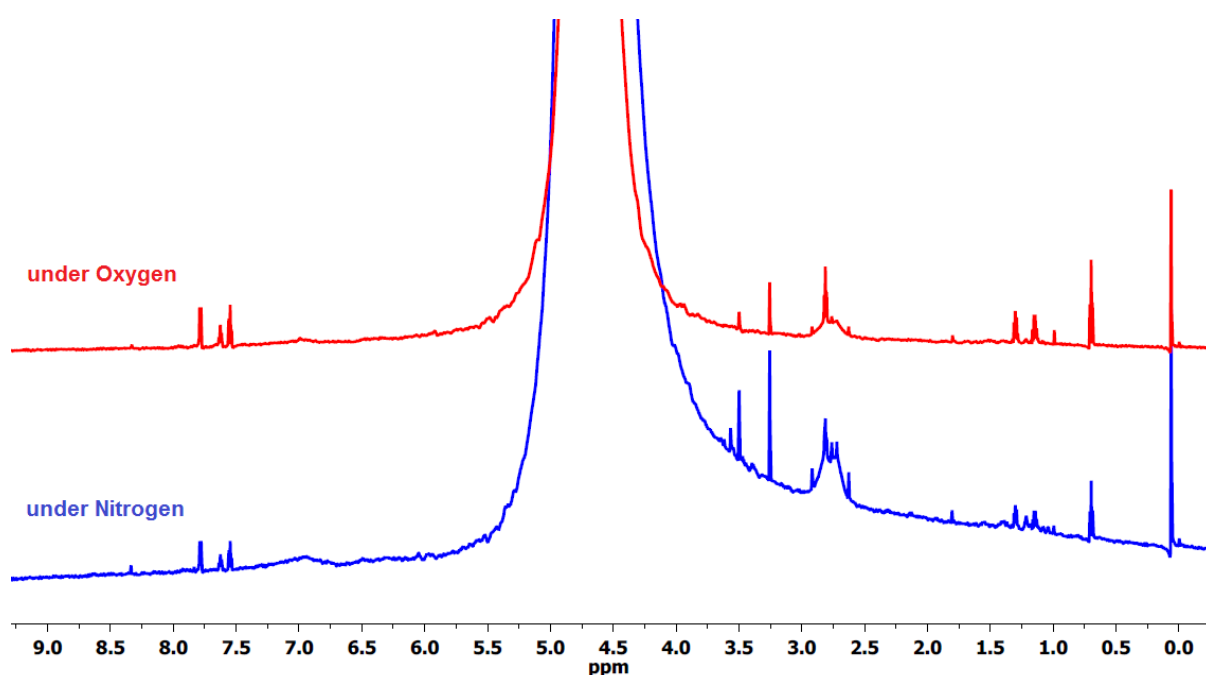


Figure 3.23. $^1$H NMR spectra of the degradation products of TMA-functionalised membranes under oxygen and nitrogen atmospheres after stability test.

The higher % IEC loss of the membrane with oxygen gas feed (29.6%) indicates faster degradation compared with 11.1 % IEC loss of the membrane with nitrogen gas feed. The faster degradation of AEM under oxygen environment is not only due to the removal of head group but also due to oxidation/auto-oxidation of the initial degradation products that result in the formation of peroxide radicals (Scheme 3.2). Therefore, at low alkalinity media typical for electrolysers and fuel cells, the degradation of AEM is chiefly driven by peroxide radical attack which occurs predominantly, compared with degradation by head group loss. This study

therefore reports the importance of oxidation in the degradation process and recommends that future research on AEM degradation be conducted at neutral pH and under oxygen-saturated conditions.

**3.15 Membrane stability of commercial membrane**

A commercially available membrane (A201) from Tokuyama Corp. was subjected to the similar stability test and the degradation in terms of IEC and ionic conductivity was compared with the fabricated AEM. Table 3.11 shows the IEC profile of the commercial A201 membrane after 720 and 1440 h degradation test. The initial IEC of the A201 membrane was measured to be 1.44 mmol $g^{-1}$ which is comparable with the IEC data reported by Tokuyama Corp. [224]. There is an observed similar trend of decreasing IEC of the membrane after each degradation period.

Table 3.11. IEC of commercial A201 membrane before and after degradation test at 60 °C in comparison with the fabricated LDPE-based AEMs

| Membrane Source | Membrane Type | Thickness (µm) | IEC (mmol $g^{-1}$) | | |
| --- | --- | --- | --- | --- | --- |
| | | | Initial | After 720 h | After 1440 h |
| Tokuyama | A201 | 28 | 1.4 | 1.2 | 0.8 |
| Fabricated LDPE-based | TMA-functionalised | 30 | 2.8 | 2.7 | 2.4 |
| | DABCO-functionalised | 30 | 2.3 | 2.2 | 2.0 |

At comparable thickness with the fabricated LDPE-based AEM (reproduced from Tables 3.2 and 3.3), the commercial membrane (A201) performed inferior having % IEC loss of 42.9% after 1440 h degradation, which is three times higher than the % IEC loss of fabricated AEMs (TMA- and DABCO-functionalised). The results indicate superior stability of the fabricated LDPE-based AEMs for electrolyser application in comparison with a commercially available membrane.

Since the chemical structure and identity of the commercial AEM is proprietary, the mechanism of membrane degradation cannot be predicted. However, based on the results, the degradation rate of the commercial membrane is faster than the fabricated membrane, which could indicate a more aggressive mechanism of OH⁻ ion attack that occurs not only to the functional head group, but also to the polymer backbone, of which the latter was not observed in the fabricated AEMs.

The measured decrease in IEC is consistent with the observed decrease in ionic conductivity for each degradation period as shown in Figure 3.24. The ionic conductivity of the OH⁻ exchanged original A201 membrane measured using a fuel cell setup at 25°C was 16.3 mS cm⁻¹ (100% RH), which was lower than the ionic conductivity advertised by Tokuyama Corp. of 42 mS cm⁻² (23°C and 90% RH) [224].
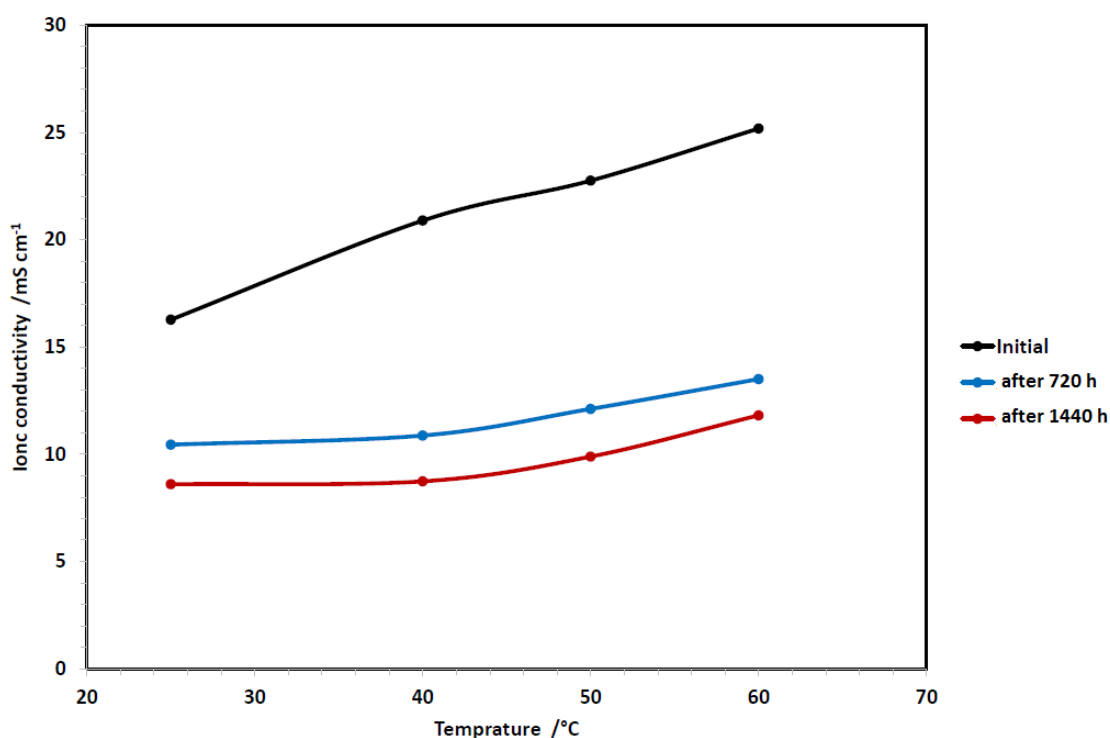


Figure 3.24. Ionic conductivity of A201 membrane before and after degradation test in a fuel cell setup.

The ionic conductivity of the A201 membrane under electrolyser operation at 80 °C using 0.5 M NaOH as the alkaline electrolyte is shown in Table 3.12. Similar with the measured ionic conductivity of the commercial A201 membrane in fully

humidified environment (fuel cell), the obtained ionic conductivity in an electrolyser setup was also low even with circulating alkaline electrolyte. The ionic conductivity of the TMA-functionalised membrane was also measured for comparison.

The fabricated TMA-functionalised membrane was expected to exhibit higher ionic conductivity than the A201 membrane because of its initial IEC double than that of the commercial membrane, which further increased due to the circulating alkaline electrolyte. However, ionic conductivity data (Table 3.12) indicates superb stability of the fabricated TMA-functionalised membrane in an electrolyser setup at 80 °C for 5 days in comparison with the day-to-day decrease in ionic conductivity of the commercial A201 membrane. Aside from the observed fast degradation rate of the A201 membrane at 60 °C in deionised water (Table 3.11), the higher degradation rate observed in Table 3.12 is the combination of increased alkaline concentration (more attacking OH$^-$ ions) and the increased operating temperature to 80 °C.

Table 3.12 Ionic conductivity of commercial A201 and TMA-functionalised AEMs at 80 °C using 0.5 M NaOH alkaline electrolyte

| Time (Day) | Average ionic conductivity (mS cm$^{-1}$) | |
| --- | --- | --- |
| | A201 membrane | TMA-functionalised AEM |
| 1 | 48 | 98 |
| 2 | 29 | 98 |
| 3 | 27 | 96 |
| 4 | 23 | 96 |
| 5 | 19 | 96 |

Prolonged use of the fabricated TMA-functionalised AEM in an electrolyser at 80 °C showed evidence of degradation due to the discoloration of the AEM exposed to the anode side (Figure 3.25). This is due to the oxidation of the membrane as oxygen is produced at the anode side coupled by the exposure of the AEM at high operating temperature. Furthermore, such oxidation reaction can be

the likely cause of the observed degradation in terms of decrease in ionic conductivity of the same TMA-functionalised membrane under vapour phase condition (fuel cell) at 80 °C (Figure 3.2). The observed discoloration (oxidation) confirms the occurrence of AEM degradation when exposed to oxygen as discussed in this research and thereby presents considerable challenge in designing and fabricating highly stable membrane for both fuel cell and electrolyser to ensure long term service life.



Figure 3.25. Discoloration of the TMA-functionalised AEM exposed to the anode side of the electrolyser setup

# CHAPTER 4
## CONCLUSION

The chemical and thermal stability of anion-exchange membrane (AEM) are important properties that dictate its service life for fuel cell and electrolyser applications. This research has investigated the stability of fabricated AEMs in both vapour phase condition and in deionised water which is the usual medium for electrolyser and fuel cell operation. After the stability test, there was an observed decrease in ion exchange capacity (IEC), hence a decrease in ionic conductivity, which is an indication of AEM degradation.

The LDPE-based membrane (71.3% DOG) was subjected to stability test for 4800 h and was found to be extremely stable at temperature of up to 80 °C for 2000 h under nitrogen, with average conductivity of 0.11 S cm$^{-1}$ and a degradation rate of 5.7 mS kh$^{-1}$. However, the membrane continuously lost conductivity when exposed to oxygen gas at 80 °C with a degradation rate of 24.3 mS kh$^{-1}$. At a conductivity cut-off point of 0.02 S cm$^{-1}$, the membrane projected life time under nitrogen is 2 years and 5 months under oxygen operating under 80 °C. The life time of the prepared membrane will however be significantly longer when it is operated at a lower temperature of typically 50 °C.

The stability of the membrane was found to be influenced by the applied gamma radiation dose rate. The use of higher radiation dose rate produces membranes with enhanced stability due to the improved VBC monomer distribution throughout the grafted monomer, hence more LDPE–VBC grafts and shorter VBC–VBC links. The increase in applied radiation dose rate from 30 to 67 Gy h$^{-1}$ (total radiation dose of 10 kGy) for the LDPE-based AEM significantly reduced the % IEC loss from 37 to 21%, respectively. The same was observed with HDPE-based AEM where the % IEC loss decreased from 50% to 28% with similar increase in radiation dose rate. The stability of the LDPE-based AEM even further improved when the applied radiation dose rate and total radiation dose were increased to 2000 Gy h$^{-1}$ and 20 kGy, respectively, with only 11% IEC loss. The ETFE-based AEMs, on the other hand, were fabricated using an electron beam radiation source and at 400 Gy h$^{-1}$ radiation dose rate demonstrated comparable stability to that of the LDPE based AEM (2000 Gy h$^{-1}$) having 13-15% IEC loss.

The use of different base polymer types among those investigated revealed minimal effect on the stability of the resulting AEM, which is mainly influenced by the structural changes (e.g. cross-linking, chain graft lengths, DOG) during radiation grafting. In terms of functional groups, TMA has emerged to offer slightly better stability than DABCO (under the same radiation dose rate).

NMR (solution and solid-state) and FTIR analyses of both the aged TMA- and DABCO-functionalised membranes and their degradation products confirmed loss of not only the functional group but also the VBC monomer which is in contrast with typically reported degradation mechanisms of AEMs where degradation under inert atmosphere and the use of simple benzyl trimethylammonium compound instead of polymer membrane in high alkaline media were mainly considered. At very low alkaline concentration, the reaction rates of membrane degradation were dependent on both oxygen concentration present in the surrounding media and on the applied radiation dose rate. As the concentration of dissolved oxygen in the solution is increased, the rate of membrane degradation due to IEC loss also increases due to increased formation of superoxide radicals that could attack the vulnerable benzylic carbon and cause the release of VBC–TMA chains. Polymer grafting performed under low radiation dose rates produces long chain grafts that leave large void spaces upon chain scission due to OH$^-$ ion attack. Moreover, $^{17}$O NMR analysis of the aged membrane and the degradation products revealed the presence of carbonyl-containing compounds suggesting that either the benzylic alcohol and TMA by-products are not the terminal form of the degradation products and could undergo further auto-oxidation leading to the loss of VBC through benzylic peroxide radicals and TMA–oxide radicals attack, or another more probable explanation is that peroxide radicals generated from dissolved oxygen through the ylide are responsible for VBC–TMA loss, wherein the degradation rate was observed to be faster with an oxygen gas feed compared with nitrogen under fuel cell operation as we have reported previously [114]. Lastly, preparation of AEMs with high radiation dose rate resulted in a lower % IEC loss and improved stability explained by shorter grafts length, which the established degradation mechanisms reported in literature have not taken into account.

The investigation on ABCO-functionalised membranes revealed similar degradation via the loss of both the VBC and head group as a whole. The DABCO-functionalised membrane (in mono-quaternised form) was found to offer better

stability than the ABCO-functionalised membrane, which is consistent with that reported in literature. Among all the amine head groups investigated in this research, TMA emerged as the most stable functionality for the AEM.

The $^1$H NMR spectra of the degradation solution confirmed the loss of the chemical components of the membrane (VBC and head group) observed in the $^{13}$C CP-MAS NMR spectra. The $^1$H NMR spectra of the degradation solution of the TMA-functionalised membrane showed presence of degradation products containing ether group compounds and benzylic hydroperoxy proton responsible to the attack on the head group and VBC chains. These degradation products containing ether group compounds and benzylic hydroperoxy proton were also observed with membranes tethered with other amine functionalities.

The degradation test under oxygen and nitrogen atmospheres confirmed the observed faster degradation in terms of ionic conductivity of the membrane under oxygen gas feed in a fuel cell setup in comparison with nitrogen gas feed. IEC measurement revealed higher % IEC loss under oxygen than with nitrogen, which agrees with the observed ionic conductivity, due to the oxidation/auto-oxidation of the degradation products leading to the formation of peroxide radicals. Hence, oxygen was found to play a significant role on faster degradation of the membrane.

A commercially available AEM (A201, Tokuyama Corp.) was subjected to the same stability test in order to compare with that of the fabricated AEMs. Results revealed that the commercial A201 membrane performs inferior compared with the fabricated AEMs. IEC measurement showed faster degradation of the commercial A201 membrane having three times higher % IEC loss than the fabricated TMA-functionalised membrane. The measured ionic conductivity of the membranes in both fuel cell and electrolyser setup agrees with the obtained IEC data. The degradation rate of the commercial membrane is faster than the fabricated membrane probably due to OH$^-$ ion attack on both the functional head group and polymer backbone, unlike that of the fabricated AEMs having polyethylene base films found to exhibit superb stability.

**RESEARCH SUMMARY**

This research has successfully fabricated polyethylene-based anion exchange membranes (AEM) promising for fuel cell and electrolyser application. The prepared AEMs were characterised in terms of degree of grafting (DOG), ion exchange capacity (IEC), water uptake and swelling, mechanical strength, ionic conductivity and fuel cell performance. The measured ionic conductivity and the IEC increased with increase in DOG where the fabricated membrane with 71.3% DOG exhibited the highest ionic conductivity of 0.12 S cm$^{-1}$ at a temperature of 70 °C prepared with 50 μm initial LDPE thickness. The fabricated TMA-functionalised membranes have an IEC of 2.7 mmol g$^{-1}$ regardless of the initial LDPE thickness. Such a high IEC is desired (IEC > 2.0 mmol g$^{-1}$) in order to achieve comparable H$^+$ ionic conductivity to that of Nafion (0.1 S cm$^{-1}$ at 80 °C, 100% RH) to compensate for the slow diffusion of hydrated OH$^-$ in comparison with that of the hydrated H$^+$. Moreover, the high IEC improves the hydrophilicity of the membrane which is necessary to stop AEM from dehydration at fuel cell operating temperatures above 60 °C.

A membrane electrode assembly based on the fabricated TMA-functionalised AEM showed high open circuit voltage of 1.08 V for AEM with 74.6% DOG. This indicates that membranes with DOG < 75% are suitable for fuel cell operation with low fuel cross over. The AEM with 74.6 % DOG and hydrated thickness of 151 μm exhibited the best performance among the fabricated AEMs achieving peak power density of 608 mW cm$^{-2}$ and maximum current density at 0.6 V of 643 mA cm$^{-2}$ under oxygen gas feed at 50 °C.

While this research has successfully synthesised alkaline AEMs exhibiting excellent ionic conductivity and cell performance, their chemical and thermal stability for long-term service life is noteworthy of investigation. The stability of the fabricated AEMs in both vapour phase (fuel cell) condition and in deionised water (electrolyser) is hereby reported. The TMA-functionalised AEM (71.3% DOG) was found to be highly stable in a fuel cell operating at temperature up to 80 °C for 2000 h under nitrogen, with average conductivity of 0.11 S cm$^{-1}$. However, the membrane showed evidence of degradation in terms of ionic conductivity when the gas feed was changed to oxygen with a degradation rate of 24.3 mS kh$^{-1}$. This indicates that oxygen plays a vital role in the stability and degradation of AEM which poses as a

critical challenge as oxygen is the usual reactant in fuel cells and product gas in electrolysers.

This research has established that the observed degradation of AEM is influenced by the applied gamma radiation dose rate. The use of a higher dose rate for the preparation of the membrane will result in enhanced stability brought about by the improved VBC monomer distribution throughout the grafted monomer (i.e. shorter VBC–VBC links and more LDPE–VBC grafts as more active sites are created). This finding is very significant as AEM degradation mechanisms reported in literature have not taken it into account.

In the investigation of the stability of the fabricated AEM, $^{13}$C CP-MAS NMR spectroscopy revealed the loss of not only the tethered head group but also the VBC monomer which is in contrast with typically reported degradation mechanisms of AEMs in literature, where degradation studies were performed under inert atmosphere use of simple TMA compounds unlike what has been done in this research of using actual polymer AEM. Furthermore, degradation tests reported in literature were mostly performed in high alkaline medium, elevated temperature and short period of exposure (hours or days). However, this study has demonstrated the occurrence of degradation of AEM even in neutral pH media and a degradation period of up to 1440 h. At very low alkaline concentration, the reaction rates of membrane degradation were dependent on both oxygen concentration and the applied radiation dose rate. The presence of dissolved oxygen in the solution caused the formation of superoxide radicals which consequently attack the benzylic carbon causing the release of VBC–TMA chains thereby resulting in the decrease in IEC of the membrane. Moreover, $^{17}$O NMR analysis confirmed the presence of carbonyl containing compounds in the degradation product and the $^{1}$H NMR spectra of the degradation solution confirmed the presence of dissolved VBC and head groups that dislodged from the membrane. The degradation solution also contains the benzylic hydroperoxy proton responsible in the head group and the VBC chains. The degradation test of membranes in deionised water with continuous flow of nitrogen and oxygen gas revealed faster rate of degradation in terms of % IEC loss under oxygen compared with that of nitrogen. Such oxidation/auto-oxidation of the AEM leading to the decrease in ionic conductivity was similarly observed under fuel cell condition as previously mentioned. With these significant findings, this research is the first to report that the degradation of the AEMs is not exclusively due to the

removal of the tethered head group, but is also attributed to the loss of VBC. An alternative degradation mechanism is hereby proposed which involves oxidation of the initial degradation products and the ylide intermediate that could explain the obtained results.

The observed degradation of TMA-functionalised membranes via the removal of both the TMA head group and the VBC led this research to consider other amine functionalities and compare them with TMA in terms of degradation, hence, DABCO, ABCO and NMP were considered. The investigation of the degradation of ABCO- and DABCO-functionalised AEM revealed degradation via the loss of the VBC and the head group as a whole, similar with that observed with TMA-functionalised AEM. However, mono-quaternised DABCO-functionalised AEM was more stable than the ABCO-functionalised membrane, consistent with that discussed in literature. The NMP-functionalised membrane, however showed loss of VBC in the $^{13}$C CP-MAS NMR spectra but only minimal presence of VBC was detected in the $^{1}$H NMR spectra of the degradation solution. This discrepancy is hereby recommended for further investigation.

Lastly, this research investigated the degradation of a commercially available AEM (A201, Tokuyama Corp.) which was compared with the fabricated AEMs. The results revealed that the fabricated AEM exhibited superior stability than the commercial A201 membrane in terms of % IEC loss and ionic conductivity, both in fuel cell and electrolyser setup. The % IEC loss of the commercial A201 membrane was 3 times that of the % IEC loss of the fabricated TMA-functionalised AEM with similar membrane thickness. Though the chemical structure of the commercial membrane is proprietary, the faster degradation rate of the A201 membrane could possibly due to the attack of OH$^{-}$ ions on both the head group on to the polymer backbone. The higher stability of the fabricated AEM compared with that of the commercial A201 membrane can be due to the superb stability of the polyethylene base polymer.

Therefore, in summary, the following are the highlights, novelty and key aspects of the study:

- Successfully fabricated LDPE-based anion exchange membranes exhibiting highest conductivity of 0.12 S cm$^{-1}$ at 70 °C and maximum current density at 0.6 V of 643 mA cm$^{-2}$ under oxygen at 50 °C.

- The stability of the fabricated anion exchange membranes in vapour phase condition was investigated.

- The use of high radiation dose rates produces membranes with enhanced stability due to the improved VBC monomer distribution through the grafted polymer.

- The degradation test of the fabricated membranes was performed in deionised water, which is the usual medium present in fuel cells and electrolyser operation, which is contrast with the degradation studies reported in the literature that are performed in high alkalinity solutions.

- The duration of the degradation study was also significantly prolonged (i.e. up to 1440 h in deionised water and 5000 h in nitrogen-saturated atmosphere) in order to confirm with certainty any observable degradation unlike those reported in literature which performed only in just few days immersion time.

- Actual fabricated polymer membranes were used in all degradation tests rather than simple benzyl trimethylammonium compound routinely reported in the literature.

- Successfully established that the degradation of the fabricated membranes is not solely due to the removal of the tethered functional group but also due to the removal of the vinylbenzyl group via oxidation (i.e. superoxide radical attack).

- The rate of membrane degradation is faster under oxygen gas feed compared to using nitrogen under fuel cell operation.

# RECOMMENDATION AND FUTURE WORK

This study was able to successfully fabricate membranes using polyethylene-based base polymer films and functionalised with different head groups under different synthesis conditions.  The prepared membranes were subsequently characterised and were found promising for fuel cell and electrolyser applications. The membranes were also subjected to degradation tests to assess their potential for efficient and long-term service of alkaline membrane fuel cells and electrolyser. Even though this research was able to present a great deal of accomplishment, there are still areas in this research that can be further investigated.

For the membrane synthesis part, although the author has successfully fabricated membranes with high ionic conductivity and ion exchange capacity due to the high degree of grafting, still a critical challenge is producing a membrane with all these desired properties but with controlled swelling and water uptake.  Very high degree of swelling and water uptake leads to dimensional deformation and structural instability of the membrane electrode assembly.

Another novelty of this research is the use of double-beam UV radiation source to prepare the polyethylene-VBC graft copolymer.  It was an attempt to address the low-energy radiation provided by a single-beam source and to ensure uniform grafting of VBC monomer on both sides of the base polymer film.

The study of the membrane degradation was complicated by the difficulty in identifying the degradation products hence, further chemical analysis of the solid membrane and the degradation solution is recommended.  Furthermore, the results of our degradation study paved the way for the future research on AEM materials and degradation studies to shift its focus on conducting investigations under pH close to neutral and in oxygen saturated environment.  The next research direction points to the design and synthesis of oxidation-resistant head groups where degradation experiments will be performed under oxygen atmosphere.

# APPENDIX A

## CASTING OF POLYETHYLENE FILM

Table A.1.  Summary of polyethylene casting runs

| Sample No. | Concentration | Casting Procedure | Findings /Remarks |
|---|---|---|---|
| 1 | 1% LDPE | 5 mL solvent evaporation at room temperature | Good cast 18 microns thickness; 43.9 mg |
| 2 | | 14 mL solvent evaporation at room temperature | Good cast 129.1 mg |
| 3 | 2% LDPE | Solvent evaporation at room temperature | Good cast 18 microns (center); 14-16 microns (edges); 153.3 mg |
| 4 | | Solvent evaporation in chamber (under pressure) and subsequently stored in oven at 97degC | Comparison before and after storing in oven produced no significant improvement |
| 5 | 5% LDPE | 5 mL solvent evaporation at 97degC in oven | Good cast 60-70 microns; 237.3 mg |
| 6 | | Heating gun casting | very fast evaporation rate |
| 7 | | Solvent evaporation at around 90-95 degC on hotplate | fast evaporation rate |
| 8 | | 5mL solvent evaporation inside chamber (vent to atmosphere); subsequently fed in furnace for 80 minutes at 150 degC | Good cast Improved transparency |
| 9 | 1% LLDPE | Solvent evaporation at above 65 degC on hotplate | Solid PE particulates and presence of holes |
| 10 | | Solvent evaporation at above 65 degC on open-oven | Solid PE particulates and presence of holes |
| 11 | 2% LLDPE | 8mL solvent evaporation inside chamber (vent to atmosphere) | Not completely casted; casting continued at ambient |
| 12 | | Heating gun casting | very fast evaporation rate |
| 13 | | 12 mL solvent evaporation at 97degC in oven | Good cast |
| 14 | 1% MDPE | Solvent evaporation at room temperature | contracted to the center of dish; strong and thick, yet brittle |
| 15 | | Solvent evaporation at above 65 degC on hotplate | Brittle |
| 16 | 2% MDPE | 5 mL solvent evaporation at 93degC in oven | very brittle |

# APPENDIX B

## RADIATION GRAFTING OF DIFFERENT POLYMER FILMS

Table B.1. DOG of membranes subjected to 10 kGy gamma radiation dose.

| Sample Description | 10/36/54 VBC/toluene/methanol | | | 31/26/43 VBC/toluene/methanol | | |
|---|---|---|---|---|---|---|
| | Initial Weight (mg) | Final Weight (mg) | Degrees of Grafting (DOG), % | Initial Weight (mg) | Final Weight (mg) | Degrees of Grafting (DOG), % |
| Cranfield | 151.2 | 158.1 | 4.36 | 147.2 | 296.8 | 50.40 |
| Cranfield | 148.1 | 157.1 | 5.73 | 150.8 | 289.2 | 47.86 |
| Entek UHMW PE | 35.4 | 44.8 | 20.98 | 36.3 | 85.3 | 57.44 |
| Entek UHMW PE | 34 | 44.4 | 23.42 | | | |
| VWR PE | 169.1 | 179.1 | 5.58 | 184.5 | 354 | 47.88 |
| VWR PE | | | | 173.2 | 358.4 | 51.67 |
| Cast 5% LDPE | 159.2 | 171.3 | 7.06 | 105.8 | 224.4 | 52.85 |
| Cast 2% LLDPE | 73.5 | 74.4 | 1.21 | 74.7 | 145.6 | 48.70 |
| Cranfield VBC with inhibitor | 145.6 | 152.3 | 4.40 | 145.1 | 307.5 | 52.81 |
| 5% LDPE Colloid | 114.2 | 106.2 | -7.53 | 112.7 | 103 | -9.42 |

Table B.2. DOG of membranes subjected to 20 kGy gamma radiation dose.

| Sample Description | 10/36/54 VBC/toluene/methanol | | | 31/26/43 VBC/toluene/methanol | | |
|---|---|---|---|---|---|---|
| | Initial Weight (mg) | Final Weight (mg) | Degrees of Grafting (DOG), % | Initial Weight (mg) | Final Weight (mg) | Degrees of Grafting (DOG), % |
| Cranfield | 152 | 181.6 | 16.30 | 153.8 | 605.4 | 74.60 |
| Cranfield | 144.8 | 174.4 | 16.97 | 172.2 | 631.5 | 72.73 |
| Entek UHMW PE | 35.9 | 66.5 | 46.02 | 35.5 | 220.7 | 83.91 |
| Entek UHMW PE | 34.4 | 58.2 | 40.89 | | | |
| VWR PE | 175.3 | 201.8 | 13.13 | 174.5 | 607.3 | 71.27 |
| VWR PE | | | | 182 | 634.1 | 71.30 |
| Cast 5% LDPE | 120 | 153.5 | 21.82 | 114 | 374.7 | 69.58 |
| Cast 2% LLDPE | 79.9 | 92.3 | 13.43 | 97.8 | 333.5 | 70.67 |
| Cranfield VBC with inhibitor | 153.6 | 178.7 | 14.05 | 146.4 | 504.6 | 70.99 |
| 5% LDPE Colloid | 113.9 | 129.5 | 12.05 | 121 | 153.9 | 21.38 |

**LIST OF PUBLICATIONS AND CONFERENCES/WORKSHOPS ATTENDED**

A. Research Publications

**R. Espiritu**, B. Golding, K. Scott and M. Mamlouk. Degradation of radiation grafted hydroxide anion exchange membranes tethered with different amine functional groups via removal of vinylbenzyl trimethylammonium hydroxide. **In preparation for submission to the Journal of Power Sources.**

**R. Espiritu**, B. Golding, K. Scott and M. Mamlouk. Degradation of radiation grafted hydroxide anion exchange membrane immersed in neutral pH: Removal of vinylbenzyl trimethylammonium hydroxide due to oxidation. **Journal of Materials Chemistry A.** 5(3), 1248-1267, 2017. **DOI: 10.1039/c6ta08232g (Open Access)**

**R. Espiritu**, M. Mamlouk, and K. Scott. Study on the Effect of the Degree of Grafting on the Performance of Polyethylene-based Anion Exchange Membrane for Fuel Cell Application. **International Journal of Hydrogen Energy**, 41(2), 1120-1133, 2016. **DOI: 10.1016/j.ijhydene.2015.10.108 (Open Access)**

K. Scott, M. Mamlouk, **R. Espiritu** and X. Wu. Progress in Alkaline Membrane Fuel Cells and Regenerative Fuel Cells. **ECS Transactions** 58(1), 1903-1906, 2013. **DOI: 10.1149/05801.1903ecst**

B. Conference Paper (SCOPUS-listed)

K. Scott, M. Mamlouk, **R. Espiritu** and X. Wu. Progress in Alkaline Membrane Fuel Cells and Electrolysers. **EFC 2013 – Proceedings of the 5th European Fuel Cell Piero Lunghi Conference and Exhibition.** Rome, Italy. December 11 to 13, 2013. Cigolotti V., Barchiesi C., and Chianella M. (Eds.). Rome: ENEA, pp. 249-250. ISBN: 978-888286297-8.

C. Papers presented in Conferences

"Stability and Degradation Studies of Polyethylene-based Anion Exchange Membrane for Alkaline Fuel Cells and Electrolyser Application". **International Conference on Renewable Energy (INCORE 2016)**. Zewail City of Science and Technology, Cairo, Egypt. February 3 to 6, 2016.

"Stability Assessment of Polyethylene-based Anion Exchange Membrane for Alkaline Fuel Cells and Electrolysers". **Workshop on Ion Exchange Membranes for Energy Applications (EMEA 2015)**. Hansens Haus am Meer, Bad Zwischenahn, Germany. June 22 to 24, 2015.

"Synthesis of Polyethylene-based Anion Exchange Membrane for Alkaline Fuel Cells and Electrolysers and their Stability Assessment". **6th International Conference on Fundamentals and Development of Fuel Cells (FDFC 2015)**. Congress Center Pierre Baudis, Toulouse, France. February 3 to 5, 2015.

"Synthesis of LDPE-based Anion Exchange Membrane via Radiation-induced Graft Copolymerization for Alkaline Fuel Cells". **20th World Hydrogen Energy Conference (WHEC 2014)**. Kimdaejung Convention Center, Gwangju Metropolitan City, South Korea. June 15 to 20, 2014.

"Progress in Alkaline Membrane Fuel Cells and Regenerative Fuel Cells". **European Fuel Cell Technology and Applications: Piero Lunghi Conference (EFC 2013)**. Fontana di Trevi Conference Center, Rome, Italy. December 11 to 13, 2013.

## D. Seminar / Workshop / Summer School Attended

Workshop on Solid State NMR: Basic Principles, Practice, Interpretation and Applications. Department of Chemistry, Durham University, United Kingdom. March 24 and 25, 2015.

Joint European Summer School for Fuel Cell, Electrolyser and Battery Technologies (JESS 2014). Pearl Beach Hotel, Rethymno, Greece. September 21 to 27, 2014.

## E. Award and Recognition

**Best Oral Presenter** entitled "Synthesis of Polyethylene-based Anion Exchange Membrane for Alkaline Fuel Cells and their Stability Assessment". School of Chemical Engineering and Advanced Materials (CEAM) Postgraduate Research Conference, Newcastle University, United Kingdom. May 19, 2014.

# REFERENCES

[1] Y.-C. Cao, X. Wang, M. Mamlouk, K. Scott, Preparation of alkaline anion exchange polymer membrane from methylated melamine grafted poly(vinylbenzyl chloride) and its fuel cell performance, Journal of Materials Chemistry, 21 (2011) 12910.

[2] A. Kirubakaran, S. Jain, R.K. Nema, A review on fuel cell technologies and power electronic interface, Renewable and Sustainable Energy Reviews, 13 (2009) 2430-2440.

[3] K. Sopian, W.R. Wan Daud, Challenges and future developments in proton exchange membrane fuel cells, Renewable Energy, 31 (2006) 719-727.

[4] E. Antolini, E.R. Gonzalez, Alkaline direct alcohol fuel cells, Journal of Power Sources, 195 (2010) 3431-3450.

[5] C.S. O'Hayre R., Colella W., Prinz F., Fuel cell fundamentals, John Wiley & Sons, Inc., 2006.

[6] F. Bidault, P.H. Middleton, 4.07 - Alkaline Fuel Cells: Theory and Application, in: Comprehensive Renewable Energy, Elsevier, Oxford, 2012, pp. 179-202.

[7] G.F. McLean, T. Niet, S. Prince-Richard, N. Djilali, An assessment of alkaline fuel cell technology, International Journal of Hydrogen Energy, 27 (2002) 507-526.

[8] K. Zeng, D. Zhang, Recent progress in alkaline water electrolysis for hydrogen production and applications, Progress in Energy and Combustion Science, 36 (2010) 307-326.

[9] A. Ursua, L.M. Gandia, P. Sanchis, Hydrogen Production From Water Electrolysis: Current Status and Future Trends, Proceedings of the IEEE, 100 (2012) 410-426.

[10] T. Smolinka, E.T. Ojong, J. Garche, Chapter 8 - Hydrogen Production from Renewable Energies—Electrolyzer Technologies, in: Electrochemical Energy Storage for Renewable Sources and Grid Balancing, Elsevier, Amsterdam, 2015, pp. 103-128.

[11] M. Carmo, D.L. Fritz, J. Mergel, D. Stolten, A comprehensive review on PEM water electrolysis, International Journal of Hydrogen Energy, 38 (2013) 4901-4934.

[12] D.L. Stojić, T.D. Grozdić, B. Umićević, A.D. Maksić, A comparison of alkaline and proton exchange membrane electrolyzers, Russian Journal of Physical Chemistry A, 82 (2008) 1958-1960.

[13] M. Mamlouk, X. Wang, K. Scott, J.A. Horsfall, C. Williams, Characterization and application of anion exchange polymer membranes with non-platinum group metals for fuel cells, Proceedings of the Institution of Mechanical Engineers, Part A: Journal of Power and Energy, 225 (2011) 152-160.

[14] J.-S. Park, S.-H. Park, S.-D. Yim, Y.-G. Yoon, W.-Y. Lee, C.-S. Kim, Performance of solid alkaline fuel cells employing anion-exchange membranes, Journal of Power Sources, 178 (2008) 620-626.

[15] Y.-C. Cao, X. Wang, K. Scott, The synthesis and characteristic of an anion conductive polymer membrane for alkaline anion exchange fuel cells, Journal of Power Sources, 201 (2012) 226-230.

[16] C.C. Pavel, F. Cecconi, C. Emiliani, S. Santiccioli, A. Scaffidi, S. Catanorchi, M. Comotti, Highly Efficient Platinum Group Metal Free Based Membrane-Electrode Assembly for Anion Exchange Membrane Water Electrolysis, Angewandte Chemie International Edition, 53 (2014) 1378-1381.

[17] S. Lu, J. Pan, A. Huang, L. Zhuang, J. Lu, Alkaline polymer electrolyte fuel cells completely free from noble metal catalysts, Proceedings of the National Academy of Sciences, 105 (2008) 20611-20614.

[18] C.G. Arges, Ramani V., and Pintauro P. N., Anion exchange membrane fuel cells, The Electrochemical Society Interface, 19 (2010) 31- 35.

[19] X. Wang, M. Li, B.T. Golding, M. Sadeghi, Y. Cao, E.H. Yu, K. Scott, A polytetrafluoroethylene-quaternary 1,4-diazabicyclo-[2.2.2]-octane polysulfone composite membrane for alkaline anion exchange membrane fuel cells, International Journal of Hydrogen Energy, 36 (2011) 10022-10026.

[20] J.R. Varcoe, M. Beillard, D.M. Halepoto, J.P. Kizewski, S. Poynton, R.C.T. Slade, Membrane and Electrode Materials for Alkaline Membrane Fuel Cells, ECS Transactions, 16 (2008) 1819-1834.

[21] J.R. Varcoe, R.C.T. Slade, Prospects for Alkaline Anion-Exchange Membranes in Low Temperature Fuel Cells, Fuel Cells, 5 (2005) 187-200.

[22] S. Srinivasan, B.B. Davé, K.A. Murugesamoorthi, A. Parthasarathy, A.J. Appleby, Overview of Fuel Cell Technology, in: L.J.M.J. Blomen, M.N. Mugerwa (Eds.) Fuel Cell Systems, Springer US, Boston, MA, 1993, pp. 37-72.

[23] J. Larminie, A. Dicks, Fuel cell systems explained, Second ed., John Wiley & Sons Ltd., England, 2003, pp. 46, 48, 67, 122.

[24] G. Merle, M. Wessling, K. Nijmeijer, Anion exchange membranes for alkaline fuel cells: A review, Journal of Membrane Science, 377 (2011) 1-35.

[25] L. Carrette, K.A. Friedrich, U. Stimming, Fuel Cells: Principles, Types, Fuels, and Applications, ChemPhysChem, 1 (2000) 162-193.

[26] H.W. Zhang, D.Z. Chen, Y. Xianze, S.B. Yin, Anion-Exchange Membranes for Fuel Cells: Synthesis Strategies, Properties and Perspectives, Fuel Cells, 15 (2015) 761-780.

[27] K.E. Ayers, E.B. Anderson, C.B. Capuano, M. Niedzwiecki, M.A. Hickner, C.-Y. Wang, Y. Leng, W. Zhao, Characterization of Anion Exchange Membrane Technology for Low Cost Electrolysis, ECS Transactions, 45 (2013) 121-130.

[28] C.K. Mittelsteadt, J.A. Staser, 10.42 - Electrolyzer Membranes, in: Polymer Science: A Comprehensive Reference, Elsevier, Amsterdam, 2012, pp. 849-871.

[29] M. Mamlouk, K. Scott, Effect of anion functional groups on the conductivity and performance of anion exchange polymer membrane fuel cells, Journal of Power Sources, 211 (2012) 140-146.

[30] J.R. Varcoe, J.P. Kizewski, D.M. Halepoto, S.D. Poynton, R.C.T. Slade, F. Zhao, FUEL CELLS – ALKALINE FUEL CELLS | Anion-Exchange Membranes, in: G. Editor-in-Chief: Jürgen (Ed.) Encyclopedia of Electrochemical Power Sources, Elsevier, Amsterdam, 2009, pp. 329-343.

[31] G. Wang, Y. Weng, D. Chu, R. Chen, D. Xie, Developing a polysulfone-based alkaline anion exchange membrane for improved ionic conductivity, Journal of Membrane Science, 332 (2009) 63-68.

[32] M.R. Hibbs, C.H. Fujimoto, C.J. Cornelius, Synthesis and Characterization of Poly(phenylene)-Based Anion Exchange Membranes for Alkaline Fuel Cells, Macromolecules, 42 (2009) 8316-8321.

[33] Y. Luo, J. Guo, C. Wang, D. Chu, Quaternized poly(methyl methacrylate-co-butyl acrylate-co-vinylbenzyl chloride) membrane for alkaline fuel cells, Journal of Power Sources, 195 (2010) 3765-3771.

[34] D. Stoica, L. Ogier, L. Akrour, F. Alloin, J.F. Fauvarque, Anionic membrane based on polyepichlorhydrin matrix for alkaline fuel cell: Synthesis, physical and electrochemical properties, Electrochimica Acta, 53 (2007) 1596-1603.

[35] H. Hou, G. Sun, R. He, B. Sun, W. Jin, H. Liu, Q. Xin, Alkali doped polybenzimidazole membrane for alkaline direct methanol fuel cell, International Journal of Hydrogen Energy, 33 (2008) 7172-7176.

[36] D. Aili, M.K. Hansen, R.F. Renzaho, Q. Li, E. Christensen, J.O. Jensen, N.J. Bjerrum, Heterogeneous anion conducting membranes based on linear and crosslinked KOH doped polybenzimidazole for alkaline water electrolysis, Journal of Membrane Science, 447 (2013) 424-432.

[37] J.O. Jensen, D. Aili, M.K. Hansen, Q. Li, N.J. Bjerrum, E. Christensen, A Stability Study of Alkali Doped PBI Membranes for Alkaline Electrolyzer Cells, ECS Transactions, 64 (2014) 1175-1184.

[38] O. Savadogo, B. Xing, Hydrogen/oxygen polymer electrolyte membrane fuel cell (PEMFC) based on acid-doped polybenzimidazole (PBI), Journal of New Materials for Electrochemical Systems, 3 (2000) 345-349.

[39] D.W. Tomlin, A.V. Fratini, M. Hunsaker, W. Wade Adams, The role of hydrogen bonding in rigid-rod polymers: the crystal structure of a polybenzobisimidazole model compound, Polymer, 41 (2000) 9003-9010.

[40] G. Couture, A. Alaaeddine, F. Boschet, B. Ameduri, Polymeric materials as anion-exchange membranes for alkaline fuel cells, Progress in Polymer Science, 36 (2011) 1521-1557.

[41] M. Zhang, H.K. Kim, E. Chalkova, F. Mark, S.N. Lvov, T.C.M. Chung, New Polyethylene Based Anion Exchange Membranes (PE–AEMs) with High Ionic Conductivity, Macromolecules, 44 (2011) 5937-5946.

[42] H.K. Kim, M. Zhang, X. Yuan, S.N. Lvov, T.C.M. Chung, Synthesis of Polyethylene-Based Proton Exchange Membranes Containing PE Backbone and Sulfonated Poly(arylene ether sulfone) Side Chains for Fuel Cell Applications, Macromolecules, 45 (2012) 2460-2470.

[43] M.M. Nasef, Radiation-Grafted Membranes for Polymer Electrolyte Fuel Cells: Current Trends and Future Directions, Chemical Reviews, 114 (2014) 12278-12329.

[44] S. Alkan Gürsel, L. Gubler, B. Gupta, G. Scherer, Radiation Grafted Membranes, in: G. Scherer (Ed.) Fuel Cells I, Springer Berlin Heidelberg, 2008, pp. 157-217.

[45] M.M. Nasef, E.-S.A. Hegazy, Preparation and applications of ion exchange membranes by radiation-induced graft copolymerization of polar monomers onto non-polar films, Progress in Polymer Science, 29 (2004) 499-561.

[46] J.P. Masson, R. Molina, E. Roth, G. Gaussens, F. Lemaire, Obtention and evaluation of polyethylene-based solid polymer electrolyte membranes for hydrogen production, International Journal of Hydrogen Energy, 7 (1982) 167-171.

[47] M. Faraj, M. Boccia, H. Miller, F. Martini, S. Borsacchi, M. Geppi, A. Pucci, New LDPE based anion-exchange membranes for alkaline solid polymeric electrolyte water electrolysis, International Journal of Hydrogen Energy, 37 (2012) 14992-15002.

[48] M. Mamlouk, J.A. Horsfall, C. Williams, K. Scott, Radiation grafted membranes for superior anion exchange polymer membrane fuel cells performance, International Journal of Hydrogen Energy, 37 (2012) 11912-11920.

[49] M. Mamlouk, K. Scott, J.A. Horsfall, C. Williams, The effect of electrode parameters on the performance of anion exchange polymer membrane fuel cells, International Journal of Hydrogen Energy, 36 (2011) 7191-7198.

[50] T.A. Sherazi, J. Yong Sohn, Y. Moo Lee, M.D. Guiver, Polyethylene-based radiation grafted anion-exchange membranes for alkaline fuel cells, Journal of Membrane Science, 441 (2013) 148-157.

[51] M. Shen, S. Roy, J. Kuhlmann, K. Scott, K. Lovell, J. Horsfall, Grafted polymer electrolyte membrane for direct methanol fuel cells, Journal of Membrane Science, 251 (2005) 121-130.

[52] H. Cheng, K. Scott, K.V. Lovell, J.A. Horsfall, S.C. Waring, Evaluation of new ion exchange membranes for direct borohydride fuel cells, Journal of Membrane Science, 288 (2007) 168-174.

[53] H.A. Kostalik, T.J. Clark, N.J. Robertson, P.F. Mutolo, J.M. Longo, H.c.D. Abruña, G.W. Coates, Solvent Processable Tetraalkylammonium-Functionalized Polyethylene for Use as an Alkaline Anion Exchange Membrane, Macromolecules, 43 (2010) 7147-7150.

[54] G.K. Kostov, S.C. Turmanova, Radiation-initiated graft copolymerization of 4-vinylpyridine onto polyethylene and polytetrafluoroethylene films and anion-exchange membranes therefrom, Journal of Applied Polymer Science, 64 (1997) 1469-1475.

[55] K.J.T. Noonan, K.M. Hugar, H.A. Kostalik, E.B. Lobkovsky, H.D. Abruña, G.W. Coates, Phosphonium-Functionalized Polyethylene: A New Class of Base-Stable Alkaline Anion Exchange Membranes, Journal of the American Chemical Society, 134 (2012) 18161-18164.

[56] J.R. Varcoe, R.C.T. Slade, E. Lam How Yee, S.D. Poynton, D.J. Driscoll, D.C. Apperley, Poly(ethylene-co-tetrafluoroethylene)-Derived Radiation-Grafted Anion-Exchange Membrane with Properties Specifically Tailored for Application in Metal-Cation-Free Alkaline Polymer Electrolyte Fuel Cells, Chemistry of Materials, 19 (2007) 2686-2693.

[57] Y. Zhao, H. Yu, F. Xie, Y. Liu, Z. Shao, B. Yi, High durability and hydroxide ion conducting pore-filled anion exchange membranes for alkaline fuel cell applications, Journal of Power Sources, 269 (2014) 1-6.

[58] A.S. Gruzd, E.S. Trofimchuk, N.I. Nikonorova, E.A. Nesterova, I.B. Meshkov, M.O. Gallyamov, A.R. Khokhlov, Novel polyolefin/silicon dioxide/H3PO4 composite membranes with spatially

heterogeneous structure for phosphoric acid fuel cell, International Journal of Hydrogen Energy, 38 (2013) 4132-4143.

[59] M.M. Nasef, S.A. Gürsel, D. Karabelli, O. Güven, Radiation-grafted materials for energy conversion and energy storage applications, Progress in Polymer Science, 63 (2016) 1-41.

[60] M.M. Franjo Ranogajec, Zvonimir Hell, Improvement of the polymer properties by radiation grafting and crosslinking, Polimeri, 29 (2008) 236-243.

[61] T.R. Dargaville, G.A. George, D.J.T. Hill, A.K. Whittaker, High energy radiation grafting of fluoropolymers, Progress in Polymer Science, 28 (2003) 1355-1376.

[62] M.M. Nasef, Fuel Cell Membranes by Radiation-Induced Graft Copolymerization: Current Status, Challenges, and Future Directions, in: S.M.J. Zaidi, T. Matsuura (Eds.) Polymer Membranes for Fuel Cells, Springer US, 2009, pp. 87-114.

[63] T. Zhou, R. Shao, S. Chen, X. He, J. Qiao, J. Zhang, A review of radiation-grafted polymer electrolyte membranes for alkaline polymer electrolyte membrane fuel cells, Journal of Power Sources, 293 (2015) 946-975.

[64] C. Padeste, S. Neuhaus, Chapter 2 - Polymer-on-Polymer Structures Based on Radiation Grafting, in: Polymer Micro- and Nanografting, William Andrew Publishing, Oxford, 2015, pp. 11-41.

[65] S.M. Tamboli, Mhaske, S T and Kale, D D, Crosslinked Polyethylene, Indian Journal of Chemical Technology, 11 (2004) 853-864.

[66] B. Qu, Y. Xu, L. Ding, B. Rånby, A new mechanism of benzophenone photoreduction in photoinitiated crosslinking of polyethylene and its model compounds, Journal of Polymer Science Part A: Polymer Chemistry, 38 (2000) 999-1005.

[67] H. Ma, R.H. Davis, C.N. Bowman, A Novel Sequential Photoinduced Living Graft Polymerization, Macromolecules, 33 (2000) 331-335.

[68] Y.-J. Choi, M.-S. Kang, J. Cho, S.-H. Moon, Preparation and characterization of LDPE/polyvinylbenzyl trimethyl ammonium salts anion-exchange membrane, Journal of Membrane Science, 221 (2003) 219-231.

[69] Y.-J. Choi, M.-S. Kang, S.-H. Kim, J. Cho, S.-H. Moon, Characterization of LDPE/polystyrene cation exchange membranes prepared by monomer sorption and UV radiation polymerization, Journal of Membrane Science, 223 (2003) 201-215.

[70] M.-L. Hwang, J.-M. Song, B.-S. Ko, J.-Y. Sohn, Y.-C. Nho, J. Shin, Radiation-induced grafting of vinylbenzyl chloride onto a poly(ether ether ketone) film, Nuclear Instruments and Methods in Physics Research Section B: Beam Interactions with Materials and Atoms, 281 (2012) 45-50.

[71] K. Scott, M. Mamlouk, R. Espiritu, X. Wu, Progress in Alkaline Membrane Fuel Cells and Regenerative Fuel Cells, ECS Transactions, 58 (2013) 1903-1906.

[72] S.M. Kolhe, A. Kumar, Preparation of strong base anion exchange membrane using 60Co gamma radiation, Radiation Physics and Chemistry, 74 (2005) 384-390.

[73] J.A. Horsfall, K.V. Lovell, Fuel Cell Performance of Radiation Grafted Sulphonic Acid Membranes, Fuel Cells, 1 (2001) 186-191.

[74] J. Fang, Y. Yang, X. Lu, M. Ye, W. Li, Y. Zhang, Cross-linked, ETFE-derived and radiation grafted membranes for anion exchange membrane fuel cell applications, International Journal of Hydrogen Energy, 37 (2012) 594-602.

[75] H. Herman, R.C.T. Slade, J.R. Varcoe, The radiation-grafting of vinylbenzyl chloride onto poly(hexafluoropropylene-co-tetrafluoroethylene) films with subsequent conversion to alkaline anion-exchange membranes: optimisation of the experimental conditions and characterisation, Journal of Membrane Science, 218 (2003) 147-163.

[76] M.J. Sundell, K.B. Ekman, B.L. Svarfvar, J.H. Näsman, Preparation of poly[ethylene-g-(vinylbenzyl chloride)] and functionalization with bis(phosphonic acid) derivatives, Reactive Polymers, 25 (1995) 1-16.

[77] W.G. Lloyd, T.E. Durocher, Kinetic observations of the quaternization of poly(ar-vinylbenzyl chloride) with trimethylamine, Journal of Applied Polymer Science, 8 (1964) 953-969.

[78] J.R. Varcoe, P. Atanassov, D.R. Dekel, A.M. Herring, M.A. Hickner, P.A. Kohl, A.R. Kucernak, W.E. Mustain, K. Nijmeijer, K. Scott, T. Xu, L. Zhuang, Anion-exchange membranes in electrochemical energy systems, Energy & Environmental Science, 7 (2014) 3135-3191.

[79] M. Nasef, Preparation and applications of ion exchange membranes by radiation-induced graft copolymerization of polar monomers onto non-polar films, Progress in Polymer Science, 29 (2004) 499-561.

[80] R. Vinodh, A. Ilakkiya, S. Elamathi, D. Sangeetha, A novel anion exchange membrane from polystyrene (ethylene butylene) polystyrene: Synthesis and characterization, Materials Science and Engineering: B, 167 (2010) 43-50.

[81] F. Karas, J. Hnát, M. Paidar, J. Schauer, K. Bouzek, Determination of the ion-exchange capacity of anion-selective membranes, International Journal of Hydrogen Energy, 39 (2014) 5054-5062.

[82] L. Gubler, S.A. Gürsel, G.G. Scherer, Radiation Grafted Membranes for Polymer Electrolyte Fuel Cells, Fuel Cells, 5 (2005) 317-335.

[83] Q. Duan, S. Ge, C.-Y. Wang, Water uptake, ionic conductivity and swelling properties of anion-exchange membrane, Journal of Power Sources, 243 (2013) 773-778.

[84] C.G. Arges, J. Parrondo, G. Johnson, A. Nadhan, V. Ramani, Assessing the influence of different cation chemistries on ionic conductivity and alkaline stability of anion exchange membranes, Journal of Materials Chemistry, 22 (2012) 3733-3744.

[85] W.-H. Lee, Y.S. Kim, C. Bae, Robust Hydroxide Ion Conducting Poly(biphenyl alkylene)s for Alkaline Fuel Cell Membranes, ACS Macro Letters, 4 (2015) 814-818.

[86] M.A. Vandiver, B.R. Caire, T.P. Pandey, Y. Li, S. Seifert, A. Kusoglu, D.M. Knauss, A.M. Herring, M.W. Liberatore, Effect of hydration on the mechanical properties and ion conduction in a polyethylene-b-poly(vinylbenzyl trimethylammonium) anion exchange membrane, Journal of Membrane Science, 497 (2016) 67-76.

[87] K.N. Grew, W.K.S. Chiu, A Dusty Fluid Model for Predicting Hydroxyl Anion Conductivity in Alkaline Anion Exchange Membranes, Journal of The Electrochemical Society, 157 (2010) B327-B337.

[88] S.J. Peighambardoust, S. Rowshanzamir, M. Amjadi, Review of the proton exchange membranes for fuel cell applications, International Journal of Hydrogen Energy, 35 (2010) 9349-9384.

[89] T.P. Pandey, H.N. Sarode, Y. Yang, Y. Yang, K. Vezzù, V.D. Noto, S. Seifert, D.M. Knauss, M.W. Liberatore, A.M. Herring, A Highly Hydroxide Conductive, Chemically Stable Anion Exchange Membrane, Poly(2,6 dimethyl 1,4 phenylene oxide)-b-Poly(vinyl benzyl trimethyl ammonium), for Electrochemical Applications, Journal of The Electrochemical Society, 163 (2016) H513-H520.

[90] Y.L. Ma, J.S. Wainright, M.H. Litt, R.F. Savinell, Conductivity of PBI Membranes for High-Temperature Polymer Electrolyte Fuel Cells, Journal of The Electrochemical Society, 151 (2004) A8-A16.

[91] C.H. Lee, H.B. Park, Y.M. Lee, R.D. Lee, Importance of Proton Conductivity Measurement in Polymer Electrolyte Membrane for Fuel Cell Application, Industrial & Engineering Chemistry Research, 44 (2005) 7617-7626.

[92] X.-Z.S. Yuan, Chaojie; Wang, Haijiang; Zhang, Jiujun, Electrochemical Impedance Spectroscopy in PEM Fuel Cells: Fundamentals and Applications, Springer, London, 2010.

[93] F. Barbir, PEM Fuel Cells: Theory and Practice, Elsevier Inc., USA, 2013.

[94] C. Kunusch, P.F. Puleston, M.A. Mayosky, J.J. Moré, Characterization and experimental results in PEM fuel cell electrical behaviour, International Journal of Hydrogen Energy, 35 (2010) 5876-5881.

[95] M.G. Santarelli, M.F. Torchio, P. Cochis, Parameters estimation of a PEM fuel cell polarization curve and analysis of their behavior with temperature, Journal of Power Sources, 159 (2006) 824-835.

[96] R. Talj, T. Azib, O. Béthoux, G. Remy, C. Marchand, E. Berthelot, Parameter analysis of PEM fuel cell hysteresis effects for transient load use, The European Physical Journal - Applied Physics, 54 (2011) null-null.

[97] J. Kim, S.M. Lee, S. Srinivasan, C.E. Chamberlin, Modeling of Proton Exchange Membrane Fuel Cell Performance with an Empirical Equation, Journal of The Electrochemical Society, 142 (1995) 2670-2674.

[98] A. Jikihara, R. Ohashi, Y. Kakihana, M. Higa, K. Kobayashi, Electrodialytic Transport Properties of Anion-Exchange Membranes Prepared from Poly(vinyl alcohol) and Poly(vinyl alcohol-co-methacryloyl aminopropyl trimethyl ammonium chloride), Membranes, 3 (2013) 1.

[99] J.A. Horsfall, K.V. Lovell, Synthesis and characterisation of sulfonic acid-containing ion exchange membranes based on hydrocarbon and fluorocarbon polymers, European Polymer Journal, 38 (2002) 1671-1682.

[100] J.V. Gulmine, P.R. Janissek, H.M. Heise, L. Akcelrud, Polyethylene characterization by FTIR, Polymer Testing, 21 (2002) 557-563.

[101] A.A. Moez, S.S. Aly, Y.H. Elshaer, Effect of gamma radiation on low density polyethylene (LDPE) films: Optical, dielectric and FTIR studies, Spectrochimica Acta Part A: Molecular and Biomolecular Spectroscopy, 93 (2012) 203-207.

[102] K. Yoko, Effects of Gamma Irradiation on Polyethylene, Polypropylene, and Polystyrene, in: Irradiation of Food and Packaging, American Chemical Society, 2004, pp. 262-276.

[103] V.J. Krasnansky, B.G. Achhammer, M.S. Parker, Effect of gamma radiation on chemical structure of plastics, Polymer Engineering & Science, 1 (1961) 133-138.

[104] H. Liu, S. Yang, S. Wang, J. Fang, L. Jiang, G. Sun, Preparation and characterization of radiation-grafted poly (tetrafluoroethylene-co-perfluoropropyl vinyl ether) membranes for alkaline anion-exchange membrane fuel cells, Journal of Membrane Science, 369 (2011) 277-283.

[105] M.R. Hibbs, M.A. Hickner, T.M. Alam, S.K. McIntyre, C.H. Fujimoto, C.J. Cornelius, Transport Properties of Hydroxide and Proton Conducting Membranes, Chemistry of Materials, 20 (2008) 2566-2573.

[106] L.A. Zook, J. Leddy, Density and Solubility of Nafion:  Recast, Annealed, and Commercial Films, Analytical Chemistry, 68 (1996) 3793-3796.

[107] Y.S. Kim, B.S. Pivovar, Moving Beyond Mass-Based Parameters for Conductivity Analysis of Sulfonated Polymers, Annual Review of Chemical and Biomolecular Engineering, 1 (2010) 123-148.

[108] S. Takamuku, P. Jannasch, Properties and degradation of hydrocarbon fuel cell membranes: a comparative study of sulfonated poly(arylene ether sulfone)s with different positions of the acid groups, Polymer Chemistry, 3 (2012) 1202-1214.

[109] T.A. Sherazi, S. Zahoor, R. Raza, A.J. Shaikh, S.A.R. Naqvi, G. Abbas, Y. Khan, S. Li, Guanidine functionalized radiation induced grafted anion-exchange membranes for solid alkaline fuel cells, International Journal of Hydrogen Energy, 40 (2015) 786-796.

[110] P. Yu Xu, K. Zhou, G. Lu Han, Q. Gen Zhang, A. Mei Zhu, Q. Lin Liu, Fluorene-containing poly(arylene ether sulfone)s as anion exchange membranes for alkaline fuel cells, Journal of Membrane Science, 457 (2014) 29-38.

[111] Y.-C. Cao, K. Scott, X. Wang, Preparation of polytetrafluoroethylene porous membrane based composite alkaline exchange membrane with improved tensile strength and its fuel cell test, International Journal of Hydrogen Energy, 37 (2012) 12688-12693.

[112] B.-S. Ko, J.-Y. Sohn, C.-Y. Kim, Y.C. Nho, J. Shin, Effect of the Thickness of a Fluoropolymer Film on the Radiotically Prepared Fuel Cell Membranes, Journal of Radiation Industry, 4 (2010) 159-163.

[113] H.-P. Brack, H.G. Buhrer, L. Bonorand, G.G. Scherer, Grafting of pre-irradiated poly(ethylene-alt-tetrafluoroethylene) films with styrene: influence of base polymer film properties and processing parameters, Journal of Materials Chemistry, 10 (2000) 1795-1803.

[114] R. Espiritu, M. Mamlouk, K. Scott, Study on the effect of the degree of grafting on the performance of polyethylene-based anion exchange membrane for fuel cell application, International Journal of Hydrogen Energy, 41 (2016) 1120-1133.

[115] K.H. Gopi, S.G. Peera, S.D. Bhat, P. Sridhar, S. Pitchumani, Preparation and characterization of quaternary ammonium functionalized poly(2,6-dimethyl-1,4-phenylene oxide) as anion exchange membrane for alkaline polymer electrolyte fuel cells, International Journal of Hydrogen Energy, 39 (2014) 2659-2668.

[116] M. Hibbs, C. Fujimoto, C. Cornelius, Poly(phenylene)-Based Anion Exchange Membranes for Alkaline Fuel Cells, (2009) 89-97.

[117] Z. Yuan, X. Li, J. Hu, W. Xu, J. Cao, H. Zhang, Degradation mechanism of sulfonated poly(ether ether ketone) (SPEEK) ion exchange membranes under vanadium flow battery medium, Physical Chemistry Chemical Physics, 16 (2014) 19841-19847.

[118] M.A. Hossain, Y. Lim, S. Lee, H. Jang, S. Choi, Y. Jeon, J. Lim, W.G. Kim, Comparison of alkaline fuel cell membranes of random & block poly(arylene ether sulfone) copolymers containing tetra quaternary ammonium hydroxides, International Journal of Hydrogen Energy, 39 (2014) 2731-2739.

[119] H. Xu, J. Fang, M. Guo, X. Lu, X. Wei, S. Tu, Novel anion exchange membrane based on copolymer of methyl methacrylate, vinylbenzyl chloride and ethyl acrylate for alkaline fuel cells, Journal of Membrane Science, 354 (2010) 206-211.

[120] X. Wu, K. Scott, A polymethacrylate-based quaternary ammonium OH− ionomer binder for non-precious metal alkaline anion exchange membrane water electrolysers, Journal of Power Sources, 214 (2012) 124-129.

[121] T.N. Danks, R.C.T. Slade, J.R. Varcoe, Comparison of PVDF- and FEP-based radiation-grafted alkaline anion-exchange membranes for use in low temperature portable DMFCs, Journal of Materials Chemistry, 12 (2002) 3371-3373.

[122] F.N. Büchi, B. Gupta, O. Haas, G.G. Scherer, Study of radiation-grafted FEP-G-polystyrene membranes as polymer electrolytes in fuel cells, Electrochimica Acta, 40 (1995) 345-353.

[123] T.N. Danks, R.C.T. Slade, J.R. Varcoe, Alkaline anion-exchange radiation-grafted membranes for possible electrochemical application in fuel cells, Journal of Materials Chemistry, 13 (2003) 712-721.

[124] S.D. Poynton, R.C.T. Slade, T.J. Omasta, W.E. Mustain, R. Escudero-Cid, P. Ocon, J.R. Varcoe, Preparation of radiation-grafted powders for use as anion exchange ionomers in alkaline polymer electrolyte fuel cells, Journal of Materials Chemistry A, 2 (2014) 5124-5130.

[125] X. Wu, K. Scott, F. Xie, N. Alford, A reversible water electrolyser with porous PTFE based OH− conductive membrane as energy storage cells, Journal of Power Sources, 246 (2014) 225-231.

[126] Y. Zhao, H. Yu, D. Xing, W. Lu, Z. Shao, B. Yi, Preparation and characterization of PTFE based composite anion exchange membranes for alkaline fuel cells, Journal of Membrane Science, 421–422 (2012) 311-317.

[127] K.S. Ngai, S. Ramesh, K. Ramesh, J.C. Juan, A review of polymer electrolytes: fundamental, approaches and applications, Ionics, 22 (2016) 1259-1279.

[128] Q. Zhang, Q. Zhang, J. Wang, S. Zhang, S. Li, Synthesis and alkaline stability of novel cardo poly(aryl ether sulfone)s with pendent quaternary ammonium aliphatic side chains for anion exchange membranes, Polymer, 51 (2010) 5407-5416.

[129] S.A. Nuñez, M.A. Hickner, Quantitative 1H NMR Analysis of Chemical Stabilities in Anion-Exchange Membranes, ACS Macro Letters, 2 (2012) 49-52.

[130] C. Fujimoto, D.-S. Kim, M. Hibbs, D. Wrobleski, Y.S. Kim, Backbone stability of quaternized polyaromatics for alkaline membrane fuel cells, Journal of Membrane Science, 423–424 (2012) 438-449.

[131] J. Parrondo, Z. Wang, M.-S.J. Jung, V. Ramani, Reactive Oxygen Species Accelerate Degradation of Anion Exchange Membranes Based on Polyphenylene Oxide in Alkaline Environments, Physical Chemistry Chemical Physics, 18 (2016) 19705-19712.

[132] C.G. Arges, V. Ramani, Two-dimensional NMR spectroscopy reveals cation-triggered backbone degradation in polysulfone-based anion exchange membranes, Proceedings of the National Academy of Sciences, 110 (2013) 2490-2495.

[133] J. Pan, Y. Li, J. Han, G. Li, L. Tan, C. Chen, J. Lu, L. Zhuang, A strategy for disentangling the conductivity-stability dilemma in alkaline polymer electrolytes, Energy & Environmental Science, 6 (2013) 2912-2915.

[134] J. Cheng, G. He, F. Zhang, A mini-review on anion exchange membranes for fuel cell applications: Stability issue and addressing strategies, International Journal of Hydrogen Energy, 40 (2015) 7348-7360.

[135] M.G. Marino, K.D. Kreuer, Alkaline Stability of Quaternary Ammonium Cations for Alkaline Fuel Cell Membranes and Ionic Liquids, ChemSusChem, 8 (2015) 513-523.

[136] H.-S. Dang, P. Jannasch, Exploring Different Cationic Alkyl Side Chain Designs for Enhanced Alkaline Stability and Hydroxide Ion Conductivity of Anion-Exchange Membranes, Macromolecules, 48 (2015) 5742-5751.

[137] J. Parrondo, M.-s.J. Jung, Z. Wang, C.G. Arges, V. Ramani, Synthesis and Alkaline Stability of Solubilized Anion Exchange Membrane Binders Based on Poly(phenylene oxide) Functionalized with Quaternary Ammonium Groups via a Hexyl Spacer, Journal of The Electrochemical Society, 162 (2015) F1236-F1242.

[138] K. Matsui, E. Tobita, K. Sugimoto, K. Kondo, T. Seita, A. Akimoto, Novel anion exchange membranes having fluorocarbon backbone: Preparation and stability, Journal of Applied Polymer Science, 32 (1986) 4137-4143.

[139] S. Gu, J. Wang, B. Zhang, R.B. Kaspar, Y. Yan, Hydroxide Exchange Membranes and Ionomers, in: Materials for Low-Temperature Fuel Cells, Wiley-VCH Verlag GmbH & Co. KGaA, 2014, pp. 125-144.

[140] O.I. Deavin, S. Murphy, A.L. Ong, S.D. Poynton, R. Zeng, H. Herman, J.R. Varcoe, Anion-exchange membranes for alkaline polymer electrolyte fuel cells: comparison of pendent benzyltrimethylammonium- and benzylmethylimidazolium-head-groups, Energy & Environmental Science, 5 (2012) 8584-8597.

[141] T. Sata, M. Tsujimoto, T. Yamaguchi, K. Matsusaki, Change of anion exchange membranes in an aqueous sodium hydroxide solution at high temperature, Journal of Membrane Science, 112 (1996) 161-170.

[142] S. Gu, R. Cai, T. Luo, Z. Chen, M. Sun, Y. Liu, G. He, Y. Yan, A Soluble and Highly Conductive Ionomer for High-Performance Hydroxide Exchange Membrane Fuel Cells, Angewandte Chemie International Edition, 48 (2009) 6499-6502.

[143] S. Chempath, J.M. Boncella, L.R. Pratt, N. Henson, B.S. Pivovar, Density Functional Theory Study of Degradation of Tetraalkylammonium Hydroxides, The Journal of Physical Chemistry C, 114 (2010) 11977-11983.

[144] A.C. Cope, A.S. Mehta, Mechanism of the Hofmann Elimination Reaction: An Ylide Intermediate in the Pyrolysis of a Highly Branched Quaternary Hydroxide, Journal of the American Chemical Society, 85 (1963) 1949-1952.

[145] Y. Yuesheng, A.E. Yossef, Chemical Stability of Anion Exchange Membranes for Alkaline Fuel Cells, in: Polymers for Energy Storage and Delivery: Polyelectrolytes for Batteries and Fuel Cells, American Chemical Society, 2012, pp. 233-251.

[146] C. Vogel, J. Meier-Haack, Preparation of ion-exchange materials and membranes, Desalination, 342 (2014) 156-174.

[147] S. Chempath, B.R. Einsla, L.R. Pratt, C.S. Macomber, J.M. Boncella, J.A. Rau, B.S. Pivovar, Mechanism of Tetraalkylammonium Headgroup Degradation in Alkaline Fuel Cell Membranes, The Journal of Physical Chemistry C, 112 (2008) 3179-3182.

[148] H. Long, K. Kim, B.S. Pivovar, Hydroxide Degradation Pathways for Substituted Trimethylammonium Cations: A DFT Study, The Journal of Physical Chemistry C, 116 (2012) 9419-9426.

[149] C.G. Arges, V.K. Ramani, Alkaline Stability and Ion Conductivity of Polysulfone Anion Exchange Membranes (AEMs) with Different Cation Chemistries, ECS Transactions, 50 (2013) 2183-2197.

[150] G. Ghigo, S. Cagnina, A. Maranzana, G. Tonachini, The mechanism of the Stevens and Sommelet–Hauser Rearrangements. A Theoretical Study, The Journal of Organic Chemistry, 75 (2010) 3608-3617.

[151] Z. Wang, Sommelet-Hauser Rearrangement, in: Comprehensive Organic Name Reactions and Reagents, John Wiley & Sons, Inc., 2010.

[152] H.K. Hall, R.B. Bates, Correlation of alkylamine nucleophilicities with their basicities, Tetrahedron Letters, 53 (2012) 1830-1832.

[153] V. Frenna, N. Vivona, G. Consiglio, D. Spinelli, Amine basicities in benzene and in water, Journal of the Chemical Society, Perkin Transactions 2, (1985) 1865-1868.

[154] P. Beltrame, G. Gelli, A. Loi, Potentiometric study of the ionization of some nitrogen bases in acetonitrile, Gazzetta Chimica Italiana, 110 (1980) 491-494.

[155] B. Bauer, H. Strathmann, F. Effenberger, Anion-exchange membranes with improved alkaline stability, Desalination, 79 (1990) 125-144.

[156] M. Mamlouk, S.M.S. Kumar, P. Gouerec, K. Scott, Electrochemical and fuel cell evaluation of Co based catalyst for oxygen reduction in anion exchange polymer membrane fuel cells, Journal of Power Sources, 196 (2011) 7594-7600.

[157] S. Maurya, S.-H. Shin, M.-K. Kim, S.-H. Yun, S.-H. Moon, Stability of composite anion exchange membranes with various functional groups and their performance for energy conversion, Journal of Membrane Science, 443 (2013) 28-35.

[158] J.B. Edson, C.S. Macomber, B.S. Pivovar, J.M. Boncella, Hydroxide based decomposition pathways of alkyltrimethylammonium cations, Journal of Membrane Science, 399–400 (2012) 49-59.

[159] M.R. Sturgeon, C.S. Macomber, C. Engtrakul, H. Long, B.S. Pivovar, Hydroxide based Benzyltrimethylammonium Degradation: Quantification of Rates and Degradation Technique Development, Journal of The Electrochemical Society, 162 (2015) F366-F372.

[160] B.R. Einsla, S. Chempath, L. Pratt, J. Boncella, J. Rau, C. Macomber, B. Pivovar, Stability of Cations for Anion Exchange Membrane Fuel Cells, ECS Transactions, 11 (2007) 1173-1180.

[161] W.K. Musker, A Reinvestigation of the Pyrolysis of Tetramethylammonium Hydroxide, Journal of the American Chemical Society, 86 (1964) 960-961.

[162] Z. Yang, J. Ran, B. Wu, L. Wu, T. Xu, Stability challenge in anion exchange membrane for fuel cells, Current Opinion in Chemical Engineering, 12 (2016) 22-30.

[163] T.S. Stevens, E.M. Creighton, A.B. Gordon, M. MacNicol, CCCCXXIII.-Degradation of quaternary ammonium salts. Part I, Journal of the Chemical Society, (1928) 3193-3197.

[164] S.W. Kantor, C.R. Hauser, Rearrangements of Benzyltrimethylammonium Ion and Related Quaternary Ammonium Ions by Sodium Amide Involving Migration into the Ring, Journal of the American Chemical Society, 73 (1951) 4122-4131.

[165] C. Iojoiu, F. Chabert, M. Maréchal, N.E. Kissi, J. Guindet, J.Y. Sanchez, From polymer chemistry to membrane elaboration: A global approach of fuel cell polymeric electrolytes, Journal of Power Sources, 153 (2006) 198-209.

[166] M.L. Di Vona, R. Narducci, L. Pasquini, K. Pelzer, P. Knauth, Anion-conducting ionomers: Study of type of functionalizing amine and macromolecular cross-linking, International Journal of Hydrogen Energy, 39 (2014) 14039-14049.

[167] J. Sun Koo, N.-S. Kwak, T.S. Hwang, Synthesis and properties of an anion-exchange membrane based on vinylbenzyl chloride–styrene–ethyl methacrylate copolymers, Journal of Membrane Science, 423-424 (2012) 293-301.

[168] H.-S. Dang, P. Jannasch, Alkali-stable and highly anion conducting poly(phenylene oxide)s carrying quaternary piperidinium cations, Journal of Materials Chemistry A, 4 (2016) 11924-11938.

[169] Y. Zhang, J. Fang, Y. Wu, H. Xu, X. Chi, W. Li, Y. Yang, G. Yan, Y. Zhuang, Novel fluoropolymer anion exchange membranes for alkaline direct methanol fuel cells, Journal of colloid and interface science, 381 (2012) 59-66.

[170] H. Zarrin, J. Wu, M. Fowler, Z. Chen, High durable PEK-based anion exchange membrane for elevated temperature alkaline fuel cells, Journal of Membrane Science, 394–395 (2012) 193-201.

[171] N. Li, M.D. Guiver, W.H. Binder, Towards High Conductivity in Anion-Exchange Membranes for Alkaline Fuel Cells, ChemSusChem, 6 (2013) 1376-1383.

[172] E.N. Komkova, D.F. Stamatialis, H. Strathmann, M. Wessling, Anion-exchange membranes containing diamines: preparation and stability in alkaline solution, Journal of Membrane Science, 244 (2004) 25-34.

[173] A.D. Mohanty, C. Bae, Mechanistic analysis of ammonium cation stability for alkaline exchange membrane fuel cells, Journal of Materials Chemistry A, 2 (2014) 17314-17320.

[174] C.G. Arges, V. Ramani, Investigation of Cation Degradation in Anion Exchange Membranes Using Multi-Dimensional NMR Spectroscopy, Journal of The Electrochemical Society, 160 (2013) F1006-F1021.

[175] J.R. Varcoe, S.D. Poynton, R.C.T. Slade, Alkaline anion-exchange membranes for low-temperature fuel cell application, in: Handbook of Fuel Cells, John Wiley & Sons, Ltd, 2010.

[176] A. Singh, Irradiation of polyethylene: Some aspects of crosslinking and oxidative degradation, Radiation Physics and Chemistry, 56 (1999) 375-380.

[177] K. Wündrich, A review of radiation resistance for plastic and elastomeric materials, Radiation Physics and Chemistry, 24 (1984) 503-510.

[178] S.S. Cota, V. Vasconcelos, M. Senne Jr, L.L. Carvalho, D.B. Rezende, R.F. Côrrea, Changes in mechanical properties due to gamma irradiation of high-density polyethylene (HDPE), Brazilian Journal of Chemical Engineering, 24 (2007) 259-265.

[179] D. Gheysari, A. Behjat, M. Haji-Saeid, The effect of high-energy electron beam on mechanical and thermal properties of LDPE and HDPE, European Polymer Journal, 37 (2001) 295-302.

[180] D. Plester, The effects of radiation sterilization on plastics, in: P. Briggs, W. Miller (Eds.) Industrial Sterilization, Duke University Press, Durham, NC, 1973, pp. 141-152.

[181] K.J. Hemmerich, Polymer materials selection for radiation-sterilized products, Medical Device and Diagnostic Industry, 22 (2000) 78-89.

[182] H.C. Sutton, J. Rotblat, Dose-Rate Effects in Radiation-Induced Chemical Reactions, Nature, 180 (1957) 1332-1333.

[183] E. Moura, E.S.R. Somessari, C.G. Silveira, H.A. Paes, C.A. Souza, W. Fernandes, J.E. Manzoli, A.B.C. Geraldo, Influence of physical parameters on mutual polymer grafting by electron beam irradiation, Radiation Physics and Chemistry, 80 (2011) 175-181.

[184] M.M. Nasef, H. Saidi, A.M. Dessouki, E.M. Ei-Nesr, Radiation-induced grafting of styrene onto poly(tetrafluoroethylene) (PTFE) films. I. Effect of grafting conditions and properties of the grafted films, Polymer International, 49 (2000) 399-406.

[185] D. Gheysari, A. Behjat, Radiation crosslinking of LDPE and HDPE with 5 and 10 MeV electron beams, European Polymer Journal, 37 (2001) 2011-2016.

[186] F. Ziaie, F. Anvari, M. Ghaffari, M. Borhani, Dose rate effect on LDPE cross-linking induced by electron beam irradiation, Nukleonika, 50 (2005) 125-127.

[187] M.R. Hibbs, Alkaline stability of poly(phenylene)-based anion exchange membranes with various cations, Journal of Polymer Science Part B: Polymer Physics, 51 (2013) 1736-1742.

[188] J. Mališ, P. Mazúr, M. Paidar, T. Bystron, K. Bouzek, Nafion 117 stability under conditions of PEM water electrolysis at elevated temperature and pressure, International Journal of Hydrogen Energy, 41 (2016) 2177-2188.

[189] C. Yang, S. Wang, W. Ma, L. Jiang, G. Sun, Comparison of alkaline stability of quaternary ammonium- and 1,2-methylimidazolium-based alkaline anion exchange membranes, Journal of Membrane Science, 487 (2015) 12-18.

[190] R.V. Law, D.C. Sherrington, C.E. Snape, I. Ando, H. Korosu, Solid State 13C MAS NMR Studies of Anion Exchange Resins and Their Precursors, Industrial & Engineering Chemistry Research, 34 (1995) 2740-2749.

[191] G.H. Penner, R. Webber, L.A. O'Dell, A multinuclear NMR and quantum chemical study of solid trimethylammonium chloride, Canadian Journal of Chemistry, 89 (2011) 1036-1046.

[192] T. Takewaki, L.W. Beck, M.E. Davis, Zeolite synthesis using 1,4-diazabicyclo[2,2,2]octane (DABCO) derivatives as structure-directing agents, Microporous and Mesoporous Materials, 33 (1999) 197-207.

[193] K.K. Laali, A. Jamalian, C. Zhao, Reaction of Selectfluor (F-TEDA-BF4) with chloromethylated-DABCO monocation salts (X = BF4, NTf2) and other nitrogen bases (Et3N; piperidine; basic ionic liquid); unexpected formation of symmetrical [N−H−N]+ trication salts, Tetrahedron Letters, 55 (2014) 6643-6646.

[194] L. Ghassemzadeh, M. Marrony, R. Barrera, K.D. Kreuer, J. Maier, K. Müller, Chemical degradation of proton conducting perflurosulfonic acid ionomer membranes studied by solid-state nuclear magnetic resonance spectroscopy, Journal of Power Sources, 186 (2009) 334-338.

[195] B. Wang, W. Sun, F. Bu, X. Li, H. Na, C. Zhao, Comparison of alkaline stability of benzyltrimethylammonium, benzylmethylimidazolium and benzyldimethylimidazolium functionalized poly(arylene ether ketone) anion exchange membranes, International Journal of Hydrogen Energy, 41 (2016) 3102-3112.

[196] T.M. Alam, M. Celina, R.A. Assink, R.L. Clough, K.T. Gillen, 17O NMR investigation of oxidative degradation in polymers under γ-irradiation, Radiation Physics and Chemistry, 60 (2001) 121-127.

[197] V. Maemets, I. Koppel, 17O and 1H NMR chemical shifts of hydroxide and hydronium ion in aqueous solutions of strong electrolytes, Journal of the Chemical Society, Faraday Transactions, 93 (1997) 1539-1542.

[198] P. Balakrishnan, A.L. Baumstark, D.W. Boykin, 17O NMR spectroscopy: unusual substituent effects in para-substituted benzyl alcohols and acetates, Tetrahedron Letters, 25 (1984) 169-172.

[199] I.P. Gerothanassis, Oxygen-17 NMR spectroscopy: Basic principles and applications (Part I), Progress in Nuclear Magnetic Resonance Spectroscopy, 56 (2010) 95-197.

[200] D. Boykin, 17O NMR Spectroscopy in Organic Chemistry, CRC Press, USA, 1990.

[201] X. Wang, D.Z. Wang, Aerobic oxidation of secondary benzylic alcohols and direct oxidative amidation of aryl aldehydes promoted by sodium hydride, Tetrahedron, 67 (2011) 3406-3411.

[202] M. Sankar, E. Nowicka, E. Carter, D.M. Murphy, D.W. Knight, D. Bethell, G.J. Hutchings, The benzaldehyde oxidation paradox explained by the interception of peroxy radical by benzyl alcohol, Nature Communications, 5 (2014).

[203] W.G. Klemperer, 17O-NMR Spectroscopy as a Structural Probe, Angewandte Chemie International Edition in English, 17 (1978) 246-254.

[204] J.-P. Kintzinger, Oxygen NMR, in: Oxygen-17 and Silicon-29, Springer Berlin Heidelberg, Berlin, Heidelberg, 1981, pp. 1-64.

[205] G. Socrates, Infrared Characteristic Group Frequencies: Tables and Charts, 2nd ed., John Wiley & Sons, England, 1994.

[206] M.M. Nasef, H. Saidi, K.Z.M. Dahlan, Electron beam irradiation effects on ethylene-tetrafluoroethylene copolymer films, Radiation Physics and Chemistry, 68 (2003) 875-883.

[207] R.B. Viana, A.B.F. da Silva, A.S. Pimentel, Infrared Spectroscopy of Anionic, Cationic, and Zwitterionic Surfactants, Advances in Physical Chemistry, 2012 (2012) 14.

[208] N.V. Venkataraman, S. Vasudevan, Conformation of Methylene Chains in an Intercalated Surfactant Bilayer, The Journal of Physical Chemistry B, 105 (2001) 1805-1812.

[209] K.M. Harmon, I. Gennick, Hydrogen bonding. V. Possible existence of strongly hydrogen-bonded water-fluoride and water-hydroxide complex anions, $(F^-.H_2O)_2^{2-}$ and $(OH^-.H_2O)_2^{2-}$, in tetramethylammonium ion salt hydrates, Inorganic Chemistry, 14 (1975) 1840-1845.

[210] N.G. Sahoo, H. Bao, Y. Pan, M. Pal, M. Kakran, H.K.F. Cheng, L. Li, L.P. Tan, Functionalized carbon nanomaterials as nanocarriers for loading and delivery of a poorly water-soluble anticancer drug: a comparative study, Chemical Communications, 47 (2011) 5235-5237.

[211] A. Hasaninejad, M. Shekouhy, N. Golzar, A. Zare, M.M. Doroodmand, Silica bonded n-propyl-4-aza-1-azoniabicyclo[2.2.2]octane chloride (SB-DABCO): A highly efficient, reusable and new heterogeneous catalyst for the synthesis of 4H-benzo[b]pyran derivatives, Applied Catalysis A: General, 402 (2011) 11-22.

[212] A. Filpi, M. Boccia, A. Pucci, F. Ciardelli, Modulation of the electrochemical properties of SBS-based anion membranes by the amine molecular structure, e-Polymers, 13 (2013) 1-14.

[213] V.I. Kovalenko, A.A. Akhmadiyarov, A.E. Vandyukov, A.R. Khamatgalimov, Experimental vibrational spectra and computational study of 1,4-diazabicyclo[2.2.2]octane, Journal of Molecular Structure, 1028 (2012) 134-140.

[214] C.O. Laoire, S. Mukerjee, K.M. Abraham, E.J. Plichta, M.A. Hendrickson, Elucidating the Mechanism of Oxygen Reduction for Lithium-Air Battery Applications, The Journal of Physical Chemistry C, 113 (2009) 20127-20134.

[215] Y.-F. He, R.-M. Wang, Y.-Y. Liu, Y. Chang, Y.-P. Wang, C.-G. Xia, J.-S. Suo, Study on oxidation mechanism of cumene based on GC-MS analysis, Journal of Molecular Catalysis A: Chemical, 159 (2000) 109-113.

[216] I. Di Somma, R. Andreozzi, M. Canterino, V. Caprio, R. Sanchirico, Thermal decomposition of cumene hydroperoxide: Chemical and kinetic characterization, AIChE Journal, 54 (2008) 1579-1584.

[217] R. Espiritu, B.T. Golding, K. Scott, M. Mamlouk, Degradation of radiation grafted hydroxide anion exchange membrane immersed in neutral pH: removal of vinylbenzyl trimethylammonium hydroxide due to oxidation, Journal of Materials Chemistry A, 5 (2017) 1248-1267.

[218] B.-S. Ko, J.-Y. Sohn, J. Shin, Radiation-induced synthesis of solid alkaline exchange membranes with quaternized 1,4-diazabicyclo[2,2,2] octane pendant groups for fuel cell application, Polymer, 53 (2012) 4652-4661.

[219] H. Komber, U. Georgi, B. Voit, 1H and 13C NMR Spectra of Highly Branched Poly(4-chloromethylstyrene). Signal Assignment, Structure Characterization, and a SCVP Kinetics Study, Macromolecules, 42 (2009) 8307-8315.

[220] J. Pan, L. Zhu, J. Han, M.A. Hickner, Mechanically Tough and Chemically Stable Anion Exchange Membranes from Rigid-Flexible Semi-Interpenetrating Networks, Chemistry of Materials, 27 (2015) 6689-6698.

[221] C.T. Viswanathan, C.A. Wilkie, Functionally substituted organolithium compounds: The lithium derivatives of the dimethylbenzylamines, Journal of Organometallic Chemistry, 54 (1973) 1-7.

[222] D. Swern, A.H. Clements, T.M. Luong, Nuclear magnetic resonance spectra of organic peroxides, Analytical Chemistry, 41 (1969) 412-416.

[223] W. Chen, X. Yan, X. Wu, S. Huang, Y. Luo, X. Gong, G. He, Tri-quaternized poly (ether sulfone) anion exchange membranes with improved hydroxide conductivity, Journal of Membrane Science, 514 (2016) 613-621.

[224] H. Yanagi, K. Fukuta, Anion Exchange Membrane and Ionomer for Alkaline Membrane Fuel Cells (AMFCs), ECS Transactions, 16 (2008) 257-262.